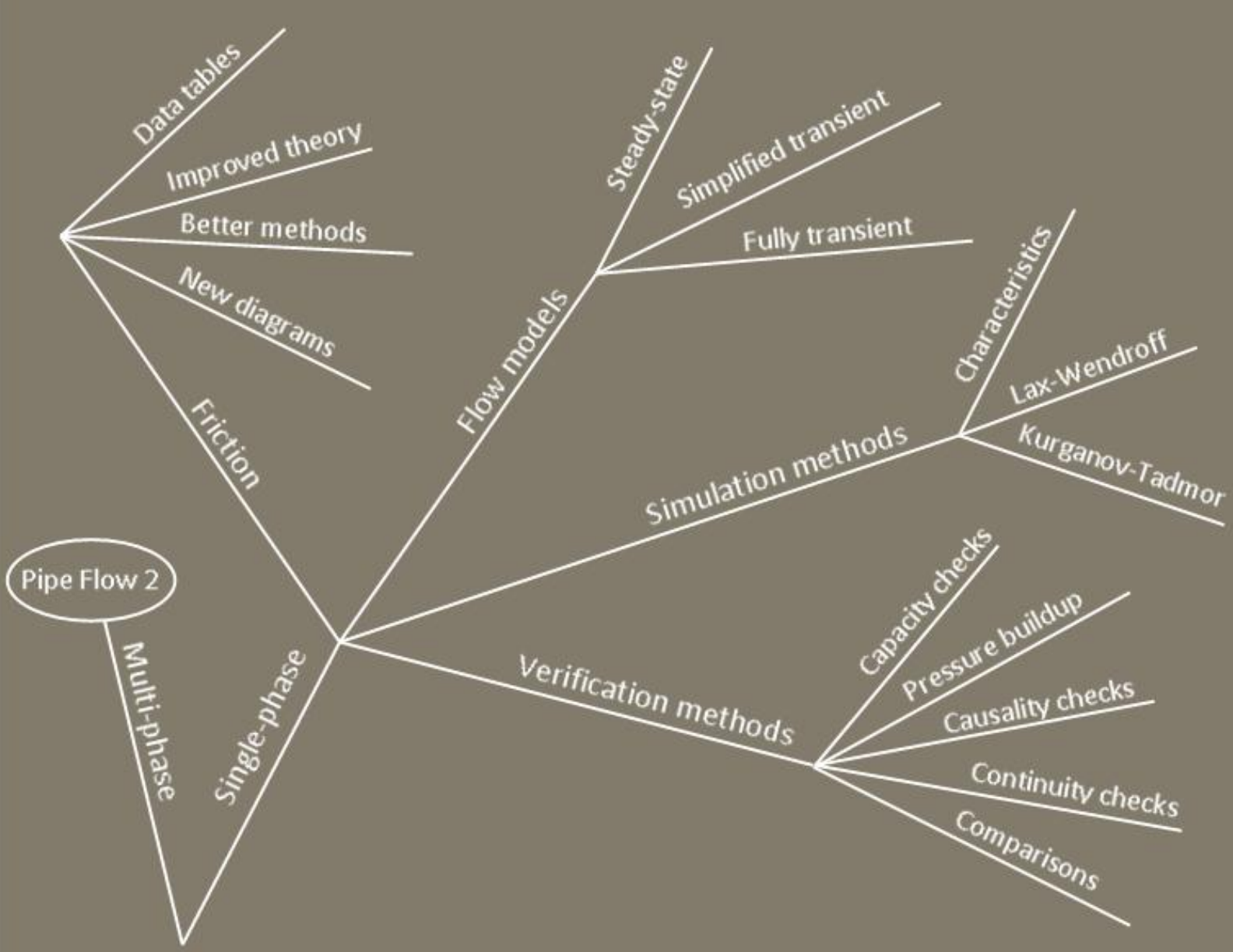




Pipe Flow 1

Single-phase Flow Assurance

Ove Bratland

© Copyright 2009 Dr. Ove Bratland
All rights reserved. No proportion of this book may be reproduced in any form or by any means, including electronic storage and retrivial systems, except by explicit, prior written permission from Dr. Ove Bratland except for brief passages excerpted for review and critical purposes.

"Intellectuals solve problems, geniuses prevent them."
Albert Einstein

Preface

Albert Einstein's wisdom regarding preventing problems before they occur certainly makes sense in pipeline and pipe network projects. Flow assurance – making sure the fluid flows as intended – relies heavily on mathematical models and the simulations they enable. Simulating the flow and everything affecting it contributes to problem prevention and efficiency, from feasibility studies through detailed engineering to operation. Ever more pipelines are being built around the world, and the number of people involved in various pipe flow calculations seems to increase daily. It is my hope that this book can be of help to everyone engaged in those tasks.

There are many commercial simulation tools available on the market, and the variation in user friendliness and underlying theoretical foundation for the various programs are astonishing. The purpose of this book is to explain how pipe flow simulation programs work and how to check results they produce. It goes into enough detail to enable the reader to create his own simulation tools and it also explains how to select and use commercial programs. It demonstrates some common sources of errors and how to avoid them.

Pipe flow is a complex phenomenon, and there have been a lot of new, valuable developments lately. Recent advancements come from such fields as fluid mechanics, mechanical engineering, chemistry, numerical mathematics, software development, control theory, and standardization. It is a challenge to keep up with it all, and this book intends to make the effort more manageable. The task is as much as possible seen from the engineer's point of view, and I have tried to avoid going too deep into details in the underlying theory.

Pipe flow problems can be categorized according to what sort of fluids we are dealing with, such as liquids, gases, dry bulk, or a mixture of several of them. This book is primarily about single-phase flow, meaning it focuses on pipes carrying either a liquid or a gas, but not both concurrently. It is still taking multi-phase flow into account in two important respects, though. It includes multi-phase simulation programs in the overview over different relevant commercial software tools in chapter 1, and it uses mathematical models very similar to the ones used for simulating multi-phase

transients. For readers who progress to multi-phase transient flow, the added equations required to do so will appear as a natural extension of the theory in this book.

In a typical pipeline project an oil company may be the project owner, while a contractor is used to carry out various phases of project execution. The contractor may do simulations in-house as part of this process, or he can sub-contract it to a company specializing in flow assurance. Results coming out of such simulations need to be verified as reliably as possible. Traditionally, this is done by using several subcontractors to do the same simulations and compare results. That can be very useful, but there are other, less well known ways of verification as well. A number of convenient verification tests have been presented in chapters 7.4.2 and 14.6, some published for the first time. The tests are meant to be useful to everyone involved in checking simulation results, including those who carry out the simulations in the first place. Given how easy some of the checks are, it does in fact seem natural to make such verification part of the contractual requirements.

A pipeline's capacity is one of the most important parameters in any design specification, and it is crucial to determine the friction accurately in order to meet that capacity as cheaply and reliably as possible. The most accepted way to determine the friction factor has been to use the traditional Moody diagram or the AGA calculation method. This book demonstrates that these traditional methods easily lead to 10 % inaccuracies in the pressure drop calculations, in some cases significantly more.

The traditional friction calculations suffer from two main weaknesses. First, they rely on measurements which do not stretch into as high Reynolds numbers as one may encounter (in high pressure export gas pipelines, for instance). Second, they rely on summarizing everything to do with surface texture into an 'equivalent sand grain roughness'. An overwhelming amount of measurements show this not to give accurate results in part of the relevant Reynolds number range.

Recently published measurements also show coating can have significant effect on capacity, so much so that internally coated pipelines can achieve the same capacity with a significantly smaller diameter than similar uncoated pipelines. A large part of the book, all of chapter 2, is dedicated to showing how friction factor accuracies can be improved. Previously un-published diagrams are also given there. Some of the proposed methods rely on carrying out measurements and can be quite costly. When expensive pipelines are to be built, though, it makes sense to go into great detail regarding friction, and even early-phase laboratory measurements can be cost-effective.

The method of characteristics is probably the most used simulation method for liquid flow. It is fast, simple, and well known, but not directly applicable to gas flow. Chapter 7 outlines which simplifications the method of characteristics relies on, how to implement it in a computer program, and how to calculate steady-state starting values. Many steady-state methods have been developed over the years, but this book outlines a previously un-published method utilizing the transient simulation program modules to simplify the overall computer code.

Most books about transient gas pipe flow focus exclusively on how to simulate perfect gases. Real gases differ from perfect gases is some important respects, and perfect gas models are most useful as a reference for testing out simulation methods or for very low pressure pipes. Perfect gas models cannot be used in general simulation programs intended for both high and low pressure pipelines. Therefore, all gas theory in this book is developed with reference to real gases, and ideal gas models are used for reference or testing purposes only.

The fully transient gas model presented in chapter 10 uses the Kurganov-Tadmor scheme of order 3 in combination with an explicit fourth-order Runge-Kutta method to solve the conservation equations. The main focus is on how easy these methods are to use in practice rather than on presenting all the advanced theory they rely on. The KT3 method has been around for nearly ten years, but the high-order, causality-safe ways of dealing with boundary conditions and ghost cells outlined in chapters 12 and 13 has to my knowledge not been published before. The new methods make traditional simplifications redundant in some cases. Avoiding model simplifications increases the results' validity and applicability significantly.

Finally, some words about how both books are published. The traditional way of publishing goes via one of the established publishers, with all their resources for checking, editing, marketing, and sales. To most advisers' dismay, I have chosen not to follow that path. New technology makes it possible to handle most publishing tasks efficiently in alternative ways. Besides, the time when a book's content was married to the paper on which it was written is long gone, and the cost of making extra digital copies is zero. So why not let unpaid students get a digital copy for free. The same goes for those who want to consider the book for commercial purposes – just download the free version first and have a look. Orders for printed copies can be made at the internet site www.drbratland.com. Some of the simulation programs used in the examples can also be found there.

Any feedback from readers is greatly appreciated and should be directed to the internet site. All will be read, and as far as time allows, serious questions and comments will also be answered.

Ove Bratland
February 2009

Acknowledgements

The author wishes to thank the following companies for various discussions and support during the work with this book: Statoil, SINTEF Petroleum Research AS, AspenTech, Simsci-Esscor, Institute for Energy Technology (IFE), SPT Group, Institut Francais du Petrole (IFP), Telvent, Schlumberger, University of Tulsa, Neotechnology Consultants, Flowmaster and Advantica.

Thanks also to Prof. Gustavo Gioia for various discussions about the turbulence model in chapter 2.8, and to Dr. Elling Sletfjerding for discussions about his friction measurements.

My good friend Mr. Jarl Helge Jensen has helped with various corrections and my warmest thanks go to him, too.

Thank you all for helping to make this book a reality.

Table of Contents

Preface .....

1 Introduction 1

1.1 The many challenges involved in pipeline projects 1

1.1.1 History 1

1.1.2 Modern pipelines and their alternatives 2

1.1.3 Pipeline politics 2

1.1.4 What this book is about 3

1.2 Codes and specifications 4

1.3 A pipeline project's different phases 4

1.3.1 Preliminary planning with feasibility study 5

1.3.2 Route selection 5

1.3.3 Acquisition of right-of-way 6

1.3.4 Various data collection 6

1.3.5 Pipeline design 6

1.3.6 Legal permits and construction 7

1.3.7 Commissioning and start-up 7

1.4 How pipe flow studies fit into a pipeline project, and which tools to use 7

1.5 Different sorts of pipe flow models and calculations 9

1.5.1 Single-phase versus multi-phase models 9

1.5.2 Steady-state versus transient simulations 10

1.5.3 The flow simulation software's different parts 11

1.6 Considerations when simulating pipe flow 13

1.6.1 General considerations 13

1.6.2 Hydrates and wax 13

1.6.3 Leak detection 14

1.6.4 Other features 14

1.7 Commercially available simulation software 14
1.7.1 Single-phase pipe flow software 14
1.7.2 Steady-state multi-phase simulation programs 16
1.7.3 Transient simulation software 16
1.8 An example of what advanced pipe flow simulations can achieve 16
References 20
2 Pipe friction 21
2.1 Basic theory 21
2.1.1 Introduction 21
2.1.2 Laminar flow 22
2.1.3 Turbulent flow 24
2.2 Simple friction considerations 28
2.3 Nikuradse's friction factor measurements 30
2.4 What surfaces look like 32
2.5 The traditional Moody diagram 36
2.6 Extracting more from Nikuradse's measurements 40
2.7 The AGA friction factor formulation 46
2.8 Towards a better understanding of the friction in turbulent pipe flow 48
2.8.1 Introduction about turbulence 48
2.8.2 Quantifying turbulence 49
2.8.3 Using Kolmogorov's theory to construct a Moody-like diagram 56
2.8.4 Comparing the theoretical results with other measurements 60
2.8.5 Large surface imperfections dominate on non-uniform surfaces 61
2.8.6 Friction behaves the same way for all Newtonian fluids. 63
2.9 Practical friction factor calculation methods 63
2.9.1 The surface-uniformity based modified Moody diagram 63
2.9.2 Improving friction factor calculation speed 67
2.10 Fitting curves to measurements 72
2.11 Friction factor accuracy 75
2.12 Tabulated surface roughness data 77
2.13 Common friction factor definitions 80

 For non-commercial use only

2.14 Transient friction 83
2.15 Other sorts of friction in straight, circular pipes 87
2.16 Friction factor summary 88
References 89
3 Friction in non-circular pipes 93
3.1 General 93
3.2 Partially-filled pipe 94
3.3 Rectangular pipe 97
3.4 Concentric annular cross-section 99
3.5 Elliptic cross-section 100
References 101
4 Friction losses in components 102
4.1 General 102
4.2 Valves 104
4.3 Bends 106
4.4 Welds joining pipe sections 108
4.5 Inlet loss 110
4.6 Diameter changes 111
4.7 Junctions 114
References 119
5 Non-Newtonian fluids and friction 121
5.1 Introduction 121
5.2 Pipe flow friction for power-law fluids 123
5.3 Pipe flow friction for Birmingham plastic fluids 127
5.4 Friction-reducing fluids 129
References 130
6 Transient flow 132
6.1 Mass conservation 132
6.2 Momentum conservation 135
6.3 Energy conservation 138
6.4 Examples to illustrate the conservation equations 142

6.4.1 Sloping liquid pipeline with steady-state flow 142
6.4.2 Horizontal gas pipeline with isothermal steady-state flow 145
6.4.3 Example: Gas pipeline cooling down after stop 148
References 150
7 Simplified liquid flow solution 152
7.1 Main principles 152
7.1.1 General 152
7.1.2 Involving fluid properties 153
7.2 Solving the equations by the characteristics method 159
7.2.1 Example: Instantaneous valve closure 163
7.3 Boundary conditions in the method of characteristics 165
7.3.1 Pipe with constant pressure at the inlet, closed outlet 166
7.3.2 Pipe with valve at the outlet 166
7.3.3 Valve located any other place than inlet or outlet 168
7.3.4 Inline centrifugal pump 169
7.3.5 Pump between reservoir and pipe inlet 173
7.3.6 Positive displacement pump 173
7.3.7 Junction 174
7.4 Instantaneous valve closure 176
7.4.1 Basic simulations 176
7.4.2 Some ways to check the simulations results manually 179
7.5 Steady-state network analysis 180
7.5.1 General 180
7.5.2 Finding initial velocities using the steady-state characteristics method 182
7.5.3 Steady-state convergence criteria 184
7.5.4 Steady-state example 185
7.6 Simulating transients in pipe networks, an example 188
7.7 Stability considerations 191
7.7.1 Frictionless flow 193
7.7.2 Flow with laminar friction 195
7.7.3 Turbulent flow 198

 For non-commercial use only

7.7.4 Some effects of the characteristic equations being nonlinear 200
7.8 Tracking the liquid 203
7.9 Checking simulation results 205
7.10 Advantages and limitations when using the method of characteristics 206
References 207
8 Heat exchange 209
8.1 General about heat through layered insulation 209
8.2 Heat transfer coefficient between fluid and pipe wall 212
8.3 Heat transfer coefficients for the pipe wall, coating and insulation layers 216
8.4 Heat transfer coefficient for outermost layer 217
8.4.1 Buried pipe 217
8.4.2 Above-ground pipe 218
8.5 The heat models' limitations 221
8.5.1 Transient versus steady-state heat flow 221
8.5.2 Other accuracy considerations 222
References 222
9 Adding heat calculations to the characteristics method 224
9.1 The energy equation's characteristic 224
9.2 Solving the energy equations using the explicit Lax-Wendroff's method 229
9.3 Boundary conditions for the thermo equation 233
9.3.1 The problem with lack of neighboring grid-points at the boundary 233
9.3.2 Junctions, pumps, valves and other components 235
9.4 Determining secondary variables 236
9.5 Computing starting values 237
9.6 Stability considerations for the energy solution 240
9.7 Numerical dissipation and dispersion 243
9.7.1 How numerical dissipation and dispersion can affect the simulations 243
9.7.2 Easy ways to reduce numerical dissipation and dispersion 245
9.7.3 Modern, effective ways to counter dissipation and dispersion 247
References 254
10 Solving the conservation equations 255

10.1 Problem formulation 255
10.2 Some initial, simplified considerations 258
10.3 The conservation equations' main properties 261
10.4 Selecting time integration and spatial discretization methods 265
10.5 How to account for friction and heat in the KT3 scheme 269
10.6 Calculating secondary from primary variables 273
10.7 Determining indirect fluid properties 276
References 278
11 Ghost cells 280
11.1 Some general considerations 280
11.2 Inserting ghost values: A simple method 281
11.3 An improved ghost cell approximation 284
11.4 Further ghost cell improvements 287
11.5 Computing state variables from flux variables 288
References 294
12 Boundary conditions 295
12.1 General 295
12.1.1 Boundary condition 1: Pressure source, inflowing fluid 296
12.1.2 Boundary condition 2: Pressure source, out-flowing fluid 297
12.1.3 Boundary condition 3: Mass flow source, in-flowing fluid 298
12.1.4 Boundary condition 4: Mass flow source, out-flowing fluid 299
12.2 Selecting boundary conditions in junctions 299
12.3 Other boundary conditions 301
References 302
13 Filling the ghost cells by using the boundary conditions directly 303
13.1 General philosophy 303
13.2 Mass flow source 305
13.2.1 Inflowing fluid 306
13.2.2 Outflowing fluid 307
13.3 Pressure source 308
References 309

 For non-commercial use only

14 Simulation results and program testing 310

14.1 Simulating one of the world's longest gas pipelines 310

14.2 Gas temperature in insulated pipelines 316

14.3 Simulating pipe rupture 318

14.4 How cooling affects the flow after shutdown 320

14.5 Comparing with other simulation programs 322

14.6 How to verify gas flow simulations, an overview 324

14.6.1 See if the integrations runs at all 324

14.6.2 Do the same checks as for liquid flow 324

14.6.3 Checking the boundary and ghost cell approximations for steady-state flow 325

14.6.4 Checking the boundary and ghost cell approximations for transient flow 326

14.6.5 Check that the program uses correct fluid properties 327

14.6.6 Check the heat flow calculations manually 328

14.6.7 Increase the velocity until choking occurs 328

14.6.8 Things which may confuse result interpretation 328

References 329

15 Simplified models 331

15.1 General 331

15.2 Steady-state calculations 332

15.3 Fully transient isothermal model 334

15.4 Neglecting part of inertia for isothermal flow 335

15.5 Neglecting all terms to do with gas inertia 336

15.5.1 Model formulation 336

15.5.2 Numerical approximations 340

15.5.3 Important observations regarding neglecting the gas inertia 341

References 342

Nomenclature 344

"Scientists discover the world that exists, engineers create the world that never was".
Theodore von Karman

1 Introduction

This chapter presents some background information, including:

- Pipeline history
- How pipeline projects work
- What flow simulations can be used for
- Different sorts of flow models
- Single-phase versus multi-phase simulations
- Overview of commercially available simulation programs

1.1 The many challenges involved in pipeline projects

1.1.1 History

Pipes appear to have been invented independently several places at nearly the same time and are known to have been in use as much as 5,000 years ago in China, Egypt, and the area presently known as Iraq. At a much later date, the Romans advanced the art of designing piping and waterworks, though the Roman empire's fall reversed all that and waterworks were largely ignored in early middle-age Europe. Towns reverted to using wells, springs, and rivers for water, and wastewater was simply disposed of into the streets. Improvements were clearly needed, and fittingly, one of the first books printed after the invention of the printing press in the fifteenth century was Frontinus' *Roman treatise on waterworks*. The advent of the industrial revolution accelerated the need for pipes while providing economic and technical means to manufacture them.

Pipes and channels have historically brought major advantages to those who had them, and successful pipeline or aqueduct projects have always required the right combination of political, economical and technical resources. History shows that most societies did not possess that combination, leaving them without advanced waterworks. Even today, a considerable part of the world's population suffers from unclean drinking water and inadequate sewage systems. The technology to solve such problems exists, but too often, poverty or economic unrest holds back the development.

Even today, a considerable part of the world's population suffers from unclean drinking water or inadequate sewage systems.

1.1.2 Modern pipelines and their alternatives

In our modern world, pipelines have more applications than in previous times. They require relatively high initial investment and typically have a designed life-span of 40 years or more. That would probably not have impressed the ancient Romans, but it is still good enough to be more economical than alternative transport forms. Liquids can sometimes be cheaper to transport by ship, at least over long distances, but gas is difficult and expensive to transport in large quantities by any other means than pipelines. Gas can be liquefied, and Liquefied Natural Gas can be shipped long distances. To do so, however, a significant part of the gas' energy has to be spent on the liquefaction itself, and gas pipelines are generally the preferred option unless very long distances, difficult terrain, prohibitive legal regimes, or other special problems prevent them from being used.

1.1.3 Pipeline politics

Oil and gas pipelines can be very long, sometimes crossing country borders. Pipeline projects are often so important they get entangled in geopolitical complications, making long and careful negotiations with many interest groups an essential part of the project. Route selection is frequently dictated by environmental or political rather than technical concerns. High level politics was on daily display when this book's author stayed some years in Azerbaijan in the 1990s, during a time when a pipeline route from Azerbaijan via Georgia and Turkey to the Mediterranean Sea was selected in competition with

 For non-commercial use only

other, mostly cheaper alternatives. More than once, the amount of dignitaries visiting Baku in order to affect that and related decisions was so high that traffic flow in the city center suffered. For those managing the project at the time it must have felt like politics was everything and technology virtually nothing.

In some recent projects we have even seen that choosing relatively expensive subsea rather than overland routes have been motivated by desires to keep the number of parties involved at a minimum. Again, politics is more than a little involved.

At the time of this writing, an equally common and related problem faces the ASEAN countries (9 South-East Asian countries, including Indonesia, Malaysia and Thailand) in their efforts to expand their pipeline networks. Differences in national gas quality specifications make it hard to trade across borders: CO_2-content can vary from nearly 30% to far less. This also complicates matters when securing backup alternatives in case of interruptions. One type of gas cannot always replace another even temporarily, and the added safety of having a gas pipeline network rather than one pipeline is reduced. Australia is an example of a country which has put intense effort into improving their gas quality standardization, and trade between different states goes more smoothly than it used to. Similar challenges related to gas quality standardization, customs for the gas as well as for spare parts, and a host of others are common all over the world wherever pipelines cross borders.

Pipeline projects are often so important they get entangled in geopolitical complications.

1.1.4 What this book is about

In addition to the geopolitical, environmental, and economical questions facing pipeline projects, there are myriads of interesting technical challenges to be solved as well. This book focuses on some of those technical challenges, specifically the ones to do with making the fluid flow the way it was intended. That is obviously affected by everything inside the pipe (inner diameter, surface roughness, and surface structure), fluid properties (there are lots of them, including viscosity, density, specific energy, and compressibility), and the pipe wall itself (thermo-properties, insulation, and elasticity). The environment affects the transported fluid's temperature, so submerged, buried and uncovered pipelines may have to be modeled slightly differently. The way the fluid flows is of course important to the pipelines' capacity, but also sets important conditions for phenomena that can damage the pipe: Corrosion, erosion, and the

potential formation of wax or other deposits fall into this category. Such damages fall outside the scope of this book, but the foundation for predicting them – the flow itself – is treated in detail.

This book focuses on technical challenges to do with making the fluid flow the way it was intended.

It is easiest to deal with flow of the single-phase type, meaning the fluid is either a homogeneous liquid or a gas, and that is what the book focuses on. But before going into details about pipe flow, let us have a brief look at some of the other aspects of relevance to pipeline projects.

1.2 Codes and specifications

A pipeline is always designed in accordance with codes and specifications. Those specifications describe nearly everything to do with the design, such as which materials to use, working stresses, seismic loads, thermal expansion, other imposed internal or external loads, as well as fabrication and installation. In addition, the design depends on factors relevant to the specific pipeline, including the fluid(s) to be transported (oil/gas/solids, single/multi-phase), length and required capacity, the environment (warm/cold climate, overland/buried/subsea, urban/countryside), and operational conditions (need for valves, compressors, pumps, surge chambers, storage capacity).

Code compliance is mandated by various governmental organizations. Codes can be legal documents, and like other laws, they vary from place to place. Contractual agreements may typically also have a say on which codes to use, and all in all selecting the right codes and standards is often one of the most important parts of the project. The different relevant specifications typically overlap, and it is essential to decide what to do when that is the case, for instance that the most restrictive code applies. Many of the legal conflicts arising in large projects have to do with how different codes should be interpreted, or even more common, when to apply which code. Frankel (1996, 2002) gives an overview over different codes relevant to pipeline engineers, and more details can be found there. As a general rule, though, it is best to stick to international codes and standards as much as possible, and to minimize the use of company- or project-specifications.

1.3 A pipeline project's different phases

The different phases in a pipeline project may vary considerably, depending on how large the project is, where it is, whether borders are crossed, whether the pipe goes over

 For non-commercial use only

land or subsea, who manages it and a multitude of other factors. The phases shown below can therefore only be seen as a typical example.

1.3.1 Preliminary planning with feasibility study

The main parameters are determined in this phase. They may include approximate pipe length with origin and destination, diameter, type of pipe, mass flow, capital cost, operating expenses with pressure loss and power consumption, main valves and pumping or compressor stations. Pipe flow simulations are very useful in this study. Both economical and technical feasibility should be considered. The project must be economical, and it obviously has to be technically possible. In addition, 'political feasibility' is a major factor since conflicts and geopolitics can pose daunting challenges.

1.3.2 Route selection

For overland pipelines, the route should be marked on various sorts of maps. This can most often be done by using existing maps in addition to taking aerial photography and surveys of the pipeline route. Route maps and property plats are created from these. Right-of-way acquisitions are normally not done in this phase, but they are taken into consideration.

In case of rock tunnels, various additional sorts of surveys may be required, such as drilling to determine rock quality.

Existing maps are often of little help for subsea pipelines. Surveying can be quite complicated and expensive, but seafloor mapping technology has developed significantly in recent years. Maps and terrain models are generated using depth data from multi-beam echo sounders mounted on the hull of survey ships, and Remotely Operated Vehicles (ROVs) are also used. Autonomous Underwater Vehicles (AUVs) have been used in some recent projects and can be more economical and faster for some surveying tasks.

Many countries have strict laws prohibiting any activities from disturbing unexcavated archeological sites, and most project managers would surely prefer not to encounter any. But archeological sites can be stumbled upon almost anywhere. In a relatively recent development, *The Ormen Lange-field* off the Norwegian coast, a shipwreck was discovered, and archeological investigations had to be carried out before pipe lying. Needless to say, planning for such possibilities is not easy.

1.3.3 Acquisition of right-of-way

How this is done is to a large extent determined by local laws, and they differ a lot. The process can take the form of voluntary negotiation with land owners, or it can be condemnation, meaning the land is acquired through an involuntary legal process. Usually, owners are entitled to compensation at a fair market value. This can be a complicated, lengthy process with many involved parties. In this respect, subsea pipelines are the easiest ones to handle. As already explained, crossing borders generally complicates this task, sometimes to unmanageable levels.

1.3.4 Various data collection

This is similar to what was discussed under *route selection*, but the work is done in greater detail. Soil borings and various soil testing may in some cases only be possible after the acquisition of right-of way is finished, so it may have to be delayed until this phase.

1.3.5 Pipeline design

Because different industries use pipelines for different purposes, the design requirements are different and the types of pipe materials vary. In the petroleum and natural gas industry, steel pipe with welded joints is most common. Using high pressures steel pipes makes it possible to have fewer booster stations along the line, and steel's ductility enables it to bend and withstand considerable impact without fracturing.

In the water and sewer industries, on the other hand, pipes are normally under relatively low, sometimes atmospheric pressure. The low pressure has led these industries to prefer low-stress, non-corroding pipe materials as PVC and concrete. Both for low-pressure and subsea pipes, it is common for external loads to exceed the internal ones.

In the petroleum and natural gas industry, steel pipe with welded joints is most common.

 For non-commercial use only

1.3.6 Legal permits and construction

Once necessary legal permits and design are approved, construction can start. For overland pipelines, that may involve clearing a path of minimum 15 m, bringing in the pipe, possibly ditching, trenching, boring, tunneling, and river crossing, followed by welding, coating, wrapping, pipe laying, and backfill with restoration of land. For subsea pipelines, it means laying the pipe from the laying vessel, in some cases including building 'underwater roads' or trenches, and to re-fill them after laying.

1.3.7 Commissioning and start-up

The various valves and instruments along the pipeline must be tested and found functional. There may be additional tests, too, such as pressure and leak tests, and various cleaning procedures may be necessary. For subsea pipelines, the fluid used to achieve the required buoyancy during lying must be removed. The procedures may include running cleaning and instrument pigs through the pipeline.

1.4 How pipe flow studies fit into a pipeline project, and which tools to use

The whole purpose of constructing a pipeline is of course to have something flow through it, and understanding how the flow behaves is essential. Pipe flow simulation is used to optimize and verify design and to throw light on various operational issues. It is used not only through all the phases described in the previous chapters, but also for training engineers and operators. During pipeline operation, simulations are used for real time system estimation and forecasting, as well as for operator training. This book is about pipe flow, and it will show how the flow theory can help us to deal with all these tasks.

There are many pipe flow simulation tools commercially available (Bratland, 2008), but using them correctly and efficiently requires understanding of what the programs do, how they work, and their limitations. State of the art simulation tools are not good enough to be reliable if they are treated as 'black boxes', and there is no substitute for understanding how they work in great detail. There is a danger that *learning how to simulate* can be misunderstood as *learning how to interface with simulation program A*, while it probably should mean something more like *understanding simulation program A's possibilities and limitations, and how to interpret and check the results*.

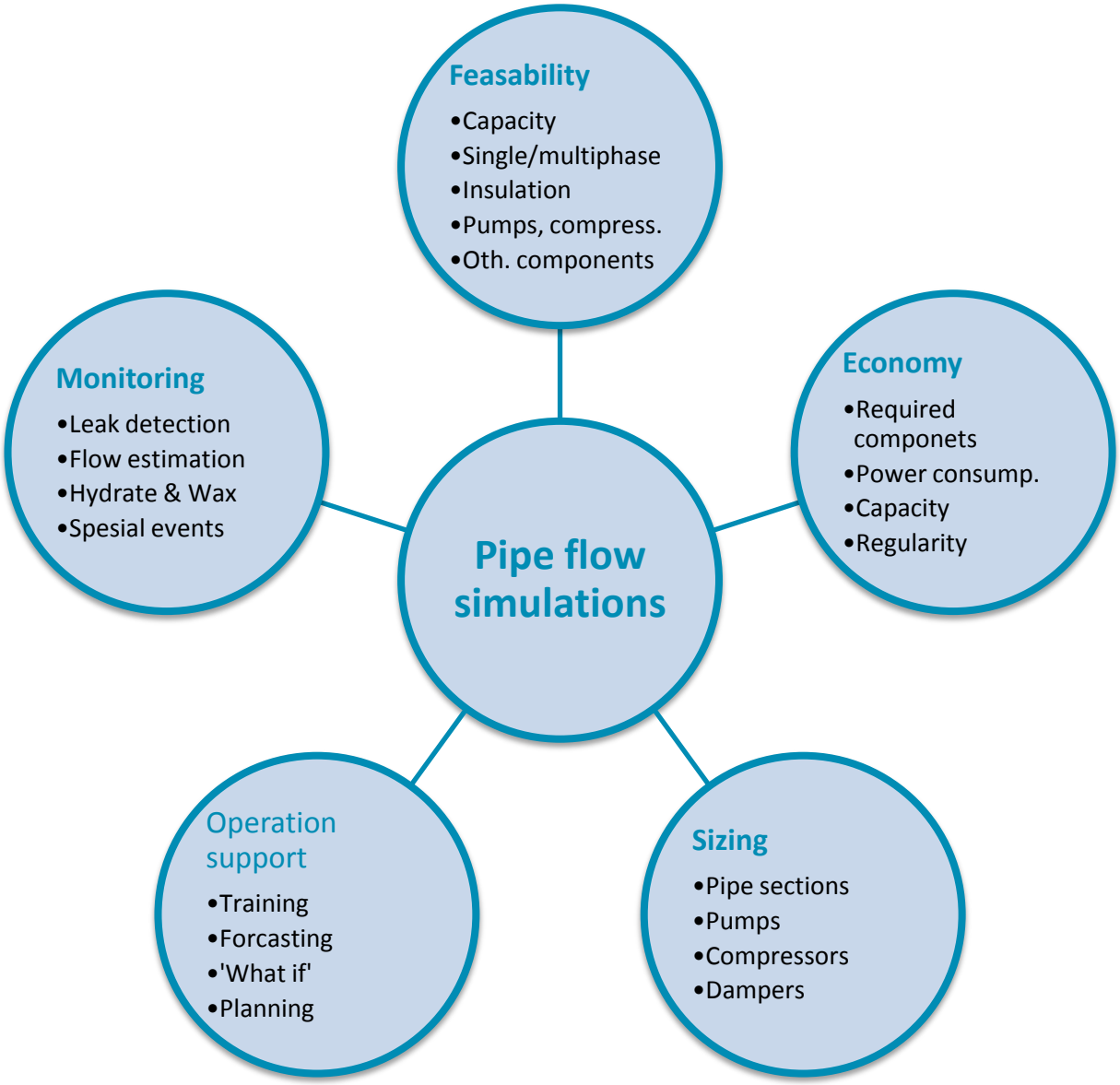


Figure 1.4.1. Various reasons to simulate pipe flow.

Considering all issues important to maintaining the fluid flow from *inlet* to *outlet* is sometimes called *Flow Assurance*. It is a term encountered frequently when studying pipe flow, particularly when hydrocarbons are involved. Still, there is no generally agreed on, clear, common definition of what Flow Assurance is. It is obviously possible to define the system boundaries *inlet* and *outlet* in different ways. For instance, when considering petroleum production, the *inlet* could be described as a reservoir or as one or several wells. Alternatively, it could simply mean the pipe inlet. The latter may have been the most common way to look at the problem in the past, but for gathering

 For non-commercial use only

networks, the trend for multi-phase simulation tools is towards integrated well and pipe network simulations. Following this trend, many of those involved in developing flow assurance tools are busy creating ever better interfaces so that almost any well simulator can communicate relatively seamlessly with any multi-phase pipe flow simulation package. The same can be said about the *outlet* end of the pipeline. The trend is to integrate with slug catchers, separators, processing facilities or whatever else the system contains.

The complexity of computing pipe flow depends on what the pipe transports and what sort of phenomena we want to investigate. Figure 1.4.2 illustrates some of the different parameters affecting how complicated it is to do those computations, arranged so that the simplest alternatives are on top.

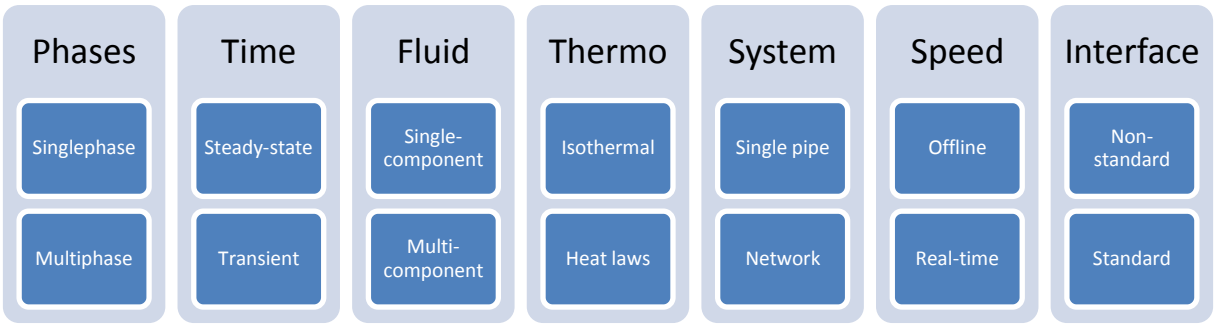


Figure 1.4.2. Various parameters affecting pipe flow computation complexity

1.5 Different sorts of pipe flow models and calculations

The simplest way to classify pipe flow models is probably by specifying how many separate fluids they can deal with simultaneously (single-phase, two-phase or three-phase), and by whether they are able to describe time-dependent phenomena (transient or purely steady-state). Let us have a look at what these differences mean in practice.

1.5.1 Single-phase versus multi-phase models

The first pipe flow models dealt with single-phase flow of water or steam, though not both at the same time. Since many phenomena are multi-phase, such single-phase models have their limitations. Early studies on transient two-phase flow were conducted in the nuclear industry, as it became mandatory to predict the transient flow behavior during potential Loss-of-Coolant Accidents for licensing pressurized water reactors.

Multi-phase flow can also occur in gas pipelines. If even a small amount of liquid condenses on the pipe wall, it will affect the flow. As we will see in later chapters, a gas pipeline's capacity can be very sensitive to the wall surface roughness, and it takes only a tiny amount of droplets on the wall to affect the friction significantly. It is essential to know whether condensate forms or not, and dew point specification is frequently part of gas sales contracts. If a small amount of condensate is present, one may get away with simply modifying the friction factor while keeping a single phase model and still get reasonably accurate simulation results. If the amount of condensate gets larger, computations based on single-phase models can no longer do the job. In some cases it is clear from the start that the flow can only be modeled sensibly with multi-phase software. That is the situation when we want to simulate a well flow of oil, gas and water mixed together. Slugging, a common problem, is very much a multi-phase phenomenon, and flow models may be used to investigate how high the gas velocity needs to be to avoid it. Defining such operational limits, the *flow envelope*, calls for multi-phase simulations.

1.5.2 Steady-state versus transient simulations

Some commercially available software packages are steady-state, meaning they can only tell how the pressure, flow, and in some cases temperature, is going to be distributed along the pipe(s) once some sort of equilibrium state has been established. They cannot tell us how conditions are on the way to that equilibrium. We see that already in the definition of a steady-state simulator some of its limitations become apparent: It cannot describe transient phenomena like line packing or pressure surges, nor can it produce a meaningful result if the system itself is unstable and therefore never converges towards a steady state. A fully transient simulator, on the other hand, computes all intermediary steps on the way to the new steady-state when such a state exists. That means transient simulations produce more information, but at the cost of using more CPU-time.

A steady-state simulation program cannot describe transient phenomena like line packing or pressure surges. Nor can it produce a meaningful result if the system itself is unstable and therefore never converges towards a steady state.

Transient programs need some steady-state solver integrated, either in the form of separate steady-state program or by mathematically solving the transient equations for

 For non-commercial use only

the time derivative being zero. Many of the transient phenomena of interest are simulated using a steady-state situation as a starting point, so transient simulations may rely on steady-state computations in order to define the initial condition on which the transient simulations should be based.

1.5.3 The flow simulation software's different parts

Figure 1.5.1 illustrates some of the main parts a simulation program may include. A commercial program package have several separate parts, it may require several licenses and may also rely on many software and hardware interfaces. Even the simplest possible simulation program must at least provide a way to give input data, typically via a *Graphical User Interface (GUI)*. It must know the chemical/physical properties of the fluid(s) involved *(PVT-data)*, and it must contain a computation module. It needs a way to communicate results, for instance via the GUI or via an *Application Programming Interface (API)* with another program.

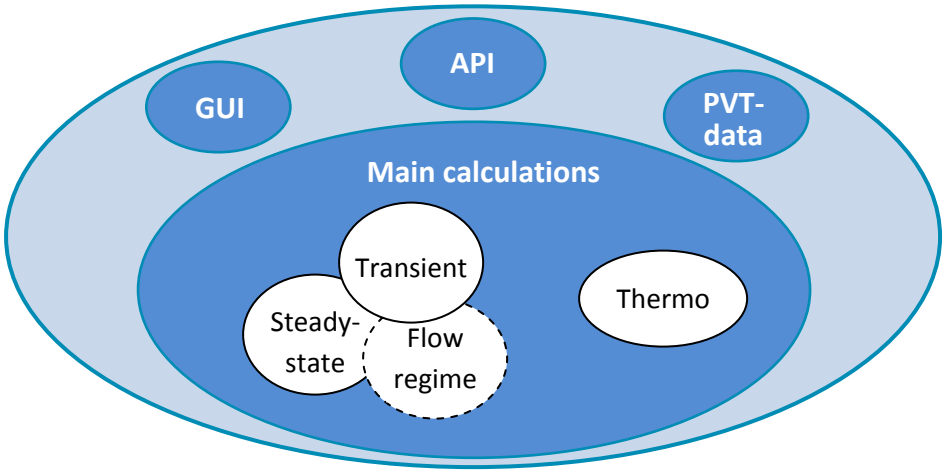


Figure 1.5.1. Typical flow simulation software structure (simplified).

Simulating a straight pipe containing water can be done with a program containing less than *10 lines* of code. Adding all whistles and bells necessary to make the program flexible and user friendly, those *10 lines* grow to many thousands. When well structured, the program parts do not all have to come from the same developer. Therefore, the different modules need convenient, preferably standard ways to talk to each other, and also to talk to the outside world. Lots of effort goes into making

different program modules integrate well on *Internet Protocol (TCP/IP)*, various *Microsoft's technologies* (*DCOM* and later *.NET*) and *industry standards* (*CAPE-OPEN, 2003, and OPC.*)

Note that the way programs are structured and which main modules they contain are the same whether the program computes single- or multi-phase flow, steady-state or transient. For instance, Simsci-Esscor's PipePhase contains one module for multi-phase steady-state simulations, and it integrates with TACITE for multi-phase transient simulations. The user interface is not much affected by the TACITE integration (but the price is!). Similarly, the same computation modules, say OLGA, can be used with many different simulation packages, even though the license typically has to be bought separately.

Computation modules vary between different programs. They generally contain fluid flow equation solvers, and they may contain one or several thermal models. For multi-phase flow, there is also some sort of flow regime identification software. That determines whether the flow is annular, bubbly, slug, or of another type. Today's multi-phase software varies somewhat in the way they determine the flow regime in each part of the pipe, but they all rely heavily on empirical data. At the same time, all multi-phase simulators are very sensitive to getting the flow regime right, even though that is one of the least accurate part of the programs.

The thermal models in use vary greatly, from the simplest isothermal models to detailed transient models of the heat flow both in the fluid, pipe wall and surroundings. The thermal model in chapter 8 discusses this in greater detail.

There is also much variation in how different programs handle PVT-data. In a water pipeline, one may get reasonable results by simply specifying the water's density, compressibility and viscosity as three constants. Those properties are in reality not constant but vary with temperature and pressure, and an improved model needs to know how those properties are related. It also makes sense to include vapor pressure data to enable the program to give warning in case of cavitation. In systems where cavitation is permitted, the program may be expected to compute exactly how the resulting 2-phase water/steam mixture behaves, and hence PVT-data needs to be available for steam as well. In addition, specific heat and surface tension must be known in order to include heat and flow regime estimation. Some fluids are much more complex than water, and several vendors have specialized in developing PVT-data packages. At the time of this writing, the most used commercially available such

 For non-commercial use only

packages seem to be the AGA Program, Gaspack™, GasVLe, Aspen HYSYS®, Multiflash, PRO/II, PVTp and PVTSim (Bratland, 2008).

Note that a simulation program must update PVT-data in all grid-points as the pressure and temperature change during computation. This means the computation module has to talk to the PVT-module continuously, and experience show that the PVT-data module easily ends up taking most of the computer's capacity. Since one of the main challenges when creating pipe flow simulation modules is to make the program fast enough, it is important for the PVT-data to be handled efficiently.

1.6 Considerations when simulating pipe flow

1.6.1 General considerations

Early phase concept studies may permit relatively inaccurate computations, in some cases favoring steady-state software over more detailed transient simulations. Note, though, that using the same software through as many phases as possible reduces the need to familiarize with many different interfaces, and depending on how the model is built up, it can also save work. The model should generally be built in several steps, starting by simulating a simplified system. It is best to neglect all nonessential components during the first runs, and get a feel for how the system is performing. Using automated routines for feeding all component data from CAD-drawings into the simulation model, as some software vendors seem to suggest, rarely makes sense, particularly not in an early phase. Components should rather be added gradually while running increasingly sophisticated simulations. Deciding which details to include and where to simplify is an important part of model building, and it happens to be a kind of task humans tend to be better at than computers.

The PVT-data module easily ends up taking most of the computer's capacity.

1.6.2 Hydrates and wax

Hydrates are ice-like structures which form when water and natural gas are in contact at high pressure and low temperature. Paraffins in crude oil or condensate can lead to wax deposits if the temperature drops to the wax appearance point. Both these phenomena depend on pressure, temperature, chemical properties, and fluid velocity. Although recent progress has been made in cold hydrate pipe flow technology, avoiding hydrates and wax for the most part comes down to keeping the flow relatively

hot and/or injecting inhibitors like methanol or glycol. Multi-phase simulations may be used to study how to avoid problems with hydrates and wax, and to some extent how to deal with them if they occur. Since avoiding problems with depositions can be expensive, it pays to use as good flow and thermal models as possible for such studies.

1.6.3 Leak detection

Using simulation-based leak detection systems is also becoming increasingly popular, and some companies' market software modules for that specific purpose. Two different detection principles are currently in use: Neural network-based decision making and calculations bases on flow models. Implementing a leak detection system involves studies of how accurately various sorts of leaks can be detected by the chosen method when fed by signals from available sensors. The required leak detection accuracy has an impact on the system's complexity and costs. Deciding which accuracy to target is a significant part of deciding what to install. Note also that the implementation phase has not always been completely successful in previous leak detection projects. It is crucial to bring all the concerned parties on board early in system planning, design and testing, and also while developing appropriate operational procedures.

1.6.4 Other features

Simulation tools may also be used for operator training and various system testing. Such software is used for operations as varied as pigging, erosion control, corrosion control, sand buildup studies, and nearly any other phenomena related to fluid flow. Again, deciding to which extent those are central issues is something to consider before deciding which details the software needs to take into account in order to satisfy ones requirements.

1.7 Commercially available simulation software

1.7.1 Single-phase pipe flow software

A simple internet search using terms like *flow assurance* or *pipeline simulation software* produces hundreds of thousands of hits. Not all of the hits are unique, and not all have to do with pipeline simulation programs, but it is still easy to see that there are lots of alternatives available. The vast majority of those programs can only simulate single-phase flow. Prices range from 0 (free!) to thousands of dollars. Given that enormous diversity no attempt has been made to give an extensive overview of the different

 For non-commercial use only

Name	Contact	Comments
Stoner Pipeline Simulator	Advantica www.advanticastoner.com	Large simulation package with many modules and support offices around the world. Relies on built-in PVT-data.
Flowmaster	Flowmaster Ltd flowmaster.com	Integrates with Matlab. Both liquid and gas. Also thermo modules. Does not focus on systems where relatively complex PVT-data are required.
Atmos Pipeline Software	Atmos atmosi.com	Involved in all sorts of singe-phase pipeline computations. Offices or representatives in 28 countries.
GASWorkS	Bradley B. Bean b3pe.com	One of the many cheap of-the-shelf steady-state gas networks simulators. Developed by a competent, but very small company.
FluidFlow3	Flite Software fluidflowinfo.com	Both gas and liquid simulations. Comes with 850 pre-defined fluids in its database. Can also handle Non-Newtonian fluids.
AFT Pipeline	Applied Flow Technology aft.com	Well designed, modularized steady-state and transient software. Has separate module for PVT-data.
PipelineStudio	Energy Solutions www.energy-solutions.com	Extensive collection of software modules for design, analysis, optimizing and forecasting oil and gas networks.
FlowDesk	Gregg Engineering greggengineering.com	Gas pipeline simulator. Focuses a lot on scheduling and forecasting.
SIMONE	Liwacom liwacom.de	Simulation and optimization of natural gas pipeline systems.
H2OCalc	MWH Soft mwhsoft.com	Specialize in various types of water pipeline computations.

Table 1.7.1. Single-phase pipe flow simulation software

software in this category, and table 1.7.1 should in no way be considered complete. Instead, it intends to illustrate that different software serves different market niches, even though they are mainly built on the same well-known theory. The most important thing to do when considering software in this category may be specifying one's requirements properly, contacting a vendor, and discussing how those requirements can be met.

1.7.2 Steady-state multi-phase simulation programs

The steady-state programs are generally relatively easy to use, and they are probably used more than the transient programs. Nearly all multi-phase simulators focus on some sort of transient capabilities, such as their ability to integrate with a third-party transient simulator. That is a strong indication that the developers recognize a trend towards transient simulations.

1.7.3 Transient simulation software

OLGA is today probably the most well documented and advanced multi-phase transient pipe flow simulator on the market, but there are also others, see table 1.7.3.

Additional multi-phase transient software packages are under development, and some of the existing ones are being improved. Interestingly, some of the oil companies sponsor several of the development projects at the same time (Bratland, 2008).

1.8 An example of what advanced pipe flow simulations can achieve

Ormen Lange is at the time of this writing (2008) the largest natural gas field under development in the Norwegian continental shelf. The field is situated *120 km* northwest of Kristiansund, where seabed depths vary between *800* and *1,100 meters*. The reservoir is approximately *40 km* long and *8 km* wide, and lies about *3,000 meters* below sea level. The Gas production is planned to become $60 \cdot 10^6$ m^3/day once full capacity is reached.

Using offshore separation of gas and liquids produced from the reservoir would have been a relatively conventional, but also expensive way to develop the project. It was concluded that offshore separation could be avoided and that the produced multi-phase flow could be sent to shore through pipelines directly. For this to be feasible, an advanced flow assurance solution was required.

Using multiphase flow to send produced gas, oil and water to shore directly can be much cheaper than offshore separation.

 For non-commercial use only

Name	Contact	Comments
HYSYS Pipe Segment	AspenTech aspentech.com	Not a very extensive model. AspenTech recommends other software for more advanced export pipelines, gathering systems or riser analysis.
HYSYS PIPESYS	AspenTech aspentech.com	Licensed separately from the Hysys Process simulation package. More advanced than Hysys Pipe Segment and used for pipeline design and analysis.
PIPESIM	Schlumberger www.slb.com	One of the most well known and most used simulation packages for multi-phase pipe flow. Developed to integrate nicely with the well simulator Eclispe. Both 2- and 3-phase.
GAP	Petroleum Experts petex.com	Part of the Integrated Production Modelling Package, which also includes various well simulation software. Both 2 and 3-phase.
PROFES	Aspen Tech aspentech.com	Dynamic multi-phase models that can be implemented within the Aspen HYSYS environment. Both 2 and 3-phase. When the Profes Transient module is included, it can also perform transient analysis.
PIPEPHASE	Simsci-Esscor (Now owned by Invensys) www.simsci-esscor.com	Developed for simulation of complex networks of pipelines and wells. Both 2 and 3-phase. Can be licensed with the TACITE transient module as an integrated part.
PIPEFLO	Neotechnology Consultants Ltd. neotec.com	One of the veteran steady-state multi-phase simulators. Comes with 2-phase capabilities.
TUFFP Pro	University of Tulsa www.tuffp.utulsa.edu	This software is integrated into PIPEPHASE and PIPESIM, but also used separately. Both 2- and 3-phase.
DPDL	University of Tulsa www.tuffp.utulsa.edu	Two-phase liquid-gas isothermal flow. Very cheap, comes with Shoham's book (Shoham, 2006). Well documented in the book.

Table 1.7.2. Multi-phase steady-state pipe flow simulation software.

An integrated flow assurance system based on the OLGA multi-phase simulator has now been installed and is in daily use. As described by Aarvik et al., (2007), it includes five sub-systems: The Pipeline Management System, the Virtual Flow Meter System, the Production Choke Control System, the Monoethyleneglycol (MEG) Injection Monitoring and Control System, and the Formation Water Monitoring System. The underlying models start at the reservoir influx zone, and include detailed representations for the subsea wells and templates, production pipelines and on-shore slug catchers. The operator is given access to liquid monitoring data throughout the system and receives recommendations on such vital parameters as choke set points and MEG injection rates. Another important feature is that the system serves as redundancy for the multi-phase flow meters. If and when the wet gas meters fail, useful flow data for each well is still going to be available from the estimates produced by the Virtual Flow Meter System.

The flow assurance system can run in four different execution modes: Real Time System Mode, Look-ahead Execution Mode, Trial Execution Mode, and Planning Execution Mode. This flexibility gives operators and planners a wide range of ways to improve their procedures and investigate 'what if'-scenarios.



Figure 1.8.1. Overview of Ormen Lange subsea production system. © Norsk Hydro.

 For non-commercial use only

Name	Contact	Comments
OLGA	SPT Group www.sptgroup.com	Currently the most used and also probably most well documented transient pipe flow simulation software. Handles both 2 and 3 phase flow. Integrates with the most used well and process simulators, in addition to most of the steady-state multi-phase pipe flow simulators.
TACITE	Simsci-Esscor www.simsci-esscor.com	Developed by Institut Francais du Petrole (IFP), but marketed by Simsci-Esscor as part of its PIPEPHASE package. Does not seem to have an open, documented API, and so can only be used together with PIPEPHASES's Graphical User Interface. The current version does not have full network capabilities. Both 2 and 3 phase.
SimSuite Pipeline	Telvent telvent.com	2-phase simulator originating in the nuclear industry, but used for both water/steam and oil/gas the last 10 years or so. It comes integrated with a steady-state simulator.
ProFES Transient	Aspen Tech aspentech.com	Developed by AEA Technology in the UK, it was formerly known as PLAC, (based on TRAC, developed for the nuclear industry), later integrated into AspenTech's ProFES simulation package to bring transient capabilities to its steady-state module. Development has been discontinued; the software is no longer marketed.
Aspen Traflow	Aspen Tech aspentech.com	Originally developed for Shell but also used in other projects. No longer developed or marketed.

Table 1.7.3. Multi-phase transient pipe flow simulation software

After the gas has been processed onshore in Norway, it is exported to Britain through a *1,200 km* subsea pipeline, the world's longest of its kind. Simulations have been used extensively in every stage of that pipeline project, too, both for selecting main pipeline parameters well as for all the other purposes mentioned in figure 1.4.1.

References

Frankel, M. (1996, 2002): *Facility Piping Systems Handbook.* Second Edition, McGraw-Hill.

CO-LaN Consortium (2003): *Documents 1.0 Documentation Set* (freely available from colan.org).

OPC Foundation: *Standards for open connectivity in industrial automation.* (available from opcfoundation.org).

Ellul, I.R., Saether, G., Shippen, M.E. Goodreau, M.J. (2004): *The Modelling of Multi-phase Systems under Steady-State and Transient Conditions – A Tutorial.* Pipeline Simulation Interest Group PSIG 0403.

Liu, H. (2005): *Pipeline Engineering.* Lewis Publishers.

Shoham, O. (2006): *Mechanistic Modeling of Gas-Liquid Two-Phase Flow in Pipes.* Society of Petroleum Engineers.

Bryn, P., Jasinski, J.W, Soreide, F. (2007): *Ormen Lange – Pipelines and Shipwrecks.* Universitetsforlaget.

Aarvik, A., Olsen, I., Vannes, K., Havre, K., Kroght, E., C. (2007): *Design and development of the Ormen Lange flow assurance simulator, 13th International Conference on Multi-phase Production technology*. p.47-64.

Bratland, O. (2008): *Update on commercially available flow assurance software tools: What they can and cannot do and how reliable they are.* 4th Asian Pipeline Conference & Exposition 2008, Kuala Lumpur.

 For non-commercial use only

"Observe the motion of the surface of the water, which resembles that of hair, which has two motions, of which one is caused by the weight of the hair, the other by the direction of the curls; thus the water has eddying motions, one part of which is due to the eddying currents, the other to the random and reverse motion."
Leonardo da Vinci on turbulence 1490 AD

2 Pipe friction

This chapter outlines how to calculate friction in straight pipes:

- The many known ways to define the friction factor
- Nikuradse's and Moody's traditional friction factor diagrams
- How surfaces affect friction
- Surface roughness values for some typical surfaces
- Recent improvements based on measurements and turbulence theory
- Friction factor accuracies
- Putting it all together

2.1 Basic theory

2.1.1 Introduction

When fluid flows through a pipe, friction between the pipe wall and the fluid tries to slow down the fluid. Unless we get assistance from gravity or naturally occurring pressure, we generally have to install pumps or compressors to counter the friction. As one would expect, many researchers have investigated it and come up with practical ways to describe it. It turns out that even for single-phase flow, pipe friction is a complex phenomenon and questionable friction calculations are surprisingly common. In addition to nature-given difficulties, there are also some historical reasons for the

current confusion: The theory has evolved gradually over the years, though some outdated definitions and methods have survived and remain in use today. Even though pipe friction is very similar for gas pipelines, oil pipelines, blood vessels and even open channels, different calculation methods are currently in use for different types of pipes or fluids. That practice tends to complicate matters and is strongly discouraged in this book.

Pipe friction is quite a complex phenomenon and questionable friction calculations are surprisingly common.

Loosely stated, pipe flow can be either laminar or turbulent, and the physics involved changes significantly when we go from one to the other. Closer inspection reveals that no such thing as a completely turbulent flow exists, there is always a laminar sub-layer closest to the wall. A pipe's surface properties become more important the more turbulent the flow gets. The traditional way of taking this into account has been by compressing the whole surface description into something called an *equivalent sand grain roughness*. This approach has the advantage of being very simple, but we will soon see that it can lead to inaccurate results.

Another important thing to remember is that most of the well established methods for calculating pipe friction were only ever intended for steady-state flow. In transient flow, our steady-state friction theory is, strictly speaking, invalid. We therefore need to establish an understanding for which conditions we can expect the results to be acceptable under.

Since friction is a very important parameter in determining a pipeline's capacity, we are going to dedicate much effort to this subject, discussing the most common calculation methods and proposing some best practices. We are also going to show which accuracies we can expect for different sorts of calculations.

For those less concerned with exactly how the theory is developed, it may not be necessary to study all of chapter 2 in-depth. Instead, the resulting diagrams in figures 2.9.1-2.9.3, as well as chapters 2.11-2.16 should be of most interest.

2.1.2 Laminar flow

For steady-state single-phase flow, the Reynolds number *Re* can be used to determine whether the flow is fully laminar. Alternative definitions of *Re* are given in equations

 For non-commercial use only

2.1.8, 2.1.10, 2.2.5 and 3.1.1. At very low *Re*, typically below *2,300*, it has been found that the flow tends to be fully laminar. For so-called Newtonian fluids, which include water, air, and most of the other fluids engineers have to deal with, Newton's law of viscosity (sometimes referred to as Stoke's law for laminar flow) states:

$$\tau = \mu \frac{\partial v}{\partial y} \tag{2.1.1}$$

Where τ *[N/m²]* is the sheer stress and v *[m/s]* is the velocity at distance y *[m]* from the wall. μ *[kg/(ms)]* is the fluid's dynamic viscosity.

In a circular pipe, y is the distance from the pipe wall, and therefore $y = d/2 - r$, where d is pipe's inner diameter and r is radius from pipe center to the studied point.

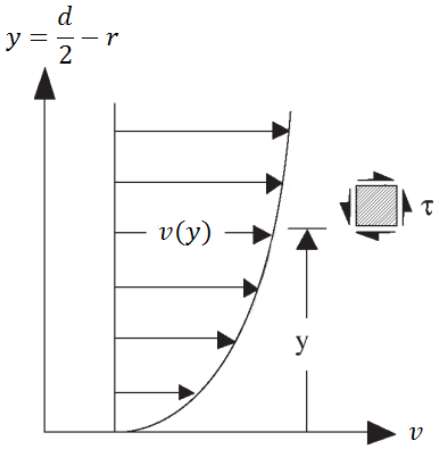


Figure 2.1.1. Velocity profile. The velocity is zero at the wall and increases towards the center.

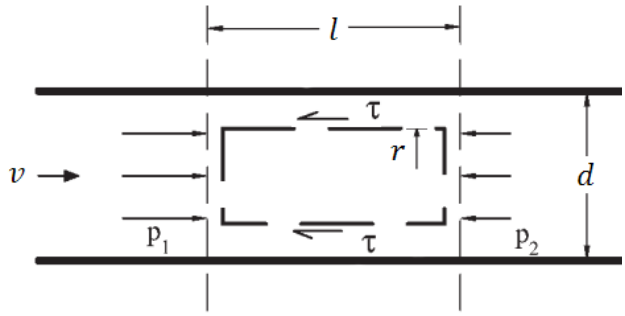


Figure 2.1.2. Shear forces on cylindrical fluid element.

During steady-state conditions, the friction shear force on any cylindrical fluid section of length l and radius r has to be balanced by an equal force due to the pressure difference $\Delta p = p_1 - p_2$ working on that cylinder's end sections:

$$shear\ force = pressure\ force$$

$$\tau \cdot 2\pi r \cdot l = \Delta p \cdot \pi r^2 \tag{2.1.2}$$

This leads to:

$$\tau = \frac{\Delta p r}{2l} \tag{2.1.3}$$

By integrating equation 2.1.1 and inserting equation 2.1.3, it can easily be shown that:

$$\Delta p = \frac{32\mu l}{d^2} v \tag{2.1.4}$$

In other words, as long as Newton's law of viscosity, equation 2.1.1, is valid, the correlation between pressure loss, Δp, and average fluid velocity, v, has to be as shown in equation 2.1.4. No empirical data was necessary to develop this correlation, so we can claim to fully understand the mechanisms at work here. In addition, the result shows that the correlation is linear, the easiest sort of equation to deal with. Less intuitively, the surface roughness is not involved in the equation, meaning a rough and a smooth surface would experience the same friction. The problem is that equation 2.1.4 is only valid for laminar flow, and most pipe flow situations of practical interest are unfortunately not laminar.

2.1.3 Turbulent flow

In turbulent flow, the viscous forces described by equation 2.1.4 also play a part, but they are no longer alone in creating friction. Turbulence means the particles move both axially and radially, so they also interact by mixing with each other. What consequences can we expect this to have for the friction? As explained by Taylor et Al, (2005), Von Karman came very close to the answer by applying some simple logic. Let us have a closer look at his reasoning.

When fluid flows in a pipe, friction creates forces between particles moving at different velocities when coming into contact with each other. The closer a particle comes to the wall, the more it tends to slow down to zero velocity. Particles in direct contact with the

 For non-commercial use only

wall are stopped completely, and the closer to the center of the pipe they get, the higher the average velocity.

In his thought experiment, Von Karman considered a particle, or a small group of particles, moving axially relatively close to the pipe wall. If the particles gradually drift towards the center of the pipe, they come into an area where the average velocity tends to be higher. For simplicity, let us assume that they collide with another similar group with a higher velocity. After the collision, both groups would end up with a velocity close to the average of their initial velocities. The velocity change for each group has to be proportional to the velocity difference.

More generally, the tendency for groups of particles to change velocity when they drift radially has to be proportional to the radial velocity gradient $\partial v/\partial y$. At first glance, we may think this would lead to a linear relationship between pressure loss and average velocity, and we would have a similar situation as for laminar flow. But the imaginary collision of the two particle groups has a secondary effect: It does in itself create additional collisions. As the two groups collide, the fluid tries to escape radially, and that increases the radial transport of momentum. This is a bit as if two drops of water of different speed collide with each other: The drops would flatten somewhat, and water would be squeezed out on the sides. In a pipe, something similar would happen if the two groups' velocity difference was negative: Fluid would fill the void by flowing in radially from neighboring areas. The total effect of increasing the average velocity, and therefore the average radial velocity gradient in a pipe, is that the *both* the average radial mass exchange *and* the amount of momentum being transported radially per unit mass is nearly proportional to the average velocity in the pipe. These two proportional effects multiply, and Von Karman concluded that we can expect the pressure drop in turbulent flow to be more or less proportional to the square of the average fluid velocity across any cross section.

The same logic also leads us to believe that the pressure loss has to be proportional to the fluid's density, since the amount of mass and therefore momentum exchange pr. volume unit of fluid flowing radially is proportional to density.

Further, the momentum balance needs to satisfy equation 2.1.2 and therefore 2.1.3 whether the flow is laminar or turbulent, and so the pressure loss needs to be proportional to the length of the pipe.

If we compare two pipes with different diameters but same average fluid velocity, and we assume the pipe's velocity profiles have identical or at least very similar shape, we realize that average $\partial v/\partial y$ has to be inverse proportional to the pipe diameter d.

This is going to be more elaborated later, but for now, we may summarize this purely hypothetical logic in the form of a simple equation:

$$\Delta p = Some\ constant\ \cdot v^2 \cdot \rho \cdot l \cdot \frac{1}{d} \tag{2.1.5}$$

It is common to re-formulate this somewhat to define what has become known as the Darcy-Weisbach friction factor *f*:

$$f \stackrel{\text{def}}{=} \frac{\Delta p}{\rho \frac{l}{d} \frac{v^2}{2}} \tag{2.1.6}$$

Note that Von Karman's theory also implies that there is no such thing as a constant velocity anywhere inside the pipe, even in situations when the average velocity across a cross section is fairly constant. The turbulence is going to result in continual velocity changes both in space and time. When we still use the term *steady-state* throughout this book, we refer to a situation where the mass flow through each cross section is constant. The velocity v is then defined as the average velocity in a cross section – a theoretical term which does not necessarily equal any particle's velocity in that cross-section at a given time.

Close to the pipe wall, the turbulence-driven radial velocity components are restricted since the fluid cannot pass through the wall. The closer we get, the less freedom the turbulent eddies have, and this is why we always have a laminar sub-layer closest to the wall. We will later see that the layer is very thin for high Reynolds numbers.

Equation 2.1.6 is valid for turbulent flow, but we can use it for laminar flow, too, even though the friction is proportional to the velocity rather than to the square of it for laminar flow. We simply adapt the laminar friction equation 2.1.4 by setting:

 For non-commercial use only

$$f = \frac{64}{Re} \tag{2.1.7}$$

for laminar flow. If we insert equation 2.1.7 into equation 2.1.6, we will see that it leads us back to equation 2.1.4.

For turbulent flow, f is not completely constant for any Re, and we will go into great detail on just how to determine accurate values for it in the following chapters. Note that the definition of Reynolds number used here is based on the pipe diameter, so that:

$$Re = \frac{vd}{\nu} \tag{2.1.8}$$

Where ν is kinematic viscosity. Dynamic viscosity μ is defined as:

$$\mu \stackrel{\text{def}}{=} \nu\rho \tag{2.1.9}$$

Therefore, equation 2.1.8 can alternatively have this form:

$$Re = \frac{vd\rho}{\mu} \tag{2.1.10}$$

2.2 Simple friction considerations

If we know the friction factor, *f*, the pressure drop due to friction in any straight pipe carrying an incompressible fluid can be calculated using the Darcy-Weisbach friction factor as defined by equation 2.1.6. Liquids can for the purpose of friction calculation most often be considered incompressible, and it follows directly from the definition of the friction factor that:

$$\Delta p = f \cdot \rho \frac{l}{d} \frac{v^2}{2} \tag{2.2.1}$$

We may choose to describe the average velocity v in terms of mass flow m and cross-sectional area $\pi d^2/4$ as:

$$\dot{m} = \rho \frac{\pi d^2}{4} v \tag{2.2.2}$$

Inserting that into equation 2.2.1 yields the following alternative expression for a liquid-carrying pipeline's capacity:

$$\dot{m} = \frac{\pi}{4} \sqrt{\left(\frac{2 d^5 \rho}{f l} \Delta p \right)} \tag{2.2.3}$$

Note that no pipe inclination has been considered, and the kinetic energy-term in the Bernoulli-equation has also been neglected. Still, equation 2.2.3 typically agrees well with observations relatively long horizontal pipes. The important question in single-phase pipeline capacity calculations, however, is how accurately we are able to determine *f*.

For compressible flow, which in this respect means gases, the pressure loss calculations are somewhat more complicated. As long as v is much lower than the speed of sound, which is the situation in most gas pipelines and networks, the mechanisms involved in creating friction are the same as those for incompressible fluids. The difference is that

 For non-commercial use only

the average velocity changes as the gas expands. In horizontal pipes, that means the velocity increases as the fluid moves towards the outlet. A more detailed development of how this affects the friction is shown in chapter 6.4.2. For now, let us accept that for isothermal flow in horizontal pipes, the mass flow for a gas can be estimated as:

$$\dot{m} = \frac{\pi}{4}\sqrt{\frac{d^5}{f\,l}\frac{M_g}{\bar{Z}RT}(p_1^2 - p_2^2)} \tag{2.2.4}$$

Where p_1 and p_2 *[Pa]* is inlet and outlet pressures, M_g *[kg/mole]* is gas mole weight, $\bar{Z}$ is dimensionless compressibility factor due to the gas not being a perfect gas (averaged, since it is not completely constant when the pressure varies), R *[J/(kg·mole)]* is the universal gas constant, and T *[K]* is absolute temperature. Details about how the density is modeled in this equation can be found in the AGA-8 report, see Starling (1992).

Note also that the Reynolds number can conveniently be described by mass flow rather than velocity. By combing equations 2.1.10 and 2.2.2, we get:

$$Re = \frac{4\dot{m}}{\pi d} \tag{2.2.5}$$

For more accurate results, it may be necessary to account for pipe inclination, for the flow not being completely isothermal, as well as additional sources of friction, such as welds, bends, and valves. We will later develop a general model for both steady-state and transient pipe flow that can be used for more accurate calculations, but equation 2.2.4 may serve well as a simple first approximation.

Now let us have a close look at how to determine f for turbulent flow. As mentioned in chapter 2.2.1, there are historical reasons for the current lack of standardization when it comes to determining or even defining f. The following chapters describe some of that history in order to explain which methods to use and which to discard.

2.3 Nikuradse's friction factor measurements



Johann Nikuradse, 1900-1980.

Nikuradse (1933) was one of the most influential researchers in the field of pipe friction. He carried out a lot of measurements on relatively small pipes and plotted the friction factors as a function of two dimensionless groups: The Reynolds number and the relative surface roughness. He created his roughness by gluing sand of one particular grain size, k_s, to the inside of each test pipe. He kept k_s/d constant and varied Re up to $3.4 \cdot 10^6$. He repeated that for different relative roughness values by using other grain sizes and diameters.

Some of Nikuradse's results can be seen in figure 2.3.2, where he varied k_s/d from 0.00099 to 0.0333. The curves contain a lot of information and have been used as a basis for many researches since they were published.

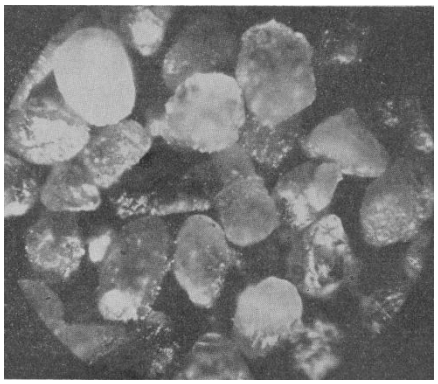


Figure 2.3.1. Photo of one of the surfaces Nikuradse created, in this case for grain size 0.5 mm.

To be able to vary Re as many orders of magnitude as he did, Nikuradse had to increase the diameter of his pipes as he increased Re, but he also increased the sand grain size so that the relation between them was kept constant for each curve. We see that the friction factor f is in fact relatively constant for a given relative roughness k_s/d, and no discontinuity is visible where both k_s and d were increased while the relation between them was kept constant. Interestingly, the Darcy-Weisbach friction factor varies very little compared to Re for each k_s/d.

The results confirm the underlying Von Karman hypothesis described in chapter 2.1.3, which presumed the pressure loss for turbulent flow to be proportional to the square of the average velocity. But the agreement is not one hundred percent: When the Reynolds number changes considerably, f changes, too, particularly for relatively low Re.

For non-commercial use only

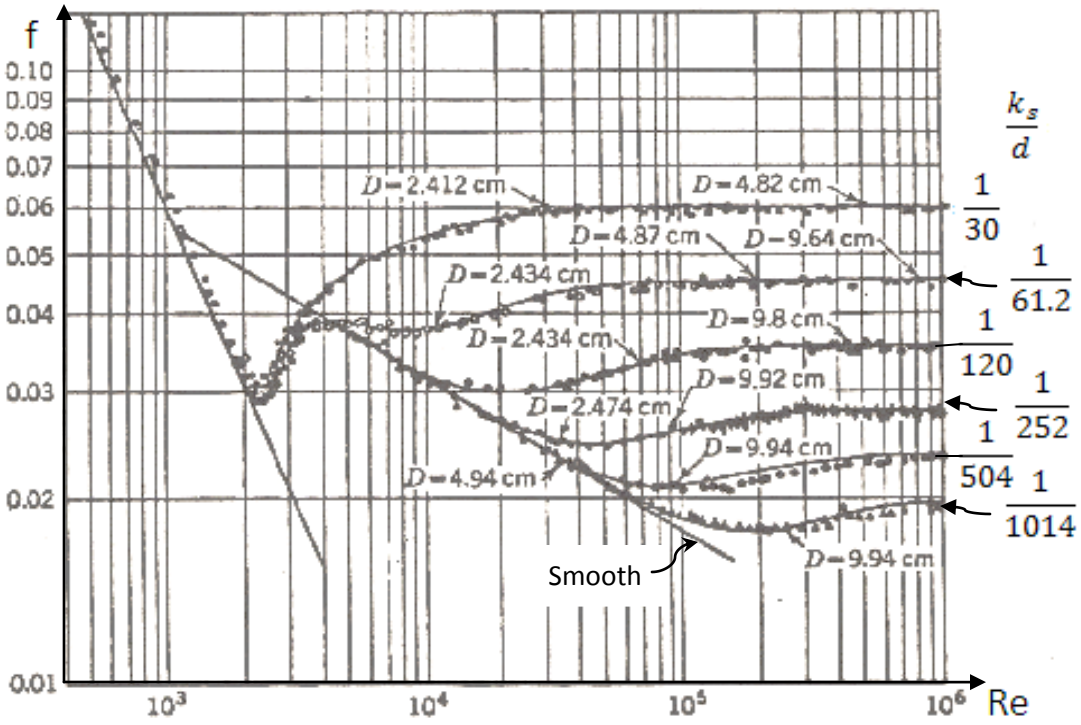


Figure 2.3.2. Results of Nikuradse's measurements.

We can make the following observations from Nikuradse's curves:

1. **High Reynolds numbers**: The friction factor depends only on the pipe's relative roughness, and *Re* does not affect the friction factor. This part of the diagram is somewhat confusingly often referred to as *fully turbulent flow*.
2. **Intermediate Reynolds numbers:** In the area between laminar and fully turbulent flow, the friction factor depends both on k_s/d and *Re*.
3. **Low Reynolds numbers:** The theoretically developed correlation for laminar flow, equation 2.1.7, is confirmed by Nikuradse's measurements. The curves also show very clearly that something happens around *Re* = *2,300*, and this is taken as evidence that the flow no longer is fully laminar for *Re* higher than this value.

Note that there are no discontinuities in the curves around *Re* = *2,300* and transition to turbulence is relatively smooth. The traditional Moody-diagram, a tool frequently used to determine *f*, violates Nikuradse's results in this respect. Transition to turbulence can probably best be explained by Kolmogorov's (1941) turbulence theory, as outlined in chapter 2.8, and we are going to modify the Moody diagram accordingly.

A much less recognized phenomenon can also be read out of the figure: For each curve except for the one with highest k_s/d, there is a minimum friction factor at one particular Reynolds number. The minima can be seen to occur for different Reynolds numbers depending on the particular pipe's roughness. This is also something the traditional Moody diagram ignores.

Nikuradse did his friction measurements on pipes with sand grains glued to their inner surface. His pipes were very different from industrial pipes, and researchers have struggeled with how to tranfer his results to practical situations ever since.

Our understanding of surface roughness and the tools to measure it is something that has come a long way since Nikuradse did his measurements, and it is now possible to understand more of how different surfaces interact with the flow.

2.4 What surfaces look like

As shown by Thomas (1982), there are many different ways to measure surface roughness. In an ideal world we would expect a surface's roughness definition and corresponding measurements to capture all surface geometry in three dimensions. In the real world, however, nobody has come close to producing anything of the kind. It is not hard to see why: Any surface – just think of the earth's surface as an example – contains a nearly infinite amount of details, and even the most thorough description of it has to rely on simplifications. So, how do we best simplify?

One of the most common ways to describe surface roughness is based on measuring the highest imperfections sticking out from it (peaks) and the lowest depressions (walleyes), and doing some statistical analysis of those measurements to compress the results into a compact form. It is also possible to measure all different heights encountered on a sample, and to investigate how they are distributed. It turns out that some surfaces show a near Gaussian (normal) height distribution. This method of describing a surface has obvious limitations, given that even two simplified surfaces like the ones shown in figure 2.4.1. may have similar distribution profiles even when the surfaces are very different. We have no guarantee that these two surfaces would lead to the same hydraulic friction.

 For non-commercial use only



Figure 2.4.1. Two different surfaces with the same peak-to-valley distributions.

Some manufacturing operations, such as milling or honing, tend to create the second sort of surface, where anything sticking out is more or less flattened, while valleys to a larger extent survive. Pipelines are often made of rolled, flat steel pipe which is pressed into O-shape and welded together. That, too, may create something quite similar to the second sort of surface. We would intuitively expect the two surfaces to lead to different friction even if they have the same average roughness, as defined by peak-to-valley measurements. What seems to be less well known is that the shape of the friction factor curves are also affected by the surface structure. A surface cannot be analyzed adequately by simply measuring the Gaussian height distribution, and even if it could, that information could not be represented as one single equivalent sand grain roughness k_s.

It is known that paint and most coatings tend to smooth both sorts of imperfections, but may at the same time produce other irregularities. Figure 2.4.2 shows an example of a coated surface. Notice the difference in length scale between height and tracing length. Unlike Nikuradse's sand grained surface, the imperfections on the coated surface stretches much further in the direction along the surface than it does perpendicular to it. The irregularities are so elongated that difference from Nikuradse's sand grains are very significant. Such relatively flat imperfections are in fact very common for most of the surfaces we encounter. Another typical characteristic of most surfaces is that they contain irregularities of many different sizes simultaneously.

The surface in figure 2.4.3 is similar to the one in figure 2.4.2, but glass spheres have been added to the coating. This can be done to make the surface stronger, but in this case it was added to increase the roughness for the sake of studying its impact on the friction factor. By simply looking at the surface profile, we get the impression that the peak-to-valley roughness must be around $50 \cdot 10^{-6}$ *m*, perhaps somewhat higher. When Sletfjerding et al. (2001) measured the pressure loss in the pipe and compared it with Nikuradse's results (or rather, with correlations based on Nikuradse's measurements, as explained in the next chapter), they concluded that the friction was the same as it

would have been in a pipe roughened with sand grains of size $90 \cdot 10^{-6} m$. Therefore, the equivalent sand grain roughness was said to be $k_s = 90 \cdot 10^{-6} m$. This may look like a surprisingly good agreement with Nikuradse's results, given that the imperfections were much further apart in the coated pipe. But the recent theory outlined in chapter 2.8 shows that the imperfection's height rather than their width is likely to be most important, and also that large imperfections must be expected to dominate over smaller ones.

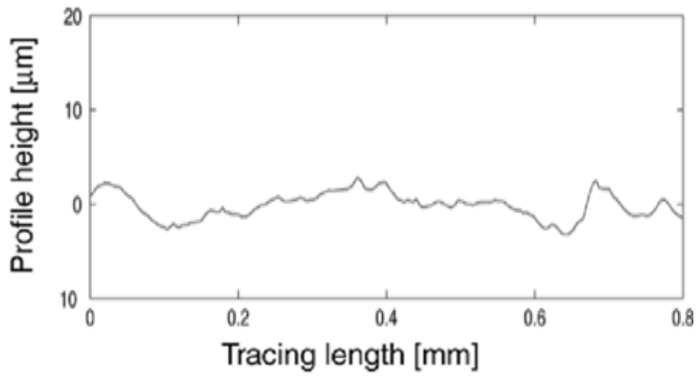


Figure 2.4.2. Measured surface profile of pipe coated with two-component epoxy coating (Sletfjerding at al., 2001).

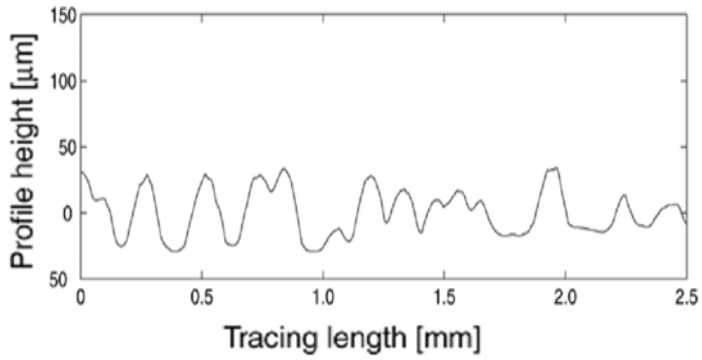


Figure 2.4.3. Measured surface profile of pipe coated with two-component glass-bead epoxy. The glass bead size was 70-90·10⁻⁶m.

Measured indirectly, from actual pressure loss: $k_s = 90 \cdot 10^{-6} m$.

Profilometer measurements showed that $R_a = 16.08 \cdot 10^{-6} m$, $R_q = 18.82 \cdot 10^{-6} m$, $R_z = 72.10 \cdot 10^{-6} m$, and $H = 1.44$. (Sletfjerding et al., 2001).

In Nikuradse's days, modern profilometers were not available, and choosing sand grains as a means to define the surfaces may have been the best way available at the time. Nowadays we can measure various sorts of surface characteristics directly. Standard instruments give readings of parameters like arithmetic mean roughness R_a, root mean square roughness R_q, mean peak-to-valley height R_z and the Hurst exponent H. Although those parameters have relatively simple definitions, for the purpose of this book it is sufficient to point out that various ways to quantify surfaces do exist.

 For non-commercial use only

Figures 2.4.4-2.4.5 shows examples of other surfaces. Again, imperfections of different sizes are present at the same time on each surface, and the scale is different along the surface and perpendicular to it.

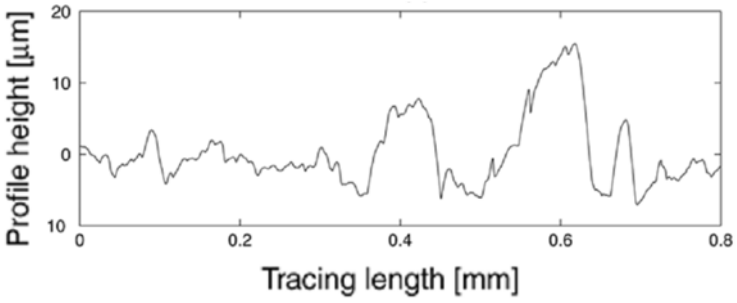


Figure 2.4.4. Honed steel pipe measured surface profile. (Sletfjerding et al., 2001)

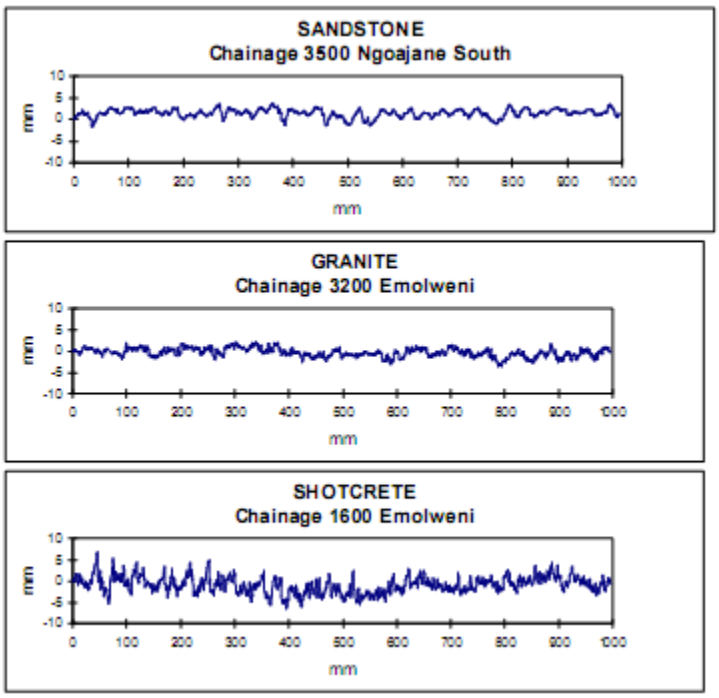


Figure 2.4.5. Measurements of different drilled rock tunnel surface profiles. (Pennington, 1998)

Another complication is caused by the fact that pipe surfaces may change over time. Corrosion, erosion, coating cracks, and various other sorts of wear and tear are common problems, and the friction factor generally tends to increase with wear. Figure 2.4.6 shows an example of a surface, part of which has a high roughness. According to Nikuradse's measurements this should lead to the friction factor curves deviating from the 'smooth pipe'-curve even at relatively low Reynolds numbers. The much lower roughness in other parts of the surface means some parts contribute to such deviation only when *Re* reaches considerably higher values.

Since the surface in effect contains a very large span of roughness values, we must expect the transition from 'smooth' to 'fully rough' friction to take part over a greater span of Reynolds numbers, and therefore to be much more gradual than for Nikuradse's single roughness experiments.

Surfaces are not only characterized by the size of their imperfections, but also by how different sorts of imperfections are distributed.

Corrosion may therefore affect both the friction factor at fully rough flow as well as the shape of the friction factor curve at lower *Re*.

As we already have seen, no real surface is uniform. It varies in some more or less random fashion, depending on the manufacturing process and wear and tear. We can therefore conclude that not only does the average roughness play a role for the friction, but so does the surface's uniformity.

High uniformity, meaning little variation in surface structure, should produce results more similar to Nikuradse's, while low uniformity can be expected to produce something more like an average of many different Nikuradse-curves.



Figure 2.4.6. Photo of corroded and later cleaned steel surface.

Ignoring the uniformity, as the traditional friction factor methods do, cannot produce accurate results for real (non-uniform) surfaces.

We will later investigate how the surface structure uniformity affect the Darcy-Weisbach friction factor curves, but let us first have a closer look at the current most common empirical correlations for *f*.

2.5 The traditional Moody diagram

Prandtl used Von Karman's theory to arrive at the following way to describe the 'smooth pipe'-line in Nikuradse's diagram (Schlichting, 1979):

 For non-commercial use only

$$\frac{1}{\sqrt{f}} = -2\log_{10}\frac{2.51}{Re\sqrt{f}} \tag{2.5.1}$$

Nikuradse (1933) himself presented a friction factor correlation valid for relatively high *Re*, a part of the diagram which sometimes confusingly has been termed 'fully turbulent flow', meaning the part where the curves are horizontal, as:

$$\frac{1}{\sqrt{f}} = -2\log_{10}\frac{k_s}{3.7d} \tag{2.5.2}$$

The most difficult part has turned out to be describing what happens between these two extremes, sometimes referred to as the 'partly turbulent' zone. Colebrook & White carried out additional experiments on commercial pipes in the late 1930s, and they presented what has since become the most widely used equation for estimating the friction factor in steady-state pipe flow (Colebrook, 1939). It is known as the Colebrook & White-correlation, and it has been constructed by summarizing the two terms on the right hand side of equations 2.5.1 and 2.5.2 while keeping the left-hand side as is:

$$\frac{1}{\sqrt{f}} = -2\,log_{10}\left(\frac{2.51}{Re\sqrt{f}} + \frac{k_s}{3.7d}\right) \tag{2.5.3}$$

In spite of this equation's popularity, we sense a problem with it immediately: It does not take the surface's uniformity into account. As concluded in the previous chapter, uniformity plays a role. That is one reason why Colebrook & White's equation is relatively inaccurate, and we will soon see it can be improved.

Another, but much less serious problem with the equation is that *f* occurs at both sides. There is no known exact analytical solution, but very simple fixed-point itereation can easily be used to find good approximations. To see how, we take the square at both sides, invert and re-formulate equation 2.5.3 to become:

$$f = \left[-2\,log_{10}\left(\frac{2.51}{Re\sqrt{f}} + \frac{k_s}{3.7d}\right)\right]^{-2} \tag{2.5.4}$$

The iteration process starts by guessing a value for f, say $f_0 = 0.02$, and inserting that into the right side of equation 2.5.4. The result, let's call it f_1, is going to be quite close to the real f. This process can be repeated several times so that:

$$f_{i+1} = \left[-2\,log_{10}\left(\frac{2.51}{Re\sqrt{f_i}} + \frac{k_s}{3.7d}\right)\right]^{-2} \tag{2.5.5}$$

For each computation, the relative iteration error may be estimated from the difference between the last and the previous result:

$$\delta_i = \frac{|f_{i+1} - f_i|}{f_{i+1}} \tag{2.5.6}$$

It rarely takes more than *6* iterations to arrive at a relative error less than 10^{-3}. Since the Colebrook & White-equation itself is at least an order of magnitude less accurate than that, there is no reason to iterate more. In fact, rather than checking the error after each iteration, one may simply iterate *5* or *6* times and thereafter accept the result.

It has been argued that solving equation 2.5.4 by iteration is relatively slow. Computation speed is only of concern when numerous computations need to be carried out, which can be an issue when we simulate fluid transients in the time domain. In such cases the next time step can use the friction factor from the previous step as a first guess. That usually brings the required number of iterations down to *1*, and iteration becomes as efficient as any explicit correlation would have been. A slightly faster but somewhat complicated convergence method for those cases when a good initial estimate is not available can be found in chapter 2.9.2.

 For non-commercial use only

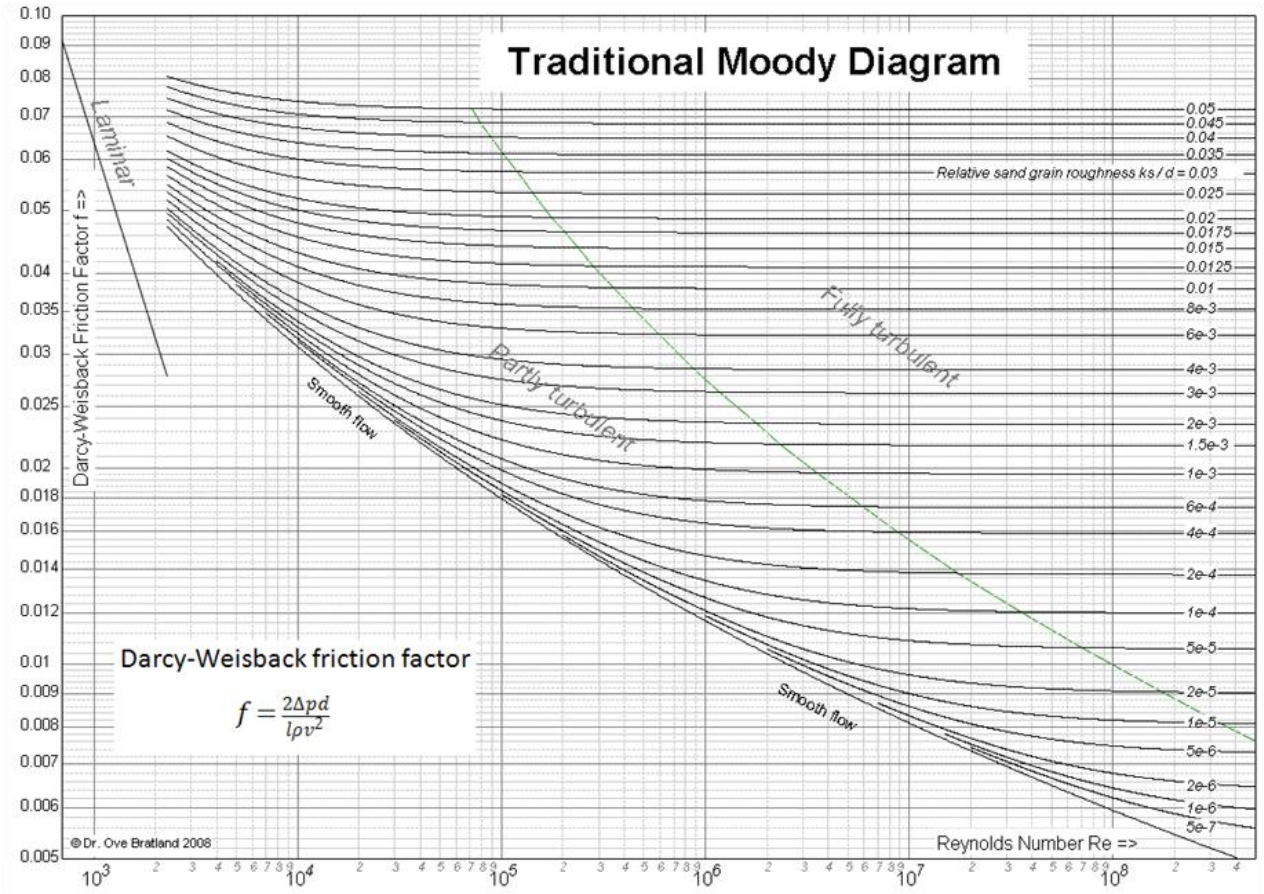


Figure 2.5.1. Traditional Moody diagram based on equations 2.1.7 (Re <= 2,300) and 2.5.3 (Re > 2,300).

Some authors have tried to establish explicit approximations of equation 2.5.3. One of the most widely used such approximation is the one proposed by Haaland (1983), equation2.5.7:

$$f = \left\{-1.8\, log_{10}\left[\frac{6.9}{Re} + \left(\frac{k_s}{3.7d}\right)^{1.11}\right]\right\}^{-2} \qquad (2.5.7)$$

Haaland's modified formula agrees with Colebrook & White's formulae to within *1.5 %* at any given point, and for most Reynolds numbers and relative roughness values, it agrees considerably better than that. That may make it somewhat faster or at least more convenient for simple hand calculations, but it has of course in all other ways inherited the weaknesses described for Colebrook & White's equation.

Rouse (1943) plotted curves based on Colebrook & White's equation in a diagram. It turned out that most engineers considered his way of plotting the curves awkward, and Moody (1944) modified it into what is shown in figure 2.5.1. The diagram now bears Moody's name, and it has been the most widely used diagram for selecting friction factors for single-phase pipe flow ever since. More knowledge is now available, however, and the time may have come to improve the traditional Moody diagram.

2.6 Extracting more from Nikuradse's measurements

The traditional explanation for why Nikuradse's measurements differ so much from the Moody diagram has always been that the Moody diagram is about commercially available pipes, while Nikuradse investigated a rather artificial sort of pipe with sand grains glued to their surface. The Moody-diagram, it is argued, is valid for typical surfaces. This shows that two assumptions are built into the Moody diagram: That such a thing as a typical surface actually exists, and that at the time when Colebrook & Whites' equation was developed, the instruments to measure surface roughness in the relevant way were available. As shown by Thomas (1982), both of these assumptions are at best questionable. One reality the differences between the two diagrams make clear, however, is that roughness does not only affect the friction factor at a particular Reynolds number, it affects the shape of the curves, too.

To get a feeling for what having several roughness sizes at the same time in one pipeline leads to, let us first consider this very simple example: Two pipes of identical length and diameter, but different roughness, are coupled in series. For a particular Re, the first pipe is going to have friction described by f_1, while the second's friction factor is f_2. The average friction factor for the two pipes together is obviously going to be $(f_1 + f_2)/2$. If the first pipe was of the Nikuradse-type and described by the *1/120*-curve and the second by the *1/1014*-curve in figure 2.3.1, the average curve would obviously lie somewhere in-between, and we realize it would have a more smoothed out minima than each individual curve.

Now suppose we had a nearly similar situation with two distinct roughness values, but instead of having them in two separate pipes, they both occur super-imposed on each other in one pipe. If they affect the flow independently, an assumption which admittedly is not completely accurate, we would end up with the same overall friction factor as for the two separate pipes described above. We can extend this theory further by combining far more different roughness values than just two. To do so, let us start by creating some simplified curve fits to Nikuradse's diagram.

 For non-commercial use only

By comparing the local minima in the partly turbulent zone of Nikuradse's measurements, figure 2.3.1, we see they become less and less prominent as the relative roughness decreases. By reading the minima carefully for all the curves and plotting them in a logarithmic diagram it can be seen that they lie in a nearly straight line described by:

$$\Delta f = 10^{(0.54773\,\mathrm{Re} - 1.1079)} \tag{2.6.1}$$

The location of the line describing where the flow becomes fully turbulent can be formulated as:

$$Re_t = 1718\left(\frac{k_s}{d}\right)^{-0.912} \tag{2.6.2}$$

We may use these results together with equations 2.5.1 and 2.5.2 for smooth and rough pipes to extrapolate Nikuradse's diagram. Figure 2.6.1 has been created that way.

The results show that for very high *Re* the partly turbulent zone becomes narrower and the friction factor is more constant than for lower *Re*. For high *Re*, the curves are in fact very similar to the diagram one may create by using AGA's recommendations, which are discussed in the next chapter. Figure 2.6.1 is based on extrapolating quite far beyond the area covered by Nikuradse's measurements, and it deals with surfaces of a kind not frequently encountered in real pipes. But it has one very distinct advantage which the classical Moody diagram does not have: It deals with only one relative roughness at a time. That gives each curve a clearer definition than those obtained by measuring on commercially available pipes, where an undefined combination of different roughness sizes exists simultaneously.

Keeping these limitations in mind, it is interesting to see how different sand grain sizes could have combined to create a friction factor curve if the grain size had a Gaussian distribution. For instance, consider a surface where the sand grain size has a *relative*

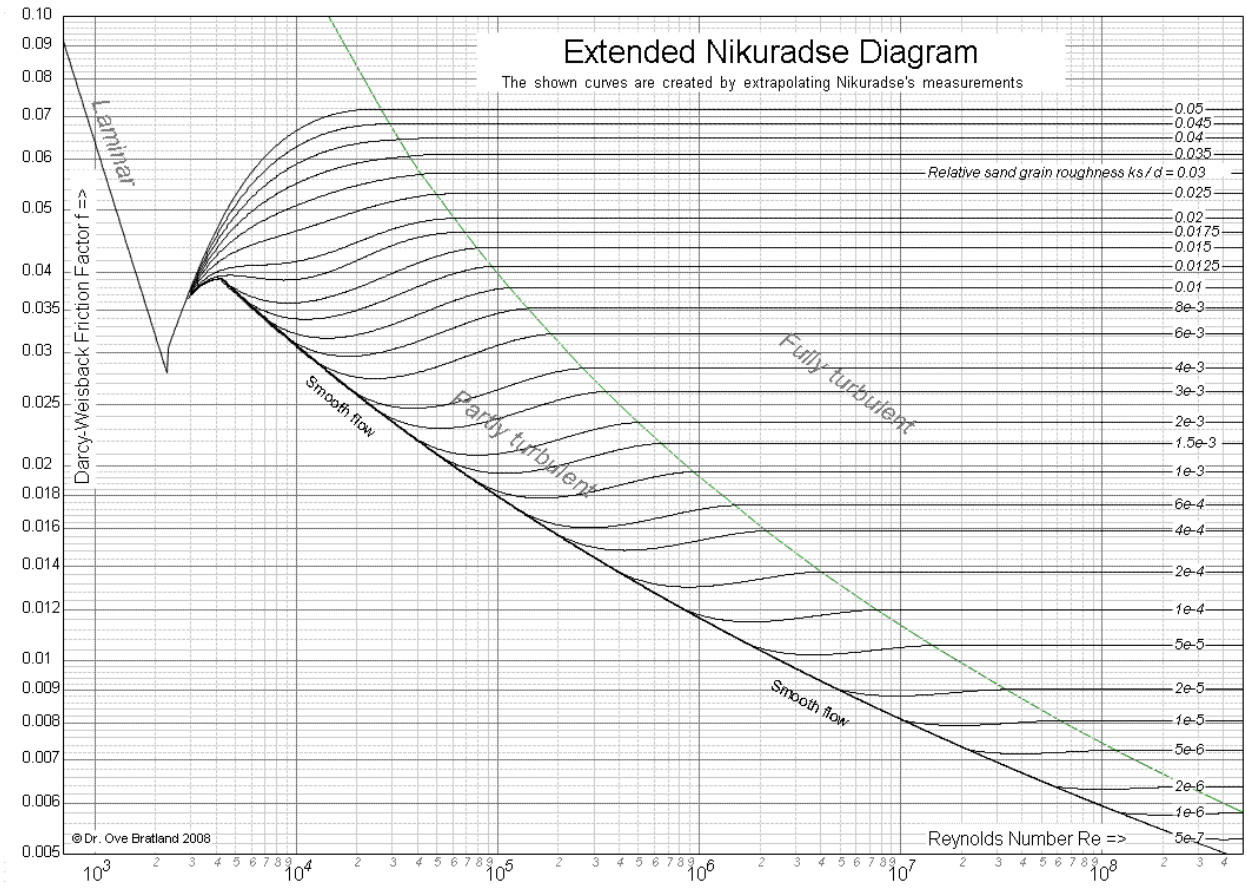


Figure 2.6.1. Extended Nikuradse diagram.

mean $\mu_s = 3 \cdot 10^{-6}$ *m and variance* $\sigma^2 = 1 \cdot 10^{-12}$ m^2. From statistics, we know the probability density function for a Gaussian distribution is:

$$\varphi_G(k_s, \mu, \sigma) = \frac{1}{2\sqrt{2\pi}} \exp\left[-\frac{(k_s - \mu)^2}{2\sigma^2}\right] \qquad (2.6.3)$$

By splitting the sand grains into 100 different sizes spread from μ_s - 3σ to μ_s + 3σ, and by weighing each grain size according to equation 2.6.3, we may use the extended Nikuradse diagram in figure 2.6.1 to compute the average weighed friction factor for that grain size. In figure 1.5.2, the curve for that has been drawn as the lowermost thick, blue line, curve 2.

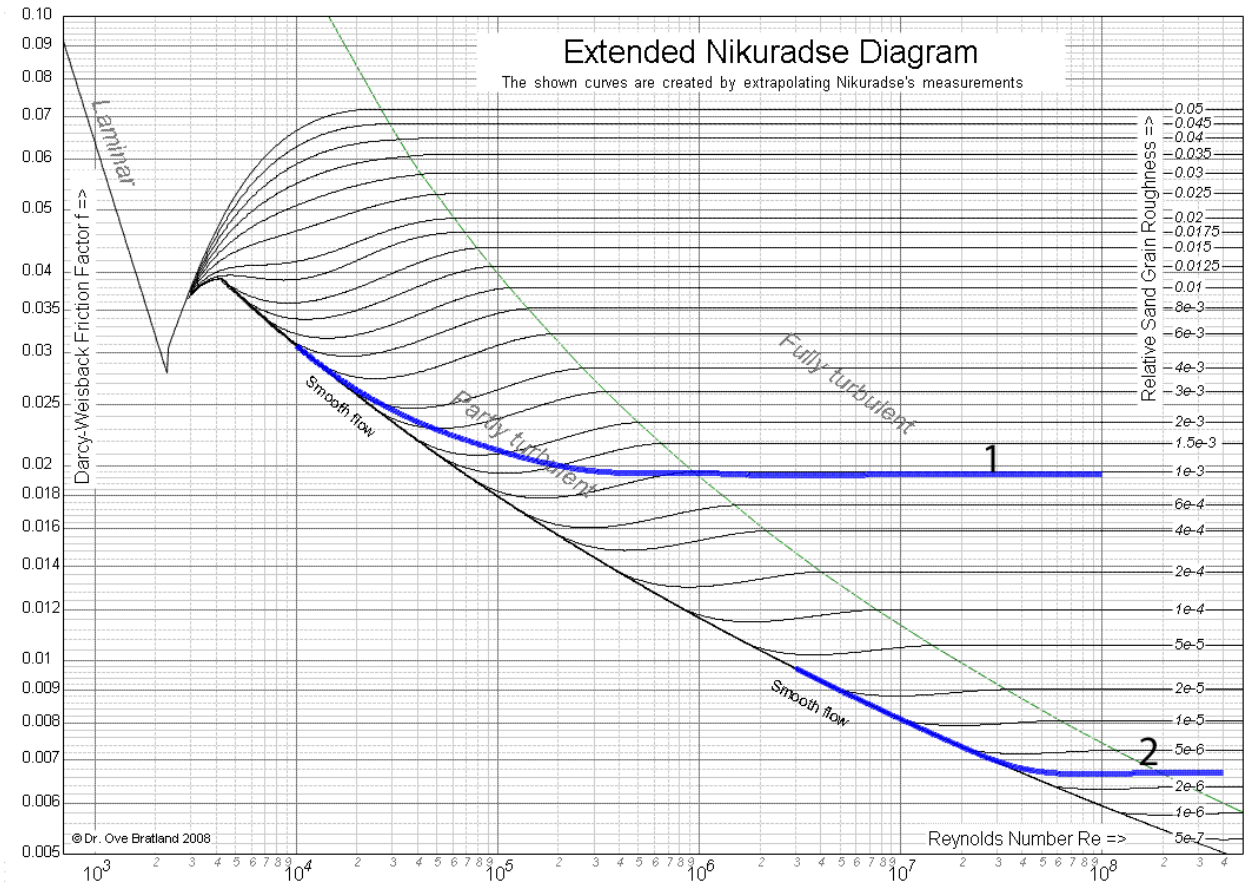


Figure 2.6.2. Theoretical pipes with Gaussian surface roughness distributions show on the extended Nikuradse diagram.

We can clearly see how this strategy leads to a smoothened curve without a dip in the partly turbulent zone, and with a less abrupt transfer to smooth pipe behavior, just like in Moody's diagram. Even though the theoretical experiment shown here assumes the different sand grain sizes can be combined linearly, something which is a very rough simplification, it does lend weight to the argument that pipes with a combination of different roughness sizes have smoother transitions between 'smooth' and 'partly turbulent' flow than do pipes with only one imperfection size.

We also realize that the larger the spread in the imperfection's sizes, the smoother the curves. That is something to keep in mind when investigating real pipes, for instance when comparing coated and un-coated pipes: Comparisons cannot be done for only one Reynolds number, since very different surfaces must be expected to lead to very differently shaped friction factor curves.

Pipes can also have non-Gaussian surfaces. Some irregularities may be inherent in the materials, others come from distinct steps in the manufacturing process. Each of these

sources of irregularities may lead to their own surface characteristics, and the final results can be some sort of weighed sum of the different roughness values. For that reason, more than one dominant roughness size may exist in one pipeline. Suppose, for instance, that a pipe is described by three distinct relative roughness values: $k_{s1}/d = 6 \cdot 10^{-3}$, $k_{s2}/d = 6 \cdot 10^{-4}$, $k_{s3}/d = 6 \cdot 10^{-5}$. Suppose also that the first roughness contributes *25%* of the total roughness, the second *50%*, and the last *25%*. By taking the friction factor from Nikuradse's diagram for each relative roughness and plotting the weighted average for many different Reynolds number, *curve 1* can be drawn.

When accurate friction calculations are required, we need more information about the surface than what can be compressed into an 'average' equvivalent sand grain roughness k_s.

Again, the tendency is that the curves begin to look more like the ones in the traditional Moody diagram. The agreement would be even better if a wider distribution of roughness values were used.

Note that no roughness distribution could be expected to create Moody-like curves for Reynolds numbers for $2{,}300 < Re < 4{,}000$. In that area, Nikuradse's measurements show all different curves merge, and transition between laminar and turbulent flow is relatively smooth. That contradicts how this area is displayed in the Moody diagram. The discrepancy was also recognized by Moody, who pointed out that his diagram is very inaccurate in this area. In fact, no convincing measurements seem to offer any support to the way the Moody diagram presents friction factors for $2{,}300 < Re < 20{,}000$, particularly not for relative roughness values $k_s/d > 0.02$.

We have seen that different surface roughness distributions can lead to different friction factors. Some of Nikuradse's results have been confirmed thoroughly by numerous measurements. Lots of measurements have shown that the friction factor curves do become horizontal for high Reynolds numbers for all normal, commercial metal pipes. We also know that in the horizontal part, corresponding to the 'fully turbulent' area of the Nikuradse charts, the friction factor is determined by the relative roughness, making it sufficient to measure it for only one pipe diameter (corresponding to one relative roughness). But how is the curve's shape affected by the pipe diameter in the 'partly turbulent' area? A commercial pipe may for instance be manufactured from a rolled steel plate. If that plate is used to manufacture 3 different pipes with different

 For non-commercial use only

diameters, the surface would be the same for all three. But the relative roughness would not. That is what is illustrated in figure 2.6.3, where the surface is assumed to have a Gaussian distribution of peaks and valleys, similar to the one described for curve 2 in figure 2.6.2. Setting $\mu_s = 3{\cdot}10^{-5}\ m$ and variance $\sigma^2 = 1{\cdot}10^{-8}\ m^2$, the curves are plotted for diameters *10, 1* and *0.1 m*, leading to average relative roughness values of $9.25{\cdot}10^{-4}$, $9.25{\cdot}10^{-5}$ and $9.25{\cdot}10^{-6}$.

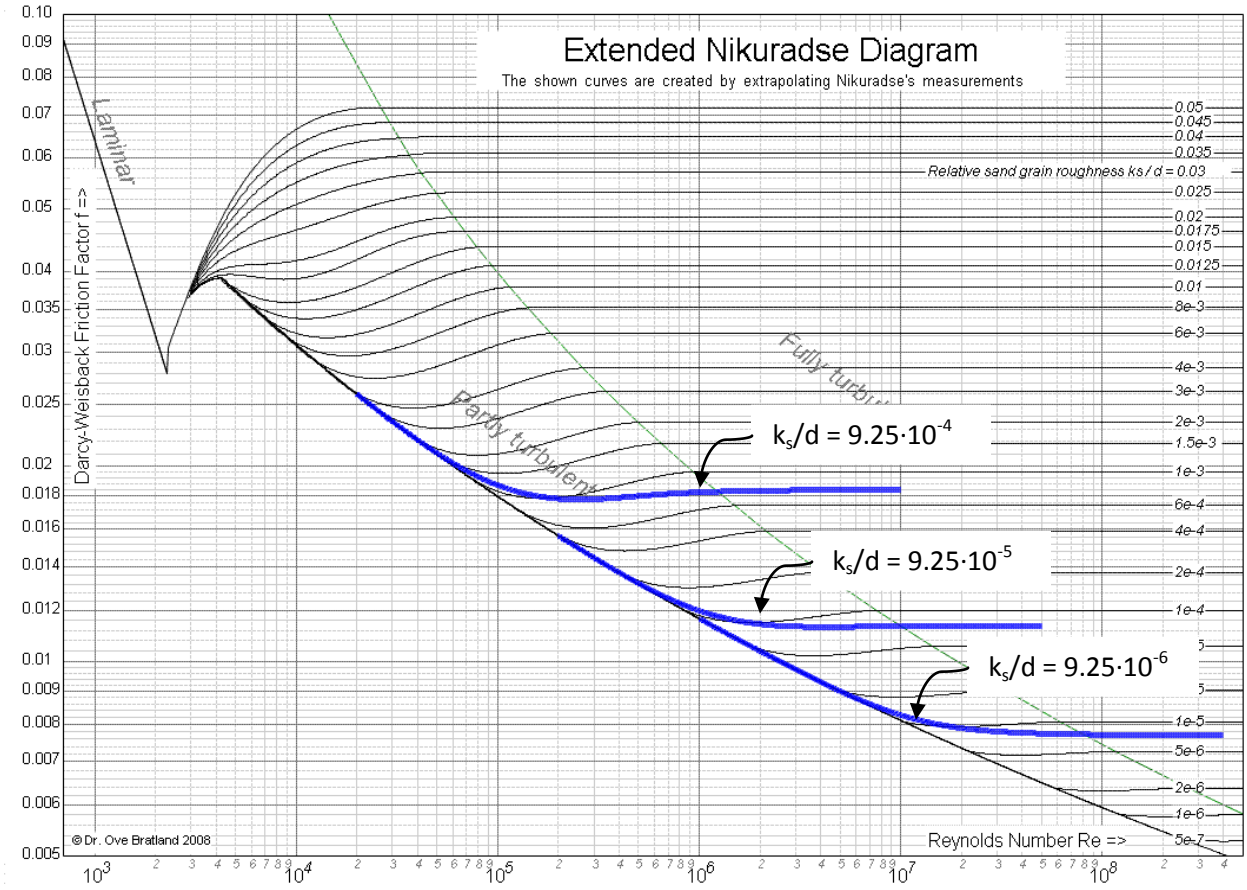


Figure 2.6.3. The same surface plotted for 3 different relative roughness values.

Figure 2.6.3 shows that this leads to relatively similar shapes. The surface structure uniformity factor u_s, which will be defined later, does in fact fit all three curves if we set $u_s = 3$. If we change μ and σ^2, the shape changes, which shows a pipe's friction properties cannot be described by k_s alone.

Put another way: No amount of effort can make it possible to compress the entire truth about a surface into a single, equivalent sand grain roughness. In the so-called 'partly turbulent' zone, we also need some way of describing the friction curve's surface-texture dependent shape.

2.7 The AGA friction factor formulation

Uhl et al. (1965) carried out a lot of measurements on gas pipes and concluded that the actual friction factor tends to be smaller in the intermediate zone than what Colebrook & White's formulae predicts.

Using a modified Prandtl equation based on Uhl et al.s measurements together with Nikuradse's equation, The AGA-report suggests that the highest of the two friction factors should be used. This is sometimes referred to as the AGA NB-13 method.

The report also gives recommendations for how to include other losses, such as those in bends and welds, but that part has been removed here to make comparison with the Moody diagram easier.

Uhl et al. used data from onshore gas pipelines in the United States as basis for his recommendations, where the operating pressure was below *7 MPa*. That is an order of magnitude lower than what is in use in gas transport pipelines in the North Sea today.

The AGA-method proposes a different equation for calculating f. First, f_r is calculated for the rough pipe law ('fully turbulent') as:

$$\frac{1}{\sqrt{f_r}} = 2log_{10}\left(\frac{k_e}{3.7d}\right) \tag{2.7.1}$$

This is very similar to the Nikuradse correlation, equation 2.5.2, except that sand grain roughness k_s has been replaced by an effective roughness k_e which accounts for both pipe surface friction and friction in bends and other components.

Next, a friction factor for smooth flow, f_s is calculated by equation 2.7.2, which represents a small modification of equation 2.5.1:

$$\frac{1}{\sqrt{f_s}} = -2F_d \log_{10}\frac{2.825}{Re\sqrt{f_s}} \tag{2.7.2}$$

 For non-commercial use only

Something called a drag factor, F_d, has been introduced. It takes into account effects of bends, valves and welds. Our purpose here is not to elaborate on how to choose F_d, but rather to compare the AGA report with the Moody diagram, so we simplify by setting $F_d = 1$.

The smaller of the two values f_r and f_s is used in the friction calculation. When plotting this, the simplified AGA diagram in figure 2.7.1 emerges. We can see that the AGA report is in fact closer to Nikuradse's diagram than the Colebrook & White formula is.

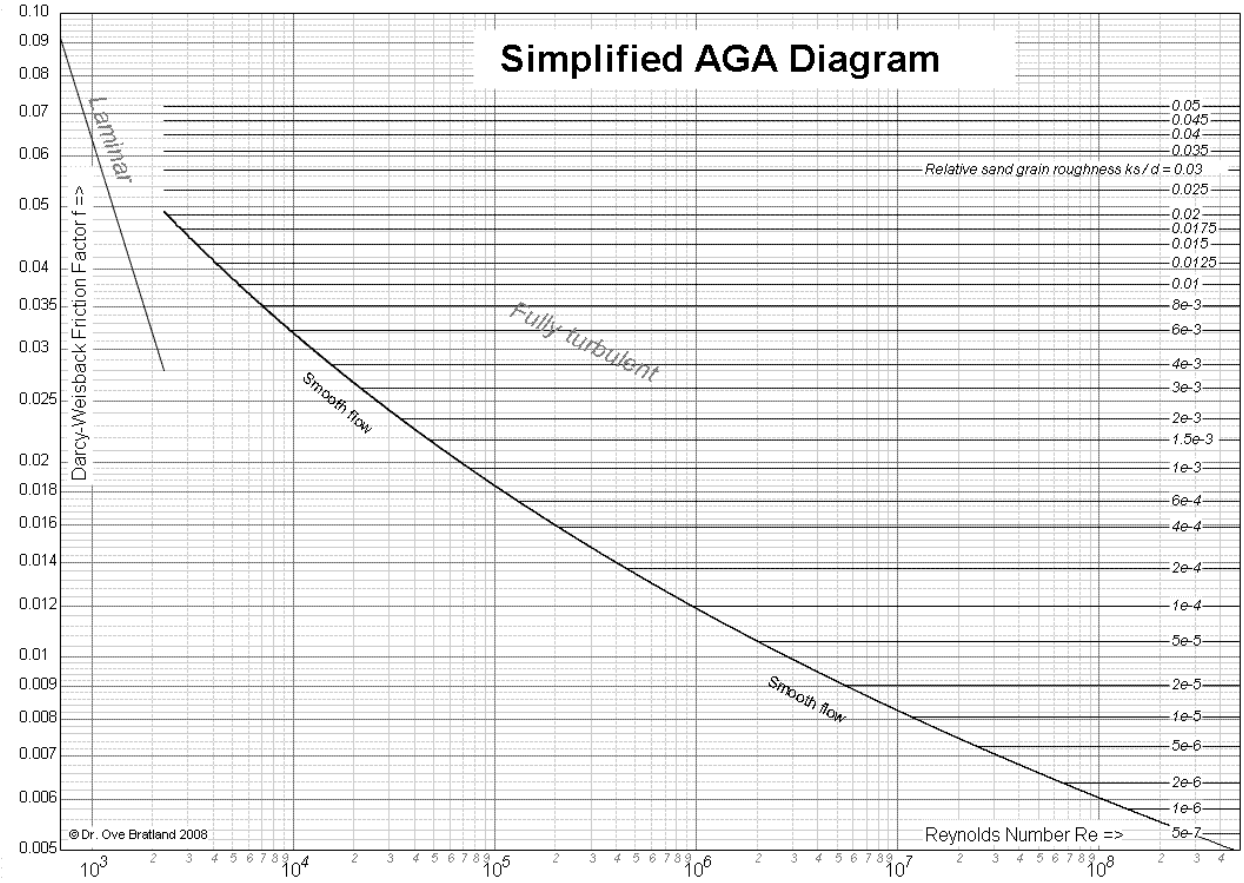


Figure 2.7.1. Moody diagram based on simplified AGA-recommendations.

We will later see that the differences in the Moody and AGA diagrams can be explained by differences in the pipe surfaces they try to describe, and that both diagrams can in fact be improved by taking into account relatively new measurements. But first, let us have a closer look at some very recent results which throw light on how the friction mechanisms work.

2.8 Towards a better understanding of the friction in turbulent pipe flow

2.8.1 Introduction about turbulence

Figure 2.8.1. Water flowing in a glass tube. Colored water is injected just upstream of the section where the photo is taken. We see that the flow is laminar. From Van Dyke (1982).



Figure 2.8.2. The Reynolds number has been increased just enough to create turbulence. Due to the thick laminar boundary layer, the eddies do not come close to the wall.



Figure 2.8.3. Fully turbulent flow.

Turbulent flow remains one of the mysteries facing modern science. That does not mean no useful theories have been developed, and we will show here that Kolmogorov's theory, as outlined by Pope (2000) and recently applied to rough pipe flow by Gioia & Chakraborty (2006), can be used to compute the Darcy-Weisbach friction factor theoretically.

The theory is not completely analytical as it relies on empirical factors. But it goes into far more detail than previous models in explaining exactly what goes on inside the pipe. In fact, when plotting the results in a diagram, we get curves quite similar to the ones measured directly by Nikuradse. As we will discover in this chapter, this leads to new, useful insights.



Andrey Nikolaevich Kolmogorov

In 1922, Richardson introduced the concept of the energy cascade (Pope, 2000). It states that the turbulence can be considered to be composed of eddies of different sizes. Energy enters the turbulence at the largest scale of motion, which for pipe flow is eddies of radius similar to the pipe's radius. This energy is thereafter transferred to smaller and smaller eddies and only at the smallest scales does it dissipate by viscous action.

For non-commercial use only

2.8.2 Quantifying turbulence

The amazingly clear-thinking Russian mathematician Kolmogorov (1941) showed the energy contained in turbulent eddies of length-scale σ *[m]* can be fitted to a correlation which has become known as the *Kolmogorov 5/3 Spectrum* (the exponent *5/3* has actually been derived from the Navier-Stokes equations analytically and is considered to be exact):

$$E(\sigma) = k_k \varepsilon^{2/3} \sigma^{5/3} \; for \; \eta \ll \sigma \ll d/2 \tag{2.8.1}$$

where k_k is a universal, dimensionless constant (by experiments determined to be around 1.5), ε *[m²/s³]* is the rate of dissipation of turbulent kinetic energy, and σ is the inverse of the so-called wave number *[1/m]* The validity boundaries are the Kolmogorov viscous micro length scale η *[m],* which is assumed to be the smallest scale of importance when describing turbulent flow, and the pipe radius *d/2 [m],* so that:

$$\eta \stackrel{\text{def}}{=} \left(\frac{\nu^3}{\varepsilon} \right)^{1/4} \tag{2.8.2}$$

The existence of a lower bound for the turbulent eddies is not something that may seem immediately obvious. Kolmogorov postulated that not only does such a lower bound exist but it can even be quantified by applying equation 2.8.2.

In order to extend the validity of Kolmogorov's spectrum, it may be multiplied by two factors C_e and C_d. They start to differ from *1* as we approach the stated validity limits of equation 2.8.1:

$$E(\sigma) = C_e C_d k_k \varepsilon^{2/3} \sigma^{5/3} \; for \; \eta \leq \sigma \leq R \tag{2.8.3}$$

When the energy spectrum is on this form, it contains information about the kinetic energy for each length scale. For eddies of size *s*, it can be shown that their average kinetic energy is described by:

$$v_{es}{}^2 = \int_0^s E(\sigma)\sigma^{-2}d\sigma \tag{2.8.4}$$

If we could solve this integral it would be possible to estimate how fast eddies of different sizes move around in the flow. Kolmogorov's hypothesis of local isotropy states that at sufficiently high Reynolds numbers the small-scale turbulent notions are statistically isotropic, meaning that they do not have any preferred direction(s). That means they move as much radially as axially. When they touch the wall, or possibly the laminar boundary layer close to the wall, they will transfer momentum from the fluid to the wall. The momentum exchanged this way obviously has to be proportional to the fluid's density and the average axial velocity, as well as the eddies' radial velocity. The average radial velocity is again considered proportional to the velocity describing the kinetic energy:

$$\tau = k_\tau \, \rho \cdot v \cdot v_{es} \tag{2.8.5}$$

where k_τ is some dimensionless constant. We do not have a value for k_τ at this stage, but we will later see how it can be estimated.

By combining equations 2.1.3 with the definition of the Darcy-Weisbach friction factor, equation 2.1.6, we see friction stress τ and f is correlated as:

$$f = \frac{8\tau}{\rho v^2} \tag{2.8.6}$$

Combining equations 2.8.5 and 2.8.6 leads to:

$$f = \frac{8k_\tau}{v} v_{es} \tag{2.8.7}$$

 For non-commercial use only

Inserting that into equation 2.8.4, we get:

$$f = \frac{8k_\tau}{v}\left[\int_0^s E(\sigma)\sigma^{-2}d\sigma\right]^{1/2} \tag{2.8.8}$$

Now let us try to express the different terms in this integral as a function of those parameters we know are of relevance to the friction - the Reynolds number *Re* and the relative roughness k_s/d.

The factor C_e is smaller than *1* for relatively low *Re*, which is referred to as the energetic range. Von Karman showed that a good approximation can be formulated as:

$$C_e = \left[1 + \gamma\left(\frac{2\sigma}{d}\right)^2\right]^{-17/6} \tag{2.8.9}$$

where γ is a dimensionless constant, estimated to be 6.78 .

The factor C_d is smaller than 1 for relatively high *Re* in the so-called dissipative range. It has been shown (Pope, 2000) that C_d can be approximated as:

$$C_d = exp\left(\frac{-\beta\eta}{\sigma}\right) \tag{2.8.10}$$

where β is a dimensionless constant, estimated to be *2.1*.

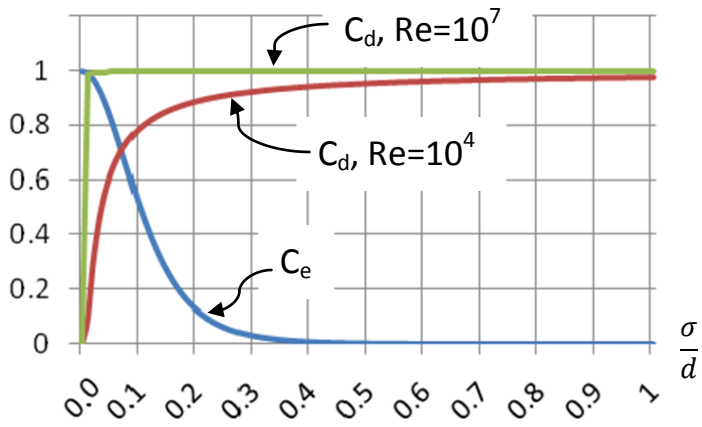


Figure 2.8.5. Dissipative and energetic factors as a function of σ/d.

As already mentioned, energy dissipation from the turbulence starts at the large-scale eddies and is fed down to ever smaller eddies, finally dissipating due to the fluid's viscosity. Taylor (1935) found the dissipation rate to be proportional to the third power of the velocity of the largest scale eddies, v_{el}, and inversely proportional to the largest scale (which in a pipe is limited by the pipe radius to $d/2$):

$$\varepsilon = \frac{2k_\varepsilon {v_{el}}^3}{d} \tag{2.8.11}$$

where k_ε is some dimensionless constant. It can actually be shown that the Kolmogorov 4/5-law leads to $k_\varepsilon = 5/4$.

The largest eddies are fed by the mean velocity v in the pipe, and it has been well documented that the correlation between them is linear:

$$v_{el} = k_l v \tag{2.8.12}$$

where k_l is some dimensionless constant. Antonia & Pearson (2000) have measured it to be 0.036 ± 0.005.

Inserting 2.8.12 into 2.8.11, we get:

 For non-commercial use only

$$\varepsilon = \frac{2k_\varepsilon {k_l}^3 v^3}{d} \tag{2.8.13}$$

A common estimate of the thickness δ_l of the laminar sub-layer near the pipe wall is to assume it to be proportional to the Kolmogorov length scale:

$$\delta_l = \kappa_\delta \eta \tag{2.8.14}$$

where κ_δ is a dimensionless constant (often set to be around 5).

Combining equations 2.8.2, 2.8.13 and 2.8.14 with the definition of *Re*, equation 2.1.8, we get:

$$\delta_l = \kappa_\delta \left(2k_\varepsilon {k_l}^3\right)^{-1/4} \mathrm{d} \cdot \mathrm{Re}^{-3/4} \tag{2.8.15}$$

Inserting the already given constants, this leads to the boundary layer thickness being a simple function of the Reynolds number:

$$\frac{\delta_l}{\mathrm{d}} = 48 \cdot \mathrm{Re}^{-3/4} \tag{2.8.16}$$

This is a very interesting correlation in itself. It states that for very low *Re*, such as for instance close to where the flow becomes laminar (say *Re*=2,300), $\delta_l/d = 0.14$, meaning a very large part of the cross-sectional area is taken up by the laminar layer close to the wall. When *Re* gets very large, say $Re = 10^8$, the boundary layer becomes $\delta_l/d = 4.8 \cdot 10^{-5}$. The surface imperfections are of course only going to rise above the laminar boundary layer if they are higher than the layer's thickness. Therefore, for any given relative roughness, we can expect the pipe to act as if it were smooth below a certain *Re*-

value. This has long been a popular explanation, but it agrees with measurements only on a qualitative basis. If we have a close look at where the different curves depart from the 'smooth pipe'-curve in the Moody (or Nikuradse) diagram, we will see it does not agree quantitatively with equation 2.8.16. We will also soon see that the complete model developed here, on the other hand, turns out to predict the curves quite accurately.

We may now insert everything into equation 2.8.8 and write:

(2.8.17)

$$f = \frac{8k_\tau}{v}\left[\int_0^s k_k\left[1+\gamma\left(\frac{2\sigma}{d}\right)^2\right]^{-\frac{17}{6}} exp\left(\frac{-\beta\frac{\mathrm{d}}{\left(2k_\varepsilon {k_l}^3\right)^{1/4}}\mathrm{Re}^{-3/4}}{\sigma}\right)\left[\frac{2k_\varepsilon {k_l}^3 v^3}{d}\right]^{2/3}\sigma^{-5/3}\sigma^{-2}d\sigma\right]^{1/2}$$

In order to transform this to the form we are familiar with from the Moody diagram, we change the integration variable by introducing:

$$x = \frac{\sigma}{d} \tag{2.8.18}$$

With this integration variable we get:

(2.8.19)

$$f = 8k_\tau {k_k}^{\frac{1}{2}}\left[2k_\varepsilon {k_l}^3\right]^{\frac{1}{3}}\left[\int_0^{s/d}(1+4\gamma x^2)^{-17/6}\cdot exp\left(\frac{-\beta\left(2k_\varepsilon {k_l}^3\right)^{-1/4}\mathrm{Re}^{-3/4}}{x}\right)x^{-1/3}dx\right]^{1/2}$$

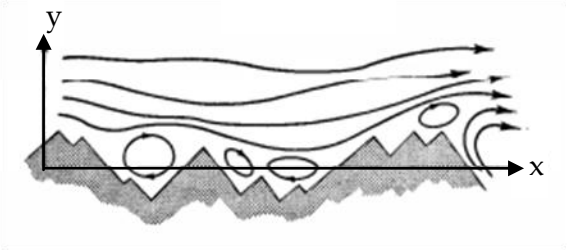


Figure 2.8.6. Eddies interacting with a real surface.

We also need to find an expression for the upper boundary, *s*, for the integral in equation 2.8.19. We recall that the factor *s* was the size of the eddies we expect to dominate in the interaction between pipe wall and the moving eddies. As indicated on figure 2.8.6, real surfaces typically have

 For non-commercial use only

a relatively complicated structure, and more than one size is likely to play a part.

Since Nikuradse's pipes were roughened with sand grains of a constant size, it seems that both the grain size and the distance between grains were in the order of k_s.

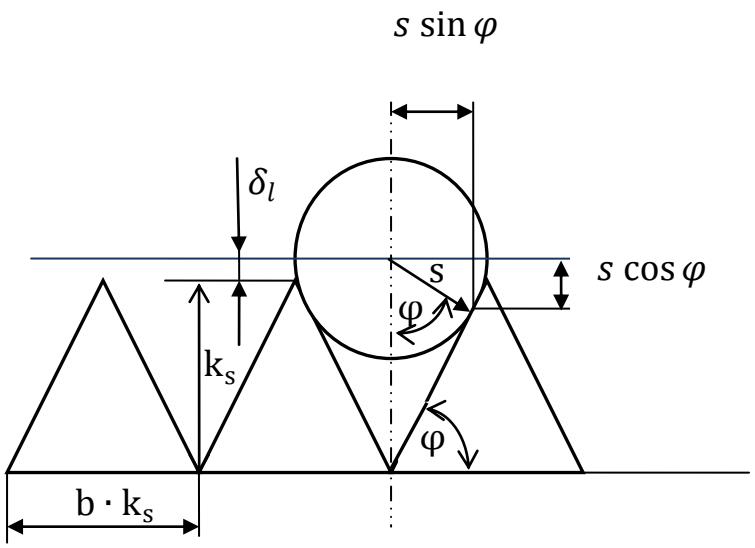


Figure 2.8.7. Eddy passing over idealized sand grains. The rectangular, pyramid-shaped grains are seen at a 45^0 angle to the pipe axis.

It is hard to come up with an accurate way of describing how the eddies interact with the pipe wall. On figure 2.8.7, the sand grains have been considered as pyramid-shaped with rectangular cross-sections. Given that the eddies are not spheres and not rigid, and that the grains are of unknown shape, the first approach to describing the eddies is simplified compared to what strict geometry and figure 2.8.7 could result in. We start out by assuming that if half the eddy manages to get into the 'wall zone', it is going to transfer its momentum to the wall:

$$s = k_s + \delta_l \tag{2.8.20}$$

The 'wall zone' is according to this simplification described as everything lying below the laminar boundary of thickness δ_l,. That boundary's thickness starts from the tips of the sand grains.

Note, though, that s is only used to determine the characteristic, average velocity v_{es}, that is the only place in the theory where s occurs. If some slightly smaller eddies or some slightly larger eddies are at work, too, they can also be expected to have average velocities relatively close to v_{es}, so the main trend in the results should hold.

Inserting equation 2.8.15 into 2.8.20 and dividing all terms with d leads to:

$$\frac{s}{d} = \frac{k_s}{d} + \kappa_\delta \left(2 k_\varepsilon {k_l}^3\right)^{-1/4} \mathrm{Re}^{-3/4} \tag{2.8.21}$$

By inserting the known constants in 2.8.19 and 2.8.21, we get:

$$f = 0.48 k_\tau \left[\int_0^{s/d} (1 + 27x^2)^{-17/6} \cdot exp\left(\frac{-20 \cdot \mathrm{Re}^{-3/4}}{x} \right) \cdot x^{-1/3} dx \right]^{1/2} \tag{2.8.22}$$

$$\frac{s}{d} = \frac{k_s}{d} + 48 \cdot \mathrm{Re}^{-3/4} \tag{2.8.23}$$

We have now managed to express the Darcy-Weisbach friction factor f as a function of Re and k_s/d. It seems impossible to solve equation 2.8.22 analytically, but it is easy to do so numerically. Finished integration programs are commercially available but it takes no more than a couple of lines of code to implement a simple integrator based on the Trapezoidal rule.

2.8.3 Using Kolmogorov's theory to construct a Moody-like diagram

Since we do not have a value for k_τ, we start by making a guess, say $k_\tau = 1$. Solving equation 2.8.22 and 2.8.23 with that value, $Re = 10^5$ and smooth pipe ($k_s/d = 0$) leads *to* $f = 0.0652$. Von Karman's smooth pipe correlation leads to $f = 0.0180$ for the same Re. Comparing those two results, we conclude that $k_\tau = 1 \cdot 0.0180/0.0652 = 0.276$.

 For non-commercial use only

With this value, we may now draw the whole diagram in the normal Moody-style, see figure 2.8.8

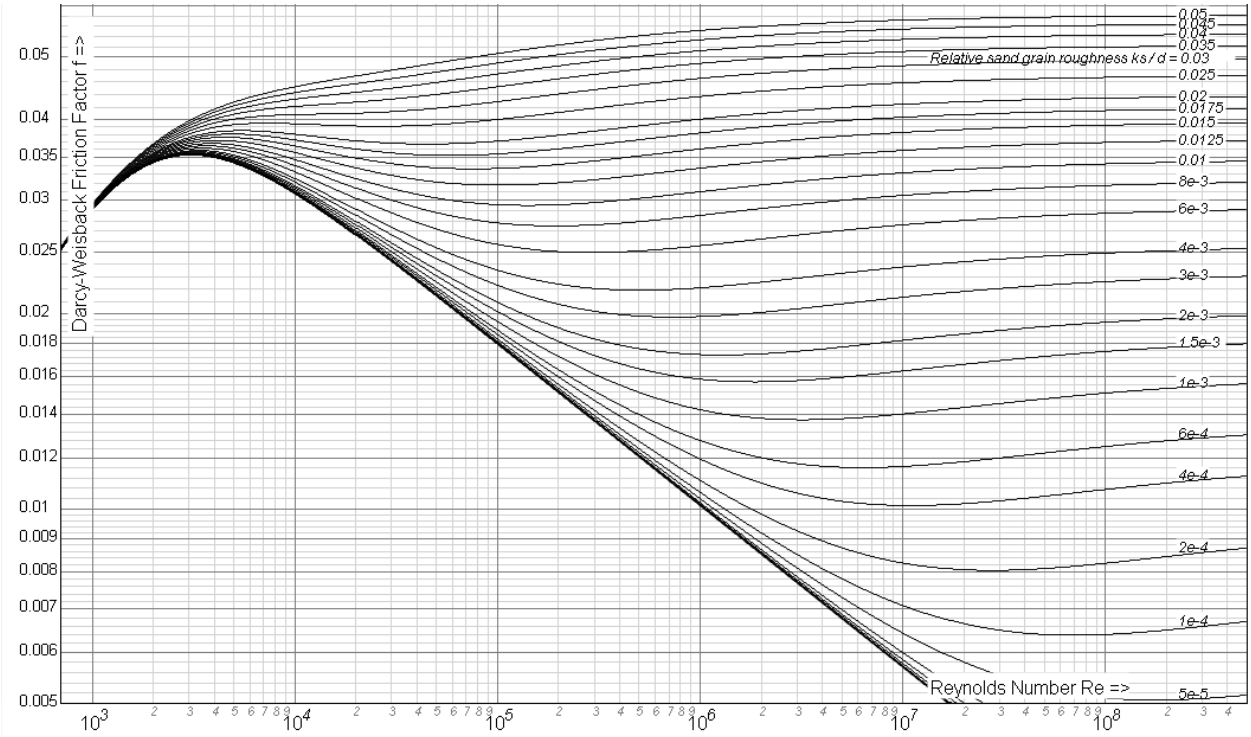


Figure 2.8.8. Moody-like diagram drawn on the basis of equation 2.8.22 and $k_\tau = 0.276$.

The results are in many ways very similar to Nikuradse's. For instance:

1. There is a maximum *f* at around *Re = 3000*. It turns out that what many authors have believed to be a gradual transition between laminar and turbulent flow can in fact be explained well by our model, where the central part of the flow is assumed to be fully turbulent, and a relatively thick boundary layer closer to the wall is laminar. We have not assumed the central part to be somewhat laminar in any way. The increase in *f* when *Re* is increased from *2,300* is due to the energetic range correction factor, C_e, taking on values lower than *1* for low *σ/d*. We can easily show that letting $\gamma = 0$ (and hence $C_e = 1$ in the whole range) results in the maxima disappearing. Lower C_e –values are according to this a result of the turbulent eddies being so large that they approach the same order as the pipe's diameter, and their radial movement is therefore restricted. The flow is not isotrop, and momentum is not transferred as efficiently from the turbulent eddies to the pipe wall if *Re* is low.

2. The local minima on the curves are apparent here, just as they were in Nukuradse's measurements. If we set $\beta = 0$, so that the dissipative range correction factor $C_d = 1$ in the whole range, this is in fact no longer the case. This shows we do not need to bring in any arguments about how the first sand grains penetrate the boundary layer in order to explain the local minima, even though some authors have experimented with such arguments in the past. It may in fact be a good idea to do away with the term 'partly turbulent' altogether, since this naming convention can be associated with the probably erroneous assumption that part of the surface irregularities are sticking out of the boundary layer.
3. The curves seem to approach a horizontal path for large *Re*, but it happens much more gradually than in Nikuradse's measurements. The curves do show sections where *f* increases with increasing *Re* for all k_s/d, including for very low k_s/d, and that agrees with the extended Nikuradse diagram in figure 2.6.2. It also agrees with the tendencies (slightly) visible in some of Sletfjerding's measurements for glass-bead coated gas pipes with $Re \sim 10^6 - 3 \cdot 10^7$ (not shown here, but can be found in Sletfjerding, 2001). The Moody diagram, by contrast, shows falling or horizontal f-curves with increasing *Re* in the whole turbulent area.

There are also some very notable differences between our theoretical results and Nikuradse's measurements:

4. The smooth-pipe curve in figure 2.8.8 is approximately a straight line, at least for $Re > 10^5$. That does not agree with known measurements on smooth pipes.
5. These curves leave the smooth-pipe line more gradually as the *Re* increases than Nikuradse's curves did. Our model was based on the 'wall zone', the area where eddies are slowed down, to be the sum of the boundary layer and the sand grain height. The upper bound in the integral will therefore never be completely independent of k_s. This suggests we need a more sophisticated model representing exactly what happens when the eddies reach the wall zone, possibly by modifying equation 2.8.20.
6. In the theoretical results, we see these curves lie closer together for high relative roughness and further apart for low relative roughness values compared to what they did in Nikuradse's measurements.

It is possible to play around with more accurate geometrical surface estimates based on figure 2.8.7 or some similar model. For instance, by assuming each eddy to be a sphere, we may set:

 For non-commercial use only

$$\varphi = \tan^{-1}\frac{k_s}{bk_s/2} \tag{2.8.24}$$

$$\frac{s}{d} = \frac{\frac{k_s}{d} + \kappa_\delta\left(2k_\varepsilon {k_l}^3\right)^{-1/4}\cdot \mathrm{Re}^{-3/4}}{\tan\varphi\sin\varphi + \cos\varphi} \quad if\ \frac{s}{d}\cos\varphi \geq \kappa_\delta\left(2k_\varepsilon {k_l}^3\right)^{-1/4}\cdot \mathrm{Re}^{-3/4} \tag{2.8.25}$$

And:

(2.8.26)

$$\frac{s}{d} = 2\sqrt{\left(\frac{bk_s}{2d}\right)^2 + \left(\kappa_\delta\left(2k_\varepsilon {k_l}^3\right)^{-1/4}\cdot \mathrm{Re}^{-3/4}\right)^2} \quad if\ \frac{s}{d}\cos\varphi < \kappa_\delta\left(2k_\varepsilon {k_l}^3\right)^{-1/4}\cdot \mathrm{Re}^{-3/4}$$

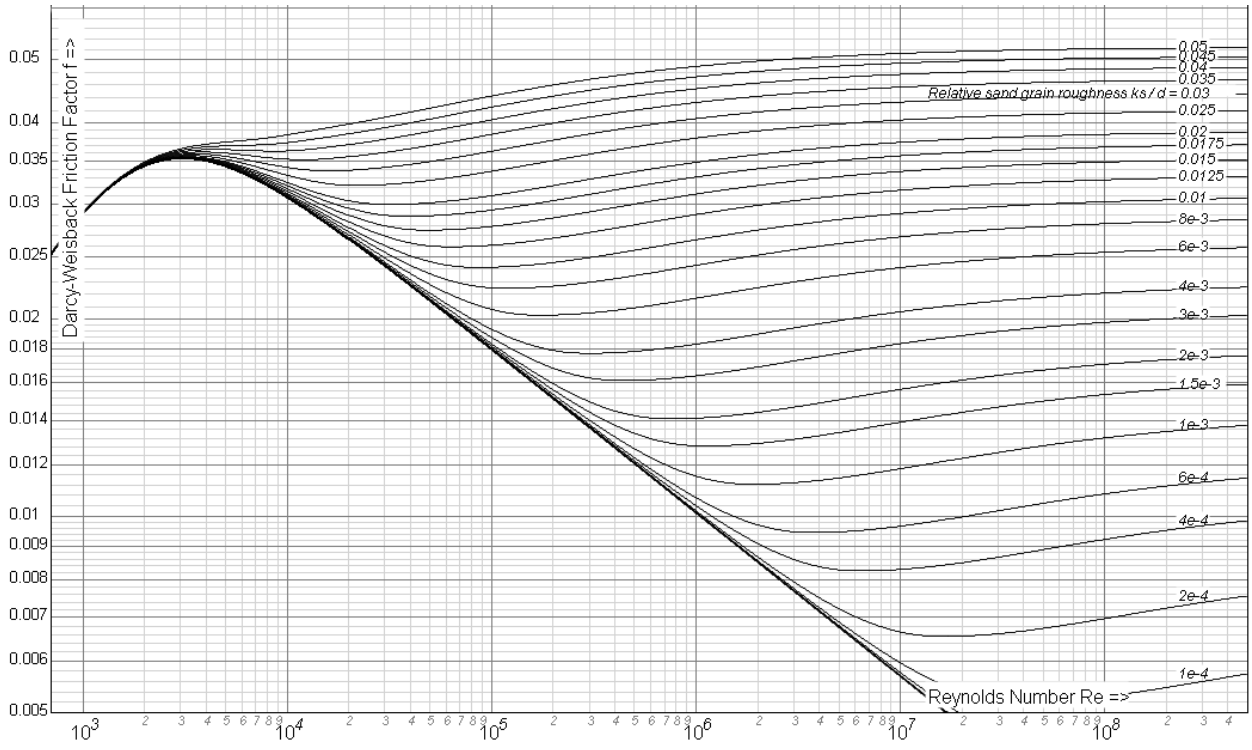


Figure 2.8.9. Results based on the same data as for figure 2.8.8, but with a more sophisticated description of the sand grain geometry.

The factor b is used to describe the sand grain width. $b = 2$ seems to be a likely value, se figure 2.8.7. Repeating the computations with these criteria as upper integration boundary we get a slightly more abrupt departure from the smooth pipe curve (the local minima having moved somewhat to the left), but the difference is not very significant, see figure 2.8.9.

Other parameter variations are possible. For instance, setting $\beta = 0.5$ leads to curves which become horizontal at much lower Re and more similar to Nikuradse's curves.

It is possible to make this model fit the measurements better by adapting the different constants and maybe even model some of them as functions of Re and k_s/d. A more thorough attempt at adapting the data is outside the scope of this book, but it looks likely that going deeper into this theory can help gain more insight into how to model pipe friction as a function of different surface roughness structures.

2.8.4 Comparing the theoretical results with other measurements

Nikuradse's measurements are far from being the only available measurements we may compare results with. The United States Department of The Interior Bureau of Reclamation published an extensive report in 1965, and has been re-printed many times since. It summarizes information obtained through field measurements and large-scale laboratory experiments compiled from world-wide sources. Charts are presented for obtaining friction factors for concrete pipe, various sorts of steel pipe, as well as wood pipe. Even though the report fails to propose anything better than the Moody diagram, it presents lots of measured curves sloping at angles which differ significantly from those in the Moody diagram, and some looking much more similar to the ones in figure 2.8.8.

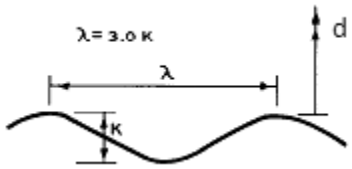


Figure 2.8.10. Corrugated metal pipe.

Another interesting report came from U.S. Army Engineers Waterways Experiment Section in 1969 (revised 1977). It shows, among other things, examples of measurements on corrugated pipes. Such pipes turn out to have up to twice as high friction factors as expected according to the Moody diagram.

The curves are also completely different, with friction factor maxima located above $Re = 10^6$. Corrugated pipes have something in common with Nikuradse's pipes in the sense

that they have one distinct dominating relative roughness. Geometrical considerations indicate that these pipes' surface roughness fit equation 2.8.20 quite well. Figure 1.6 shows a large spread in the measurements, but it is clear that f can reach maxima at Reynolds numbers of $5{\cdot}10^7$ or more. That trend is in fact also visible in figure 2.8.8, leading us to believe that our theoretical model captures the essence in how the friction mechanisms work.

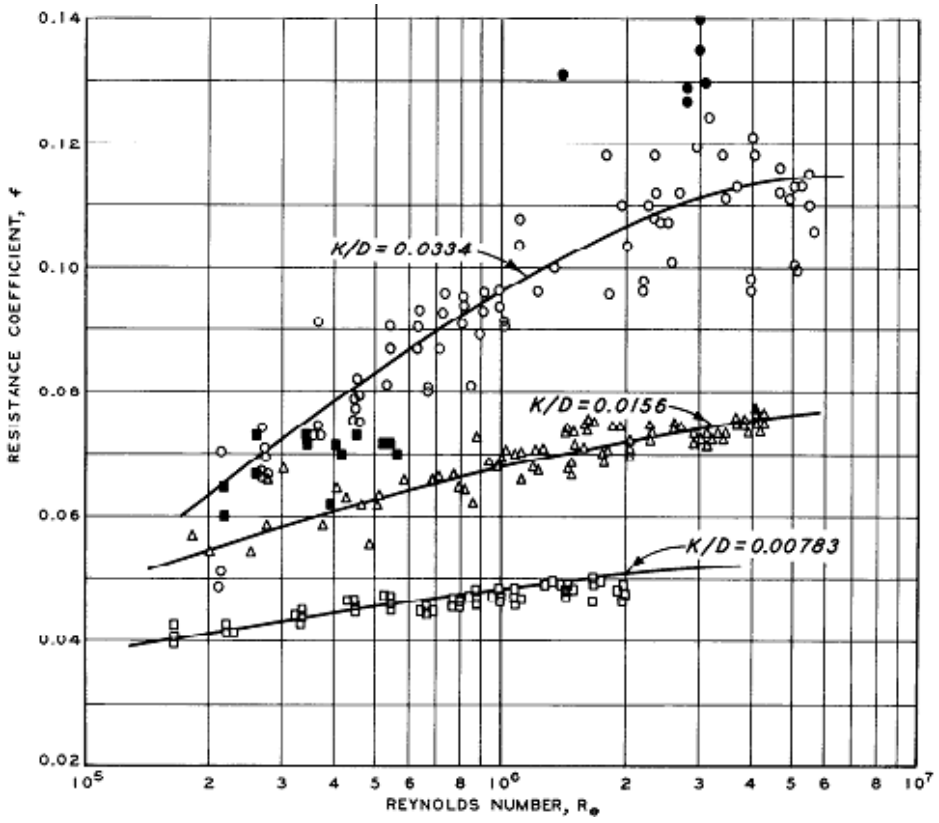


Figure 2.8.11. Measurements on corrugated pipes.

2.8.5 Large surface imperfections dominate on non-uniform surfaces

The fact this relatively new theory agrees so well with measurements gives us confidence in its ability to capture the main mechanisms involved in creating friction. We saw that one of the main assumptions was the turbulence is composed of eddies, and these eddies start out with a radius similar to the pipe radius. As they travel along the pipe they break down to ever smaller eddies. When they become small enough to be absorbed by the laminar boundary layer and/or the surface imperfections, they transfer momentum to the pipe wall and create friction. When the surface structure was completely uniform, reasonable agreement with measurements could be achieved by assuming the eddies would be absorbed once they became small enough to be

'captured' by the length scale of relevance with that particular roughness. But what does this theory say about what happens if we have more than one roughness size at the same time, for instance a surface of the type indicated on figure 2.8.6?

Some pipe surfaces turn out to produce very different friction factors than those plotted in the traditional Moody diagram.

Let us first consider a simplified pipe surface consisting of only two different textures, one quite rough, and one quite smooth. Each texture covers 50% of the surface area. Eddies travel along the surface and get into contact with it occasionally. If a large eddy touches a rough part it gets absorbed. If it contacts a smooth part, nothing significant happens and it continues its journey. Half of the eddies happen to get in contact with a rough surface part on their first encounter. If they are smaller than what corresponds to the rough part they are adsorbed. Of the eddies which happen to contact the smooth part first, fewer are going to be small enough to be absorbed, and some of the ones that bounce back are going to come into contact with a rough part and be absorbed on their second encounter. In sum, that means the rough part contributes more to the dissipation than the smooth part, and the overall friction factor will be closer to the one corresponding to the rough part of the surface than the one for the smooth part.

The explanation above relates to a surface consisting of only two different surface roughness sizes, but the logic holds for a general surface of an infinite amount of surface roughness values, too. Constructing some sort of average surface roughness by simply averaging the geometrical imperfections, as some recent authors have attempted (and as we did in chapter 2.6) cannot be expected to lead to accurate results, at least not for surfaces having a large spread in the different surface roughness sizes.

The model supports the view that the hard-to-model part of the Moody diagram, the area where the curves are affected both by relative roughness and Reynolds number, is affected by all the different types of imperfections occurring on it. The largest imperfections are more important than their frequency would suggest if weighed linearly with the other imperfections. Therefore, we need to include some sort of factor to take this into account. The factor we are looking for should preferably be a surface property. In that case it does not change if we manufacture a different diameter pipe with an identical surface by using the same rolled steel plate. We will soon see other authors have been very close to defining such a factor, even though they do not seem to

 For non-commercial use only

have explicitly stated their factor to be a surface property which could have been determined and tabulated, just like the equivalent sand grain roughness k_s.

2.8.6 Friction behaves the same way for all Newtonian fluids.

We see from equation 2.8.19 that the parameters determining the steady-state friction factor include the relative surface roughness and diameter, as well as such fluid properties as viscosity and density. It does not depend on whether the fluid is a liquid. It is therefore a mistake to pretend different friction factor equations should be used for liquid and gas. It is for instance a common misconception that the AGA-equations somehow fit gas flow better than liquid flow while the traditional Moody diagram is best for liquids. No theory supports this, and the differences in the two diagrams are in direct conflict with each other. The reasons for the differences are that the AGA diagram, as explained in chapter 2.7.1, is built on a more updated correlation for the 'smooth pipe'- curve, and obviously also on a different surface uniformity distribution. We can therefore say the different diagrams assume different types of pipe surfaces, not different types of liquid.

2.9 Practical friction factor calculation methods

2.9.1 The surface-uniformity based modified Moody diagram

Although the turbulence model method shown in the previous chapter was useful when trying to gain insight into the friction mechanisms in single-phase pipe flow, it is not accurate enough to be used for calculating f directly. Instead, we need to rely on empirical correlations similar the one proposed by Colebrook & White, but we should include some of the knowledge which has accumulated since Moody diagram was first published.

One of the most extensive and systematic relatively recent series of measurements are those of Zagarola (1996). He has carried out measurements for $3.1 \cdot 10^4 \leq Re \leq 3.5 \cdot 10^7$, and he has proposed two alternative friction correlations for smooth pipes. Smooth pipe correlations are of course of great importance, given that both the traditional Moody diagram and the AGA recommendations rely on them. Any new, improved smooth-pipe correlation can therefore be used 'Moody-style' or 'AGA-Style' without changing the philosophy behind the diagrams as such.

Zagarola's two correlations give very similar results for high Reynolds numbers. The simpler of the two, which seems more than adequate considering the many uncertainties involved in normal pressure loss calculations, is:

$$\frac{1}{\sqrt{f}} = 1.889 \log_{10}\left(Re\sqrt{f}\right) - 0.3577 \tag{2.9.1}$$

We can bring this over to a more familiar form:

$$\frac{1}{\sqrt{f}} = -2log_{10}\left[\left(\frac{1.547}{Re\sqrt{f}}\right)^{0.9445}\right] \tag{2.9.2}$$

By multiplying out the exponents and using the analogy for how Colebrook & White combined the smooth equation with the fully rough flow, we get:

$$\frac{1}{\sqrt{f}} = -2log_{10}\left[\left(\frac{1.547}{Re\sqrt{f}}\right)^{0.9445} + \frac{k_s}{3.7d}\right] \tag{2.9.3}$$

It was shown by Haaland (1983) that the sharpness in the transition from smooth to fully rough flow can be neatly adjusted by rising each of the terms in the parenthesis into a power he called *n*. We already showed in chapters 2.6 and 2.8 that the more uniform the surface, meaning the more different surface imperfections show similarity with each other in shape and size, the more abrupt the transition between smooth and rough flow becomes. Utilizing this result, we define a dimensionless surface structure uniformity factor, u_s, and include it in a way similar to Haaland's mathematical exponent n, and write :

 For non-commercial use only

$$\frac{1}{\sqrt{f}} = -\frac{2}{u_s} log_{10}\left[\left(\frac{1.547}{Re\sqrt{f}}\right)^{0.9445u_s} + \left(\frac{k_s}{3.7d}\right)^{u_s}\right] \quad (2.9.4)$$

The surface uniformity-based friction factor equation, equation 2.9.4 represents a clear improvement compared to Colebrook & White's correlation and the conventional Moody diagram for two reasons: It relies on improved measurements covering a greater span of Reynolds numbers (those of Zagarola). In addition, it has a better representation of the pipe's surface roughness (using both k_s and u_s). It also recognizes that the factor u_s is a surface property, and we have chosen to call 2.9.4 the surface uniformity-based friction factor equation. We see that unlike k_s, u_s is dimensionless as it stands – it does not have to be divided by d or anything else.

Since u_s is a property, it can be tabulated for different types of surfaces, just like k_s. We cannot be sure, though, that u_s is completely independent of Re for all different relative roughness values. We remember that the way equations 2.9.2 and 2.5.2 were combined to form 2.9.3 was based on convenience rather than science. Equation 2.9.3 agrees with equations 2.9.2 and 2.5.4 for very high and very low Re, but does not take into account what happens in the intermediate range. We can adjust that somewhat by choosing different u_s –values and at least make better approximations with equation 2.9.4 than what is possible with the Darcy-Weisbach or the AGA-equations.

Solving equation 2.9.4 is done just as easily as for the original Colebrook & White correlation by setting:

$$f = \left\{-\frac{2}{u_s} log_{10}\left[\left(\frac{1.547}{Re\sqrt{f}}\right)^{0.9445u_s} + \left(\frac{k_s}{3.7d}\right)^{u_s}\right]\right\}^{-2} \quad (2.9.5)$$

We start out by guessing an f, say $f = 0.02$, and correcting that guess by computing an ever improved f in the same way as it was explained for equation 2.5.4.

If we set $u_s = 1$, equation 2.9.4 becomes identical to 2.9.3. Further, if can be seen that for any value of u_s, f approaches the 'smooth flow'-line when Re is small, and that it approaches the Nikuradse fully turbulent equation for large Re.

The traditional Moody diagram shows – in clear contrast both to Nikuradse's measurements and the theoretical diagrams in figures 2.8.8 and 2.8.9 – an abrupt jump in the friction factor close to $Re = 3{,}000$. Although the literature contains numerous claims that such a jump is supposed to exist, it is difficult to find hard evidence in the form of measurements to support it. It looks like the claims sometimes are based on the Moody diagram rather than the diagram reflecting realities in this respect. In addition it is easy to see that poorly arranged test setups could lead to instabilities in the transition zone, and that could also occasionally produce erroneous claims about abrupt friction factor changes. Test rig setups where the velocity starts to decline as the friction increases when the flow becomes turbulent can lead to the flow switching back to laminar again, followed by increased velocity due to lower friction and so on. Such system instability can occur for other reasons than abrupt and apparently random transition between laminar and turbulent flow, but it can easily be misinterpreted when observed.

On the following pages, diagrams based on equation 2.9.4 are presented for $u_s = 1$, $u_s = 3$ and $u_s = 10$. They use equation 2.1.7 for the laminar part of the flow. To achieve better agreements with measurements and theory in the transition between laminar and turbulent flow, some additional modifications have been introduced. All curves follow the same, straight line from a point p_1, corresponding to laminar flow at $Re_1 = 2{,}300$ and $f_1 = \frac{64}{Re}$, to a point p_2 (estimated from Nikuradse's diagram), where $Re_2 = 3{,}100$ and $f_2 = 0.04$. When the different relative roughness curves start to spread out, it clearly happens more gradually than the traditional Moody diagram suggests, and all curves in the new diagrams are therefore assumed to follow straight lines from point p_2 to points p_3, where $Re_3 = 20{,}000$, and f_3 is computed from equation 2.9.4.

The modified Moody diagrams in figures 2.9.1-1.9.3 have been based on these assumptions. Recognizing that although the transition zone for $2{,}300 < Re < 20{,}000$ has been improved compared to the traditional Moody diagram, this is still considered the least reliable part, and a blue area has been added to visualize that.

Since all turbulent pipe flow consists of a laminar layer close to the wall in addition to a turbulent zone in the center, it does not appear useful to mark any part of the diagram 'partly turbulent' or 'fully turbulent'.

 For non-commercial use only

2.9.2 Improving friction factor calculation speed

As previously mentioned, equation 2.9.4 can be solved nicely with fixed-point iteration, and that simple alternative should be the method of choice for most users.

Equation 2.9.4 can alternatively be solved by Newton-iteration. We start by defining a function y and re-formulated the problem to solve the equation

$$y = \frac{1}{\sqrt{f}} + \frac{2}{u_s} log_{10}\left[\left(\frac{1.547}{Re\sqrt{f}}\right)^{0.9445u_s} + \left(\frac{k_s}{3.7d}\right)^{u_s}\right] = 0 \tag{2.9.6}$$

This can be done by Newton-iteration by first calculating the partial derivative:

$$\frac{\partial y}{\partial f} = -\frac{1}{2}f^{-3/2} - \frac{\frac{2}{u_s \cdot ln(10)} \cdot \left(\frac{1.547}{Re}\right)^{0.9445u_s} \cdot \frac{0.9445u_s}{2} f^{-\frac{0.9445u_s}{2}-1}}{\left[\left(\frac{1.547}{Re\sqrt{f}}\right)^{0.9445u_s} + \left(\frac{k_s}{3.7d}\right)^{u_s}\right]} \tag{2.9.7}$$

This simplifies to:

$$\frac{\partial y}{\partial f} = -\frac{1}{2}f^{-3/2} - \frac{0.4102\left(\frac{1.547}{Re}\right)^{0.9445u_s} f^{-0.4723u_s-1}}{\left[\left(\frac{1.547}{Re\sqrt{f}}\right)^{0.9445u_s} + \left(\frac{k_s}{3.7d}\right)^{u_s}\right]} \tag{2.9.8}$$

Newton-iteration means setting:

$$f_{i+1} = f_i - \frac{y_i}{\left(\frac{\partial y}{\partial f}\right)_i} \tag{2.9.9}$$

It is possible to overshoot and get a negative *f* in the first iteration if the initial value is much higher than what turns out to be the correct one. A negative *f* would of course make the next iteration crash, but this can easily be prevented by never allowing it to fall below its smallest possible physical value, for instance by replacing equation 2.9.9 with:

$$f_{i+1} = Max\left[0.005,\ f_i - \frac{y_i}{\left(\frac{\partial y}{\partial f}\right)_i}\right] \tag{2.9.10}$$

The best initial guess for *f* may as already mentioned typically be the one from previous time step, which tends to be very close to the correct value and therefore leads to only one iteration. If we prefer to avoid using memory to remember all the old friction factors, we can instead let the friction factor function remember the factor it last calculated without keeping track of where on that pipe or even which pipe the calculation was relevant for. Most of the time such a value is closer to the real value than a constant starting value, say f = *0.02*, would have been. Using Haaland's explicit approximation for the first calculation, equation 2.5.7, is also possible, but most of the time slower for transient pipeline calculations.

Note that many of the factors in equation 2.9.8 and 2.9.10 are constant during the iteration and can be calculated once and for all outside the iteration loop. Also, some of the same factors are found in both the y and the $\partial y/\partial f$ expression. Careful utilization of these facts makes for fast calculations.

One might wonder whether it actually makes sense to use such a complicated method as this, given the equation converges nicely after only a few iterations even if the simpler fixed-point iteration is used. Newton-iteration may typically save an iteration or two, and consequently can be worthwhile only for heavy simulations.

 For non-commercial use only

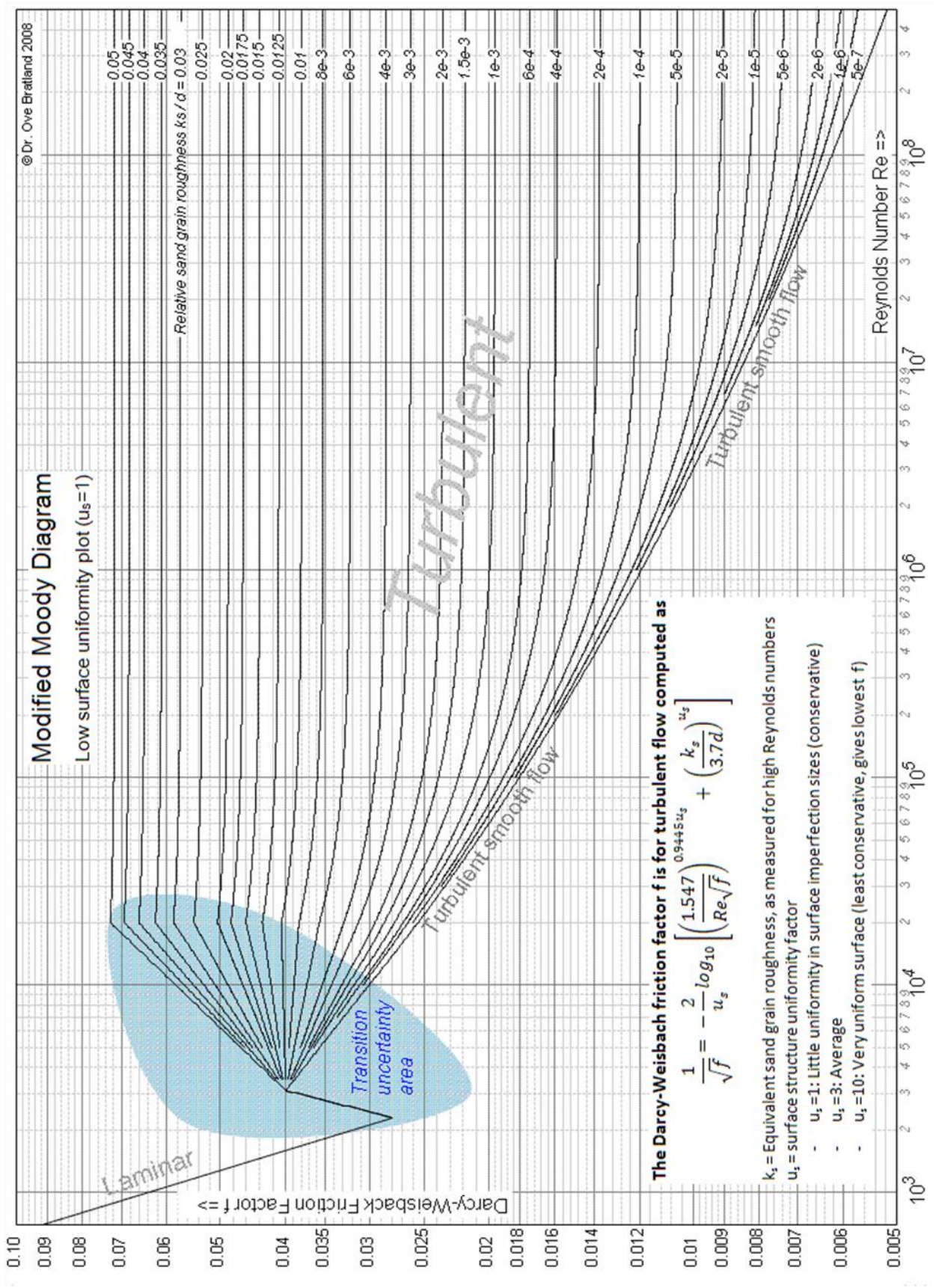

©Dr. Ove Bratland 2008
Modified Moody Diagram
Low surface uniformity plot (u_s=1)
Relative sand grain roughness ks / d = 0.03
0.05
0.045
0.04
0.035
0.025
0.02
0.0175
0.015
0.0125
0.01
8e-3
6e-3
4e-3
3e-3
2e-3
1.5e-3
1e-3
6e-4
4e-4
2e-4
1e-4
5e-5
2e-5
1e-5
5e-6
2e-6
1e-6
5e-7
Turbulent
Turbulent smooth flow
Turbulent smooth flow
Transition uncertainty area
Laminar
Darcy-Weisbach Friction Factor f =>
Reynolds Number Re =>
The Darcy-Weisbach friction factor f is for turbulent flow computed as
$\frac{1}{\sqrt{f}} = -\frac{2}{u_s} log_{10}\left[\left(\frac{1.547}{Re\sqrt{f}}\right)^{0.9445u_s} + \left(\frac{k_s}{3.7d}\right)^{u_s}\right]$
k_s = Equivalent sand grain roughness, as measured for high Reynolds numbers
u_s = surface structure uniformity factor
- u_s =1: Little uniformity in surface imperfection sizes (conservative)
- u_s =3: Average
- u_s =10: Very uniform surface (least conservative, gives lowest f)

Figure 2.9.1.

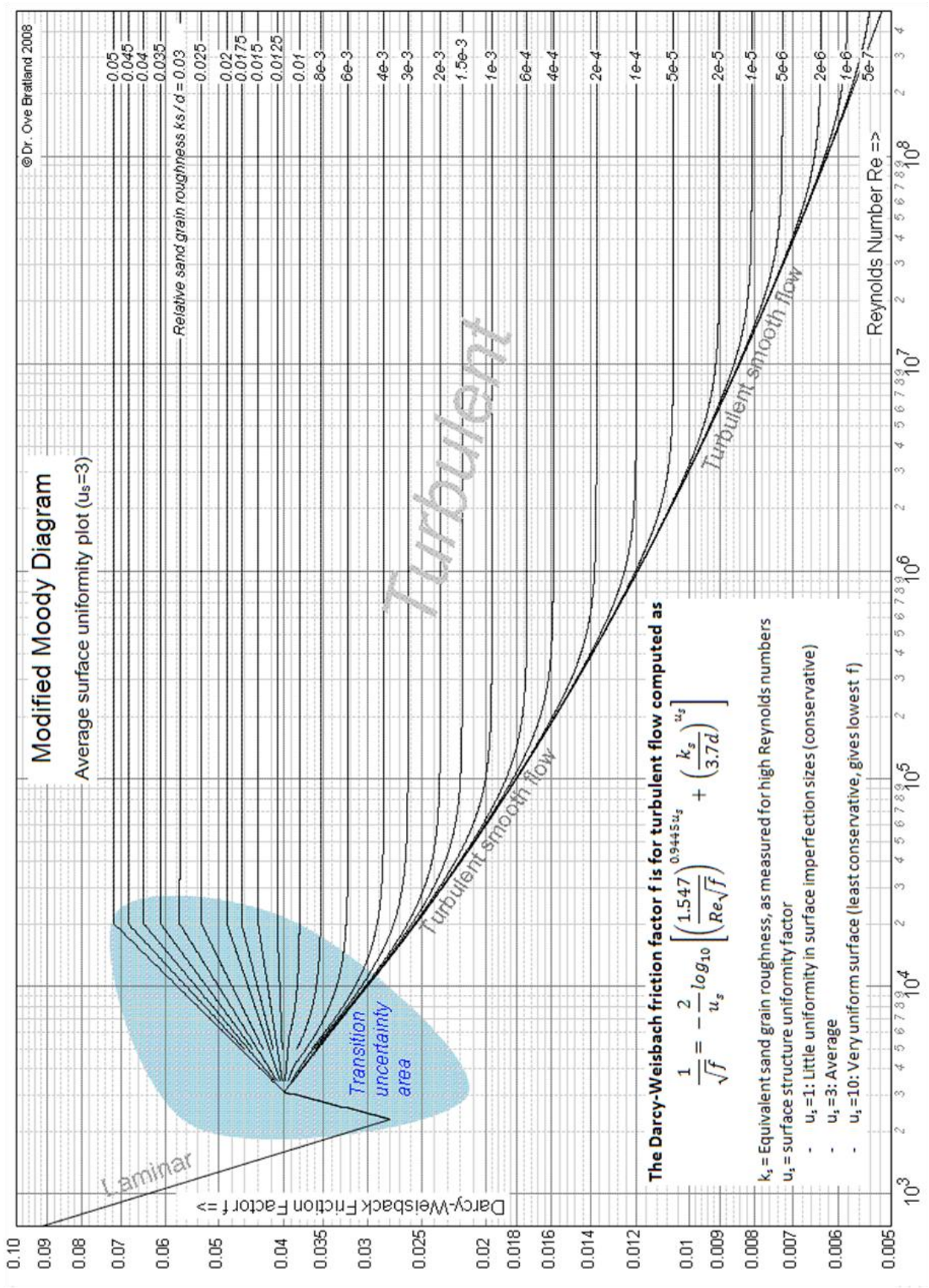


Figure 2.9.2.

For non-commercial use only

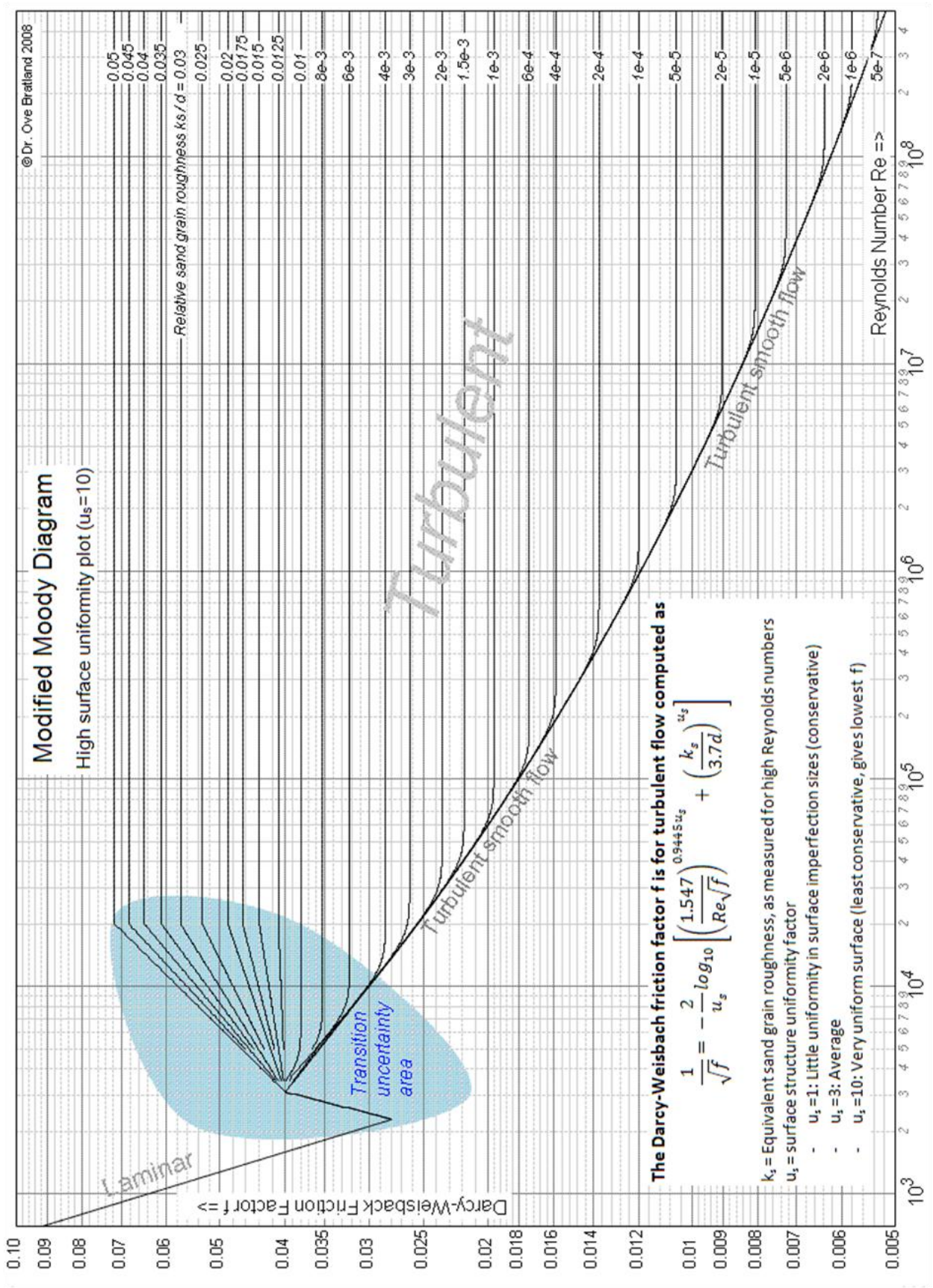


Figure 2.9.3.

For non-commercial use only

2.10 Fitting curves to measurements

As mentioned already, there are many measurements on industrial pipes where local friction factor minima of a similar type as those visible in Nikuradse's curves do exist. When we evaluate different surface treatment options in large pipeline projects, it may even make sense to perform full flow measurements on a short test-section of the pipe in order to establish accurate data. If those data show our pipeline to have local minima, as we know they may, how do we model that?

One way to attack the problem would be to try to reduce the influence from the second term in equation 2.9.4 somewhat in the area where a local minimum has been found to exist, but allow it to regain its influence for higher *Re*. We could modify it to:

$$\frac{1}{\sqrt{f}} = -\frac{2}{u_s} log_{10}\left[\left(\frac{1.547}{Re\sqrt{f}}\right)^{0.9445 u_s} + \left(k_d \frac{k_s}{3.7d}\right)^{u_s}\right] \tag{2.10.1}$$

Where k_d is a 'delay-factor', defined so that it has to grow from a low value where the curve has its minimum, for instance *0*, and approaching *1* for higher *Re* where we want the curves to follow the traditional rough pipe correlation. One mathematical function which has such properties is the so-called *sigmoid* function, which we can modify somewhat for our purpose by writing:

$$k_d = \frac{1}{1 + e^{(Re_d - Re)/{Re_d}^{n_d}}} \tag{2.10.2}$$

Where Re_d is the Reynolds number where we want a local minimum to be located (or very close to it), and n_d is a factor relatively close to *1*, which may be used to determine how wide the belly-like minima should be.

Some of the most convincing resent measurements covering the largest span of Reynolds numbers are those presented by Shockling et al. (2006). Their measurements were carried out on a drawn and thereafter honed *0.129 m* diameter aluminum tube carrying high-pressure gas. The surface elevation was found to have a Gaussian distribution. Their measurements clearly show an example of a curve with a local minimum, see figure 2.10.1. In the same diagram, we have played around with the four

 For non-commercial use only

parameters describing the pipe surface in equations 2.10.1 and 2.10.2, and have found the curve can be made to fit the measurements by letting $k_s/d = 6 \cdot 10^{-5}$, $u_s = 2.4$, $Re_d = 7 \cdot 10^5$ and $n_d = 1.1$.

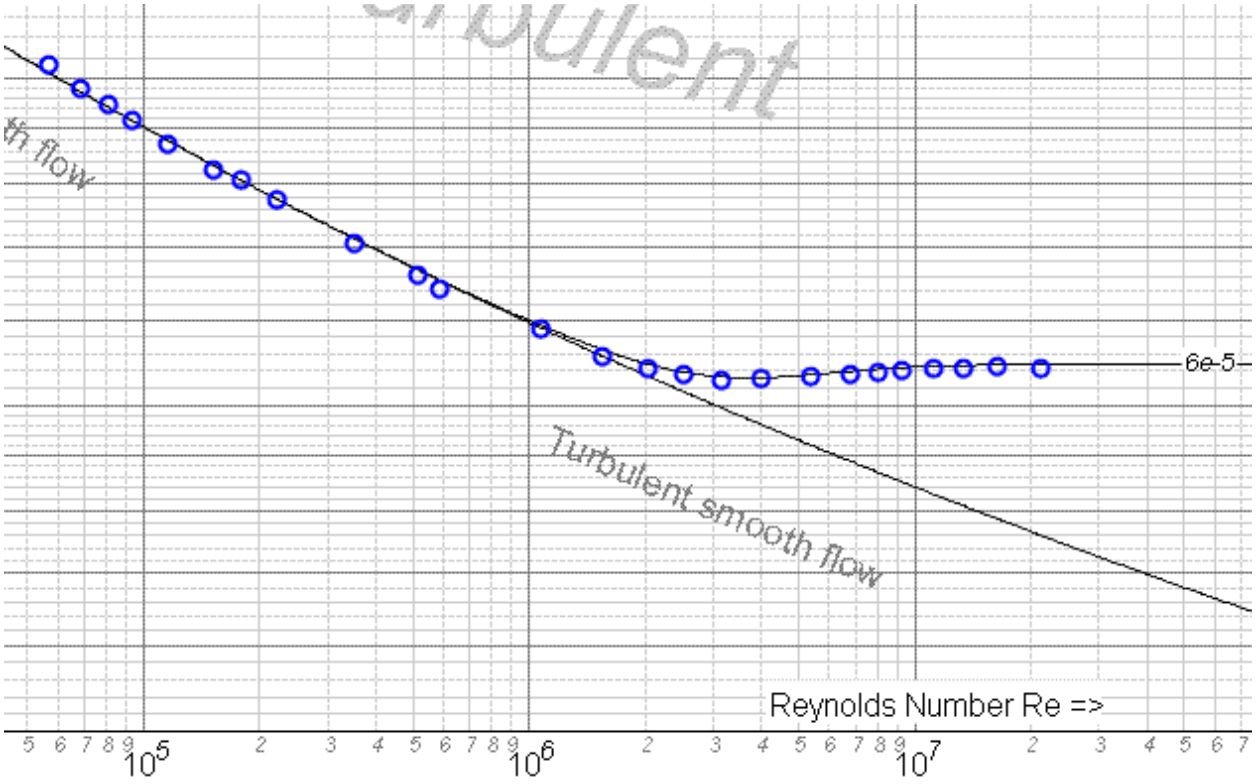
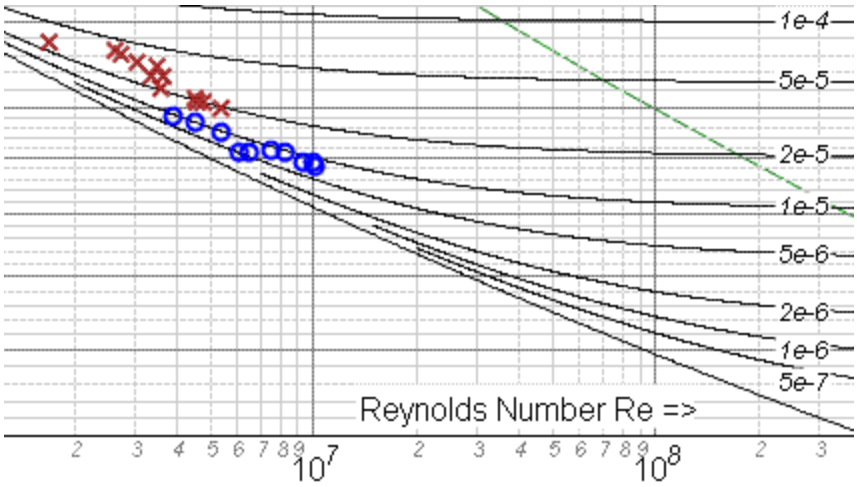
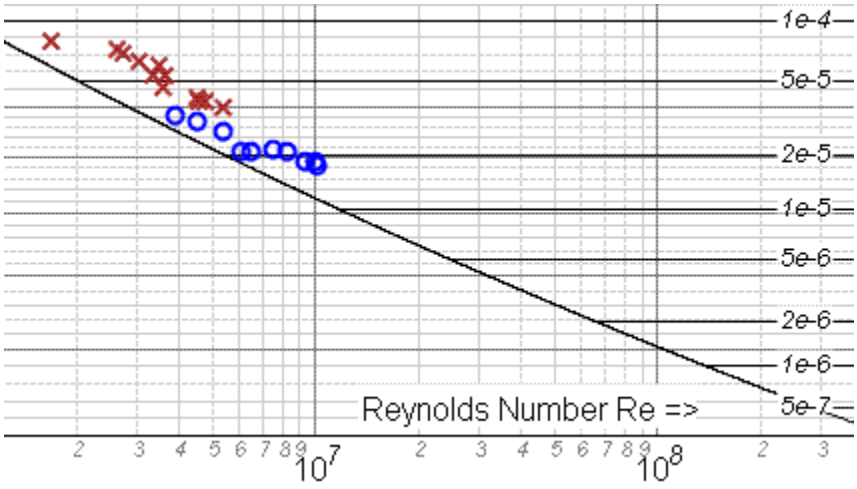


Figure 2.10.1. Curve fitted to measurements which show local minima for f. The measurements show that the fully rough, horizontal part of the modified Moody-curve corresponds to $k_s/d = 6 \cdot 10^{-5}$.

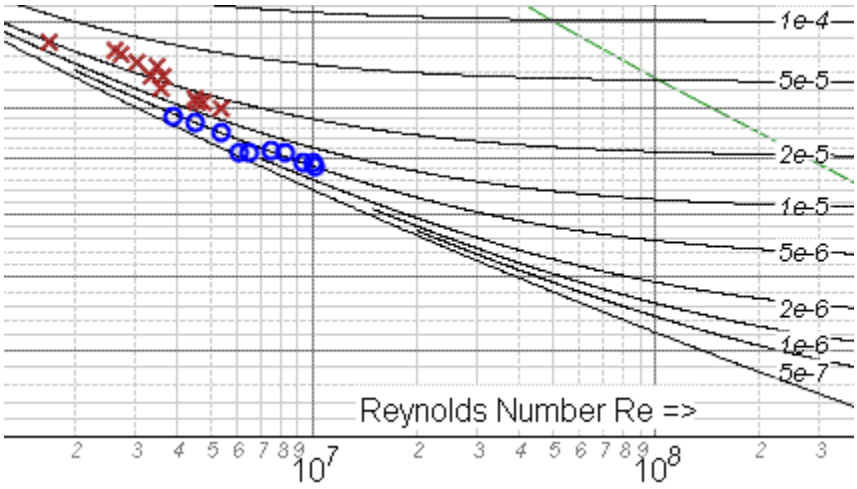
One may wonder why not equation 2.9.4 is simply replaced by equations 2.10.1 and 2.10.2 when plotting the general uniformity-based diagrams in figures 2.9.1 - 2.9.3 in the first place. The answer is it could have been, but there are some practical problems involved in doing so: We do not have sufficient knowledge to decide exactly how uniform a surface needs to be before it produces a local minimum, and we do not know where the local minimum would be located (and could therefore not select the right Re_d). Therefore, we would not be able to pick the right curves from more general diagrams even if we went ahead and created them. Besides, equations 2.10.1 and 2.10.2 contain too many empirical factors and therefore too many dimensions to allow easy plotting. This intricacy simply reflects the fact that real surfaces are so complex they cannot generally be represented by only one parameter. We can hope that the future brings more understanding of how surface structures are correlated to Darcy-Weisbach



Measurements from two hydro-power stations: Lucendro, Germany (red crosses), and Grytaaga, Norway (blue circles), plotted in the traditional Colebrook & White diagram. Interpreted this way, the two pipeline's relative roughness values look like they are in the order of $k_{s\ Lucendro}/d \approx 3 \cdot 10^{-5}$ *and* $k_{s\ Grytaaga}/d \approx 9 \cdot 10^{-6}$.



Assuming more surface uniformity (in this case by using the simplified AGA-diagram) , we reach quite different conclusions for the same measurements: $k_{s\ Lucendro}/d \approx 5 \cdot 10^{-5}$ *and* $k_{s\ Grytaaga}/d \approx 2 \cdot 10^{-5}$.



Using improved knowledge about smooth flow (as shown in the modified Moody diagram, figure 1.9.1 ($u_s = 1$*), we may estimate* $k_{s\ Lucendro}/d \approx 2 \cdot 10^{-5}$ *and* $k_{s\ Grytaaga}/d \approx 5 \cdot 10^{-6}$ *or less*

Figure 2.11.1. Alternative ways of interpreting the same measurements (data from Alming, 1977).

For non-commercial use only

friction factor curves, so that we will be able to predict the complete curve for any pipe with known surface structure. In the meantime, the most accurate method available is to fit curves for individual pipes based on hydraulic measurements the way it has been shown here. For the majority of engineering tasks, however, using equation 2.9.4 or the diagrams in figures 2.9.1 to 2.9.3 is the most realistic alternative. Since that is so, let us have a look at which sorts of accuracies we can expect to end up with when using equation 2.9.4 or the improved Moody diagrams in figures 2.9.1 - 2.9.3.

2.11 Friction factor accuracy

Literature about pipe flow contains numerous tables showing typical surface roughness values for different sorts of pipes. The Reynolds numbers and relative roughness values the data relate to should ideally have been stated, too, but that is rarely the case. The problems are exemplified by the measurements shown if figure 2.11.1.

Using different diagrams as basis leads to very different conclusions about the pipes' surface roughness. If we had used those data to make new estimates for relatively similar Reynolds numbers and relatively similar relative roughness values, the results might have been acceptable. That would no longer be the case of if we used the data far away from where they were measured. Note that the problem cannot be solved by simply always sticking to the same diagram. Even though the traditional Moody diagram has formed the basis for most published k_s-measurements, the fact that the real curves do not follow that diagram means extrapolation into other Re than those used in the measurements is going to be inaccurate.

So what sort of accuracy can we expect to achieve when we try to estimate the Darcy-Weisbach friction factor by using available tables, diagrams, and correlations, but without carrying out any measurements? It is an important, but difficult question. Let us start with the simplest part of the modified Moody diagrams: Laminar flow. Even there, where we already stated that the surface roughness does not play a role, it may indirectly do so since severe roughness may displace some of the pipe's effective cross-sectional area. Also, the pipe's tolerances affects the accuracy even for laminar flow, but all of these effects are in most cases very small compared to other errors. For simplicity, we here presume they are zero.

For turbulent flow, the error can be estimated by comparing the friction factor determined by equation 2.9.4 for $u_s = 1$, which corresponds to a Colebrook & White-like calculation (but based on improved knowledge of smooth pipe friction), and a large

structure uniformity factor (u_s = 20 is used here), which correspond to an AGA-like friction calculation (but also here with improved smooth pipe correlation):

$$\frac{\Delta f}{f} = \frac{f(u_s = 1) - f(u_s = 20)}{f(u_s = 1)} \tag{2.11.1}$$

As we can see, this error estimate is actually based on the fact that we do not know which u_s to use, since tables generally only give us k_s, not u_s.

In addition, an error for the uncertainties in the smooth-pipe curve fit, as given by Zagarola, needs to be added. He claimed that the errors could be kept within *1.2%* for *Re* from $3.1 \cdot 10^{-4}$ *to* $3.5 \cdot 10^{-7}$ for his most accurate equation. By comparing this with the equation we have used, an error below 1.3 % is assumed, and this is expected to grow towards 4% for Reynolds numbers below $3.1 \cdot 10^4$.

It is more difficult to estimate the error in the transition zone. It requires knowledge of exactly how transition takes place. On the other hand, it is less critical to have accurate knowledge of k_s and u_s in that zone, since the curves lie closer together. For the traditional Moody diagram, the error in this area would be in the order of the difference between laminar and turbulent estimates, since even a relatively moderate error in the Reynolds number could lead to choosing the wrong correlation. That could easily lead to errors in the order of up to 100 %. The modified Moody diagram has been designed to minimize this error, most likely down to a third or less of what the traditional Moody diagram could have produced. A combination of these considerations has been used to create figure 2.11.2.

The results show that the friction factor error may easily become 10 or even 15 % in the 'partly rough' zone. Best agreement can be expected for 'smooth' and 'fully rough' flow, where the error may be in the order of 2 %.

The main source of error is often going to be inaccuracy for the k_s-value selected from tabulated data (this error is not included in figure 2.11.2), not the modified Moody diagram as such. For instance, the tabulated k_s for newly painted steel is in table 2.12.2 given as "0.01-0.02 mm", the error involved in choosing k_s = *0,01* mm if our paint-job is somewhat below average (k_s = *0.02*, say,) can lead to a factor 2 between the correct and the used relative roughness. By looking at the modified Moody diagrams in figures 2.9.1 to 2.9.3, we see that this may easily lead to a 20 % error in the friction factor,

 For non-commercial use only

depending on where in the diagram it refers to. This error, though, gets smaller and smaller the closer we come to the 'smooth flow'-line, while the errors in figure 2.11.2 have local maxima for partly rough flow. Still, it may all in all be quite common to end up with errors in the order of 20 % or more for friction factors predicted at the design stage if no relevant measurements or reliable surface data from the manufacturer is available. That may be acceptable for some applications, but it is important to be aware of the moderate accuracy. For costly pipeline projects, carrying out early tailor-made laboratory measurements may sometimes make sense.

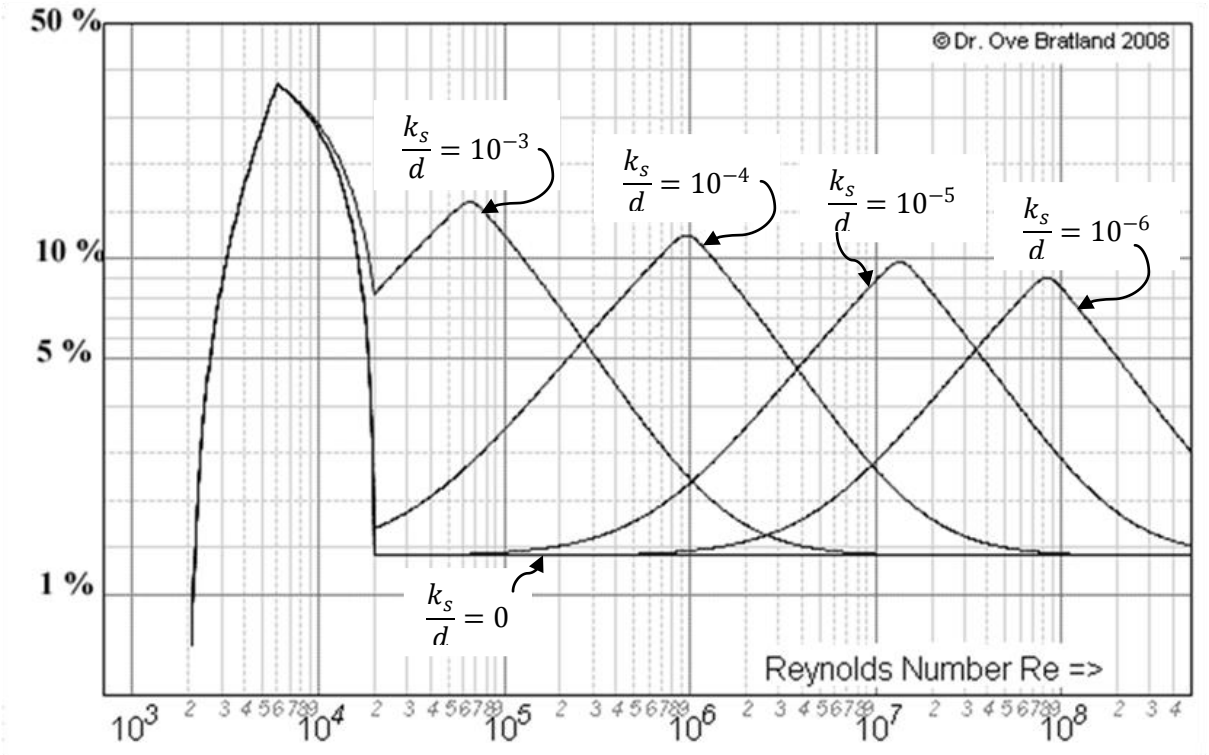


Figure 2.11.2. Friction factor errors for the modified Moody diagram, mainly due to not knowing u_s accurately.

2.12 Tabulated surface roughness data

Sletfjerding (1999) carried out measurements on 8 operational Norwegian high-pressure gas export pipelines with Reynolds numbers around $2 \cdot 10^7$, se table 2.12.1. Measured pressure losses were adjusted for expected weld losses according to the equations given in chapter 4.4, and after that, the Darcy-Weisbach friction factors were calculated. Three of the pipelines appear to lay slightly below Zagarola's 'smooth pipe'-curve, but none of them by more than 1.2%, which is within stated error margins.

Sletfjerding was unable to vary the Reynolds numbers in his field measurements, so it was not possible to see which diagram those measurements agreed best with. But he included sufficient data to enable us to calculate the equivalent absolute sand roughness k_s based on different diagrams.

Sletfjerding made progress in determining the equivalent sand grain roughness k_s from direct surface roughness measurements, rather than measuring the pressure loss and computing k_s from that, as has been the normal procedure for most other investigators. He concluded that of the different sorts of surface roughness parameters one may measure, the two of most relevance to pressure loss were something called the root mean square roughness, R_q, and a texture parameter he called H' (somewhat similar to the Hurst exponent mentioned in chapter 2.4). He found that it was possible to predict the friction factor in his relatively smooth, honed, artificially roughened large-diameter steel pipes according to:

$$\frac{1}{\sqrt{f}} = -\frac{1.89}{n} log_{10}\left[\left(\frac{1.55}{Re\sqrt{f}}\right)^n + \left(\frac{R_q/H'}{0.865d}\right)^n\right] \tag{2.12.1}$$

It implies that the Nikuradse's correlation, equation 2.5.2, can be replaced by:

$$\frac{1}{\sqrt{f}} = -1.89 log_{10}\left(\frac{R_q/H'}{0.865d}\right) \tag{2.12.2}$$

for the particular sorts of pipes Sletfjerding studied. His correlation does not in itself help in determining n (or u_s in equation 2.9.4), but is a step forward compared to always having to measure k_s hydraulically. Others have found that $k_s \approx 3k_{rms}$, where k_{rms} is surface root-mean-square-roughness-height, Zagarola et al. (1998) and Shockling et al. (2006). Like R_q and H', k_{rms} can conveniently be measured directly with surface measuring devices, meaning it can be found without carrying out any hydraulic experiments. Both Sletfjerding's, Zagarola et al.'s and Shockling al.'s measurements were done on relatively smooth pipes (k_s/d around 10^{-5}) and high Reynolds numbers (Re around 10^6), and it is not clear how they compare to drilled rock surfaces or any other very different sort of pipes. The concerns explained in chapter 2.8.5 lead us to believe

 For non-commercial use only

that this method works better for surfaces with high surface uniformity than those with low uniformity.

Sletfjerding also measured the pressure losses in some of the main high-pressure gas pipelines in the North Sea. In table 2.12.1, we have taken the raw data from those measurements as well as the k_s his measurements would have lead to if different diagrams were used as basis for the computations, see table 2.12.1. Chapter 2.11 and figure 2.11.1 explain in greater detail why different diagrams lead to different k_s for the same measurements.

Surface	d [m]	Re	f	Absolute roughness k_s [10^{-6} m]				
				Moody	AGA	Modified Moody u_s=1	Modified Moody u_s =5	Modified Moody u_s =10
Coated	0.9664	$1.84 \cdot 10^7$	0.00764	1.2	8.8	0	0	0
Coated	0.9664	$2.63 \cdot 10^7$	0.00738	1.5	5.4	0.05	2.8	4.2
Coated	0.9664	$1.61 \cdot 10^7$	0.00781	1.6	7.9	0	0	0
Coated	1.034	$1.89 \cdot 10^7$	0.00864	11	16	8.7	16	16
Coated	0.9664	$2.90 \cdot 10^7$	0.00721	1.0	4.6	0	0	0
Coated	1.034	$3.32 \cdot 10^7$	0.00776	4.8	8.1	3.6	8.0	8.1
Uncoated	0.6698	$1.81 \cdot 10^7$	0.00885	8.3	12	7.1	12	12
Coated	0.9664	$2.72 \cdot 10^7$	0.00747	2.0	5.9	0.7	5.0	5.7

Table 2.12.1. Estimated analog sand grain roughness k_s for 8 Norwegian high-pressure gas export steel pipelines.

Given that no surface can have zero roughness, those 3 which appear to be zero (underlined in table 2.12.1), are simply interpreted to have relative roughness below the point where the friction factor curves leave the 'smooth flow'-curve, leading to an absolute roughness of no more than $5.0 \cdot 10^{-6}$ *m* for the smoothest of them. According to these results, the 7 coated pipes have absolute surface roughness between $5 \cdot 10^{-6}$ and $16 \cdot 10^{-6}$ *m*. But we clearly face the same problem as explained for figure 2.11.1: It is not possible to define k_s without knowing u_s, so it is not possible to know what the pressure loss would have been at other *Re* than the ones used during the measurements.

The Crane report (1982) also gives data for some typical surfaces. It specifically states that the data is based on measurements for 'fully turbulent' flow. That gives a good definition for the friction we get at high *Re*, since all diagrams are based on the same correlation for fully rough flow. It does not, however, imply which diagram to use for partly rough flow.

Surface type	k_s [10^{-6} m]	Ref. diagram	Source
Drawn tubing	500	Moody	
Steel pipe, new, not painted	40-100	Moody	Muller&Stratman d~1-3m, Re~1-12·10^6
Steel, newly painted	10-20	Moody	Muller&Stratman, d~1-3m, Re~1-12·10^6
Steel, newly coated	05-16	Recomm., u_s = 10 (fig.2.9.3)	Sletfjerding see table 2.12.1 and description
Steel, paint partly flaked off	80-100	Moody	Muller&Stratman d~1-3m, Re~1-12·10^6
Steel, light corrosion	100-200		Muller&Stratman d~1-3m, Re~1-12·10^6
Steel, considerable corrosion	500-1000	Moody	Muller&Stratman d~1-3m, Re~1-12·10^6
Steel, severe corrosion	1000-3000	Moody	Muller&Stratman d~1-3m, Re~1-12·10^6
Asphalted cast iron	120	Any	Crane, fully turbulent
Galvanized iron	150	Any	Crane, fully turbulent
Cast iron	260	Any	Crane, fully turbulent
Concrete, smooth	0.3	Any	Crane, fully turbulent
Concrete, average	1.6	Any	Crane, fully turbulent
Concrete, rough	3.0	Any	Crane, fully turbulent
Riveted steel, smooth	910	Any	Crane, fully turbulent
Riveted steel, average	3,000	Any	Crane, fully turbulent
Riveted steel, rough	9,100	Any	Crane, fully turbulent
Wood stave	180-910	Any	Crane, fully turbulent
PVC, drawn tubing, glass	15	Any	Crane, fully turbulent

Table 2.12.2. Tabulated absolute equivalent sand roughness k_s for various surfaces.

2.13 Common friction factor definitions

The long history behind the current knowledge and common practice in single-phase pipe flow friction calculation has resulted in many different empirical correlations, and quite a few of them are still in use. That may create confusion sometimes. Mixing together the Darcy-Weisbach friction factor with Fanning's factor is probably one of the most common sources of error, since much of the literature call them both either f or λ.

As described by Schroeder (2001), Coelho et al. (2007) and many others, these are in fact far from being the only equations in use where the friction factor does not take the Darcy-Weisbach form. The Spitzglass equation, the Weimouth equation and the Panhandle A and B equations were originally developed for the gas industry. They all suffer from the same disadvantage as the Chezy, Hazen-Williams, and Manning correlations: The

 For non-commercial use only

friction factor is not dimensionless, and so it changes when switching from one unit system to another. It also suffers from the inconvenient practice that different industries sometimes invent their own ways of calculating pipe friction, making communication between different engineers and researchers more complicated than necessary.

Source	Equation	Comments
Antonine Chezy's coefficient C. C is not dimensionless. *Not recommended.*	$\Delta p = \frac{8\rho g}{C^2}\frac{l}{d}\frac{v^2}{2}$	Extremely novel when presented around 1770, but now discouraged.
H. Darcy & J. Weisback ***Recommended.***	$\boldsymbol{\Delta p = f\rho\frac{l}{d}\frac{v^2}{2}}$	Their publications from around 1850 never actually proposed the definition now bearing their name.
J.T. Fanning's factor f_f. ***Not recommended.***	$\Delta p = 4f_f\rho\frac{l}{d}\frac{v^2}{2}$	Frequently causes confusion since $f = 4f_f$. Using the more common Darcy-Weisbach f is recommended.
Hazen-Williams formula C_h is not dimensionless, and tabulating it requires the surface roughness to be given in an absolute, unit-system dependent manner. *Not recommended.*	$\Delta p = \frac{4.52}{{C_h}^{1.85}}\frac{Q^{1.85}}{d^{4.87}}$	Linked to one particular unit system (US shown here). The Darcy-Weisbach factor f and its corresponding pressure loss formula is both more general and more common.
Manning's formula Used for determining average velocity v, and thereby depth, in open channel flow. The roughness coefficient n_M is not dimensionless. s_m is slope in m/m. ***Not recommended.***	$v = \frac{1}{n_M}{s_m}^{1/2}\left(\frac{d}{4}\right)^{2/3}$	Frequently used for natural streams and floodplains, and a lot of data for n_M has been accumulated in tables. Still, the Darcy-Weisbach formulation should now be preferred (how to use it for open channels is elaborated later)

Table 2.13.1. Different friction factor definitions

Encountering different friction factor definitions is not the only challenge we face. Even when we use the preferred one – the Darcy-Weisbach friction factor – there are a number of competing formulas in use to calculate it. All this fragmentation probably goes a long way towards explaining why it has taken so long for even relatively old improvements in our knowledge base, such as ways to refine the Moody diagram, to become common engineering practice. Table 2.13.2 gives a brief overview of the most common traditional Darcy-Weisbach friction factor correlations.

Source	Equation	Comment
Blausius, smooth pipes.	$f = \frac{0.3164}{Re^{0.25}}$	4,000 < Re < 80,000. Limited application.
Prandtl-Von Karman, smooth pipes.	$\frac{1}{\sqrt{f}} = -2\log_{10}\frac{2.51}{Re\sqrt{f}}$	Based on Re<3.4·10^6
Nikuradse, fully turbulent regime.	$\frac{1}{\sqrt{f}} = -2\log_{10}\frac{k_s}{3.7d}$	Based on Re<3.4·10^6
Colebrook & White Much used, but has important limitations.	$\frac{1}{\sqrt{f}} = -2\,log_{10}\left(\frac{2.51}{Re\sqrt{f}} + \frac{k_s}{3.7d}\right)$	Basis for the traditional Moody diagram
Uhl et al., based on Prandtl	$\frac{1}{\sqrt{f}} = -2\log_{10}\frac{2.825}{Re\sqrt{f}}$	Only valid for smooth pipes.
Haaland's explicit approximation of Colebrook & White's original equation.	$\frac{1}{\sqrt{f}} = -1.8\,log_{10}\left[\frac{6.9}{Re} + \left(\frac{\varepsilon}{3.7d}\right)^{1.11}\right]$	Agrees within 1.5% relative error with Colebrook & White's equation.
AGA simplified (stripped of AGA's factors for bends)	$\frac{1}{\sqrt{f}} = -2\log_{10}\frac{2.825}{Re\sqrt{f}}$ $\frac{1}{\sqrt{f_t}} = -2\log_{10}\frac{k_s}{3.7d}$ $f = min(f_s, f_t)$	Gives somewhat lower friction factor than Colebrooke & White in the transition zone.

Table 2.13.2. Traditional Darcy-Weisbach friction factor correlations

Source	Equation	Comment
Surface uniformity-based. For 2,300 < Re ≤ 3,100, it is based on Nikradse's measurements and Kolmogorov's turbulence theory.	Re ≤ 2,300 (laminar, correlation a): $f = \frac{64}{Re}$ Re ≥ 20,200 (turbulent, correlation b): $\frac{1}{\sqrt{f}} = -\frac{2}{u_s}log_{10}\left[\left(\frac{1.547}{Re\sqrt{f}}\right)^{0.9445u_s} + \left(\frac{k_s}{3.7d}\right)^{u_s}\right]$ 2,300 < Re ≤ 3,100 (turbulent, correlation c): Straight line from point p_1 to point p_2, where *p_1(Re=2,300; $f = \frac{64}{Re}$), p_2(Re=3,100; f=0.04)* 3,100 < Re ≤ 20,000 (turbulent, correlation d): Straight line from point p_2 to point p_3, where *p_3(Re=20,000; f computed as for correlation b)*	Much in common with Sletfjerding's and Gersten's correlations, but interprets u_s as a surface uniformity property independent of liquid properties. Also, it improves accuracy for 2,300<Re<20,000. Diagrams in figure 2.9.1 - 2.9.3 are based on these correlations.

Table 2.13.3. Friction factor correlations proposed in this book, no measurements available

For non-commercial use only

This book's recommendations for normal friction calculations are shown in table 2.13.3. These equations are also illustrated in the modified Moody-diagrams in figures 2.9.1-2.9.3.

When measurements are available, better curve fit can normally be achieved with the equations in table 2.13.4.

Source	Equation	Comment
Surface uniformity based, suited for curve fit when measurements are available	$\frac{1}{\sqrt{f}} = -\frac{2}{u_s} log_{10}\left[\left(\frac{1.547}{Re\sqrt{f}}\right)^{0.9445u_s} + \left(k_d \frac{k_s}{3.7d}\right)^{u_s}\right]$ $k_d = \frac{1}{1 + e^{(Re_d - Re)/{Re_d}^n d}}$	One extra term added to the surface uniformity based equation, to enable it to re-produce minima,

Table 2.13.4. Friction factor correlation proposed in this book, used for curve fitting to measurements when they exist

2.14 Transient friction

The presented friction factor diagrams and correlations are all based on the flow being steady-state. But how can we calculate the friction when the flow varies over time? As shown by Zielke (1968), Trikha (1975), Ham (1982), and Bratland (1986), there are several methods available for calculating transient friction very accurately for laminar flow, and doing so must now be considered relatively trivial.

Transient turbulent friction, a much more frequently encountered phenomenon, is generally not as well understood, but it is clear that the transients can make the friction several orders of magnitude higher than the steady-state friction. Brekke (1984) has developed a frequency-domain model for improved stability analysis of hydro power plants, and it has a built-in transient friction estimator which seems to work well for pulsations superimposed on a relatively high average flow. Somewhat more general models have been presented by Zarzycki (2000), Vardy et al. (1994) and several others, and their models represent clear improvements compared to using steady-state friction factors directly. But the subject is complicated, and no one has succeeded in developing a general, well documented and practical theory.

Instead of going into details about the available models, let us try to give some rules for when we can get away with using steady-state friction rather than going to greater sophistication.

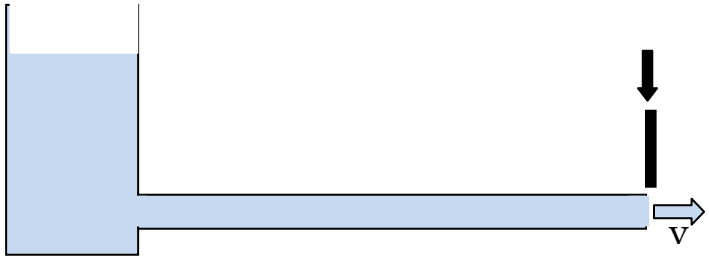


Figure 2.14.1. Straight pipe with fast-closing valve at the end.

To illustrate which mechanisms affect the friction factor, consider first a pipe with laminar flow. By using Newton's law, equation 2.2.1, it is relatively easy to show that steady-state laminar velocity profiles are described by:

$$\frac{v(r)}{v_{max}} = \left(1 - \frac{r}{R}\right)^2 \tag{2.14.1}$$

Suppose a valve at the end of the pipe is suddenly closed. One may at first expect this to stop all the fluid immediately after the closure so all particles near the valve come to rest. For that to happen, however, particles near the center of the pipe, which has a higher initial velocity than those closer to the wall, would have to be stopped simultaneously. Instead, the instantaneous pressure step resulting from the closure leads to the same velocity step for all fluid particles in each cross section, and continuity means the average velocity becomes zero. Those particles close to the center continue at a reduced speed towards the closed valve, while those close to the wall are forced backwards away from it. Therefore, closure does not mean the fluid just upstream from the valve comes to rest immediately.

This is illustrated in figure 2.14.2. *Curve 1* is the velocity profile before closure and *curve 2* the profile just after. *Curve 2* is very similar to curve 1, but it has been moved to the left so that the flow is zero. This leads to a very sharp velocity gradient near the wall, and the instantaneous friction can become very high just after closure. Gradually, friction removes more and more of the kinetic energy, and after awhile, the velocity

 For non-commercial use only

profile looks like curve 3, before the fluid eventually comes to rest. The curves are actual simulations of how flow develops, not mere illustrations. The results have been shown to agree with measurements carried out by Holboe & Rouleau (1967), (Bratland 1986).

What is of interest here, though, is observing that velocity gradients near the wall can become very steep after fast changes in the average velocity. In this particular example, the average velocity obviously becomes zero after closure, but the friction does not. The Darcy-Weisbach friction factor f would have to be infinite to describe the non-zero friction! It is also possible for the fluid closest to the wall to temporarily go in the opposite direction of the average velocity, leading to a negative f.

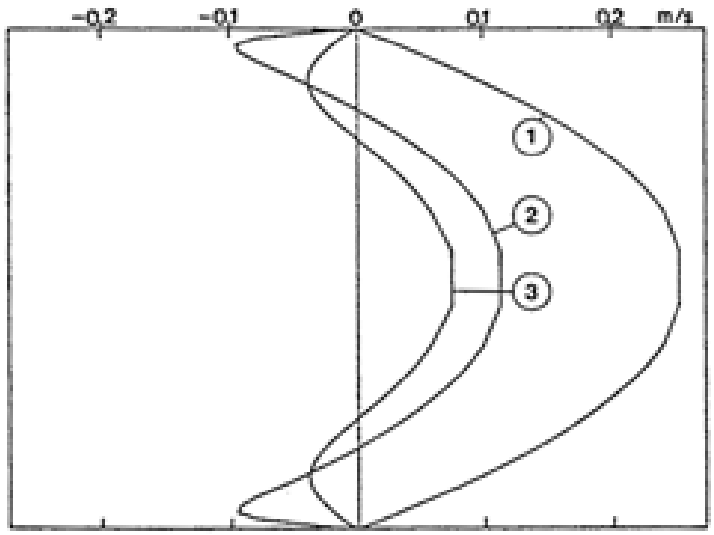


Figure 2.14.2. Velocity profiles near the valve at different times after closure, laminar flow.

In turbulent flow, both the steady-state and the transient velocity profiles appear slightly different than these laminar profiles, but the main mechanisms remain the same: Transients deform the velocity profile, and that makes f differ from what steady-state correlations predict. The frequency-dependent friction, as it is sometimes called, tends on average to be much higher than steady-state friction.

If Re is constant over a relatively long period of time, the friction factor approaches the steady-state value. Accurate criteria for how long it takes to reach steady-state do not exist. But one may compare with how a velocity profile develops at a pipe's inlet, where it is generally accepted that the profile is fully developed around *30 diameters* into the pipe. It is therefore reasonable to assume steady-state friction once the average velocity has been relatively constant as long as it takes to travel 30 diameters:

$$t_{steady} = \frac{30d}{v_{steady}} \tag{2.14.2}$$

where t_{steady} is the time it takes for from the velocity, v_{steady}, becomes constant until the friction has become steady-state, too, meaning the normal Darcy-Weisbach friction calculations have become valid.

In very long pipelines, it takes hours and even days to change the velocity significantly, and under such conditions, transient friction can safely be neglected. The friction factor may simply be computed from equation 2.9.4 and updated every time the Reynolds number changes. That is good news to the engineer since it means frequency-dependent friction is not something to worry about in most cases. The exceptions are systems where fast changes in Reynolds number occur, and where those changes can have significant effect on the problems of interest. There are at least two important situations when transient friction cannot be neglected:

In long pipelines with slow pressure and mass flow variations the friction can be calculated as if it were steady-state.

1. In some cases we are interested in studying hydraulic noise attenuation, for instance downstream of pumps. The noise corresponds to velocity transients and may be in the range of hundreds or thousands of Hz. Under such conditions, the frequency-dependent part of the friction may be orders of magnitude higher than the steady-state part, and the noise ripples are damped much faster than the steady-state friction would suggest. Accurate prediction of the damping is obviously not possible by using steady-state friction. In the case of laminar flow, Ham's frequency-domain model may offer the simplest and most effective approach (Ham, 1982), but as mentioned above, time-domain models are also available.
2. In many hydropower plants, regulators maintain constant turbine speed during varying load conditions by controlling the water flow through each turbine. If, for instance, a consumer switches off his air conditioner, the regulator responds to the reduced load by reducing the nozzle or guide vane opening. The water in the penstock may have high enough inertia for the retardation to lead to a significant pressure increase at first, and that in turn gives higher rather than lower power output. Stabilizing such regulators is therefore difficult, and large, expensive surge tanks are often needed to ensure proper operation. The frequency-dependent

 For non-commercial use only

friction works to improve stability, and accurate prediction and utilization of it enables cheaper designs.

Much of the theoretical work done on transient turbulent friction has focused on instantaneous valve closure and how the reflected pressure surges gradually dissipate after the first, initial surge. Such cases represent a well-defined reference, but paradoxically, they are of little interest in most engineering situations. The maximum pressure occurring in first surge is not much affected by the friction's frequency dependence, and the later reflections are typically smaller than the first one, making the exact damping of those of little concern. When the average flow is non-zero, which is what we have to deal with when studying noise propagation or highly dynamic regulators, the turbulent eddies responsible for most of the friction are constantly re-energized, and it is not obvious that the newer, relatively fragile models give adequate results under such conditions.

2.15 Other sorts of friction in straight, circular pipes

All the friction discussed so far is of the hydraulic type. But energy may also dissipate in the pipe wall itself. That sort of friction is not hydraulic, it has nothing to do with the type of fluid or surface roughness, and it only affects transients. To understand how it works, consider a pipe carrying fluid under increasing pressure. Since any material is elastic to at least some extent, the pipe wall expands, and it stores potential energy in the process. If the pressure later falls, that energy is fully regained, at least if the pipe wall is completely elastic. But for high pressure hydraulic hoses, for instance, the different layers in the hose may move against each other, and the materials may also be partly visco-elastic. Therefore, some of the energy is not re-gained, and the overall effect appears in much the same way as hydraulic friction. It has been shown that this can be the dominating way in which noise and vibrations dissipate. It also plays an important part for blood flow pulsations (Bohle et al, 2004).

Energy dissipation due to internal friction in the pipe wall is very low in steel pipes and can safely be neglected in most pipelines.

For steady-state calculations, visco-elastic pipe wall friction does not play a role, and it can nearly always be ignored for transient calculations for metal pipes, too. Relatively accurate, easy-to-use models exist, and details can be found in Bratland (1995) and Stein et al. (2004).

2.16 Friction factor summary

For circular pipes carrying single-phase Newtonian fluids, friction calculations can be summarized as follows:

1. The preferred definition of the friction factor f is the Darcy-Weisbach definition, as shown in equation 2.1.6.
2. The traditional Moody diagram is still the most used way to determine f, even though some major limitations apply to it: It over-estimates the 'smooth pipe'-friction for $Re > 10^6$, and it is very inaccurate around $Re = 10^4$. Also, it neglects the fact that different pipes have different shaped friction factor curves. Therefore, the Moody diagram should be replaced by the surface uniformity factor based diagrams shown in figures 2.9.1-2.9.3. They are based on equation 2.1.7 for $Re \leq 2{,}300$ and equation 2.9.4 for $Re \geq 20{,}0000$ and a gradual transition between those equations in the area around $Re = 10^4$, as outlined in chapter 2.9 and table 2.13.3.
3. When the surface structure uniformity factor u_s is unknown, one may opt for the most conservative estimate by setting $u_s = 1$. The expected friction factor accuracy can be read out of figure 2.11.2 as a function of relative roughness and Reynolds number. Errors may be larger than 10% even when an accurate roughness value is available, and up to 20% or even more when relatively inexact, tabulated roughness values must be relied on.
4. For large pipeline projects, it may be cost-effective to improve accuracy by carrying out measurements on pipeline sections in the laboratory before making the final decision on diameter and inner surface treatment. The measurements need to focus on both k_s and u_s, meaning the friction factor needs to be measured for a range of Reynolds numbers. Even better curve fits can be produced by using equations 2.10.a and 2.10.2.
5. When operating pipelines close to the 'smooth pipe'-line, as is often the case for high pressure gas pipelines, very high sensitivity to surface roughness must be expected. The friction factor may often be reduced very significantly by choosing appropriate coating or other surface treatment.
6. Even moderate changes in relative roughness due to corrosion, wear, coating damage, and other unfavorable developments with time can have very significant effect on a pipeline's capacity. It is therefore desirable to estimate these effects during design, and to consider over-sizing according to uncertainties in those estimates.

 For non-commercial use only

7. In some calculations, transient friction is important. This is most likely to be the case when investigating noise due to hydraulic pulsations or when stabilizing fast-acting regulators, such as those governing water turbines. The pipe wall's visco-elastic properties can in some rare cases also be of importance, particularly for non-metallic pipes.

References

Blasius, H. (1913): *Das Ähnlichkeitsgesetz bei Reibungsvorgängen in Flüssigkeite.,* Forschungs-Arbeit des Ingenieur-Wesens 131. (In German).

Richardson, L. F (1922): *Weather Prediction by Numerical Process.* Cambridge University Press.

Nikuradse, J. (1932): *Gesetzmessigkeiten der Turbuklenten Stromung in Glatten Rohren.* In Forschungsheft 356, Volume B. VDI Verlag Berlin, Sept/Oct. Translated in NASA TT F-10, 359. (In German)

Nikurdse, J. (1933): *Stromungsgsetze in Rauhen Rohren.* In Forschungsheft 361, Volume B. VDI Verlag Berlin, Jul/Aug. Translated in NACA Technical Memorandum Nr. 1292, 1950. (In German)

Colebrook, C. F. and White, C. M. (1937): *Experiments with fluid-friction in roughened pipes.* Proc. Royal Soc. London, 161, 367-381.

Colebrook, C.F. (1939): *Turbulent Flow in Pipes, With Particular Reference to The Transition Regime between Smooth and Rough Pipe Laws.* Institution of Civ. Eng. Journal,11:133-156, paper No. 5204.

Kolmogorov, A. N. (1941): *The local structure of turbulence in incompressible viscous fluid for very large Reynolds numbers.* Dokl. Akademik Nauk SSSR 30, 299-303 (In Russian).

Rouse, H. (1943): *Evaluation of boundary roughness.* Proceedings Second Hydraulics Conference, Univ. of Iowa Studies in Engrg., Bulletin No. 27.

Moody, L. F. (1944): *Friction factors for pipe flow.* Trans. ASME, 66:671-678

Clauser, F.H. (1956): *The turbulent boundary layer.* Advan. Appl. Mech., 4, 1.

Ito, H. (1960): *Pressure Losses in Smooth Pipe Bends*, Trans. ASME, J. Basic Eng., Vol. 82, p. 131.

Gunn, D.J., Darling, C.W.W. (1963): *Fluid Flow and Energy Losses in Non Circular Conduits*, Trans Inst Cham Eng. No. 41, 163.

Uhl, A.E. (1965): *Steady Flow in Gas Pipelines.* Institute of Gas Technology, Technical Report No. 10, American Gas Association.

U.S. Department of the Interior, Bureau of Reclamation (1965): *Friction Factors for Large Conduits Flowing Full. Engineering Monograph No. 7.*

Holmboe, E.L., Rouleau, W.T. (1967): *The Effect of Viscous Shear on Transient In Liquid Lines*, ASMEJ. Basic Eng., 89(1), pp. 174-180.

U.S. Army Engineers Waterways Experiment Section. (1969, revised 1977): *Hydraulic Design Criteria, Sheet 224-1/1 Resistance Coefficients Steel Conduits.*

Bird, R.B., Stewart, W.E., Lightfoot, E.N. (1973): *Transport Phenomena*, John Wiley and Sons, New York City.

Trikha, A. K. (1975): *An efficient method for simulating frequency-dependent friction in liquid flow* J. Fluids Eng., Vol 97(1), 97 – 105.

Alming, K. Hydro *power plants.* (1977): *Lecture notes from Subject 63550 Water Turbines and Pumps*. The Norwegian Institute of Technology, The Water Power Laboratory. (In Norwegian).

Crane Technical Paper No. 410 M. (1982): *Flow of fluids through valves, fittings and pipe*, Crane Co.

Thomas, T. (1982): *Rough Surfaces.* Longman Group Limited, London.

Ham, A. (1982): *On The Dynamics of Hydraulic Lines Supplying Servosystems.* Laboratorium Voor Verktuigkundige Meet – En Regeltechniek, Delft.

Van Dyke, M. (1982): *An Album of Fluid Motion.* The Parabolic Press, Stanford.

Haaland, S.E. (1983): *Simple and Explisit Formulas for The Friction Factor in Pipe Flow.* Journal of Fluids Engineering, 105:89-90.

Brekke, H. (1984): *A stability study on hydro power plant governing including the influence from a quasi non-linear damping of oscillatory from the turbine characteristics.* Dr. techn. dissertation, NTNU, Trondheim.

Bratland, O. (1986): *Frequency-Dependent Friction and Radial Kinetic Energy Variation in Transient Pipe Flow*. 5th International Conference on Pressure Surges, Paper D2, BHRA.

Vardy, A.E., Hwang, K. (1991): *A Characteristics Model of Transient Friction*, Journal of Hydraulics Research 29, No. 5: 669-684.

Idelchik, I.E. (1992): *Handbook of Hydraulic Resistance*. 3. Edition, Moscow Machine Institute (In Russian). (2. Edition exists in English translation from Hemisphere Publishing Corporation.)

Caetano, E.F., Shoham, O., Brill, J.P. (1992): *Upward vertical Two-Phase Flow Through an Annulus, Part I: Single-phase Friction Factor, Taylor Bubble Rise Velocity and Flow Pattern Prediction*. J. Energy Res. Tech, 114, 1.

Frish, U. (1995): *Turbulence: The Legacy of A.N. Kolmogorov.* Cambridge University Press

Bratland, O. (1995): *Simulation Models of Subsea Umbilicals, Flowlines and Fire Pump Systems.* Offshore Technology Center, 7715

Zagarola, M.V. (1996): *Mean-Flow Scaling of Turbulent Pipe Flow.* PhD Thesis, Priceton University.

Pennington, M.S. (1998): *Hydraulic Roughness of Bored Tunnels.* IPENZ Transactions, Vol. 25, No.1/CE, 1998.

Zagarola, M.V., Smits, A.J. (1998): *Mean-flow Scaling of Turbulent Pipe Flow*. Journal of Fluid Mechanics.

Sletfjerding, E. (1999): *Friction Factor in Smooth and Rough Gas Pipelines*. Ph.D. Thesis, The Norwegian Institute of Technology, Trondheim.

Gersten, K., Papenfuss, H. –D., Kurschat, T., Genilliion, P., Fernández Pérez, F., Revell, N. (2000): *New transmission-factor formula proposed for gas pipelines*. Oil and Gas Journal, February 14.

Pope, S.P. (2000): *Turbulent Flows.* Cambridge University Press. Reprinted with corrections (2003).

Antonia, R.A., Pearson, P.R. (2000): *Reynolds number dependence of velocity structure functions in a turbulent pipe flow*. Flow, Turbulence and Combustion, 64 95-117 (2000) [C1]

Zarzycki, Z. (2000): *On Weighing Function for Wall Shear Stress During Unsteady Turbulent Pipe Flow*, Proc. of the 8th International Conf. on Pressure Surges, BHRGroup, The Hague, The Netherlands.

Sletfjerding, E., Gudmundsson, J.S., (2001): *Friction Factor in High Pressure Natural Gas Pipelines from Roughness Measurements.* International Gas Research Conference, November 5-8, Amsterdam.

Schroeder, D.W. (2001): *A Tutorial on Pipe Flow Equations.* Pipeline Simulation Interest Group, paper 0112.

Oertel, H., Bohle, M., Etling, D., Muller, U., Screenivasan, K.R., Riedel, U., Warnatz, J. (2004): *Prandtl's Essentials of Fluid Mechanics.* Springer.

Stein, E., Borst, R.D., Hughes, T.J.R., (2004): *Encyclopedia of Computational Mechanics*. Wiley.

Taylor, J.B, Carrano, A.L., Kandlikar, S.G. (2005): *Characterization of The Effect of Surface Roughness and Texture on Fluid Flow – Past, Present and Future.* Proceedings of ICMM2005, 3rd International Conference on Microchannels and Minichannels, Paper No. ICMM2005-75075.

Gioia, G., P. Chakraborty. (2006): *Trubulent Friction in Rough Pipes and the Energy Spectrum of the Phenomenological Theory.* Physical Review Letters, PBRL 96, 044502.

Shockling, M.A., Allen, J.J., Smits, A.J. (2006): *Roughness Effects in Turbulent Pipe Flow.* Journal of Fluid Mechanics.

Coelho, P.M., Pinho, C. (2007): *Considerations about equations for steady state flow in natural gas pipelines.* Journal of the Brazilian Society of Mechanical Sciences and Engineering, Print ISSN 1678-5878.

Langelandsvik, L.I., Kunkel, G.J., Smiths, A.J. (2007): *Flow in a commercial steel pipe.* Journal of Fluid Mechanics.

"Everything flows, nothing stands still."
Heraclitus of Ephesus

3 Friction in non-circular pipes

This chapter covers:

- Hydraulic diameter for non-circular pipes
- Friction in partially-filled pipes
- Friction in rectangular, annular and elliptic cross-sections

3.1 General

For circular pipes flowing full, the Reynolds number was defined by the diameter d in equation 2.1.8. For non-circular pipes or open channels, there is of course no such thing as a diameter. To be able to define Re, we replace d with hydraulic diameter d_h:

$$Re = \frac{v d_h}{\nu} \tag{3.1.1}$$

Where d_h is defined from the pipe's cross sectional area, A, and the vetted perimeter of the cross section, O, meaning the part of the perimeter in contact with the liquid, as:

$$d_h \overset{\text{def}}{\equiv} \frac{4A}{O} \tag{3.1.2}$$

In particular case of a circular pipe, this definition leads to the hydraulic diameter being the same as the pipe's inner diameter. Note that equation 3.1.2 is simply a definition, not a claim that any differently shaped cross-section must result in the same friction if the hydraulic diameter is identical. We will soon see that a rectangular pipe, for instance, does not have exactly the same friction loss as a circular pipe even when they have the same d_h. But it turns out that the difference tends to be small for relatively similar cross sections. Let us have a look at some examples.

3.2 Partially-filled pipe

A partially-filled pipe containing liquid, as shown in figure 3.2.1, is a situation encountered frequently in drain pipes. How is the friction in such a situation?

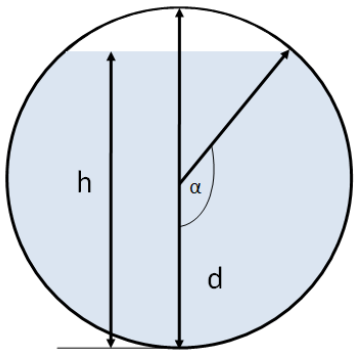


Figure 3.2.1. Partly-filled pipe.

As far as the liquid is concerned, the empty part of the pipe does not exist in the sense the liquid experiences no influence from it (not completely true if the 'empty' part contains something else, such as air, but a fair approximation in this case). O is the part of the pipe wall in contact with the fluid (the lower part, where the liquid touches the pipe wall on figure 3.2.1):

$$O = \alpha d \tag{3.2.1}$$

The filled part of the cross-section is:

$$A = \frac{d^2}{4}\left(\alpha - \frac{\sin 2\alpha}{2}\right) \tag{3.2.2}$$

And the hydraulic diameter becomes:

$$d_h = d\left(1 - \frac{\sin 2\alpha}{2\alpha}\right) \tag{3.2.3}$$

This result leads to further conclusions if we observe the following: If this is steady-state flow, it means both h and a stay constant (liquid does not accumulate or disappear). For this to be the case, the pipe has to slope downwards at a constant angle, and the friction force has to balance the gravitational force. This is the same situation we generally have in an open channel, which is what the pipe behaves like here.

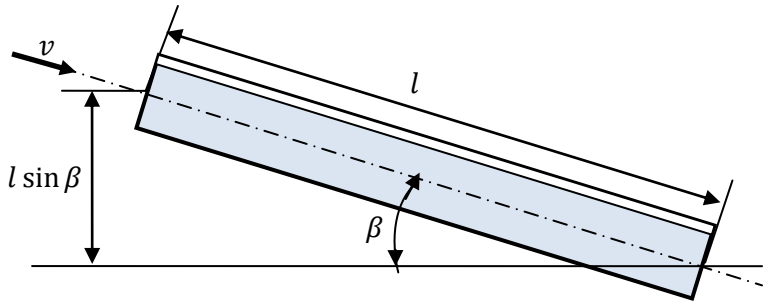


Figure 3.2.2. Partly filled pipe sloping downwards.

If the downward angle is called β, the friction loss of a length l of the pipe can be used to establish the following balance:

$$Required\ pressure\ to\ hold\ a\ static\ head\ of\ l\sin\beta = friction\ loss$$

$$\rho g l \sin\beta = \frac{f\rho l}{2d_h}v^2 \tag{3.2.4}$$

This leads to:

$$v = \sqrt{\frac{2gd_h \sin\beta}{f}} \tag{3.2.5}$$

We see the velocity is a function of the hydraulic diameter, d_h, which we already found an expression for in equation 3.2.3. If we change d_h, that will obviously affect the Reynolds number and hence the friction factor f. To avoid getting lost in details, we will here neglect that and pretend f is constant, so that:

$$v = Const \cdot \sqrt{d_h} \tag{3.2.6}$$

h on figure 3.2.1 can be expressed as:

$$h = \frac{d}{2}(1 + \cos\alpha) \tag{3.2.7}$$

We are able to plot the velocity as a function of how full the pipe is, see figure 3.2.3.

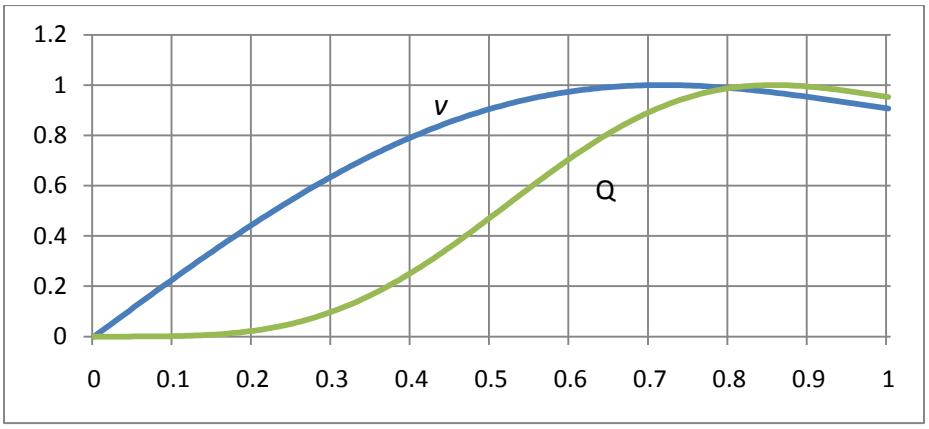


Figure 3.2.3. Velocity v and flow Q as function of h.

In the same diagram, we have also plotted the flow $Q = A \cdot v$. Both the average velocity and the flow reach maxima some time before the pipe flows full. The reason is that filling the pipe completely increases the friction by bringing a larger part of the liquid in contact with the wall.

 For non-commercial use only

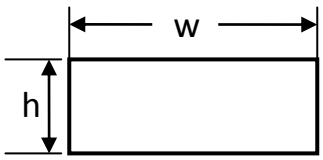
In spite of the relatively rough approximations made here, the result corresponds with phenomena observed in real life. A drain pipe, for instance, can be more or less empty on a dry day. When it starts raining, it gradually fills up as it must handle an ever increasing flow. Once the water surface reaches between *80* and *90 %* of the diameter, further increase in level leads to reduced capacity. This is an unstable situation: Increased h leads to lower capacity, which in turn leads to even higher h and so on, and the pipe fills quickly once the maximum capacity-level has been reached. The instability makes it unpractical to try to increase pipe capacity by controlling the level to just below full. We see the potential gain is minimal, and avoiding the pipe getting full is difficult once the level has risen to near-full.

3.3 Rectangular pipe

In the partly-filled pipe example, we pretended that a Reynolds number based on the hydraulic diameter can be used directly to calculate the Darcy-Weisbach friction factor from the same correlations as for a circular pipe. That works relatively well for many sorts of cross-sections, but the geometry may have impact on more than just the Reynolds number. In the general case it is therefore necessary to include a geometric correction factor, k_g, to account for this effect, so the total friction factor becomes:

$$f = k_g f_{circular} \tag{3.3.1}$$

$f_{circular}$ is determined in the same way as explained for circular pipes in chapter 2. For instance, a rectangular pipe of width w and height h has a hydraulic diameter of:



$$d_h = \frac{2wh}{w+h} \tag{3.3.2}$$

Figure 3.3.1. Rectangular cross-section.

The geometric correction factor, k_g, is according to Idelchik (1992) as shown in the curves in figure 3.3.2:

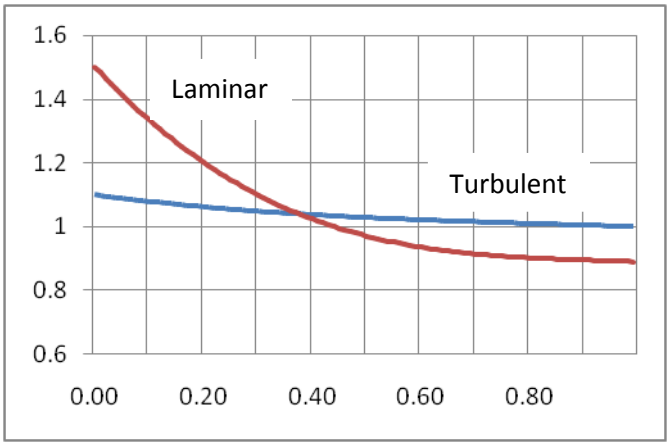


Figure 3.3.2. k_g for laminar and turbulent flow in a rectangular duct.

For more convenient programming, we may use curve-fitting to describe figure 3.3.2 as:

$$k_g = -0.65143\left(\frac{h}{w}\right)^3 + 1.9003\left(\frac{h}{w}\right)^2 - 1.8516\left(\frac{h}{w}\right) + 1.5019 \qquad (3.3.3)$$

for laminar flow, and:

$$k_g = -0.077828\left(\frac{h}{w}\right)^3 + 0.2022\left(\frac{h}{w}\right)^2 - 0.22419\left(\frac{h}{w}\right) + 1.0998 \qquad (3.3.3)$$

for turbulent flow. Both cover the whole range of possible rectangular cross-sections: $0 \leq h/w \leq 1$.

 For non-commercial use only

3.4 Concentric annular cross-section

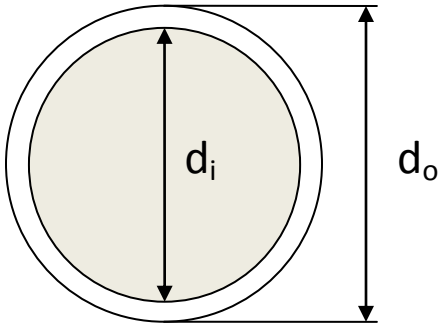


Figure 3.4.1. Concentric annular cross-section.

Note that the correlations for rectangular cross-sections described above can in some cases also be used to estimate the flow in annular cross-sections. If the inner cylinder is concentrically located in the outer cylinder and the annular space is relatively narrow, it can be regarded as a (bent) rectangle of width $\pi(d_o/2 + d_i/2)$ and height $d_o/2 - d_i/2$. For larger differences between d_o and d_i, the correlations shown below are better suited.

The definition of hydraulic diameter immediately leads to:

$$d_h = d_o - d_i \tag{3.4.1}$$

For laminar flow in a concentric annulus, Idelchik (1992) has collected results from many investigators. For laminar flow his results may be written as:

$$f = k_g \frac{64}{Re} \tag{3.4.2}$$

where the geometric correction factor can be found analytically, and turns out to be:

$$k_g = \frac{\left(1 - \frac{d_i}{d_o}\right)^2}{1 + \left(\frac{d_i}{d_o}\right)^2 - \frac{1 - \left(\frac{d_i}{d_o}\right)^2}{ln\left(\frac{d_o}{d_i}\right)}} \tag{3.4.3}$$

The geometric correction factor for turbulent flow is closer to one. By curve-fitting empirical results, we may express k_g for turbulent flow as:

$$k_g = 0.0786\left(\frac{d_i}{d_o}\right)^3 - 0.209\left(\frac{d_i}{d_o}\right)^2 + 0.184\left(\frac{d_i}{d_o}\right) + 1 \tag{3.4.4}$$

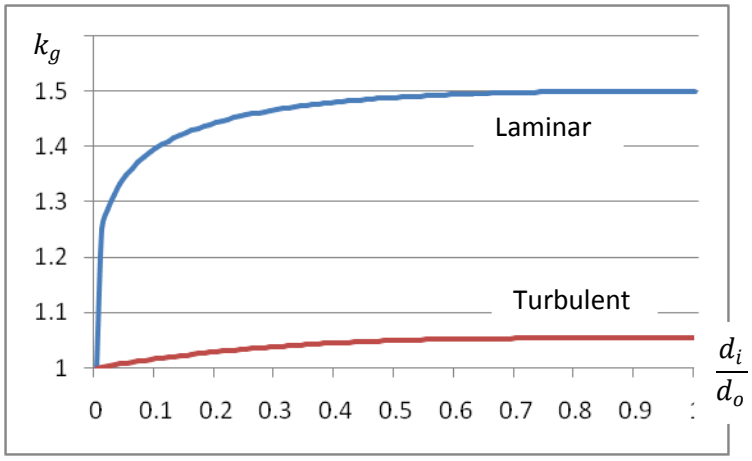
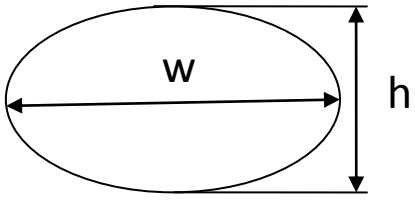


Figure 3.4.2. Concentric annular cross-section, laminar and turbulent geometric correction factors k_g.

In case the inner cylinder is eccentrically located in the outer cylinder, the friction factor will be lower. For turbulent flow, the reduction can be up to 30 %, and for laminar flow even more. More accurate correlations for eccentric annulus can be found in Idelchik (1992).

3.5 Elliptic cross-section

For an ellipse of width w and height h, the hydraulic diameter can be estimated as:



$$d = \frac{wh}{0.75(w+h) - \frac{1}{2}\sqrt{wh}} \tag{3.5.1}$$

Figure 3.5.1. Elliptic cross-section.

For non-commercial use only

For turbulent flow, experiments have shown that $f_g = 1$ for all Reynolds numbers. For laminar flow, it is possible to develop f_g analytically, and it turns out:

$$f_g = \frac{1}{2}\left(\frac{d}{h}\right)^2\left[1+\left(\frac{h}{w}\right)^2\right] \tag{3.5.2}$$

This shows that for laminar flow, f_g grows to around 1.3 when the ellipse gets very flat, while it of course has to become 1 for $w = h$, which is a circle.

References

Crane Technical Paper No. 410 M. (1982): *Flow of fluids through valves, fittings and pipe*, Crane Co.

Idelchik, I.E. (1992): *Handbook of Hydraulic Resistance*. 3. Edition, Moscow Machine Institute (In Russian). (2. Edition exists in English translation from Hemisphere Publishing Corporation.)

Brill, J.P., Mukherjee, H. (1999): *Multi-phase flow in Wells*. First printing, Henry L. Doherty Memorial Fund of AIME, Society of Petroleum Engineers Inc.

"K_f-values, C_v-coefficients and K_v-factors, does it have to be that complicated? Why does the world use local definitions when physical laws are global?"
Frustrated engineer

4 Friction losses in components

This chapter explains how to determine friction in common components:

- Valves
- Bends
- Pipe inlets
- Diameter changes
- Junctions

4.1 General

Typically, the dominating loss element in pipelines or piping systems is the straight run of the pipe itself. But additional components, such as bends, welds and valves lead to additional friction. More accurate computations may require them to be taken into account as well. Empirical and semi-empirical data are helpful when estimating such losses, and we generally express them in terms of a dimensionless factor. Different authors use different notation, for instance *K-factors,* to correlate friction head in *m* with velocity in *m/s*, or a *flow coefficient C* to correlate pressure drop in *Pa* with flow in m^3/s. No matter which definition one uses, it is best to make the coefficients dimensionless so that they remain equally valid in any unit system. Here, we have chosen to define a dimensionless friction factor, K_f, as:

 For non-commercial use only

$$\Delta p = K_f \frac{\rho v^2}{2} \tag{4.1.1}$$

where v refers to the average velocity in the pipe, just as it did in the straight-pipe calculations. If we introduce the flow Q *[m³/s]:*

$$Q = Av \tag{4.1.2}$$

where A *[m²]* is the valve's cross-sectional area. We can alternatively write:

$$\Delta p = K_f \frac{\rho}{2A^2} Q^2 \tag{4.1.3}$$

In some cases the friction is expressed in terms of the equivalent length of straight pipe which would lead to the same pressure loss. When using that notation, we have:

$$f \frac{l_e}{d} \frac{\rho v^2}{2} = K_f \frac{\rho v^2}{2} \tag{4.1.4}$$

This means the equivalent length, l_e, is defined as:

$$l_e = K_f \frac{d}{f} \tag{4.1.5}$$

This definition leads to an equivalent length which depends on the Darcy-Weisbach friction factor, f, which again depends on Re. Piping components do in reality also have friction factors K_f which to some extent depend on Re, though not necessarily in exactly

the same way as f does, and so l_e is not completely independent of Re. In practice, l_e is usually treated as constant anyway, and the error involved in doing so is typically small.

4.2 Valves

Valves do of course play an important role in most pipelines and pipe networks. Handbooks like those of Idelchik (1992) and Crane (1982) are useful when modeling valve losses. Due to the enormous variety in valve designs available, however, no general books cover all, and one often needs to rely on manufacturers' data when computing the resistance for flow-stopping, throttling and controlling devices. For most engineers, the challenge comes down to interpreting the data given by manufacturers. Unfortunately, different manufacturers give their valve data in different ways. When manufacturers talk of *K-values*, they usually refer to the dimensionless factor termed K_f in equation 4.1.1. The most favored form for equation 4.1.1 seems to be to divide each side of the equation 4.1.1 with density ρ and gravity g in order to express head loss Δh:

$$\Delta h = \frac{\Delta p}{\rho g} = K_f \frac{v^2}{2g} \tag{4.2.1}$$

K_f in equation 4.2.1 is obviously the same dimensionless one as in equation 4.1.1, so it needs no conversion if we go from one unit system to the next, say from Imperial units to SI units.

It is unfortunately also quite common to give valve properties in the form of a factor which is not dimensionless. By re-arranging equation 4.1.3, we get:

$$Q = A \sqrt{\frac{2}{K_f}} \cdot \sqrt{\frac{\Delta p}{\rho}} \tag{4.2.2}$$

This may be modified somewhat by introducing water density ρ_v:

 For non-commercial use only

$$Q = \left(A\sqrt{\frac{2}{K_f \rho_v}} \right) \cdot \sqrt{\frac{\Delta p}{\frac{\rho}{\rho_v}}} \tag{4.2.3}$$

Although this book uses the SI-system, it cannot escape the fact that many manufacturers, particularly those based in the USA, define everything in the parenthesis of equation 4.2.3 as a flow coefficient, C_v *[in $^{7/2}lb^{-1/2}$]*, for imperial units:

$$\left(Q = C_v \cdot \sqrt{\frac{\Delta p}{\frac{\rho}{\rho_v}}} \right)_{imperial} \tag{4.2.4}$$

Q is measured in *US gallons/min*, Δp in *psi*, and the equation refers to water at *60 ^0F (16 ^0C)*. The philosophy is that C_v is defined for a density similar to that of water at *60 ^0F*, while ρ/ρ_v takes care of the necessary modification in case we have a density differing from that.

When the correlation between pressure drop and flow through a valve is written for the SI-system in a similar form as equation 4.2.4, it is common to define a flow factor, K_v, with units $m^{7/2}kg^{-1/2}$:

$$Q = K_v \cdot \sqrt{\frac{\Delta p}{\frac{\rho}{\rho_v}}} \tag{4.2.5}$$

By comparing imperial and SI units, it can easily be shown that:

$$K_v = 0.862\ C_v \tag{4.2.6}$$

Armed with these definitions, valve data from different manufacturers is easily obtainable from various catalogs available on the internet.

4.3 Bends

When a pipe changes direction, it leads to extra friction compared with how it would have been had the pipe been straight. How large the extra friction becomes is affected by how the bend is designed, how smooth it is, the bend angle, θ, and the bend radius, R_0, and also how far it is from other bends. Rapid direction changes can also lead to secondary effects such as cavitation and erosion. Presence or absence of guide vanes in the bend can also be important, and all in all there are a lot of details one may go into in this field. Here, we are only going to present some empirical data for smooth, circular bends. In fully developed turbulent flow (meaning the bend is located at least 30 diameters downstream from other disturbances), Ito (1960) and Idelchik (1992) give the probably most used recommendations for such friction losses. Here, only Idelchik's method is shown, as that is the most general of the two.

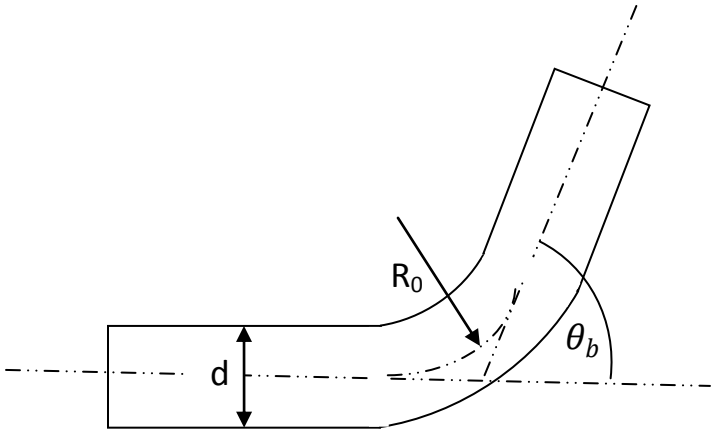


Figure 4.3.1. Pipe bend of angle θ_b.

He sets:

$$K_f = k_1 k_2 + 0.0175 f \theta_b \frac{R_0}{d} \tag{4.3.1}$$

 For non-commercial use only

where f is the Daarcy-Weisbach friction factor, and the two factors k_1 and k_2 are constants. k_1 is a function of $\frac{R_0}{d}$ and is given as:

$$k_1 = \frac{0.21}{\left(\frac{R_0}{d}\right)^{2.5}} \; for \; 0.5 \leq \frac{R_0}{d} \leq 1$$

$$k_1 = \frac{0.21}{\left(\frac{R_0}{d}\right)^{0.5}} \; for \; \frac{R_0}{d} > 1 \qquad (4.3.2)$$

k_2 is a function of bend angle θ_b. It is not given as a simple empirical formula directly by Idelchik, but his tabulated data can be approximated as:

$$k_2 = 1.9244 \cdot 10^{-7}{\theta_b}^3 - 9.0438 \cdot 10^{-5}{\theta_b}^2 + 0.017871\theta_b \qquad (4.3.3)$$

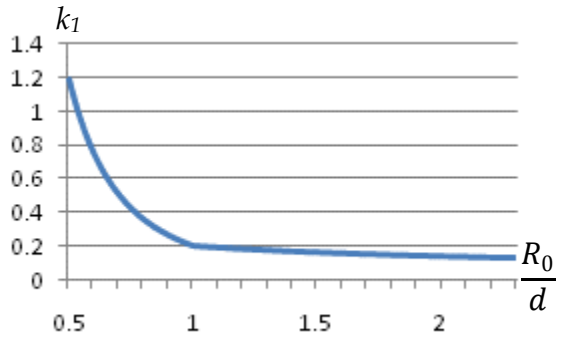


Figure 4.3.2. k_1 as function of $\frac{R_0}{d}$

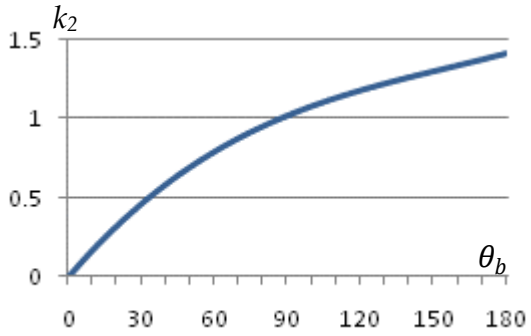


Figure 4.3.3. k_2 as function of θ_b

As we would expect, the empirical correlation shows that the loss is smallest in bends with small bend radiuses R_0 (k_1 falls with increased R_0/d), and it is of course higher the more it is bent (k_2 increases with θ_b). This is also the overall trend for K_f when all terms in equation 4.3.1 are taken into account.

4.4 Welds joining pipe sections

For long pipelines, the welds between each pipe section may contribute significantly to the total friction. Idelchik (1992) gives some guidelines for how large the friction becomes.

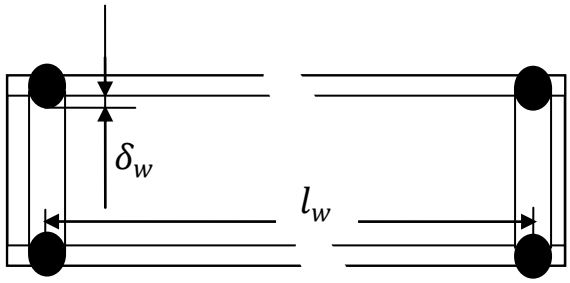


Figure 4.4.1. Pipe sections joined by welds

For relatively short distances l_w between each weld, the welds affect each other, and each weld has less influence than it would have if the distance between them were larger. If $\frac{l_w}{d} < 30$:

$$K_f = k_1 \left(\frac{\delta_w}{d}\right)^{3/2} \tag{4.4.1}$$

The data given for k_1 can be curve-fitted as:

$$k_1 = 0.000582 \left(\frac{l_w}{d}\right)^3 - 0.0369 \left(\frac{l_w}{d}\right)^2 + 1.012 \frac{l_w}{d} \tag{4.4.2}$$

For non-commercial use only

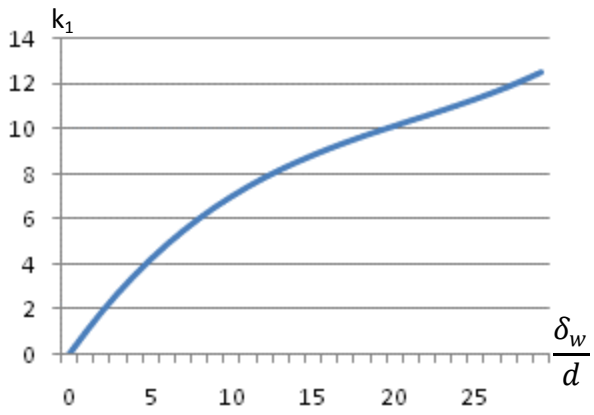


Figure 4.4.2. k_1 as a function of relative joint spacing $\frac{l_w}{d}$

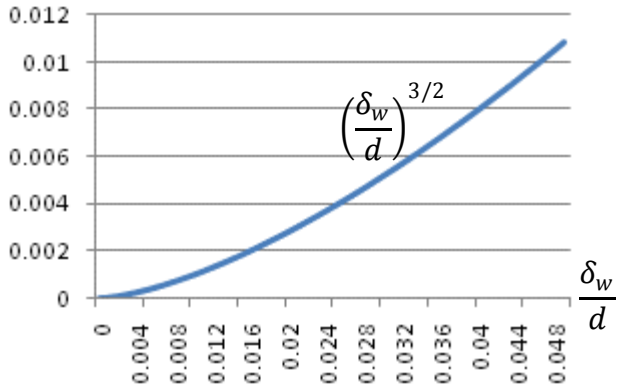


Figure 4.4.3. $\left(\frac{\delta_w}{d}\right)^{3/2}$ as a function of $\frac{\delta_w}{d}$

When the welds are far apart, specifically when $\frac{l_w}{d} \geq 30$, Idelchik gives K_f directly as a function of pipe diameter, but only for $\delta_w = 0.003$ m and $d \leq 0.2m \leq 0.9m$. K_f is expected to be a function of the weld's relative size δ/d, so the data can be generalized and used for other weld sizes. His data can be curve-fitted as:

$$K_f = \exp\left[1.76log10\left(\frac{\delta_w}{d}\right) + 1.65\right] \quad (4.4.3)$$

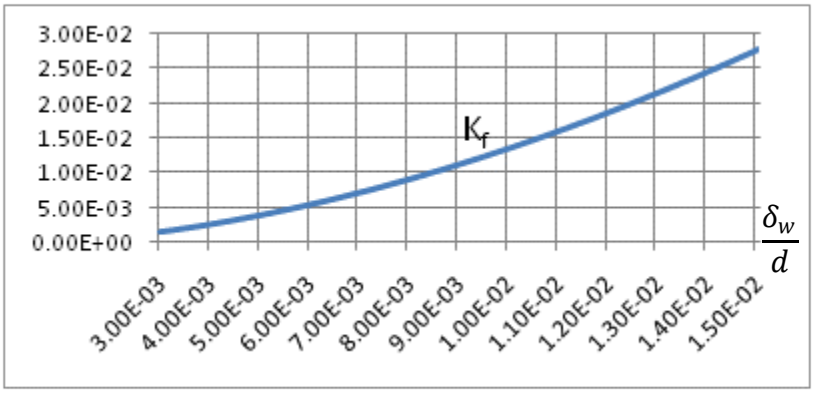


Figure 4.4.1. K_f as a function of $\frac{\delta_w}{d}$

When using these results as explained for the general equation 4.1.1, we get the pressure loss per weld as:

$$\Delta p_j = K_f \frac{v^2}{2\rho} \tag{4.4.4}$$

K_f is found either from equations 4.4.1 and 4.4.2 or from equation 4.4.3, depending on $\frac{l_w}{d}$.

4.5 Inlet loss

When dealing with long pipelines, the inlet losses are normally negligible compared to the total friction in the rest of the pipeline. But there may be other reasons why we want to know it more accurately, such as investigating the possibility of cavitation due to low pressure at pump inlets.

Before describing the loss itself, let us first point out that when fluid at rest accelerates towards a pipe inlet, it gains kinetic energy. This energy is taken from the pressure, which therefore is reduced accordingly. This pressure reduction, though, is not a loss, but simply a result of some pressure energy being transferred to kinetic energy. It can easily be shown that the Bernoulli pressure reduction is described by:

$$\Delta p_{Bernoulli} = \frac{\rho v^2}{2} \tag{4.5.1}$$

This pressure reduction comes in addition to the losses described below. Crane (1982) gives values for the inlet loss as shown in figure 4.5.2.

 For non-commercial use only

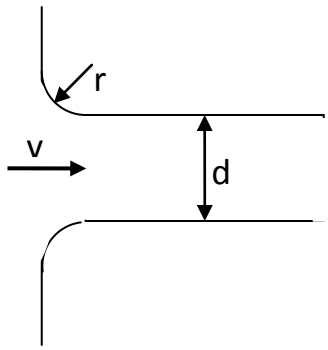


Figure 4.5.1. Pipe entrance loss

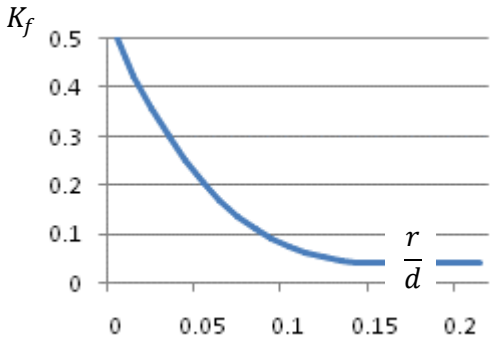


Figure 4.5.2. K_f as a function of $\frac{r}{d}$

The curve in figure 4.5.2 can be described by the following curve-fit:

$$K_f = -89\left(\frac{r}{d}\right)^3 + 46\left(\frac{r}{d}\right)^2 - 7.96\frac{r}{d} + 0.50 \; for \; 0 \leq \frac{r}{d} < 0.15 \tag{4.5.2}$$

$$K_f = 0.04 \; for \; \frac{r}{d} \geq 0.15 \tag{4.5.3}$$

This means the inlet loss coefficient, K_f, varies between 0.5 for sharp inlets to 0.15 for well rounded inlet.

There is also another sort of added friction near the pipe inlet. The Darcy-Weisbach friction factor can be around 2.5 times as high in the first diameter length of pipe compared to what it is in stabilized flow. This effect rapidly diminishes as the velocity profile reaches its normal shape some 20-30 diameters downstream (Idelchik, 1992). It is difficult to quantify this extra loss accurately, and it is common to neglect it, but it is still worth keeping in mind that the total inlet loss is somewhat higher than predicted by equation 4.5.2 or 4.5.3.

4.6 Diameter changes

When the diameter changes, the friction losses become higher than they would have been in a straight pipe.

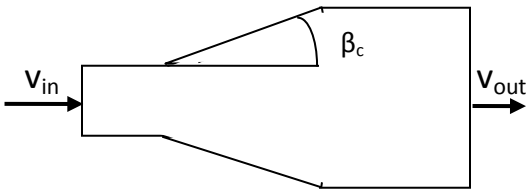


Figure 4.6.1. Conical diffuser.

Just like for the pipe inlet discussed in chapter 4.5, the friction loss is not the only mechanism at work here: The Bernoulli energy equation tells us that when the velocity is reduced, such as in a diffuser, some of the kinetic energy is transformed to pressure energy.

If the flow had been lossless, the pressure change for incompressible flow in a diffuser would be:

$$p_{out} - p_{in} = \frac{\rho {v_{in}}^2}{2} - \frac{\rho {v_{out}}^2}{2} = \left[1 - \left(\frac{d_{in}}{d_{out}}\right)^4\right]\frac{\rho {v_{in}}^2}{2} \tag{4.6.1}$$

Since $d_{out} > d_{in}$, clearly $p_{out} > p_{in}$, as expected. That is what happens in the draft tube of a Francis or Kaplan water turbine: The diameter is increased behind the turbine to extract as much of the kinetic energy from the flowing water as possible. But in addition to this energy transformation, there is also an energy loss due to increased friction. That loss has the opposite effect on $p_{out} - p_{in}$.

In general, very small angles β_c lead to a smooth flow with relatively small losses, and the flow follows the conical geometry without separating from the wall. Increasing β beyond a certain point leads to separation, and the losses increase. At exactly which angle separation starts depends on both *Re*, $\frac{d_{in}}{d_{out}}$ and any upstream disturbances. Measurements carried out by Idelchik (1992) indicate that *if* $\beta_c \leq 2^0$, no separation occurs under any circumstances, and losses are kept to a minimum. For relatively large β_c, separation becomes so dominant that the conical section has no effect, and one may as well use an abrupt diameter step ($\beta_c = 90^0$). Crane's simplified correlations take this into account, and are adequate for most engineering applications:

$$K_f = 2.6\left[1 - \left(\frac{d_{in}}{d_{out}}\right)^2\right]^2 \sin\beta_c \;\; for\; \beta_c \leq 22.5^0 \tag{4.6.2}$$

 For non-commercial use only

$$K_f = \left[1 - \left(\frac{d_{in}}{d_{out}}\right)^2\right]^2 \quad for\ 22.5^0 \le \beta_c \le 90^0$$

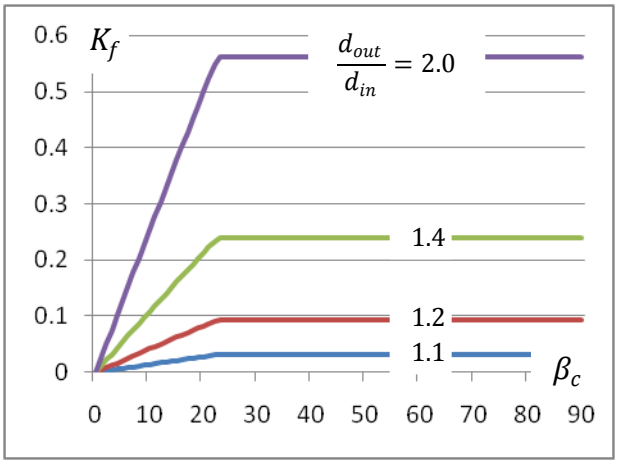


Figure 4.6.2. Loss coefficient for conical diffuser.

Note that K_f is defined according to the velocity in the smallest diameter section, the inlet, so that:

$$\Delta p_{loss} = p_{in} - p_{out} = K_f \frac{\rho v_{in}^2}{2} \qquad (4.6.3)$$

If we compare the pressure gain described by equation 4.6.1 with the empirical friction losses modeled by equation 4.6.2, we will see that which one is largest depends on the diffuser's construction – it is obviously possible to construct diffusers where the pressure increases and diffusers where it is reduced.

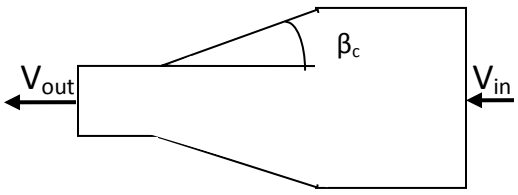


Figure 4.6.3. Conical contraction.

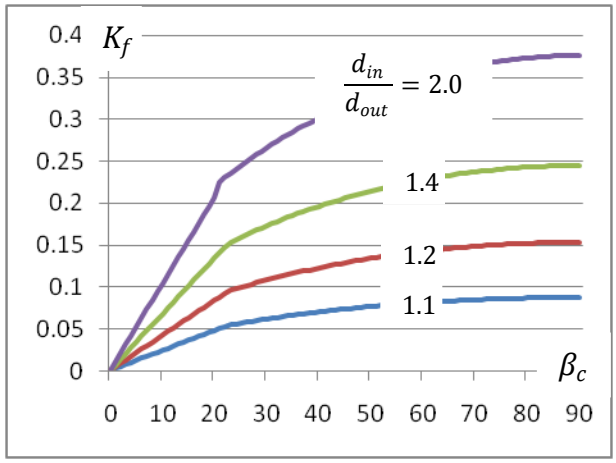


Figure 4.6.4. Loss coefficient for conical

contraction.

On equation form, the curves in figure 4.6.1 can be written as:

$$K_f = 0.8\left[1-\left(\frac{d_{out}}{d_{in}}\right)^2\right]\sin\beta_c \;\; for\; \beta_c \leq 22.5^0$$

$$K_f = 0.5\left[1-\left(\frac{d_{out}}{d_{in}}\right)^2\right]\sqrt{\sin\beta_c} \;\; for\; 22.5^0 \leq \beta_c \leq 90^0 \tag{4.6.4}$$

In this case, too, the Bernoulli-effect also contributes, but both the acceleration and the friction lead to pressure reductions.

4.7 Junctions

Friction losses in pipe junctions are somewhat different from the other losses discussed so far in that junctions are characterized by very many different variables. The geometries may differ various ways, such as angles, cross sections, and even number of branches. The flow situation also plays a role, such as how the flow is distributed between the different inlet(s) and outlet(s), and whether the junction is used to merge or split flows. Needles to say, it is not possible to cover all potential combinations in a single empirical correlation, and a vast amount of articles regarding how to estimate losses in different junctions exists. In this chapter only some of the most common situations are covered.

When two pipes meet, there are generally going to be losses of four different types: Due to turbulent mixing of two streams moving with different velocities, due to flow turning when it passes from the side branch into the common channel (sometimes enhanced by separation), due to flow expansion in case of diffuser effect or acceleration in case of a nozzle effect, and due to normal pipe friction.

Both Vazsonyi (1944) and Benson et al. (1966) carried out measurements on merging flows of the type seen on figure. 4.7.1. All branches had the same diameter, and the

 For non-commercial use only

outlet was perpendicular to the two inlets. The two papers show relatively similar results. When taking the average of the two, we can write the results as:

$$K_{f\ in1-out} = 0.68\frac{v_{in1}}{v_{out}} + 0.64 \qquad (4.7.1)$$

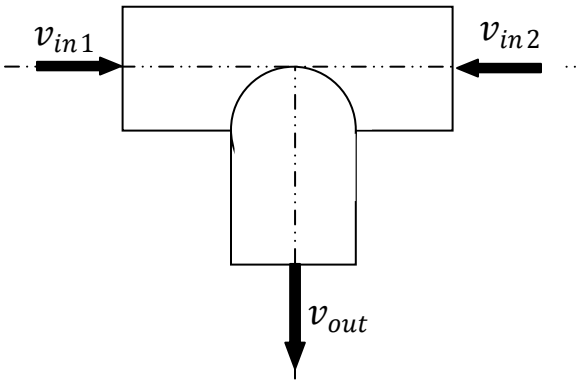


Figure 4.7.1. Merging flows, all cross-sections equal.

As before, the coefficient refers to the velocity in the inlet branch:

$$\Delta p_{in1-out} = K_{f\ in1-out}\frac{\rho {v_{in1}}^2}{2} \qquad (4.7.2)$$

Due to symmetry, $\Delta p_{in2-out}$ can be computed by simply re-indexing everything so that 1 becomes 2 and vice versa.

For diverging flows, a similar linear estimate of K_f can be obtained by combining the measurements of Vazsoniy (1944) and Benson et al. (1966):

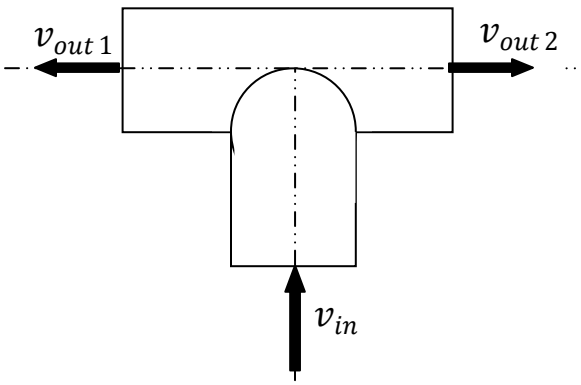


Figure 4.7.2. Diverging flows, all cross-sections equal.

$$K_{f\ in-out\,1} = 0.60\frac{v_{out\,1}}{v_{in}} + 0.85 \qquad (4.7.3)$$

And:

$$\Delta p_{in-out\,1} = K_{f\ in1-out}\frac{\rho {v_{out\,1}}^2}{2} \qquad (4.7.4)$$

Again, symmetry implies that $\Delta p_{in-out\,2}$ can be computed by simple re-indexing to make 1 become 2 and vice versa.

A more general case of merging flows for branches with equal diameters can be extracted from Vazsonyi's results (1944). The curves he presented have here been curve-fitted in order to enable easy programming:

$$K_{f\ in1-out} = k_1 \left(\frac{v_{in1}}{v_{out}}\right)^2 + 1 - 2\left[\frac{v_{in1}}{v_{out}}\frac{Q_{in1}}{Q_{out}}\cos\beta_c{}' + \frac{v_{in2}}{v_{out}}\frac{Q_{in2}}{Q_{out}}\cos\alpha_c{}'\right] \quad (4.7.5)$$

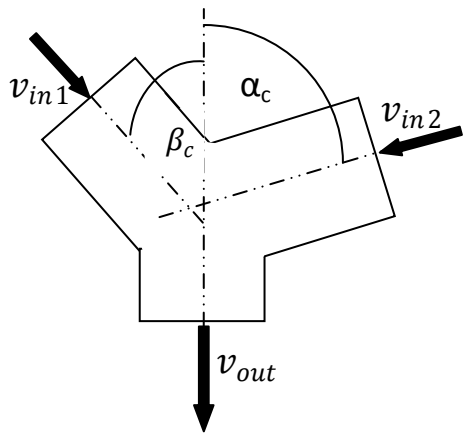


Figure 4.7.3. General, merging flows, all cross-sections equal

Where $K_{f\ in1-out}$ again refers to the inlet velocity, and equation 4.7.2 can be used to calculate the pressure loss. The factors:

$$k_1 = 6.28 \cdot 10^{-7}\beta_c{}^3 - 1.47 \cdot 10^{-4}\beta_c{}^2 + 0.00496\beta_c + 0.961 \quad (4.7.6)$$

$$\alpha_c{}' = 1.41\alpha_c - 0.00594\alpha_c{}^2 \quad (4.7.7)$$

$$\beta_c{}' = 1.41\alpha - 0.00594\beta_c{}^2 \quad (4.7.8)$$

Vazsonyi's results can also be used to estimate pressure losses in diverging flows, but only for 90^0 T-junctions angled as shown on Figure 4.7.4:

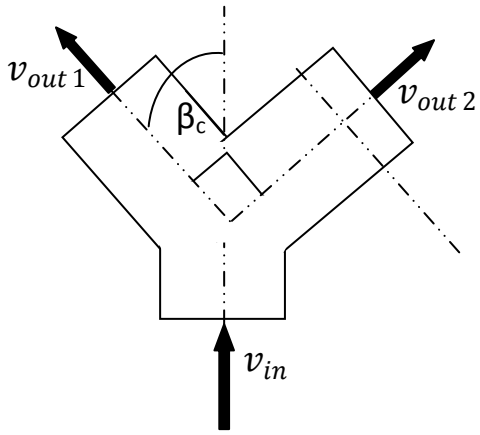


Figure 4.7.4. Diverging flows, all cross-sections equal.

For non-commercial use only

$$K_{f\ in-out\,1} = k_2 + (2k_3 - k_2)\left(\frac{v_{out\,1}}{v_{in}}\right)^2 - 2k_3\frac{v_{out\,1}}{v_{in}}\cos\alpha'$$

$$k_2 = 0.0712\alpha^{0.7041} + 0.37\ for\ \alpha < 22.5^0$$
$$k_2 = 1\ for\ \alpha \geq 22.5^0 \qquad (4.7.9)$$

$$k_3 = 0.0592\alpha^{0.7029} + 0.37\ for\ \alpha < 22.5^0$$
$$k_3 = 0.9\ for\ \alpha \geq 22.5^0$$

α' is as before computed by equation 4.7.7, and $\Delta p_{in-out\,1}$ by equation 4.7.4.

The last type of branch to be considered here is a pipe of constant diameter receiving fluid from an angled branch of a smaller diameter.

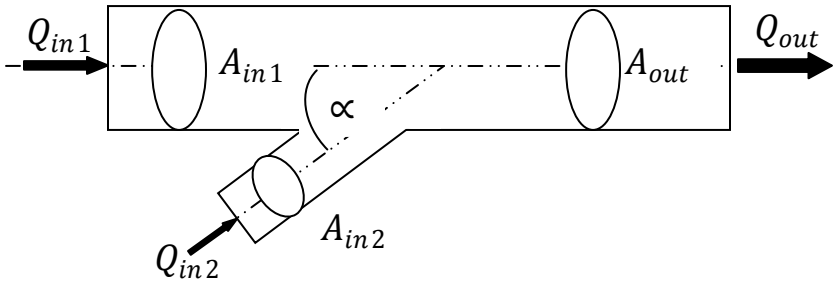


Figure 4.7.5. Merging flows, cross-sections $A_{in\,1} = A_{out}$

Idelchik (1992) reports results for many different distinct values of α. Those results may be compressed into the following:

$$K_{f\ in\,1-out} = 1 - \left(1 - \frac{Q_{in\,2}}{Q_{out}}\right)^2 - k_\propto \frac{A_{out}}{A_{in\,2}}\left(\frac{Q_{in\,2}}{Q_{out}}\right)^2 \qquad (4.7.10)$$

$$K_{f\ in\,2-out} = k_1\left[1 + \left(\frac{A_{out}\,Q_{in\,2}}{A_{in\,2}Q_{out}}\right)^2 - 2\left(1 + \frac{Q_{in\,2}}{Q_{out}}\right)^2 - k_\propto \frac{A_{out}}{A_{in\,2}}\left(\frac{Q_{in\,2}}{Q_{out}}\right)^2\right] \qquad (4.7.11)$$

where k_1 is taken from table 4.7.1.

$\frac{A_{in2}}{A_{out}}$	≤ 0.35	> 0.35	
$\frac{Q_{in2}}{Q_{out}}$	$0 - 1.0$	≤ 0.4	> 0.4
k_1	1.0	$0.9\left(1 - \frac{Q_{in2}}{Q_{out}}\right)$	0.55

Table 4.7.1. Values of k_1.

$k_\propto$ is a factor which takes the branch angle α (measured in degrees) into account. For $30 \leq \propto \leq 60^0$, $k_\propto$ varies between 1.7 and 1 in the following way:

$$k_\propto = 1.47 \cdot 10^{-4} \propto^2 - 0.0113 \propto +2.21 \tag{4.7.12}$$

When calculating $C_{f\ in2-out}$, the equation above remains valid all the way up to 90^0, while something appears to happen with $C_{f\ in1-out}$ as the angle approaches 90^0 so that:

$$K_{f\ in1-out\ 90^0} = 1.55\frac{Q_{in2}}{Q_{out}} - \left(\frac{Q_{in2}}{Q_{out}}\right)^2 \tag{4.7.13}$$

With these correlations, the pressure loss in each flow-path can then be computed as:

$$\Delta p_{in1-out} = K_{f\ in1-out}\frac{\rho {v_{in1}}^2}{2} \tag{4.7.14}$$

$$\Delta p_{in2-out} = K_{f\ in2-out}\frac{\rho {v_{in1}}^2}{2} \tag{4.7.15}$$

For non-commercial use only

As we can see, these equations are nicely suited to be included in a computer program. All data are given in the form of equations, and we may easily write an algorithm which computes both $\Delta p_{in1-out}$ and $\Delta p_{in2-out}$ as a function of for instance $\propto$, A_{out}, A_{in2}, Q_{in1} and Q_{in2}.

To get s feeling for what the correlations express, the loss factors for some angles and cross-sectional areas have been plotted in figures 4.7.6 and 4.7.7:

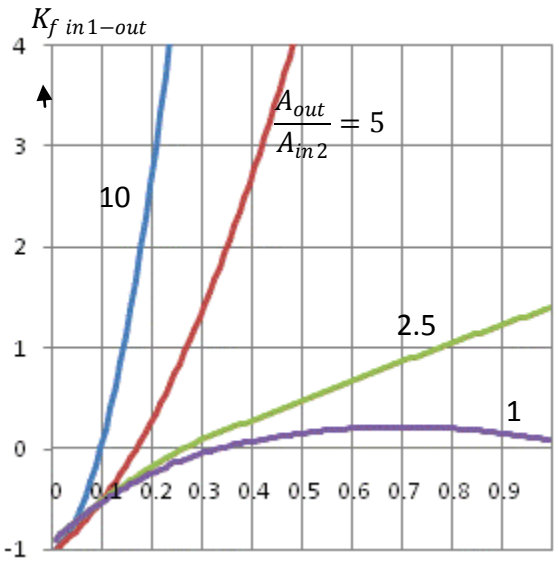


Figure 4.7.6. $K_{f\ in1-out}$ *as a function of* $\frac{Q_{in2}}{Q_{out}}$ *for* $a = 30^0$.

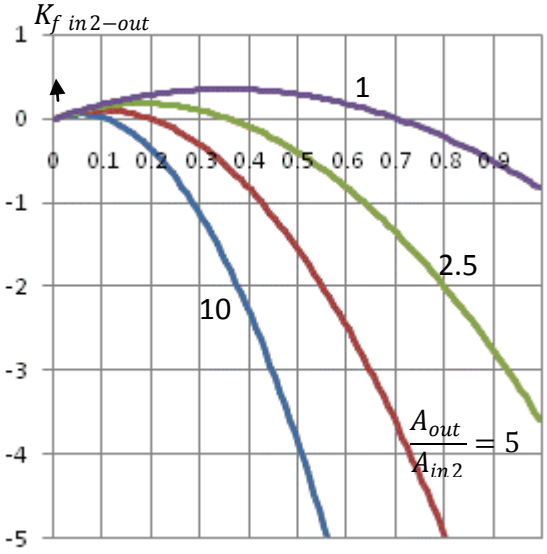


Figure 4.7.7. $K_{f\ in2-out}$ *as a function of* $\frac{Q_{in2}}{Q_{out}}$ *for* $a = 30^0$.

References

Vazsonyi, A. (1944): *Pressure loss in elbows and duct branches*. Trans ASMA, April, p. 177

Benson, R.S., Wollatt, D. (1966): Compressible *flow loss coefficients at bends and T-junctions.* Engineer, Vol. 222, January, p. 153.

Benedict, R.P. (1980): *Fundamentals of Pipe Flow.* John Wiley & Sons.

Crane Technical Paper No. 410 M. (1982): *Flow of fluids through valves, fittings and pipe.* Crane Co.

Idelchik, I.E. (1992): *Handbook of Hydraulic Resistance*. 3. Edition, Moscow Machine Institute (In Russian). (2. Edition exists in English translation from Hemisphere Publishing Corporation.)

 For non-commercial use only

"Blood is a non-Newtonian fluid; its viscosity automatically adjusts to the blood vessel's diameter."
Author unknown

5 Non-Newtonian fluids and friction

Non-Newtonian fluids differ from other fluids:

- Various sorts of non-Newtonian fluids
- How to define the Reynolds number for non-Newtonian fluids
- Transition between laminar and turbulent flow
- Friction models

5.1 Introduction

In most engineering applications, the fluids encountered are of the Newtonian sort, meaning the shear stress in laminar flow is proportional to the liquid's velocity gradient. We saw in equation 2.2.1 that this can be described as:

$$\tau = \mu \frac{\partial v}{\partial y} \tag{5.1.1}$$

Where μ is dynamic viscosity and y refers to the direction of the velocity gradient (orthogonal to the velocity). Pure fluids such as water and air are Newtonian fluids. Solutions or suspensions of particles may not obey this equation, and if they don't, they

are called non-Newtonian. The most important types of non-Newtonian fluids may be categorized as shown in figure 5.1.1.

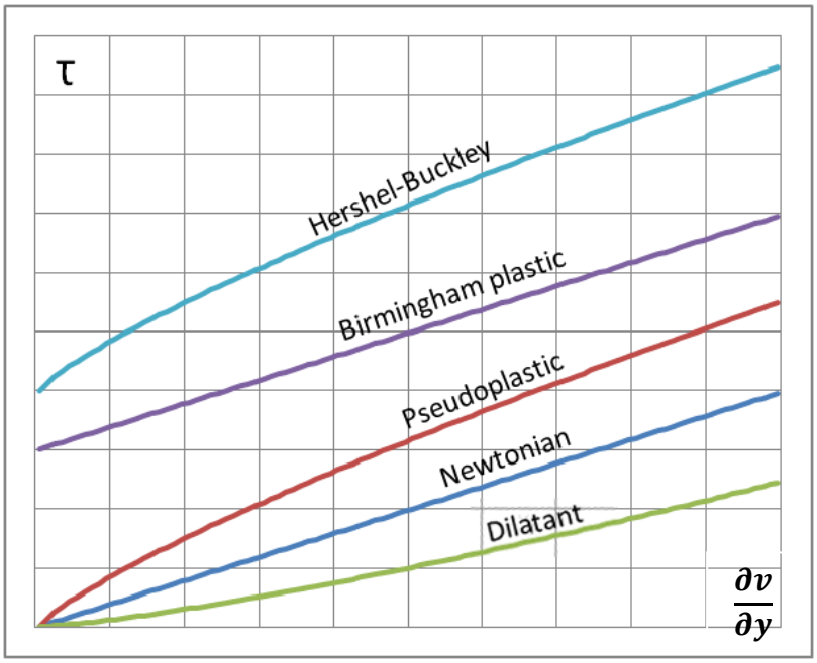


Figure 5.1.1. Various sorts of viscous, time-independent fluids

Birmingham plastic fluids need a minimum yield stress, τ_0, in order to allow a velocity gradient at all. Such properties can be desirable for some fluids. Shaving foam, for instance, needs to be 'thin' enough not to generate much force on a razor blade surface even if the razor is moves relatively fast. Had the foam acted like a Newtonian fluid, the relatively low viscosity would cause it to flow quickly off the shaver's face. But shaving foam is Birmingham plastic, and gravity is not strong enough to make the foam move. Other, more industrially significant kinds of Birmingham fluids include water suspensions of clay, fly ash, sewage sludge, paint, and fine minerals, such as coal slurry.

Human blood can also be approximately described by Birmingham models. For low shear forces, blood is viscous enough to keep the flow laminar in nearly all blood vessels. Amazingly, higher shear stress in the thinnest capillaries makes the red blood cells arrange themselves and even deform in ways which reduce the viscosity, and consequently they tend to concentrate in the center. The result is that blood flows well even in *10 μm* diameter capillaries, but is viscous enough to maintain laminar flow almost up to the largest diameters, which may be *20 mm* for the aorta. Water carrying

 For non-commercial use only

cellulose fibers is also non-Newtonian, and it shows some of the same characteristics as blood.

The yield stress τ_0 for Birmingham fluids (the maximum τ_0 we can achieve at $\partial v/\partial y = 0$) may be very small (less than 10^{-6} N/m^2 for some types of sewage sludge) or very large (more than 10^5 N/m^2 for some asphalts and bitumens).

Some clay-water suspensions at intermediate levels of concentration exhibit Hershel-Buckley (sometimes called yield-pseudoplastic) properties.

There are also non-Newtonian fluids which actually change properties over time, and they are said to have time-dependent rheological properties. One important example is water suspension of bentonitic clay, which is much used in drillmuds. It is an example of what is called a thixotropic fluid, and has the peculiar property that its viscosity under constant shear decreases with time.

This chapter gives a brief overview over some of the most important friction models available for non-Newtonain fluids. A more extensive overview can be found in Chhabra (1999).

5.2 Pipe flow friction for power-law fluids

Just like for Newtonian fluids, laminar flow is easier to deal with than turbulent flow for non-Newtonian fluids. There is one difference, though: Many types of non-Newtonian fluids have relatively high viscosity, and laminar flow is quite common. In this chapter, we will look at how to describe pipe friction for different types of non-Newtonian fluids for laminar flow. We will also establish criteria for when the flow becomes turbulent and present some of the theories regarding how to estimate turbulent friction factors.

First, let us start by describing mathematically what characterizes different types of non-Newtonian fluids.

Both pseudoplastic and dilatant fluids follow a power law described by:

$$\tau = K_0 \left(\frac{\partial v}{\partial y}\right)^n \tag{5.2.1}$$

Newtonian fluids also follow that law, since setting $n = 1$ and $K_0 = \mu$ leads us back to equation 5.1.1. For other values of n we define the apparent viscosity as:

$$\mu_a = K_0 \left(\frac{\partial v}{\partial y}\right)^{n-1} \tag{5.2.2}$$

which also obviously fits the Newtonian case nicely.

It can be shown without too much effort that for laminar flow, this leads to a velocity profile described by:

$$v(r) = \left(\frac{\Delta p}{2K_0 l}\right)^{\frac{1}{n}} \frac{n}{n+1}\left[\left(\frac{d}{2}\right)^{\frac{n+1}{n}} - r^{\frac{n+1}{n}}\right] \tag{5.2.3}$$

This profile is shown for 3 different values of n in figure 5.2.1.

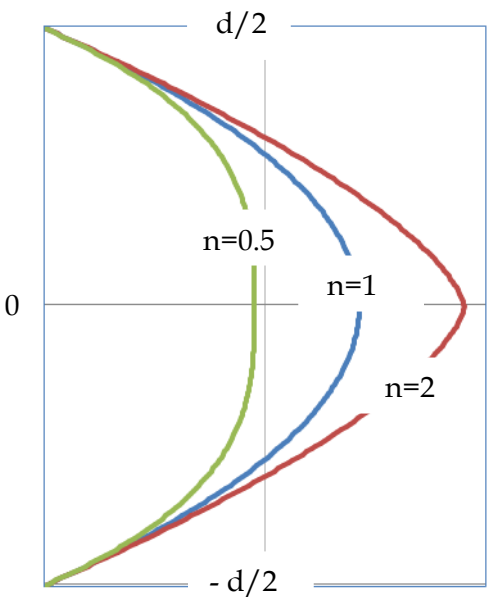


Figure 5.2.1. Laminar velocity profiles for power law fluids, constant $\Delta p, K_0$ and l.

The velocity profile can be integrated to give us the average velocity v. As a boundary condition, we may use the same steady-state momentum correlation in equation 2.1.4:

$$\tau_w = \frac{\Delta p\, d}{4l} \tag{5.2.4}$$

This leads to the Darcy-Weisbach friction factor for laminar flow being:

$$f = \frac{8K_0}{\rho d^n v^{2-n}}\left(\frac{6n+2}{n}\right)^n \tag{5.2.5}$$

 For non-commercial use only

The following power-law Reynolds number definition based on the average velocity integrated from equation 5.2.3 is useful:

$$Re_p = \frac{\rho d^n v^{2-n}}{8^{n-1} K_0} \left(\frac{4n}{3n+1} \right)^n \tag{5.2.6}$$

In case the fluid is Newtonian, $n = 1$ and $K_0 = \mu$, and we see that equation 5.2.6 leads us back to the familiar Reynolds number definition $Re = vd\rho/\mu$.

We may combine equations 5.2.5 and 5.2.6 and show that for laminar flow:

$$f = \frac{64}{Re_p} \tag{5.2.7}$$

This shows that if we simply describe the Reynolds number according to equation 5.2.6, we may compute the laminar friction factor for any power-law fluid in the same way as for Newtonian fluids.

One curiosity worth noting is that by the definition of Re_p according to equation 5.2.6, Re becomes less and less affected by v the closer n is to 2, and if $n = 2$, Re is in fact independent of v. This may seem somewhat counter-intuitive, but since dilatant fluids 'thicken' as the shear increases, this is actually possible. $n = 2$ must therefore lead to the flow always being turbulent or always laminar. If $n > 2$, Re falls as v increases, leading to laminar flow at high rather than low velocities. If we combine equations 5.2.7, 5.2.6 and 2.1.6, we see this means the pressure loss becomes proportional to v^n. If n is close to 2, this behavior is in fact not so different from turbulent flow for Newtonian fluids.

It turns out the Reynolds number where the flow switches from laminar to turbulent flow depends on n. Ryan and Johnson (1959) used stability analysis to come up with the following result:

$$Re_p < \frac{6464n(2+n)^{\frac{2+n}{1+n}}}{(1+3n)^2} => Laminar\ flow \tag{5.2.8}$$

Later work by Mishra and Tripathi (1971) gives another criterion:

$$Re_p < \frac{2100(4n+2)(5n+3)}{3(1+3n)^2} => Laminar\ flow \tag{5.2.9}$$

When we plot these two criteria in the same diagram, as we have done in figure 5.2.2, we see they give different results, particularly for $n < 0.5$. Tadashi (1978) points out that Ryan's results mainly are based on measurements of $n > 0.5$, and Dodge and Mezner (1959) seem to support Mishra's results. It therefore seems plausible to prefer the Mishra-correlation.

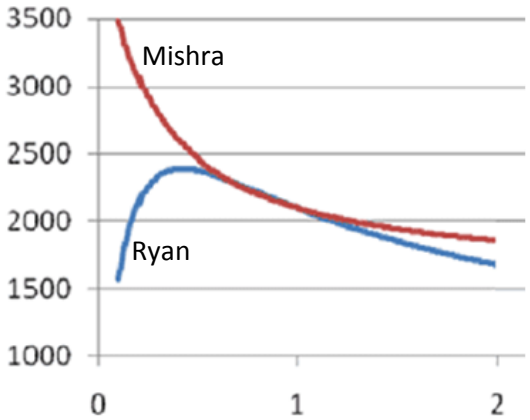


Figure 5.2.2. Critical power law Reynolds number as a function of n.

To estimate the Darcy-Weisbach friction factor for turbulent flow, we again have to rely on empirical data. The most common estimate for power law fluids is probably the one reported by Grovier and Aziz (1972). They defined yet another power-law Reynolds number, Re_m, as well as a modified Darcy-Weisbach friction factor, f_m, as follows:

 For non-commercial use only

$$Re_m = \frac{6\left(\frac{1+3n}{n}\right)^{1-n} \rho d^n v^{2-n}}{2^n \frac{1+2n}{n} K_0} \tag{5.2.10}$$

$$f_m = \frac{8d\Delta p(1+2n)}{3l\rho v^2(1+3n)} \tag{5.2.11}$$

Using these definitions, results agreed with the Prandtl-Von Karman correlation for smooth pipes, equation 2.5.1, by letting f_m replace f:

$$\frac{1}{\sqrt{f_m}} = -2\log_{10}\frac{2.51}{Re_m\sqrt{f_m}} \tag{5.2.12}$$

It has been suggested these clever results show the methods developed in chapter 2 may be used to determine friction factors for any power-law fluid. That seems to be the best method available, but it cannot at this stage be called a reliable and well documented method.

5.3 Pipe flow friction for Birmingham plastic fluids

For Birmingham plastic fluids, we have:

$$\mu_p = \frac{\tau - \tau_0}{\frac{\partial v}{\partial y}} \tag{5.3.1}$$

Where τ_0 is the minimum stress required to initiate flow. If the shear stress is smaller than τ_0, the fluid does not flow at all. It means:

$$\frac{\partial v}{\partial y} = 0 \; if \; \tau \leq \tau_0$$

$$\frac{\partial v}{\partial y} = \frac{1}{\mu_p}(\tau_0 - \tau) \; if \; \tau > \tau_0 \tag{5.3.2}$$

It is obvious that the sort of flow we get in a pipe carrying a Birmingham plastic fluid is going to be very different from those carrying Newtonian fluids. For instance, since the shear stress is always smaller near the center of a pipe than it is closer to the wall (equation 2.1.3 shows that), the shear stress is going to be lower than τ_0 near the axis. That means the velocity profile is flat in the center.

Govier and Aziz (1972) give the same laminar friction factor as for power-law fluids:

$$f = \frac{64}{Re_p} \tag{5.3.3}$$

For turbulent Birmingham fluids they give:

$$\frac{1}{\sqrt{f}} = -4.53 \log_{10}\left(1 - \frac{2\tau_0}{f\rho v^2}\right) + 4.53 \log_{10}\left(\frac{vd\rho}{\mu_p}\sqrt{f}\right) - 2.3 \tag{5.3.4}$$

According to Hanks (1963), laminar flow can be expected when:

$$\frac{vd\rho}{\mu_p + \frac{d\tau_0}{6v}} < 2{,}100 \tag{5.3.5}$$

 For non-commercial use only

5.4 Friction-reducing fluids

Certain long-chain polymers have the remarkable property of apparently reducing the turbulent friction for some liquids. The amount of additives needed is far lower than what would be needed to reduce the viscosity itself, so it is obvious other mechanisms are at work. Even though this was discovered as early as in 1948, the phenomenon is still not understood in full detail, but it is believed the additives' long polymer chains may dampen the turbulent eddies and thereby reduce the part of the friction which has to do with fluid travelling radially. As shown in chapter 2.8, the friction is considered proportional to the turbulent eddies' radial velocity, and reducing that movement therefore leads to a direct reduction in friction. Simply put: Drag-reducing Agents (DRA) reduce turbulence, and that in turn leads to reduced friction. DRA's do obviously not work for laminar flow.

Some companies specialize in producing DRAs. The market is considerable, and significant pipeline capacity gains have been reported. In its simplest form, a system may consist of a tap, an injection pump and a storage tank. Installing that may be a much quicker way of increasing capacity compared to increasing pumping power or pipe diameter. On the other hand, it is difficult to predict the effect accurately in advance. It can also be a problem that some products - aviation fuel, for instance - may not be allowed to mix with any additives.

Injecting friction-reducing fluids may be the fastest way of increasing a pipeline's capacity.

The long polymer chains are relatively fragile, and they seem to be at least partly destroyed when they pass through pumps, valves or even bends, so DRA's should be injected downstream of such disturbances.

According to Isaksen et al. (2003), DRAs may even have an effect when injected in pure gas flow. In their experiments, this seemed to be due to the direct smoothing effect the DRA's had on the pipe's roughness. They concluded that the main mechanism at work was the DRA liquid sticking to the pipe wall and thereby allowing the gas to experience a smoother surface. That turned out to have nothing to do with the turbulence reduction caused by polymer chains, and could probably have been achieved by other types of fluids as well. Also, the potential gain will obviously depend on how smooth the pipe is to begin with. Only relatively rough surfaces, in practice meaning uncoated gas pipelines, can expect to get lower rather than higher surface roughness when a layer of liquid is created. Trying to increase a gas pipeline's capacity this way must be

considered experimental, and it can potentially lead to completely different results if various two-phase flow phenomena occur due to the liquid fraction becoming too high.

More details about DRAs can be found in the papers by Pietsch et al. (1999) and Somandepalli et al. (2006). One of the most promising, recent publications presenting a well-founded turbulence theory for how DRAs work is that of Proccacia et al. (2008).

It is also easy to find more material by doing an Internet search for Drag Reducing Agents. It will reveal numerous articles and suppliers relevant to the subject. The supplier brochures may at times reflect the fact that no generally accepted theory behind the technology exists, and some of the marketing claims should be viewed with caution.

References

Ryan, N.W., Johnson, M.M. (1959): *Transition from Laminar to Turbulent Flow in Pipes.* AIChE J. 5: 433-435.

Dodge, D.W., Metzner, A.B. (1959): *Turbulent Flow of Non-Newtonian Systems* . AIChEJ Vol. 5 No. 2, p. 189.

Hanks, R.W. (1963): *Laminar-turbulent Transition of Fluids with a Yield Strength.* AIChEJ J. 9: 306-309.

Govier, G.W., Aziz, K. (1972): *The Flow of Complex Mixtures in Pipes.* Van Nostrand Reinhold, New York.

Mishra, P., Tripathi, G., (1971): Chemical Engineering Science Vol. 26, No. 2.

Tadashi, M., Toshio, K. (1978): *On Lower Critical Reynolds Number of Non-Newtonian Fluid Flow.* Bulletin of JSMA, Vol. 2, No. 155, pp 848-853.

Starling, K. E. (1992): *Compressibility Factors of Natural Gas and Other Related Hydrocarbon Gases*. Transmission Measurement Committee Report no. 8, American Gas Association.

Barnes, H.A., Hutton, J.F., Walters, K. (1993): *An Introduction to Rheology.* Elsevier, Science Publishers, Third Edition.

Steffe, J.F. (1992): *Rheological Methods in Food Process Engineering.* Second Edition. Freeman Press.

 For non-commercial use only

Chhabra, R.P., Richardson, J.F. (1999): *Non-Newtonian Flow in the Process Industries, Fundamentals and Engineering Applications.* Butterworth-Heinemann.

Pietsch, U., Koberstein, B. (1999): *Establishing Parameters required for Real-Time On-Line Drag-Reducing Agent Modelling*. PSIG 9914. Pipeline Simulation Interest Group.

Oertel, H., Bohle, M., Etling, D., Muller, U., Screenivasan, K.R., Riedel, U., Warnatz, J. (2004): *Prandtl's Essentials of Fluid Mechanics*. Springer.

Liu, H. (2003): *Pipeline Engineering*. Lewis Publishers.

Gaard, S., Isaksen, O.T. (2003): *Experiments with Different Drag-Reducing Additives in Turbulent Flow in Dense Phase Gas Pipelines.* PSIG 03B3, Pipeline Simulation Interest Group.

Somandepalli, V.S.R., Mungal, M.G. (2006): *Combined PIV and PLIF Measurements in a Polymer Drag Reduced Turbulent Boundary Layer*. Report No. TSD-169, Stanford University.

Procaccia, I., L'vov, V.S., Benzi, R. (2008): *Theory of Drag Reduction by Polymers in Wall Bounded Turbulence*. Reviews of Modern Physics, v 80, 225.

"As far as the laws of mathematics refer to reality, they are not certain, and as far as they are certain, they do not refer to reality."
Albert Einstein

6 Transient flow

This chapter shows conservation equations on a general form:

- Mass conservation
- Momentum conservation
- Energy conservation
- Examples illustrating the conservation equations

6.1 Mass conservation

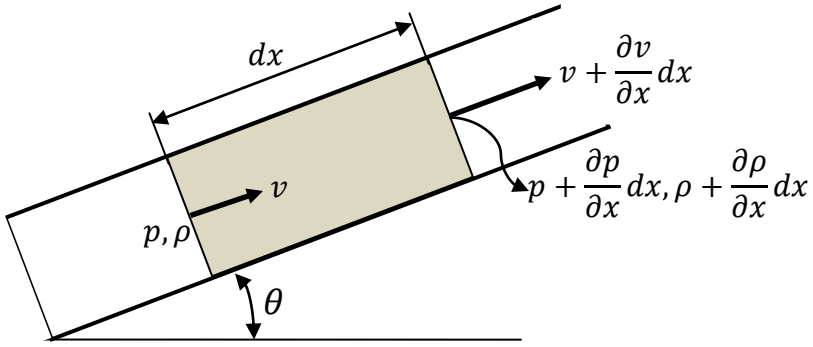


Figure 6.1.1. Compressible single-phase fluid flowing through a pipe.

Consider a control volume V of a pipe. The mass m in that volume may change over time due to density change and due to changes in what flows in and out of the volume. Since pipe materials to at least some extent are elastic, the volume also changes, but let

 For non-commercial use only

us for now neglect that fact. Mass balance for a single-phase flow can then be expressed as follows:

$$\frac{dm}{dt} = \int_V \frac{\partial \rho}{\partial t} dV + \int_S (\rho v) n_s dS \tag{6.1.1}$$

The first term on the right-hand side of equation 6.1.1 accounts for all the density changes over time integrated over the total control volume. Neglecting higher order terms in this integral, meaning $\partial\rho/\partial t$ is assumed to be constant within the control volume V, leads to:

$$\int_V \frac{\partial \rho}{\partial t} dV = \frac{\partial \rho}{\partial t} V = \frac{\partial \rho}{\partial t} dx\, A \tag{6.1.2}$$

The second term integrates all mass entering and leaving the control volume. S is the control volume's surface, and n_s is the vector normal to it. By convention, n_s always points out of the control volume. Since the flow is assumed to go parallel to the pipe's axis, and no fluid flows through the pipe wall, the net result of this integral is simply the change in mass flow along dx:

$$\int_S (\rho v) n dS = \frac{\partial (\rho v)}{\partial x}\, dx\, A \tag{6.1.3}$$

If we allow the boundaries of our control volume to follow the flow in such a way that the mass is kept constant within the control volume, we may simplify equation 3.1, since it implies that dm/dt=0. Equation 3.1 can be written as:

$$0 = \frac{\partial \rho}{\partial t} dx\, A + \frac{\partial (\rho v)}{\partial x}\, dx\, A \tag{6.1.4}$$

By re-arranging:

$$\frac{\partial \rho}{\partial t} + \frac{\partial (\rho v)}{\partial x} = 0 \tag{6.1.5}$$

This is the continuity equation written on what is called conservation form. Looking at it we can immediately read out a couple of interesting results. For instance, equation 6.1.5 implies that if the velocity changes inversely proportional to the density along the pipe, so the product ρv stays constant, then $\partial(\rho v)/\partial x = 0$. If so, we must also have that $\partial \rho/\partial t = 0$, meaning there is no density change over time at any given pipe position. That seems credible. If the mass flow is constant though all cross-sections, there will not be any build-up of mass or changing density anywhere. The argument can of course also be reversed, implying that if the density is constant over time at a given point, then the mass flow is also constant at that point.

As shown by Anderson (1995) and many others, the same equation can be arrived at by approaching the problem in slightly different ways. Considering a finite or infinitesimally small control volume, either stationary or moving with the flow, lead to similar equations, but on slightly different form.

Looking at figure 6.1.1 again, we assume the control volume to be stationary. The mass balance becomes:

$$\textit{mass accumulation rate} = \textit{mass flow in} - \textit{mass flow out}$$

$$\mathrm{A} \cdot \mathrm{dx} \frac{\partial \rho}{\partial t} = A\rho v - A \cdot \left(\rho + \frac{\partial \rho}{\partial x} dx\right)\left(v + \frac{\partial v}{\partial x} dx\right) \tag{6.1.6}$$

Neglecting higher order terms, this leads to:

$$\frac{\partial \rho}{\partial t} + v\frac{\partial \rho}{\partial x} + \rho\frac{\partial v}{\partial x} = 0 \tag{6.1.7}$$

 For non-commercial use only

This can be further transformed by observing that the two last terms describe the derivatives of a product, and we have:

$$v\frac{\partial \rho}{\partial x} + \rho\frac{\partial v}{\partial x} = \frac{\partial(\rho v)}{\partial x} \tag{6.1.8}$$

If we insert equation 6.1.8 into 6.1.7, we arrive at equation 6.1.5 again. It shows that equation 6.1.7, which is called the non-conservation form, is actually identical to the so-called conservation form shown in equation 6.1.5.

The form used by Streeter & Wylie (1983) in their book *Fluid Transients* – a book used by nearly everyone in the field of transient single-phase pipe flow – is most similar to 6.1.7. There is one difference, though: Unlike Streeter & Wylie, we have chosen not to involve any fluid properties in our continuity equation. For instance, we have not yet mentioned anything about how pressure p and density ρ is correlated for a particular gas or liquid, since different fluid can be very different in this respect. Equations 6.1.7 and 6.1.5 are therefore general and valid for any single-phase fluid, but fluid properties must be introduced later to close the system.

6.2 Momentum conservation

By applying Newton's second law to the control volume in figure 6.1.1 we get:

$$\text{Mass} \cdot \text{acceleration} = \text{net pressure force} + \text{friction} + \text{gravity}$$

$$Adx\rho\frac{dv}{dt} = pA - \left(p + \frac{\partial p}{\partial x}dx\right)A - \frac{f\rho dx}{2d}v|v|A - Adx\rho g\,sin\theta \tag{6.2.1}$$

Remember that acceleration is defined as dv/dt, not $\partial v/\partial x$ or $\partial v/\partial t$. This definition means position changes in addition to time, and the control volume is moving with the fluid. That is different to how we chose to formulate the continuity equation 6.1.6.

Equation 6.2.1 can be formulated as:

$$\rho \frac{dv}{dt} = -\frac{\partial \rho}{\partial x} - \frac{f\rho}{2d} v|v| - \rho g \sin\theta \tag{6.2.2}$$

Equation 6.2.2 contains a mixture of derivatives and partial derivatives, so we seek an alternative way of expressing the left hand side. From the definition of a partial derivative, it follows that:

$$dv = \frac{\partial v}{\partial t} dt + \frac{\partial v}{\partial x} dx \tag{6.2.3}$$

The definition of velocity means:

$$\frac{dx}{dt} = v \tag{6.2.4}$$

We get:

$$\frac{dv}{dt} = \frac{\partial v}{\partial t} + v \frac{\partial v}{\partial x} \tag{6.2.5}$$

Inserting equation 6.2.5 into 6.2.2:

$$\rho \frac{\partial v}{\partial t} + \rho v \frac{\partial v}{\partial x} = -\frac{\partial p}{\partial x} - \frac{f\rho}{2d} v|v| - \rho g sin\theta \tag{6.2.6}$$

The left hand side of equation 6.2.6 describes the inertia-part of Newton's equation. It has two terms, indicating that each fluid particle can accelerate both in time and space.

This equation can be used as it stands, or it may be re-arranged somewhat. We observe that:

 For non-commercial use only

$$\frac{\partial(\rho v)}{\partial t} = \rho\frac{\partial v}{\partial t} + v\frac{\partial \rho}{\partial t} \tag{6.2.7}$$

And therefore:

$$\rho\frac{\partial v}{\partial t} = \frac{\partial(\rho v)}{\partial t} - v\frac{\partial \rho}{\partial t} \tag{6.2.8}$$

We will also soon see that the following general mathematical relation, describing the (partial) derivative of a product, may be useful:

$$\frac{\partial}{\partial x}(\rho v^2) = \rho v\frac{\partial v}{\partial x} + v\frac{\partial(\rho v)}{\partial x} \tag{6.2.9}$$

That can be written as:

$$\rho v\frac{\partial v}{\partial x} = \frac{\partial}{\partial x}(\rho v^2) - v\frac{\partial(\rho v)}{\partial x} \tag{6.2.10}$$

By inserting equations 6.2.8 and 6.2.10 into 6.2.6, we get:

$$\frac{\partial \rho}{\partial t} + \frac{\partial}{\partial x}(\rho v^2) - v\left[\frac{\partial \rho}{\partial t} + \frac{\partial(\rho v)}{\partial x}\right] = -\frac{\partial p}{\partial x} - \frac{f\rho}{2d}v|v| - \rho g sin\theta \tag{6.2.11}$$

It turns out the term in brackets is simply the left hand side of the continuity equation 6.1.5, and hence the term is zero. That means the momentum equation 6.2.6 can be reduced to:

$$\frac{\partial(\rho v)}{\partial t}+\frac{\partial(\rho v^2)}{\partial x}=-\frac{\partial p}{\partial x}-\frac{f\rho}{2d}v|v|-\rho g sin\theta \tag{6.2.12}$$

This form of the momentum equation is the one most similar to the ones we use when simulating gas flow in later chapters. Many textbooks about liquid transients, including Streeter & Wylie's (1983) use something more similar to 6.2.6, though. We have avoided including any fluid properties in any of them at this stage, so both equation 6.2.12 and 6.2.6 are valid for any single-phase fluid.

6.3 Energy conservation

We have so far studied two equations derived from mass and momentum conservation principles. Those are direct flow considerations, and they cannot alone reveal anything about how the temperature develops in the fluid. Heat flow can have a major impact on pipeline hydraulics, and accurate pipeline simulations often require the underlying model to include thermal effects. This is particularly true for gas flow, since the fluid's temperature strongly affects density. There are many situations where thermodynamics may be important in pure liquid pipe flow as well. Some crude pipelines, for instance, would be destroyed as the crude turned into tar had the cooling-down been allowed to proceed to equilibrium in a situation where the flow has been stopped.

Many different approaches to thermal modeling are in common use, ranging from simple assumptions of constant temperature (isothermal flow) or no heat loss (adiabatic flow) to detailed models of heat flow in the fluid, through the pipe wall (with its insulation, if any), and to the surroundings. At first, we only focus on the fluid and do not include anything about exactly how heat flows through the pipe wall, that part is left to chapter 8.

Let us go back to figure 6.1.1 and study the energy equation for a small element following the flow. We define the boundaries such that the element's mass is kept constant, just as we did when developing the mass conservation equation. Energy conservation means the net energy coming in to the element has to accumulate within it:

 For non-commercial use only

Rate of change of energy inside element	=	Net heat flux into element	+	Rate of work done on element

The left-hand side of this equation can be written as:

$$LHS = \frac{d}{dt}(\rho A dx \cdot E_s) \tag{6.3.1}$$

Where $\rho A dx$ is the control volume's total mass and E_s is the control volume's total energy pr. unit mass. At this stage will not worry about exactly which components E_s consists of, but instead observe that since $\rho A dx$ is constant, we may write:

$$LHS = \rho A dx \frac{dE_s}{dt} \tag{6.3.2}$$

This may be re-formulated as:

$$LHS = \rho A dx \left(\frac{\partial E_s}{\partial t} + v\frac{\partial E_s}{\partial x}\right) \tag{6.3.3}$$

From mathematics, we know that:

$$\frac{\partial(\rho E_s)}{\partial t} + \frac{\partial(\rho v E_s)}{\partial x} = \rho\frac{\partial E_s}{\partial t} + E_s\frac{\partial \rho}{\partial t} + E_s\frac{\partial(\rho v)}{\partial x} + \rho v\frac{\partial E_s}{\partial x} \tag{6.3.4}$$

The continuity equation 6.1.5 implies:

$$E_s \frac{\partial \rho}{\partial t} + E_s \frac{\partial (\rho v)}{\partial x} = 0 \tag{6.3.5}$$

And therefore, 6.3.4 reduces to:

$$\frac{\partial (\rho E_s)}{\partial t} + \frac{\partial (\rho v E_s)}{\partial x} = \rho \left(\frac{\partial E_s}{\partial t} + v \frac{\partial E_s}{\partial x} \right) \tag{6.3.6}$$

By inserting equation 6.3.6 into 6.3.3 we get:

$$LHS = Adx \left(\frac{\partial (\rho E_s)}{\partial t} + \frac{\partial (\rho v E_s)}{\partial x} \right) \tag{6.3.7}$$

The specific energy E_s in the control volume has 3 parts:

$$E_s = u + \frac{v^2}{2} + gz \tag{6.3.8}$$

Two of those terms are familiar from the well-known Bernoulli's energy equation: $v^2/2$ comes from the kinetic energy, and gz is the potential energy due to the element's elevation z from a reference level. u is the fluid's specific internal energy, which is simply the energy of all the molecules in the control volume. For gases, the familiar Brownian motion is caused by this energy, and it consists of translational, rotational, vibratory, and electronic parts.

On the right hand side of the equation, the only heat coming from the surroundings into the pipe element is the convection going through the pipe wall. The heat pr. unit volume of pipe, q, is the net heat flux into the element.

 For non-commercial use only

The last term, rate of work done on the element, is the net rate of work done by pressure in the axial direction x. Since forces in the positive x-direction do positive work, a growing pv means negative work is done, and so:

$$RHS = \rho q A dx - \frac{\partial (pv)}{\partial x} dx A + w \tag{6.3.9}$$

Where the term w, accounting for other possible sources of power added to the flow (such as shaft work by pumps), has also been added. Combining the equations, we get:

$$\frac{\partial}{\partial t}\left[\rho\left(u + \frac{v^2}{2} + gz\right)\right] = -\frac{\partial}{\partial x}\left[\rho v\left(u + \frac{v^2}{2} + gz + \frac{p}{\rho}\right)\right] + q + w \tag{6.3.10}$$

Introducing the enthalpy h, which by definition is:

$$h \stackrel{\text{def}}{=} u + \frac{p}{\rho} \tag{6.3.11}$$

equation 6.3.10 is transformed into its final form:

$$\frac{\partial}{\partial t}\left[\rho\left(u + \frac{v^2}{2} + gz\right)\right] = -\frac{\partial}{\partial x}\left[\rho v\left(h + \frac{v^2}{2} + gz\right)\right] + q + w \tag{6.3.12}$$

This energy balance equation has a very general form. Just as in the mass and momentum conservation equations, we have not yet included any fluid-specific properties, such as a relation between pressure, density, and temperature. Nor have we mentioned anything about how enthalpy varies with temperature and pressure. Since we have not said anything about how heat flows through the pipe wall, we have not introduced any pipeline-specific properties either.

Equation 6.3.12 as it appears here, together with equations 6.1.5 and 6.2.12, apply to any single-phase liquid or gas flow and any sort of pipe insulation. The disadvantage of being so general is that the equations are not complete – we see that we have more unknowns than equations. In later chapters, we will see how closure can be achieved by including fluid and pipe properties.

6.4 Examples to illustrate the conservation equations

The continuity, momentum and energy equations are mainly used to create simulation models, but they can also be used to solve simple and even some not-so-simple problems manually. The examples below give us an opportunity to some familiarization with the equations.

6.4.1 Sloping liquid pipeline with steady-state flow

Problem: As an example of how the momentum equation can be applied, let's investigate a pipeline carrying an uncompressible fluid from inlet to outlet. We want to determine what the steady-state mass flow rate will be.

Solution: Since we are focusing on steady-state conditions, nothing is going to change over time, and $\partial(\rho v)/\partial t$ must be zero. Mass conservation (use either equation 6.1.5 or 6.1.7) shows, unsurprisingly, that $\partial v/\partial x = 0$. Note also that since there is no time derivative, all partial derivatives become identical to the ordinary type. The momentum equation 6.2.12 reduces to:

$$0 = -\frac{dp}{dx} - \frac{f\rho l}{2d} v|v| - \rho g sin\theta \tag{6.4.1}$$

Equation 6.4.1 can be separated, and the pressure can be integrated from inlet pressure p_1 to outlet pressure p_2, the position from inlet, where $x = 0$, to outlet, where $x = l$:

$$-\int_{p_1}^{p_2} dp = \int_0^l \left(\frac{f\rho l}{2d} v|v| + \rho g sin\theta\right) dx \tag{6.4.2}$$

 For non-commercial use only

If the pipe's slope is constant, all terms are constants, and integration becomes very easy:

$$-p_2 + p_1 = \frac{f\rho l}{2d} v|v| + \rho g l sin\theta \tag{6.4.3}$$

If the inlet and outlet elevations are z_1 and z_2:

$$p_1 - p_2 = \frac{f\rho l}{2d} v|v| + \rho g(z_2 - z_1) \tag{6.4.4}$$

Or:

$$\frac{p_1}{\rho g} + z_1 = \frac{p_2}{\rho g} + z_2 + \frac{fl}{2gd} v|v| \tag{6.4.5}$$

The result may at first glance appear somewhat surprising, given that equation 6.4.5 looks like the well-known Bernoulli energy equation, though with some terms lacking. Bernoulli's equation looks like this:

$$\frac{v_1^2}{2g} + \frac{p_1}{\rho g} + z_1 = \frac{v_2^2}{2g} + \frac{p_2}{\rho g} + z_2 + \frac{fl}{2gd} v|v| \tag{6.4.6}$$

When developing the momentum equation in 6.2.12, we used figure 6.1.1, where all focus was on what goes on inside the pipe. It does not take into account what happens at the boundaries, for instance when fluid at rest in a reservoir and accelerates towards the inlet. The kinetic energy-terms in Bernoulli's equation describe exactly that: It takes $v_2^2/2g$ of pressure head to bring each fluid particle from rest and up to the pipe velocity v_2. But as long as $v_1 = v_2$, equations 6.4.5 and 6.4.6 lead to the same result. Alternatively, if we set $v_1 = 0$ on equation 6.4.6 (starting in an u upstream reservoir, but neglecting any extra losses such as the one due to sharp inlet edges), we get:

$$v_2 = \sqrt{\frac{2[(p_1 - p_2) + \rho(z_1 - z_2)]}{\rho\left(\frac{fl}{d} + 1\right)}} \tag{6.4.7}$$

Expressed as mass flow:

$$\dot{m} = \sqrt{\frac{\rho\pi^2 d^4[(p_1 - p_2) + \rho(z_1 - z_2)]}{8\rho\left(\frac{fl}{d} + 1\right)}} \tag{6.4.8}$$

If we alternatively use the momentum equation 6.4.5, which means neglecting the velocity head, we get:

$$m = \sqrt{\frac{\rho\pi^2 d^4[(p_1 - p_2) + \rho(z_1 - z_2)]}{8\rho\left(\frac{fl}{d}\right)}} \tag{6.4.9}$$

And hence:

$$m = \sqrt{\frac{\rho\pi^2 d^5[(p_1 - p_2) + \rho(z_1 - z_2)]}{8\rho fl}} \tag{6.4.10}$$

Since the velocity head in long liquid pipelines is very small compared to the other terms, equations 6.4.10 and 6.4.8 usually give virtually the same result.

To summarize: This little example shows the transient momentum conservation equation 6.2.12, or its alternative formulation 6.2.16, can be reduced to Bernoulli's equation 6.4.6 for incompressible steady-state flow in a pipe. We may also include the

 For non-commercial use only

(normally negligible) pressure reduction when the fluid accelerates from a reservoir just outside the pipe inlet by setting the pipe inlet pressure $\rho v^2/2$ lower than the upstream reservoir pressure.

6.4.2 Horizontal gas pipeline with isothermal steady-state flow

Problem: Now let's consider an example quite similar to the previous one in chapter 6.4.1, but this time with a compressible fluid: A horizontal pipeline of length l transports gas. The upstream pressure is p_1, downstream it is p_2. What is the mass flow through the pipe going to be under steady-state conditions?

Solution: Again, steady-state conditions mean nothing varies with time. The only sort of derivation remaining in the momentum equation is then as a function of x, and so partial derivation is once again identical to ordinary derivation. Equation 6.2.6 reduces to

$$\rho v \frac{dv}{dx} = -\frac{dp}{dx} - \frac{f\rho}{2d} v^2 \tag{6.4.11}$$

Recalling that the left hand side of the equation describes the fluid's acceleration, it is clear that only acceleration due to the gas' gradual expansion as the pressure falls toward the outlet end creates acceleration. In a long pipeline with the gas flowing much slower than the velocity of sound, most of the pressure loss is due to friction, not acceleration. It means:

$$\rho v \frac{dv}{dx} \ll \frac{dp}{dx} \tag{6.4.12}$$

This approximation is sometimes referred to as one of the two Allievi simplifications, and we will later see it is also used when developing the method of characteristics for transient liquid flow. In this example, it is sufficient to observe that it simplifies equation 6.4.11 to:

$$\frac{dp}{dx} + \frac{f\rho}{2d}v^2 = 0 \tag{6.4.13}$$

Since mass flow does not vary along the pipeline, it is convenient to express velocity and density in terms of mass flow by multiplying velocity with cross-sectional area and density:

$$\frac{dp}{dx} = -\frac{8f}{\pi\rho d^5}\dot{m}^2 \tag{6.4.14}$$

To get further from here it is necessary to introduce a relation between the gas' pressure and density. The gas law for real gases (taking into account that gases are not perfect) can be written on this form:

$$\rho = \frac{M_g p}{ZRT} \tag{6.4.15}$$

Where Z is the compressibility factor, R is the universal gas constant, M_g is gas molar mass and T is absolute temperature. Inserting equation 6.4.15 into 6.4.14 and integrating the pressure from inlet to outlet along the pipe, we get:

$$\int_{p_1}^{p_2} p dp = -\int_0^l \frac{8fZRT}{\pi^2 d^5 M_g}\dot{m}^2 dx \tag{6.4.16}$$

If things happen slowly enough for the pipe wall to exchange heat with the gas at such a rate that the temperature stays constant over time t and position x, we have isothermal conditions. Then everything to the left of dx on the right hand side of the equation is constant along the pipe, and integrating is straight forward. Note, though,

 For non-commercial use only

that the gas property Z also varies somewhat with the pressure, so we need to use some average for the whole pipelines, let us call it $\bar{Z}$.

After re-arranging the result, we arrive at the mass flow as:

$$\dot{m} = \frac{\pi}{4}\sqrt{\frac{d^5}{f\,l}\frac{M_g}{\bar{Z}RT}(p_1^2 - p_2^2)} \tag{6.4.17}$$

Remember that equation 6.4.17 was developed under the assumption that the pipe is horizontal. It is not sufficient for the inlet and outlet ends to be at the same elevation. In low-lying regions of the pipe, for instance, the pressure is going to be higher due to the increased static head. Since the gas is compressible, that leads to a higher density, and hence a lower velocity for the given mass flow. As a result, a pipeline with mid-section located lower than the inlet and outlet, say an export pipeline along the seabed from Norway to France, is going to have a somewhat higher capacity than equation 6.4.17 indicates. The opposite holds true for pipelines passing over a mountain range. The difference is not huge, though, and it is common to neglect it for approximate calculations or moderate elevations.

This simple example gives us some clues as to why steady-state computations are so popular: Neglecting time-dependent phenomena reduces complexity even when transient equations are used as a basis. Unfortunately, steady-state methods cannot reveal much about most transient phenomena, so what they gain in convenience is generally paid for by reduced validity.

Given these limitations, we may use the equation to estimate the capacity for one of the world's longest subsea gas pipelines, *where* $l = 8.13{\cdot}10^5$ *m (813 km)* and $d = 0.9664$ *m*. The pipe's inside is coated and found to be hydraulically smooth up to $Re = 3.0{\cdot}10^7$. Suppose we run the pipeline with inlet pressure $p_1 = 1.5{\cdot}10^7$ *Pa (15 MPa)* and outlet pressure $p_2 = 9.6{\cdot}10^6$ *Pa* (*9.6 MPa*), and that the gas temperature in the whole pipeline is $T = 278$ *K* with a gas having $M_g = 0.0185$ *kg/mol*, $\bar{Z} = 0.70$ and $\square = 16.9 \cdot 10^{-6}$ *kg/(m·s²)*, what is the mass flow going to be?

At first we do not know *Re*, and can therefore not pick the correct friction factor *f(Re, k_s/d)*. Since this is a large-diameter, high pressure gas pipeline, we expect *Re* to be in the

order of 10^7. According to the surface uniformity-based diagram in figures 2.9.1-2.9.3 (all 3 diagrams are identical for smooth pipe), that should correspond to $f \sim 8.4 \cdot 10^{-3}$.

Inserting that, as well as a universal gas constant $R = 8.32$ *J/(K·mol)* into equation 6.4.17 leads to $\dot{m} = 340$ *kg/s*. We may now correct *Re* according to equation 2.2.5, and we get $Re = 2.65 \cdot 10^7$. Using the modified Moody diagram again, we read $f = 7.37 \cdot 10^{-3}$. Iterating once more by using this *f*-value in equation 6.4.17, we get $\dot{m} = 362$ *kg/s*.

6.4.3 Example: Gas pipeline cooling down after stop

Problem: Due to an unintended shut-down, the gas in a subsea pipeline is suddenly stopped. How long time t_1 does it take for the temperature to drop from the initial temperature T_0 down to T_1?

Solution: We will later see how such problems can be solved quite accurately by simulations. At this stage, though, the problem is simplified to make it within reach of hand calculations. The following assumptions are made:

i) The flow has had time to come to rest when we start our calculations (steady-state). This is not always a very good assumption for long pipelines since it can take days and even weeks before the pressure evens out and the gas comes to rest.

ii) The inside gas temperature is the same in the whole pipeline (isothermal flow). This may or may not be a good assumption, depending on such parameters as pipe length, outside temperature, gas inlet temperature, insulation and so on.

iii) The heat loss q_l pr. unit length is constant over the studied time period. This may be a good approximation as long as we study a relatively small part of the temperature reduction, such as for instance the reduction corresponding to one hour of cooling. But after a longer time, when the inside gas temperature approaches the outside temperature, q_l is obviously going to diminish and eventually become zero.

Simplifications i) and ii) imply that all variations along the pipeline is zero, meaning anything to do with $\partial/\partial x$ in equation 6.3.12 has to be zero. That means the only derivation left is the one to do with time, and therefore $\partial/\partial t$ is the same as d/dt. No work is done, so $w = 0$. Everything being at rest means $v = 0$, and we are left with:

 For non-commercial use only

$$\frac{d}{dt}(\rho u + \rho g z) = q \tag{6.4.18}$$

Since the gas volume is locked in, the mass stays constant, and so does the density. The term $\rho g z$ stays constant, and its derivative becomes zero. The equation simplifies to:

$$\frac{d}{dt}(\rho u) = q \tag{6.4.19}$$

By introducing the specific heat at constant volume:

$$u = c_v T \tag{6.4.20}$$

We get:

$$\frac{d(\rho c_v T)}{dt} = q \tag{6.4.21}$$

This equation is separable and can be integrated as follows:

$$\rho c_v \int_{T=T_0}^{T_1} dT = q \int_{t=0}^{t_1} dt \tag{6.4.22}$$

This solves as:

$$t_1 = \frac{\rho c_v}{q}(T_1 - T_0) \tag{6.4.23}$$

Recalling that q is heat pr. unit volume, while q_l was given in heat per unit length of pipe, we may set the following balance for the full length l of the pipeline:

$$qAl = q_l l \tag{6.4.24}$$

And so:

$$q = \frac{q_l}{A} \tag{6.4.25}$$

The final result becomes:

$$t_1 = \frac{A\rho c_v}{q_l}(T_1 - T_0) \tag{6.4.26}$$

A is the pipe's cross-section. This example illustrates that it can be possible to do manual checks of the heat calculation results produced by simulation programs. If we have conditions similar to the assumptions used here, a manual calculation is quite straight forward. The method can be extended to including the heat exchange equations outlined in chapter 8.

References

Streeter, V.L., Wylie, E.B., (1983): *Fluid Transients.* FEB Press.

Anderson, J.D. (1995): *Computational Fluid Dynamics: The Basics with Applications.* McGraw Hill.

Tosun, I. (2002): *Modeling in Transport Phenomena. A Conceptual Approach.* Elsevier.

 For non-commercial use only

Menon, E.S. (2005): *Gas Pipeline Hydraulics*. Taylor & Francis Group, LLC.

Prosperetti, A., Tryggvason, G. (2007): *Computational Methods for Multi-phase Flow*. Cambridge University Press.

"I do not fear computers. I fear the lack of them."
Isaac Asimov

7 Simplified liquid flow solution

Simplified liquid solutions of the two first conservation equations:

- Allievi's simplifications and the method of characteristics
- Boundary methods for the method of characteristics
- How to include valves, pumps and junctions
- Simple pipes and pipe networks simulation examples
- Modifications for fast steady-state network solutions
- Stability considerations
- Ways to check simulation results

7.1 Main principles

7.1.1 General

Liquid flow is somewhat simpler than gas flow in that the density does not change much as a function of pressure or temperature. In fact, temperature does not affect the transients significantly for liquid flow, and we do not need to include the energy equation unless the temperature is of interest for other reasons, such as to determine the viscosity more accurately. If we first presume the flow to be isothermal, or if we simply neglect temperature variations, we will see that a complete, closed simulation model

 For non-commercial use only

can be formulated using only the continuity and momentum equations, together with a very simple correlation between density and pressure.

7.1.2 Involving fluid properties

A fluid's compressibility, k_c, is described by its speed of sound, a_s, and density, ρ, as follows:

$$a_s = \sqrt{\frac{k_c}{\rho}} \tag{7.1.1}$$

As one would intuitively expect, this correlation shows that the speed of sound increases if the compressibility increases (since compressibility, unlike volume elasticity, takes higher values the 'stiffer' the fluid), and it decreases if density is increased. In water, for instance, the speed of sound is around *1500 m/s*. In case a small amount of fine air bubbles are dissolved in the water, the fluid may still behave like a single phase, but compressibility drops to a fraction of that of pure water. That leads to significantly reduced speed of sound; it can even become lower than that of pure air.

In addition, pipes are elastic, making the speed of sound in a pipe lower than the one described by 7.1.1. As shown by Wylie et al. (1983), this can be accounted for by adding an extra factor to equation 7.1.1:

$$a_s = \sqrt{\frac{1}{1 + \frac{k_c d}{E_w \delta_w}}} \sqrt{\frac{k_c}{\rho}} \tag{7.1.2}$$

Where E_w is the pipe wall material's modulus of elasticity, and δ_w is the pipe wall's thickness.

The speed of sound is a quantity that may be measured directly. Note, though, that friction may affect the measurements. If the friction is high, it can smooth away the fastest part of the wave front, and one is left with measurable disturbances which

propagate slower than equation 7.1.2 predicts. Details about that can be found in Ham (1982) and Bratland et al. (1989).

The compressibility of a liquid is expressed as:

$$k_c = V_0 \frac{\partial p}{\partial V} \tag{7.1.3}$$

Where ∂p is the increase in pressure resulting from compressing a volume V_0 by reducing it an amount ∂V. By combining equations 7.1.1, 7.1.3 and the definition of density, we get:

$$\partial \rho = \frac{1}{{a_s}^2} \partial p \tag{7.1.4}$$

The other significant liquid property, the viscosity, is a function of temperature and pressure. For isothermal flow, only the pressure varies. If the flow is highly turbulent, the friction does not vary much with the Reynolds number, and assuming constant viscosity is often acceptable. More sophisticated viscosity models for various liquids exist, se for instance Reid et al. (1987), but we are not going to discuss them in more detail here.

Once the velocity of sound has been determined, either by equation 7.1.2 or by direct measurements, we can use equation 7.1.4 to correlate pressure and density. To make our model as similar as possible to the most used form, the one presented by Wylie at al. (1983), we use the versions shown in 6.1.7 (rather than 6.1.5) and 6.2.6 (rather than 6.2.12). Doing so, continuity becomes:

$$\frac{\partial p}{\partial t} + v \frac{\partial p}{\partial x} + \rho {a_s}^2 \frac{\partial v}{\partial x} = 0 \tag{7.1.5}$$

And momentum:

 For non-commercial use only

$$\rho\frac{\partial v}{\partial t}+\rho v\frac{\partial v}{\partial x}=-\frac{\partial p}{\partial x}-\frac{f\rho}{2d}v|v|-\rho g sin\theta \tag{7.1.6}$$

The density does not change much even if the pressure does, and ρ can be treated as a constant in equations 7.1.5 and 7.1.6.

There are several ways to solve these two equations. The most used method is to simplify the equations first, and thereafter use the method of characteristics to solve them. Allievi (1913) showed that as long as v << a_s, something which is nearly always the case for pipes carrying liquid, two of the terms can be neglected:

$$\begin{aligned}\frac{\partial p}{\partial t}\gg v\frac{\partial p}{\partial x}&=>\ v\frac{\partial p}{\partial x}\sim 0\\ \frac{\partial v}{\partial t}\gg v\frac{\partial v}{\partial x}&=>\ v\frac{\partial v}{\partial x}\sim 0\end{aligned} \tag{7.1.7}$$

With Allievi's simplifications, the continuity and momentum equations become:

$$\frac{\partial p}{\partial t}+\rho {a_s}^2\frac{\partial v}{\partial x}=0 \tag{7.1.8}$$

$$\frac{\partial v}{\partial t}+\frac{1}{\rho}\frac{\partial p}{\partial x}+\frac{f}{2d}v|v|+gsin\theta=0 \tag{7.1.9}$$

These are two simple equations. Written on matrix form:

$$\frac{\partial}{\partial t}\begin{bmatrix}p\\ v\end{bmatrix}+\begin{bmatrix}0 & \rho {a_s}^2\\ \frac{1}{\rho} & 0\end{bmatrix}\frac{\partial}{\partial x}\begin{bmatrix}p\\ v\end{bmatrix}=\begin{bmatrix}0\\ -\frac{f}{2d}v|v|-gsin\theta\end{bmatrix} \tag{7.1.10}$$

As explained by Ployanin et al. (2004) and many other mathematicians, such a set of partial differential equations can be characterized by the square matrix in front of $\partial/\partial x$. The system's eigenvalues λ are defined by the determinant of that matrix as:

$$\begin{vmatrix} -\lambda & \rho {a_s}^2 \\ \frac{1}{\rho} & -\lambda \end{vmatrix} = 0 \tag{7.1.11}$$

The solution shows this system has two eigenvalues: $\lambda_1 = a_s$ and $\lambda_2 = -a_s$. Since they are both real, it tells us that our system as defined by equations 7.1.8 and 7.1.9 are hyperbolic. It is known that hyperbolic partial differential equations can be represented as a system of ordinary differential equations along curves called characteristic lines. We will now see how this can be done.

First, let us repeat how normal derivation and partial derivation is correlated:

$$dp = \frac{\partial p}{\partial x} dx + \frac{\partial p}{\partial t} dt \tag{7.1.12}$$

And therefore:

$$\frac{dp}{dt} = \frac{\partial p}{\partial x}\frac{dx}{dt} + \frac{\partial p}{\partial t} \tag{7.1.13}$$

A similar correlation must of course be valid for the velocity:

$$\frac{dv}{dt} = \frac{\partial v}{\partial x}\frac{dx}{dt} + \frac{\partial v}{\partial t} \tag{7.1.14}$$

 For non-commercial use only

To see how this can be used to transform the equations, let us summarize equations 7.1.8 and 7.1.9:

$$n_0\left(\frac{\partial p}{\partial t}+\rho {a_s}^2\frac{\partial v}{\partial x}\right)+\left(\frac{\partial v}{\partial t}+\frac{1}{\rho}\frac{\partial p}{\partial x}+\frac{f}{2d}v|v|+gsin\theta\right)=0 \qquad (7.1.15)$$

The first parenthesis contains the left side of equation 7.1.8, which is zero, and the second parenthesis contains the left side of equation 7.1.9, which is also zero. Multiplying one of those two zeros with any number n_0, and summarizing, is still going to be zero. If we do that and also re-organize the equation somewhat, we get:

$$n_0\left(\frac{\partial p}{\partial x}\frac{1}{n_0\rho}+\frac{\partial p}{\partial t}\right)+\left(\frac{\partial v}{\partial x}n_0\rho {a_s}^2+\frac{\partial v}{\partial t}\right)+\frac{f}{2d}v|v|+gsin\theta=0 \qquad (7.1.16)$$

It turns out the first parenthesis in equation 7.1.15 happens to be very similar to the right-hand side of equation 7.1.13. The same can be said about the second parenthesis and equation 7.1.14. Since equation 7.1.16 is valid for any value of n_0, we are free to choose it so it maintains similarity with both equations:

$$\frac{dx}{dt}=\frac{1}{n_0\rho}=n_0\rho {a_s}^2 \qquad (7.1.17)$$

This produces two possible solutions for n_0:

$$n_0=\pm\frac{1}{\rho a_s} \qquad (7.1.18)$$

By inserting these two values into equation 7.1.16 and 7.1.17, we get the following sets of equations:

$$\frac{1}{\rho a_s}\frac{dp}{dt}+\frac{dv}{dt}+\frac{f}{2d}v|v|+gsin\theta=0\ for\ \frac{dx}{dt}=a_s \qquad (7.1.19)$$

And:

$$-\frac{1}{\rho a_s}\frac{dp}{dt}+\frac{dv}{dt}+\frac{f}{2d}v|v|+gsin\theta=0\ for\ \frac{dx}{dt}=-a_s \qquad (7.1.20)$$

These remarkable results show that as long as we make sure $dx/dt = \pm a_s$, equations 7.1.19 and 7.1.20 describe how the liquid flows in the pipe. At first it may not be obvious why this set of ordinary differential equations is preferable to the original, partial ones, but they do have two very significant advantages: They are relatively easy to solve numerically, and they show us that liquid flow in pipes can be described by characteristic lines, meaning they propagate as waves.

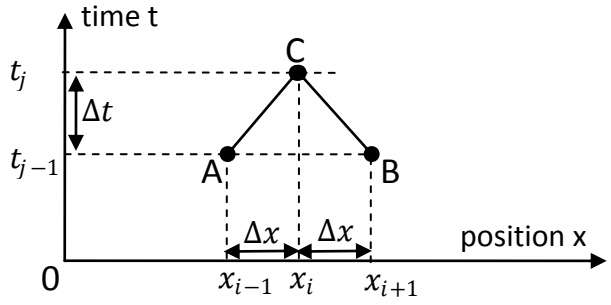


Figure 7.1.1. Characteristic lines in the xt-plane.

Figure 7.1.1 illustrates the characteristic lines. A-C is the line corresponding to $dx/dt = a_s$, while B-C shows $dx/dt = -a_s$. The only thing affecting the state in point C, meaning affecting the pressure and velocity at position x_i at time t_j, is the state in point A and B. Nothing else matters – or rather – no other points in time or space influence the conditions in C than those in A and B (or anywhere in-between).

This is an interesting result. It states any disturbance, or wave, can propagate only at the speed of sound, a_s. This is actually similar to what we observe around us every day. For instance, if an explosion takes place a kilometer away, we are only going to hear it about 3 seconds later, corresponding to a speed of sound of around *330 m/s*. Another way to put it would be to say that anything we hear 3 seconds after it happened has to come from one kilometer away. Had our world been one-dimensional, as a pipeline in

 For non-commercial use only

this respect is, there would only be two places the sound could come from if the distance was one kilometer. Had the distance been different, the time would change accordingly so that the relation between them was kept constant. This explains why a particular value of *dx/dt* emerges from the mathematical model as special, namely the *dx/dt* corresponding to the speed of sound.

The sound-wave-like behavior also leads to some interesting conclusions which may seem counter-intuitive. For instance, imagine a long pipe leading water from an upper to a lower reservoir. At some point in time, somebody closes a valve at the middle of the pipe. We may expect the water to come to rest once the closure has been completed. But according to our results, that cannot happen instantaneously since no information can travel faster than the speed of sound. Just after the closure, water will continue flowing into the pipe as if nothing happened (if the pipe is long enough for the wave not to have reached the inlet). The inlet point does not even know closure has taken place. It is (at first) not only true that the inlet velocity has not had time to slow down – it has not even started! This obviously has to lead to a high pressure buildup and it is in fact one of the situations we may study with the model being developed here.

The results imply that as long as we compare points on the characteristic lines, the ones indicated in figure 7.1.1, we can use equations 7.1.19 and 7.1.20 to simulate the flow in the pipe.

7.2 Solving the equations by the characteristics method

If we have a pipeline of length l, we may divide it into N_x equal parts on length:

$$\Delta x = \frac{l}{N_x} \tag{7.2.1}$$

When simulating the pipe in the time domain, we need to divide time similarly. A natural choice of mesh size is then obviously:

$$\Delta t = \frac{\Delta x}{a_s} \tag{7.2.2}$$

To solve equations 7.1.19 and 7.1.20 numerically, we need to approximate dp/dt and dv/dt. The simplest way is to use a first-order approximation. Applying the notations illustrated in figure 7.1.1 we get:

$$\frac{dp}{dt} = \frac{p_C - p_A}{\Delta t} \; for \; \frac{dx}{dt} = a_s$$

$$\frac{dp}{dt} = \frac{p_C - p_B}{\Delta t} \; for \; \frac{dx}{dt} = -a_s \tag{7.2.3}$$

And:

$$\frac{dv}{dt} = \frac{v_C - v_A}{\Delta t} \; for \; \frac{dx}{dt} = a_s$$

$$\frac{dv}{dt} = \frac{v_C - v_B}{\Delta t} \; for \; \frac{dx}{dt} = -a_s \tag{7.2.4}$$

By inserting this into equations 7.1.19 and 7.1.20:

$$\frac{1}{\rho a_s}\frac{p_C - p_A}{\Delta t} + \frac{v_C - v_A}{\Delta t} + \frac{f}{2d} v|v| + gsin\theta = 0 \; for \; \frac{dx}{dt} = a_s \tag{7.2.5}$$

And:

$$-\frac{1}{\rho a_s}\frac{p_C - p_B}{\Delta t} + \frac{v_C - v_B}{\Delta t} + \frac{f}{2d}v|v| + gsin\theta = 0 \; for \; \frac{dx}{dt} = -a_s \tag{7.2.6}$$

The velocity to be used in the friction term in equation 7.2.5 should ideally be an average of the velocity in A and C, and an average of those in B and C for equation 7.2.6. For simplicity, we approximate by using only the velocity in the previous time step (A and B respectively) instead. The same is done for the pipe's slope θ. If we use equations 7.2.5 and 7.2.6 to eliminate v_c and find an expression for p_c, we get:

$$p_C = \frac{1}{2}\Big[(p_A + p_B) + \rho a(v_A - v_B) - \rho a_s \Delta t\left(\frac{f_A}{2d}v_A|v_A| + gsin\theta_A - \frac{f_B}{2d}v_B|v_B| - gsin\theta_B\right)\Big] \tag{7.2.7}$$

Similarly, we may eliminate p_c and find an expression for v_c:

$$v_C = \frac{1}{2}\Big[\frac{1}{\rho a_s}(p_A - p_B) + (v_A + v_B) - \Delta t\left(\frac{f_A}{2d}v_A|v_A| + gsin\theta_A + \frac{f_B}{2d}v_B|v_B| + gsin\theta_B\right)\Big] \tag{7.2.8}$$

As shown in chapter 7.7, this way of solving the equations happens to lead to a numerically stable solution for nearly any N_x - a very unusual situation for an explicit numerical method. Since the method is explicit, computing p_c and v_c for the next time step requires only knowledge from the previous time step, so no iteration is necessary to achieve a solution. A larger N_x leads to a finer resolution both in space (equation 7.2.1) and time (equation 7.2.2), and therefore a better approximation for the derivatives in equations 7.2.3 and 7.2.4. All in all, that produces a more accurate result, but at the cost of requiring more computing capacity. That is rarely a limitation when using the method of characteristics for single-phase pipe flow these days.

The computing efficiency can be improved if we economize somewhat and avoid repeating some of the same computations for both p_c and v_c. Some of the terms are

similar in both equations 7.2.7 and 7.2.8. It is convenient to define two constants to hold intermediate values:

$$K_A = p_A + \rho a_s v_A - \rho a_s \Delta t \left(\frac{f_A}{2d} v_A |v_A| + g sin\theta_A \right) \tag{7.2.9}$$

$$K_B = p_B - \rho a_s v_B + \rho a_s \Delta t \left(\frac{f_B}{2d} v_B |v_B| + g sin\theta_B \right) \tag{7.2.10}$$

If we compare equations 7.2.9 and 7.2.10 with 7.2.7 and 7.2.8, we see that p_c and v_c can be expressed as:

$$p_C = \frac{1}{2}(K_A + K_B) \tag{7.2.11}$$

$$v_C = \frac{1}{2\rho a_s}(K_A - K_B) \tag{7.2.12}$$

At the boundaries, meaning at the ends of the pipe, it is sometimes the pressure or velocity which is known, while K_A or K_B is not. Combining equations 7.2.11 and 7.2.12 makes it possible to eliminate or express the unknown, for instance as:

$$p_C = K_B + \rho a_s v_C \tag{7.2.13}$$

or

 For non-commercial use only

$$p_C = K_A - \rho a_s v_C \tag{7.2.14}$$

In the next chapter, we will see that equations 7.2.9 - 7.2.14 make it very easy both to compute pressures and velocities in each grid point inside the pipe, as well as to formulate various sorts of boundary conditions, including for valves, pumps and junctions.

7.2.1 Example: Instantaneous valve closure

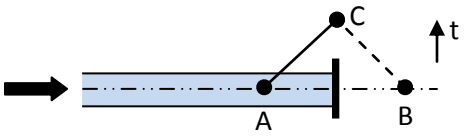


Figure 7.2.1. Fast-closing valve at outlet.

Suppose a valve is closed instantaneously in a pipe where the initial velocity v_0. What is the pressure going to be upstream of the valve just after closure?

This is a classic problem, and we will see that the solution is actually very simple – and very useful.

We know v_c by the valve after closure: It has to be zero. Therefore, equation 7.2.12 implies $K_A = K_B$. The problem is that the valve has no pipe-point to the downstream side of it, so K_B is not actually defined. But we may define an imaginary K_B outside, since we are able to establish its value ($= K_A$). Inserting that into 7.2.11 shows $p_C = K_A$, something we could also have seen directly from equation 7.2.14. From equation 7.2.9 it follows:

$$p_C = p_A + \rho a_s v_A - \rho a_s \Delta t \left(\frac{f_A}{2d} v_A |v_A| + g sin\theta_A \right) \tag{7.2.15}$$

For simplicity, we neglect any friction or elevation so everything inside the parenthesis vanishes. Since no information can travel through the pipe faster than the speed of sound, it is going to take some time before the pressure or velocity at point A, somewhat upstream of the valve, can feel any impact of what happens elsewhere. Immediately after closure, point A still has its original pressure p_A (which must have been the same as the surrounding pressure during the steady-state situation, given that there is no friction or elevation). We end up with:

$$\Delta p = \rho a_s v_0 \tag{7.2.16}$$

This equation is a simple and accurate tool to estimate the potential pressure increase in front of a fast-closing valve (or the pressure reduction behind it). It shows the pressure rise due to a velocity reduction v_0 is directly proportional to that velocity reduction. It also shows the only factors involved in determining the pressure rise are the fluid density ρ and the speed of sound a_s. Keep in mind, though, that the model used to derive this result is based on the Allievi-simplifications, and that limits the results to liquids. For gases, it can be used only if the pressure step is small compared to the mean pressure.

It may at first look surprising that the pipe's length is not involved, since a longer pipe would hold more liquid to stop. But the pressure surge travels at a constant speed, and the amount of liquid stopped per unit time is the same whether the pipe is long or short, so the result makes sense. The length does play a role when the actual closure time is taken into consideration, however. The maximum pressure rise, as calculated by equation 7.2.16, is only going to occur if the valve closes faster than the reflection time $T = 2l/a$, which rarely happens for very short pipes.

As an example, consider the plumbing in a domestic house. If a valve is located at the end of a $l = 10\ m$ long pipe ($10\ m$ from the nearest branch point), $a_s = 1{,}200\ m/s$, $\rho = 1000\ kg/m^3$ and $v_0 = 5\ m/s$. Instantaneous closure would, according to equation 7.2.16, mean a pressure increase of $6\ MPa$, which is significantly more than domestic plumbing is rated for. But given that the branch point would 'know' about the closure after $l/a_s = 0.01\ s$, and the inflow would stop (backflow would start), a reverse surge reaches back to the valve $0.02\ s$ after closure. Therefore, the maximum pressure, as predicted by equation 7.2.16, is only going to occur if the valve is closed faster than $0.002\ s$. An obvious protection strategy is to make sure no valves can close that fast, and to have large enough pipe diameters to avoid high velocities to begin with.

Notice also that if there is a pipe downstream of the valve, closure will cause a similar pressure *reduction* at the downstream end. If the surrounding pressure is one atmosphere ($\sim 0.1\ MPa$), it does not take much to approach zero, and water would start to boil. Once that happens, our single-phase equations will no longer be valid, and so they cannot tell us what happens afterwards. But equation 7.2.16 is valid until the onset

 For non-commercial use only

of cavitation, so it can tell us whether that is a danger. This example shows cavitation very easily occur in domestic plumbing systems if any of the valves have pipes connected to its downstream end.

7.3 Boundary conditions in the method of characteristics

In the previous chapter, we saw the method of characteristics enables us to compute pressure and velocity in the next time step at many positions based on knowledge of those same data for the current time. But when we look at figure 7.1.1, we realize that there is going to be a problem when we get close to the pipe's ends. For instance, the left end of the pipe is not going to have any points to the left of it, and so the characteristic from A to C is not defined if C's location is at the end of the pipe. K_A in equation 7.2.9 is therefore not defined. The same applies at the right boundary: There is no B-point to the right of it, and K_B is not defined. Fortunately, there is a simple way around that problem. As we will soon se, it is generally possible to define an imaginary K_A or K_B where no real one exists, as we did in the special example in chapter 7.2.1. This is in fact one additional advantage of using the method of characteristics: Handling the boundary conditions is very easy.

7.3.1 Pipe with constant pressure at the inlet, closed outlet

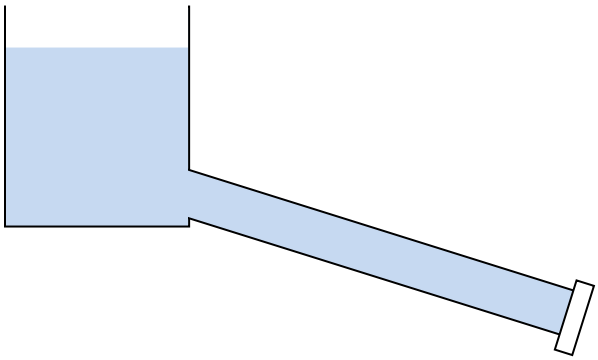


Figure 7.3.1. Pipe with closed outlet.

Suppose we have a pipe with constant pressure p_0 at the inlet (for simplicity, we neglect the inlet loss and the Bernoulli pressure reduction) and a closed valve at the outlet. This is not necessarily a situation where everything is at rest – the valve may just have been closed - and surges could still travel up and down the pipe. The task at hand is to formulate the boundary conditions.

At the inlet, K_b is easy enough to compute with equation 7.2.10. K_A, on the other hand, cannot be computed from equation 7.2.9, since there is no A-point to its left of it. Instead, we compute an imaginary K_A from equation 7.2.11 as:

$$K_A = 2p_0 - K_B \tag{7.3.1}$$

It is then possible to compute the velocity at the inlet according to equation 7.2.12. At the right boundary, the velocity is zero, and an imaginary K_B can be found from equation 7.2.12:

$$K_B = K_A \tag{7.3.2}$$

Using that value, p_C follows from equation 7.2.11.

7.3.2 Pipe with valve at the outlet

Consider the same pipe as in figure 7.3.1, but this time with a partially open valve at the outlet end. The valve may have any opening, and we know neither the pressure by or

 For non-commercial use only

flow through it, but we do know a correlation between pressure and flow. Suppose the valve is characterized by a valve factor K_f of the sort we discussed in equation 4.1.1:

$$\Delta p = K_f \frac{\rho v^2}{2} \tag{7.3.3}$$

If the outside pressure is p_0, we may simply insert equations 7.2.11 and 7.2.12 into equation 7.3.3:

$$\frac{1}{2}(K_A + K_B) - p_0 = \frac{K_f \rho}{2}\left[\frac{1}{2\rho a_s}(K_A - K_B)\right]^2 \tag{7.3.4}$$

This equation can be solved to establish an 'imaginary' K_B so that p_C and v_C can be calculated from equations 7.2.11 and 7.2.12. Of the two solutions mathematically possible, it turns out the one with a negative sign in front of the root is the correct one:

$$K_B = \frac{1}{2}\left[2K_A + \frac{4\rho {a_s}^2}{K_f} - \sqrt{\left(2K_A + \frac{4\rho {a_s}^2}{K_f}\right)^2 - 4\left[{K_A}^2 + \frac{4\rho {a_s}^2}{K_f}(2p_0 - K_A)\right]}\right] \tag{7.3.5}$$

Although using equation 7.3.5 is straight forward calculation, it has inherited one disadvantage from equation 7.3.3: Completely closing the valve – a common occurrence in many pipelines – requires $K_f \to \infty$. Since that is not numerically possible to do in a simulation program, we need to handle closure in some other way. The simplest solution would be to allow K_f to approach some very high, but finite value. That would mean a small leak would prevail even after 'closure', but for some computations, that may not matter. Instead, the terms where K_f is part ($4\rho {a_s}^2/K_f$, that is), could be computed as a separate factor, and that factor is allowed to become zero on closure. A similar problem exists when the valve is fully open, implying $K_f = 0$. Inserting that value in equation 7.3.5 would obviously create problems for the computer, and one may set a lower limit for how far down K_f is allowed to be adjusted. That limit must be low

enough for the pressure loss across the valve to be negligible or as low as the minimum K_f for the actual valve.

7.3.3 Valve located any other place than inlet or outlet

In the previous example, we saw if the valve is located at the outlet of a pipe, simple algebra could deliver a simple equation for computing an imaginary K_B at the boundary. If the valve was located at the inlet, K_A could be determined in a similar way. But what happens if the valve is located somewhere along a pipe? We will see that 'cleanest' formulation of the problem leads us to a relatively complicated set of equations, but those equations may be solved relatively easily with Newton-iteration.

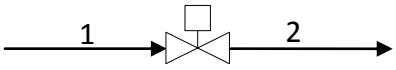


Figure 7.3.2. Inline valve.

The valve is again described by equation 7.3.3, but the valve equation is now relevant at both sides of the valve.

The pipe where the valve is located is computationally regarded as two pipes connected via the valve.

At the valve boundary of pipe 1, equations 7.2.13 and 7.2.14 allow us to express p_c as a function of the known quantity K_{A1} and v_c:

$$p_{C1} = K_{A1} - \rho a_{s1} v_{C1} \tag{7.3.6}$$

The density is not indexed, meaning we assume it is the same everywhere. Speed of sound, on the other hand, may differ in the different pipes, so we need to put an index on it when more than one pipe is involved.

Similarly, at pipe 2's inlet, we express:

$$p_{C2} = K_{B2} + \rho a_{s2} v_{C2} \tag{7.3.7}$$

Continuity means $v_{C1} = v_{C2}$, and $p_{C1} - p_{C2}$ must equal the pressure loss in the valve according to equation 7.3.3:

 For non-commercial use only

$$(K_{A1} - \rho a_{s1} v_C) - (K_{B2} + \rho a_{s2} v_C) = K_f \frac{\rho {v_C}^2}{2} \tag{7.3.8}$$

The pressure loss goes the other way through the valve in case of backflow, so equation 7.3.8 is in fact valid only if $v_C \geq 0$. If $v_C < 0$, we get:

$$(K_{A1} - \rho a_{s1} v_C) - (K_{B2} + \rho a_{s2} v_C) = -K_f \frac{\rho {v_C}^2}{2} \tag{7.3.9}$$

The criteria for which direction the liquid flows will be the same as if the valve was not there. According to equation 7.2.12, that means $v_C \geq 0 \; if \; K_{A1} \geq K_{B2}$.

These equations solve as:

$$v_C = \frac{1}{K_f \rho}\left[-\rho(a_{s1} + a_{s2}) + \sqrt{\rho^2 (a_{s1} + a_{s2})^2 + 2K_f \rho (K_{A1} - K_{B2})}\right] if \; K_{A1} \geq K_{B2}.$$

$$v_C = -\frac{1}{K_f \rho}\left[-\rho(a_{s1} + a_{s2}) + \sqrt{\rho^2 (a_{s1} + a_{s2})^2 - 2K_f \rho (K_{A1} - K_{B2})}\right] \; if \; K_{A1} < K_{B2}. \tag{7.3.10}$$

Equation 7.3.10 makes it easy to compute v_c. After that, p_c can be computed with equation 7.2.14.

7.3.4 Inline centrifugal pump

Pumps come in various different makes, and it is impossible to describe them all with one simple mathematical model. Centrifugal pumps have characteristics which for our purpose are quite similar to the opposite of a valve: Rather than reducing the pressure, as a valve does, a pump increases it. But there is one more important difference: As we saw in chapter 7.3.2, the Δp-v relationship for a valve can be approximated quite well by a simple constant K_f (which changes when the valve opening is changed, but it follows equation 7.3.3 for each distinct valve opening). Pumps, on the other hand, have more

complicated characteristics, and the manufacturers generally measure them and present those measurements in the form of charts. Including centrifugal pump characteristics in our transient liquid flow simulation program comes down to representing those measurements in a convenient way. There are many books and manufacturer documentation documents showing measured pump characteristics, one of the most well known being Stepanoff's book from 1957. Measured centrifugal pump characteristics may look something like the ones in figure 7.3.2, and generally fit relatively well to equation 7.3.11:

$$\Delta h = k_{p1} Q^2 + k_{p2} \left(\frac{n}{n_0}\right) Q + k_{p3} \left(\frac{n}{n_0}\right)^2 \qquad (7.3.11)$$

Where Δh is the pump's head measured in meters, n is the impeller speed compared to a reference speed n_0, and kp_1, kp_2 and kp_3 are empirical constants. The 'constants' tend to vary somewhat in different areas of the diagram, so it may be necessary to update them regularly during the computations. Note also that pump characteristics only tend to follow equation 7.3.11 in the first quadrant of the diagram, meaning for positive flow and positive pressure head. It can therefore not be expected to work well when simulating backflow through the pump, or when more flow is forced through it than it would have delivered with a positive pressure buildup. In those cases a more sophisticated pump model is required.

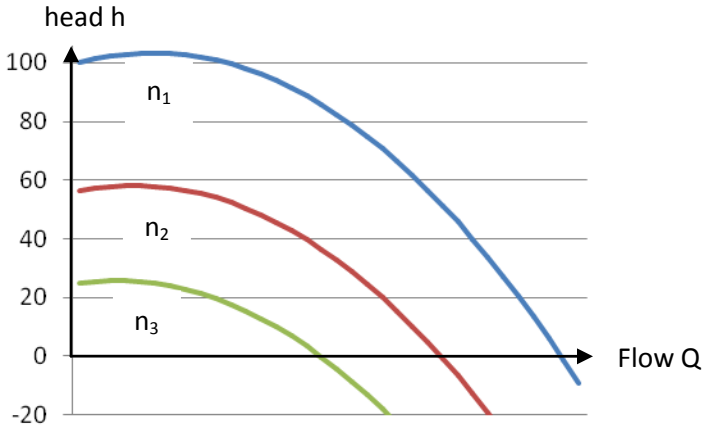


Figure 7.3.2. Centrifugal pump head as a function of discharge flow for 3 different impeller speeds.

The pump discharge cross-sectional area is sometimes smaller than the pipe area. To make the pump equation fit the pipe equations 7.2.11 and 7.2.12, we need to express flow in terms of fluid velocity in the pipe, and head has to be converted to pressure by multiplying with ρg. Equation 7.3.11 is transferred to:

$$\Delta p = \rho g \left[k_{p1}(Av)^2 + k_{p2}\left(\frac{n}{n_0}\right) Av + k_{p3}\left(\frac{n}{n_0}\right)^2 \right] \tag{7.3.12}$$

One situation frequently investigated by simulations is fast pump stop, often to find out what would happen if electrical or mechanical failure forced the pump(s) to stop faster than intended.

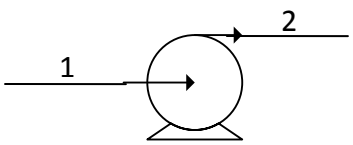


Figure 7.3.3. Inline pump.

The pressure at *pipe 1*'s outlet (pump suction) is described by equation 7.3.6. The pressure at *pipe 2*'s inlet (pump discharge) is according to equation 7.3.7. Combining this with equation 7.3.12, we get:

(7.3.13)

$$(K_{B2} + \rho a_2 v_C) - (K_{A1} - \rho a_1 v_C) = \rho g A^2 k_{p1} {v_c}^2 + \left(\frac{n}{n_0}\right) \rho g A k_{p2} v_c + \left(\frac{n}{n_0}\right)^2 \rho g k_{p3}$$

That leads to:

(7.3.14)

$$\left[\rho g A^2 k_{p1}\right] {v_c}^2 + \left[\left(\frac{n}{n_0}\right) \rho g A k_{p2} - \rho a_1 - \rho a_2\right] v_c + \left[\left(\frac{n}{n_0}\right)^2 \rho g k_{p3} + K_{A1} - K_{B2}\right] = 0$$

To simplify the expression, we define the factors a_c, b_c and a_c:

(7.3.15)

$$a_c = \rho g A^2 k_{p1},\ b_c = \left(\frac{n}{n_0}\right)\rho g A k_{p2} - \rho a_{s1} - \rho a_{s2},\ c_c = \left(\frac{n}{n_0}\right)^2 \rho g k_{p3} + K_{A1} - K_{B2}$$

Equation 7.3.14 has two roots. By trying out different values, one determines this to be the valid one:

$$v_c = \frac{1}{2a_c}\left[-b_c \pm \sqrt{b_c{}^2 - 4a_c\, c_c}\right] \qquad (7.3.16)$$

Since the pump characteristic is an inverted parabola, k_{p1} is a negative number, and so is a_c. Therefore, the ± sign means + for all points to the right of the curve maxima in figure 7.3.3, while the negative sign applies to points to the left of it. In some situations we may have two possible velocities corresponding to the same pressure for pumps like this. This can lead to physical instabilities by allowing the pump to alternate between different points.

As for the inline valve, p_c is easily found from equation 7.3.6 once v_c is known.

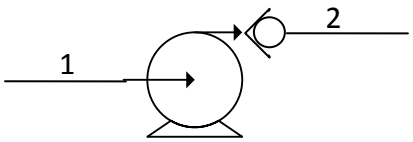


Figure 7.3.4. Inline pump with check-valve.

The pump has a check-valve in series with it to prevent backflow. For simplicity, we neglect any pressure loss in the valve when it is open. This can easily be modeled by setting $v_c = 0$ in case equation 7.3.16 returns a negative value for v_c. By comparing with equation 7.2.12, one sees that doing so actually produces the same values for K_{B1} and K_{A2} as a closed valve would have, namely $K_{B1} = K_{A1}$ and $K_{B2} = K_{A2}$.

We can see from equation 7.3.11 and its illustration in figure 7.3.3 that the pump has a maximum head for any particular pump speed. If the pressure downstream of the pump becomes so high (or upstream pressure so low) that this maximum is exceeded (for instance due to returning pressure waves), no velocity v_c corresponding to that Δp exists, and no solution exists for equation 7.3.12. That reveals itself as $b_c{}^2 - 4a_c\, c_c < 0$. To avoid numerical problems, the program should check this for every time step, and simply set $v_c = 0\ if\ b_c{}^2 - 4a_c\, c_c < 0$. When the simple model in equation 7.3.11 is used, the pump's backflow characteristics are not included to begin with, and that pump

 For non-commercial use only

model it is in fact only valid for a pump with the check-valve-configuration illustrated on figure 7.3.4.

7.3.5 Pump between reservoir and pipe inlet

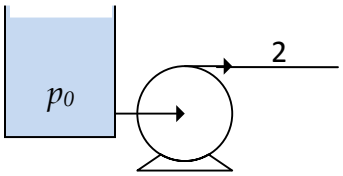


Figure 7.3.5. Inline pump.

This situation is very similar to the inline pump in the previous chapter, but equation 7.3.13 needs to be modified somewhat:

(7.3.17)

$$(K_{B2} + \rho a_2 v_C) - p_0 = \rho g A^2 k_{p1} {v_c}^2 + \left(\frac{n}{n_0}\right) \rho g A k_{p2} v_c + \left(\frac{n}{n_0}\right)^2 \rho g k_{p3}$$

This leads to slightly different intermediate factors a_c, b_c and a_c:

(7.3.18)

$$a_c = \rho g A^2 k_{p1},\ b_c = \left(\frac{n}{n_0}\right) \rho g A k_{p2} - \rho a_2,\ c_c = \left(\frac{n}{n_0}\right)^2 \rho g k_{p3} + p_0 - K_{B2}$$

v_c is then just as easily solved by equation 7.3.16 as it was for the inline centrifugal pump.

7.3.6 Positive displacement pump

Positive displacement pumps, such as piston pumps, gear pumps or vane pumps, tend to produce a discharge flow which is relatively independent of pressure. Real piston pumps do of course have some leaks between piston and cylinder, and those leaks increase when the pressure increases. It is often acceptable to neglect that and pretend the flow is independent of pressure. If so, we know the flow (and therefore velocity v_c) as a function of time directly from the pump speed. Modeling the pump as a known inlet flow is actually very similar to modeling a known inlet pressure, as we did in

example 7.3.1, where equation 7.3.1 became the result. This time, though, we use equation 7.2.12 to get:

$$K_B = K_A - 2\rho a_s v_c \tag{7.3.19}$$

v_c does not have to be constant. It may vary with pump speed, and it may also take into account velocity pulsations caused by a finite number of pistons or gears in the pump.

7.3.7 Junction

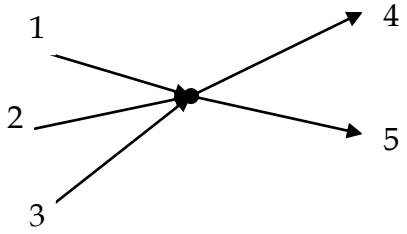


Figure 7.3.6. Junction of 5 pipes.

This is also a situation where we need to combine equations to come up with boundary conditions the computer program can use. Figure 7.3.6, illustrates a junction with 5 pipes. Positive direction is chosen to be into the junction for three of them, while it is defined as out of the junction for the remaining two. Pipes 1, 2 and 3 lack a B-point downstream, in the same way as it was described for the pipe in example 7.2.3. Similarly, pipes 4 and 5 lack an A-point. All pipes feel the same pressure in the junction, which together with equation 7.2.11 tells us that:

$$K_{A1} + K_{B1} = K_{A2} + K_{B2} = K_{A3} + K_{B3} = K_{A4} + K_{B4} = K_{A5} + K_{B5} \tag{7.3.20}$$

Continuity means the sum of flows into the junction equals the sum of flows out of it. When using that together with equation 7.2.12 multiplied by each pipe's cross-section A, we get:

$$\frac{A_1}{a_{s1}}(K_{A1} - K_{B1}) + \frac{A_2}{a_{s2}}(K_{A2} - K_{B2}) + \frac{A_3}{a_{s3}}(K_{A3} - K_{B3}) = \frac{A_4}{a_{s4}}(K_{A4} - K_{B4}) + \frac{A_5}{a_{s5}}(K_{A5} - K_{B5}) \tag{7.3.21}$$

 For non-commercial use only

The densities are assumed to be the same in all pipes (meaning ρ has been eliminated), while the speed of sound may differ between pipes ($a_1 = a_2$ or $a_1 \neq a_2$ ….).

Keeping in mind K_{A1}, K_{A2} *and* K_{A3} are known from equation 7.2.9 while K_{B4} and K_{B5} are known from 7.2.10, the unknowns are $K_{B1}, K_{B2}, K_{B3}, K_{A4}$ and K_{A5}. We use that to express the unknowns in equation 7.3.20 by one single unknown, K_{B1}, and then insert it into 7.3.21 and solve:

(7.3.22)

$$K_{B1} = \frac{K_{A1}\left(\frac{A_1}{a_{s1}} - \frac{A_2}{a_{s2}} - \frac{A_3}{a_{s3}} - \frac{A_4}{a_{s4}} - \frac{A_5}{a_{s5}}\right) + 2\left(\frac{A_2}{a_{s2}}K_{A2} + \frac{A_3}{a_{s3}}K_{A3} + \frac{A_4}{a_{s4}}K_{B4} + \frac{A_5}{a_{s5}}K_{B5}\right)}{\frac{A_1}{a_{s1}} + \frac{A_2}{a_{s2}} + \frac{A_3}{a_{s3}} + \frac{A_4}{a_{s4}} + \frac{A_5}{a_{s5}}}$$

Once K_{B1} has been computed, it is easy to find the other unknowns from equation 7.3.20, and pressures and flow become available from equations 7.2.11 and 7.2.12.

Equation 7.3.22 can easily be extended to cover a general junction of any number of pipes. If pipe No. n has positive direction in to the node (as pipe 1 in figure 7.3.6), we get:

(7.3.23)

$$K_{Bn} = \frac{K_{An}\left(\frac{A_n}{a_{sn}} - \sum_{All\ j \neq n}\frac{A_j}{a_{sj}}\right) + 2\left(\sum_{All\ j\ to\ node \neq n}\frac{A_j}{a_{sj}}K_{Aj} + \sum_{All\ j\ from\ node \neq n}\frac{A_j}{a_{sj}}K_{Bj}\right)}{\sum_{All\ j}\frac{A_j}{a_{sj}}}$$

One additional problem we face when binding pipes together is that each of the pipes needs to be split into a finite number of grid-points. The number of grid-points must of course be an integer. $\Delta l/\Delta t = a_s$ everywhere, at the same time as Δt needs to be identical in all pipes. This is not always possible, and we will usually have to modify either the pipe lengths or the velocity of sound for some of the pipes. Modifying the velocity of sound – a parameter which is not very accurately known anyway – is generally

considered the best option. One may choose to distribute grid-points in the shortest pipe first, for instance by setting the number of pipe sections to $N_x = 10$ (meaning we get 11 grid-points, since there is one at each end). If the next shortest pipe is 15 % longer than the shortest, and the pipes were of similar make (so the speed of sound was the same in both), we would need to have $N_x = 11.5$ (12.5 grid-points) in the second shortest, something which is clearly not possible since N_x has to be an integer. But we could choose to set $N_x = 11$, and use a speed of sound which is $11.5/11 = 1.045$ times as large as the correct value.

Let us now have a look at how the different boundary conditions can be used to simulate complete networks.

7.4 Instantaneous valve closure

7.4.1 Basic simulations

Consider a horizontal pipe with water flowing through it. When the water has had time to reach steady-state flow, a valve is closed at the end. This is a re-visit to the example from chapter 7.2.1, but this time we carry out simulations to get more complete results.

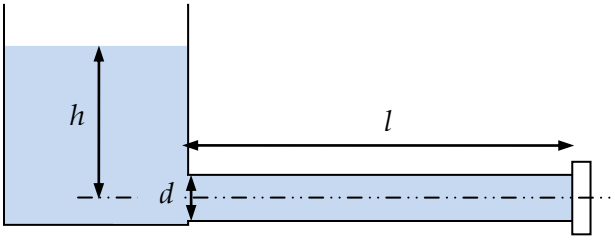


Figure 7.4.1. Instantaneous valve closure.

Pipe length $l = 100$ km
Pipe diameter $d = 1.0$ m
Pipe absolute roughness $k_s = 10^{-5}$ m
Pipe surface structure uniformity factor $u_s = 1$
Inlet pressure head $h = 102$ m, leading to an inlet pressure (ρgh) of 1.0 MPa
Outlet pressure: 0 Pa
Speed of sound $a_s = 1000$ m/s
Pipe inclination $z_2 - z_1 = 0$ m (horizontal)
Liquid density $\rho = 1000$ kg/m^3
Liquid kinematic viscosity $\nu = 10^{-6}$ m^2/s

From the simulation results in figure 7.4.2, we see that the pressure rises instantaneously at time $t = 100$ s, which is when the valve is closed. According to figure 7.4.3, the steady-state velocity is around 1.33 m/s. Once the when the valve is closed, the velocity falls to zero just upstream of the valve. The pressure rises and we see that the surge travels upstream at the speed of sound. 50 s after closure (150 s after simulation started), it reaches the middle of the pipe, and the water stops there, too. It does not

 For non-commercial use only

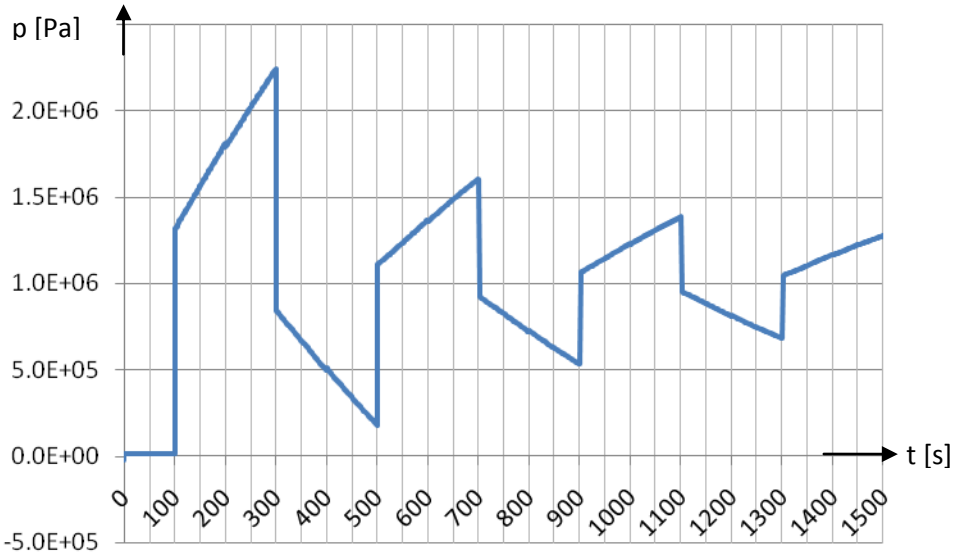


Figure 7.4.2. Pressure by the valve after instantaneous closure at t = 100 s.

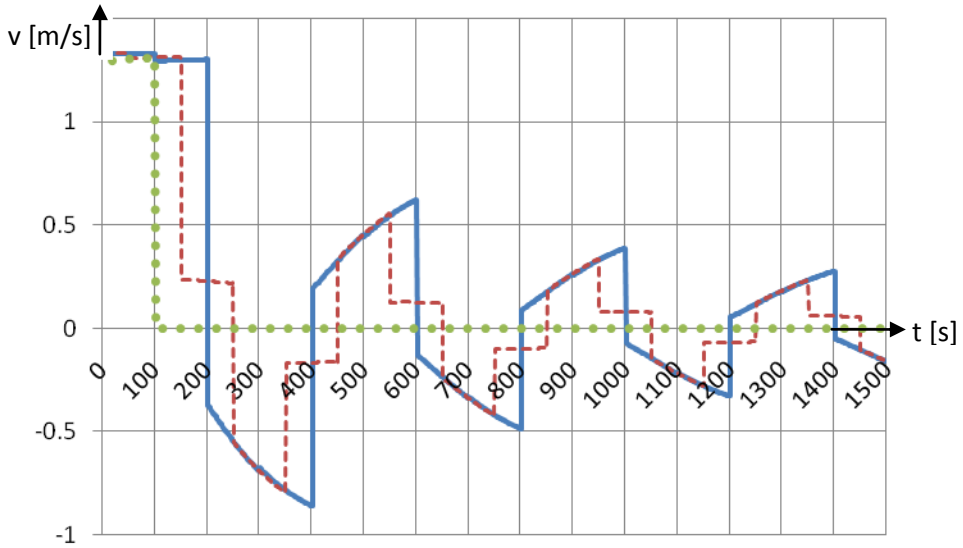


Figure 7.4.3. Velocities through the valve (round dots), at the middle of the pipe (rectangular dots) and by the valve (solid line) after instantaneous closure.

stop completely though, because the pressure by the valve continues to rise. That happens because the friction loss, which used to result in the pressure becoming lower and lower the closer we came to the outlet, becomes (nearly) zero in an ever larger part of the pipe. The kinetic energy has been transformed to potential energy by compressing the water (and some energy has been lost to friction). It is therefore room

for more water to the right of the middle-point, since the water becomes denser and the pipe expands as the pressure continues to increase.

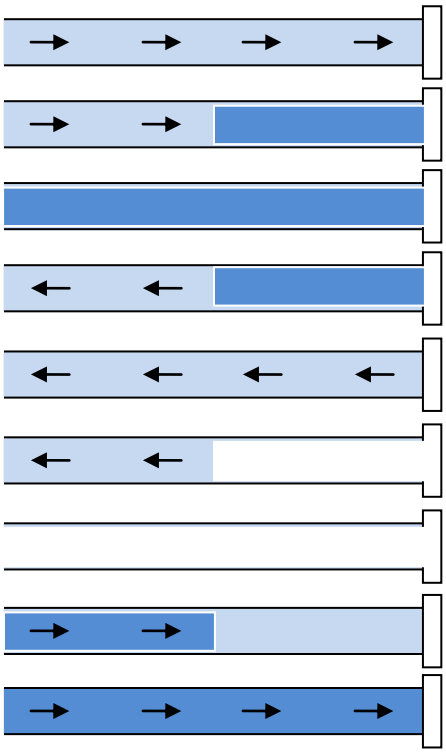
	Time from closure	Time from start
	0	100 s
	$t = \frac{l/2}{a_s}$	150 s
	$t = \frac{l}{a_s}$	200 s
	$t = \frac{3/2l}{a_s}$	250 s
	$t = \frac{2l}{a_s}$	300 s
	$t = \frac{5/2l}{a_s}$	350 s
	$t = \frac{3l}{a_s}$	400 s
	$t = \frac{7/2l}{a}$	450 s
	$t = \frac{4l}{a_s}$	500 s

Table 7.4.1. Flow pattern and pressures (dark means high pressure) at different times.

Only *200 s* after the closure does the inlet point 'become aware' of the fact the pipe no longer has an open outlet, and the water stops flowing in. The entire pipe is pressurized at this point in time, and the flow back into the inlet tank starts immediately. The backflow-wave reaches middle point *250 s* after simulation started, and it reaches the valve after *300 s*. At that moment the water is flowing towards the tank in the entire pipe, and that creates low pressure by the valve. Therefore, a surge stopping the backflow travels from the valve towards the tank. *400 s* after simulation started, water starts to flow back in again. The process repeats itself, but we see the amplitude diminishes as time goes by and friction dissipates ever more of the energy. Had we allowed the simulation to go on for a very long time, the system would eventually stabilize at zero velocity and a pressure equal to the inlet pressure.

 For non-commercial use only

This example illustrates very well how the dynamics in a single-phase liquid pipe system works. Any disturbance – valve closure, pump startup, earthquake or whatever – creates transients. Those transients travel along the pipe(s) and are to at least some extent reflected everywhere the flow-path changes, such as in valves, pumps, junctions and reservoirs. Even bends, diameter changes and wall thickness variations can result in reflections.

7.4.2 Some ways to check the simulations results manually

The simulations offer us many ways to manually check whether the computations are correct or not. The simplest check is to see whether the surge propagates at the speed of sound. That test is easy in our case, since friction is moderate enough to allow very distinct surge propagation – a typical situation in large diameter liquid pipes like this one. Figure 7.4.3 shows that the inlet velocity starts to respond to the closure *100 s* after the closure occurred. Since the pipe is *100 km* long, that means the surge has propagated at *1000 m/s*, and as expected, that corresponds to the given speed of sound.

The initial velocity in figure 7.4.3 appears to be around *1.3 m/s*. That corresponds to a Reynolds number of $1.3 \cdot 10^6$. Since the relative roughness is 10^{-5}, the uniformity-based diagram in figure 2.9.1 shows the friction factor is around $f = 0.0122$, and the pressure loss should be around *1.04 MPa*. That agrees reasonably well with the inlet pressure we had here, but not quite. If we look very closely at the solid line in figure 7.4.3, corresponding to the inlet velocity, we see that it does in fact start to fall slightly before the surge reaches it. That indicates the simulations have used a somewhat larger initial velocity than it should have, since the first part of the simulations seems to converge towards a slightly lower value than used in the simulations. That inaccuracy in the initial velocity can explain the inaccuracy in initial pressure loss. In sum, this check leads us to recommend a closer look at how the initial conditions were computed.

The pressure rise by the valve immediately after closure should according to equation 7.2.16 be *1.3 MPa*, and that turns out to agree fairly well with figure 7.4.2.

The section from *100* to *300 s* on figure 7.4.2 offers a fourth way to check the results. The pressure rise in this period is due to the friction becoming zero as more and more of the fluid is stopped. At the last part of the period – *200* to *300 s* after closure – some of the fluid is flowing backwards. That happens so far from the valve that no information has had time to reach the valve. The difference between the pressure at $t = 100$ *s* and $t = 300$ *s* should therefore be the same as the initial pressure loss in the pipe, which was *1.0*

MPa (at least if the initial velocity has been 100 % correctly computed). We see that the results agree well with expectations in this respect.

7.5 Steady-state network analysis

7.5.1 General

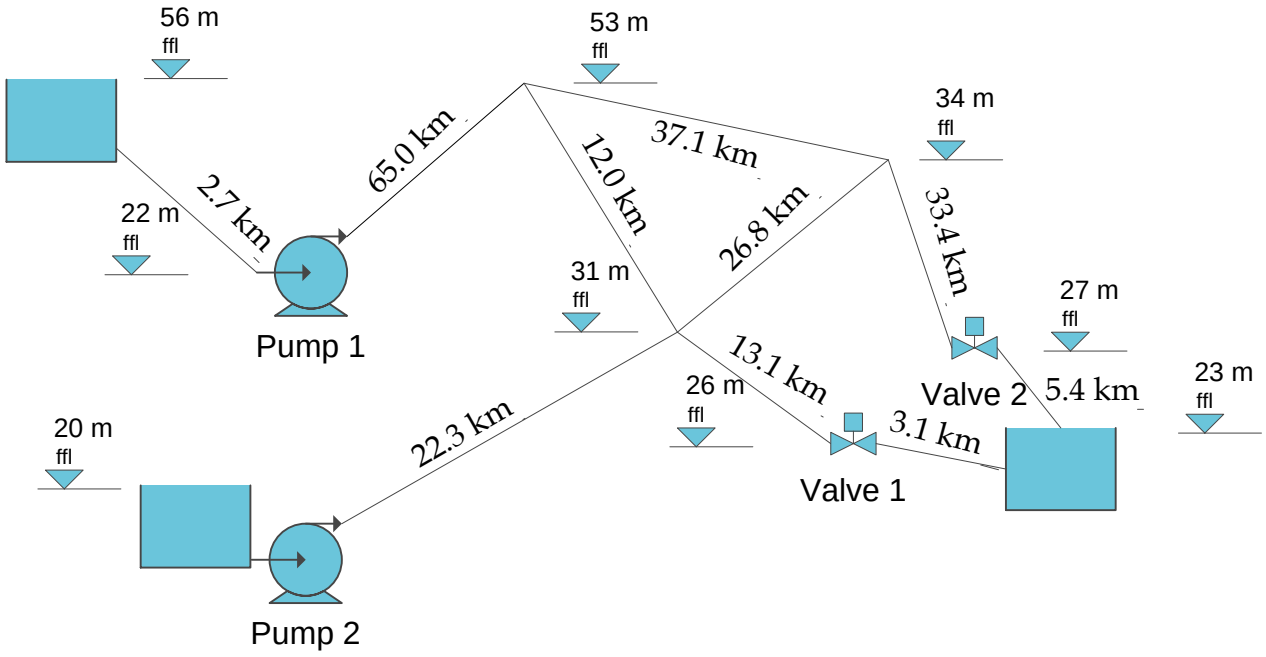


Figure 7.5.1. Example of pipe network with lengths and elevations shown.

We want to simulate the system in figure 7.5.1. One of the first problems faced is the fact that any transient simulation needs to start from some steady-state initial condition. The simplest initial condition imaginable would be to set all velocities to zero. That would not mean the pressures are all identical, of course, since the elevations are different. One possible approach would be to set them to a constant value anyway, for instance equal to the surrounding pressure, typically *1 atmosphere*. That would lead to false transients once the simulations start and the system approaches its true equilibrium. If we are interested in investigating pump failure, say, our most interesting initial condition could be full capacity pumping. To get the main study started, the

 For non-commercial use only

program has to determine both the velocities and the pressures for steady-state pumping.

One obvious way around having to deal with formulating separate steady-state equations would be to simply allow the simulation program to run for a long time until everything stabilizes. The false transients this generates may take a relatively long time to die out after the pump has reached its normal operation speed – the time it takes depends on such parameters as Reynolds number, pipe network design and how gently the pump was started. But sooner or later a steady-state condition is going to be reached in the simulations, just as it would in the real system. Once that is the case, the transient pump failure analysis can begin – by abruptly stopping the pump, say.

This way of defining the steady-state condition is intuitive and simple to implement. But if the system in question is very complex and with little damping, it may take very much computing power. Although ever-increasing computer capacity makes this problem less and less severe, it still carries a lot of weight, and it is unacceptable to rely on this method in general transient pipe flow programs.

Many alternative methods of calculating steady-state velocities in liquid networks have been developed over the years. The most well-known of them is probably the Hardy Cross method (Cross, 1946, and Streeter et al., 1983). These methods are generally straight forward to implement in a computer program, they are well documented, and many of them are even described on the internet – a search for *hardy cross networks* or *pipes networks sparse matrix* yields lots of results, for instance. The most popular steady-state methods suffer from one major disadvantage, however: They increase the total simulation program's complexity significantly. Implementing the steady-state program modules requires nearly as much work as implementing the transient modules, and unless great care is taken, the interfaces with pumps, valves, junctions and any other boundary conditions end up being programmed twice. This increases the total cost of developing and maintaining the computer code.

Instead of going into the classical models, we will look at a way to speed up the convergence when we use the transient modules in the computer program to determine steady-state. The convergence properties are comparable to those of the traditional steady-state methods, but the implementation is quicker. This method appears not to have been published before, but this book's author has utilized it in numerous simulations of moderately complex networks. As we will soon see, we are able to develop convergence and stability criteria which ensure that the method works. The method has been termed *the steady-state characteristics method*.

7.5.2 Finding initial velocities using the steady-state characteristics method

As described in chapter 7.3.7, it is usually necessary to modify the velocity of sound somewhat due to pipe length differences. When trying to find the steady-state velocities, we may simply utilize this by going further along the same line: Setting N_x = 2 in all pipes, and modifying the speed of sound so Δt becomes the same in all pipes.

When we look at the simplified continuity equation 7.1.8, we realize that in the steady-state case, nothing changes with time, and $\partial p/\partial t = 0$. We also realize that since ρ and a are assumed to be constant in this simplified model, $\partial v/\partial x = 0$, too. Therefore, this model will predict constant velocity in the entire pipe once steady-state is reached. That is not quite in agreement with reality – the velocity would increase somewhat as the fluid expands towards the low-pressure end of the pipe – but the effect is negligible for liquids. The important point is that the method of characteristics is not going to distinguish between a pipe with high or low velocity of sound once the flow has become steady-state. So when it comes to determining the steady-state pressures and velocities, we are free to use any speed of sound we desire.

The equations created to find the steady-state solution can be thought of as the model of a pipe system having the same pipe diameters, lengths, etc., as our real system, but where the pipes differ in flexibility (as measured by the speed of sound). We know from simple steady-state examples in previous chapters that the speed of sound is not involved in friction calculations, and this provides an alternative way to conclude that any selected speed of sound will lead to the same steady-state end result.

Setting N_x = 2 in all pipes speeds up convergence in two ways: We get only 3 grid-points in each pipe, meaning there are a relatively low number of equations to solve. Therefore, short wavelength disturbances – the many small ripples typically initiated by the transients we introduce when starting the simulations – are unable to survive in such a rough grid. As a result, the system reaches its steady-state condition relatively quickly.

Setting N_x = 2 also means we end up with quite a large time step. We want to use as large time steps as possible, since that brings us fast into the future where transients in our imaginary system can be expected to have died out. The time step size is not going to affect accuracy, since we are going to continue until no transients existt. From equation 7.2.7 we see directly that once the velocity has become constant in the whole pipe (when $v_A = v_b$), $p_c = 1/2(p_A + p_B)$. If, for instance, p_A and p_B are boundary

 For non-commercial use only

conditions, this sais the pressure at the middle of the pipe is going to be the average of those two boundary pressures once the velocities have stabilized. Similar considerations for equation 7.2.8 show the friction is going to be the same regardless of how long time step we use. The logic can be extended to other boundary conditions, showing that accuracy is not compromised even if the time step chosen is very long.

We have not yet discussed the method of characteristics' stability, but in chapter 7.7 it has been shown that the friction puts stability limitations on how large time steps we can take. For turbulent flow, the integration is going to be stable if the time step is chosen so that each pipe satisfies:

$$\Delta t \leq \frac{2}{max\left(\frac{f_{i,j}}{d}|v_{i,j}|\right)} \tag{7.5.1}$$

This means stability depends on the maximum velocity we encounter, together with the Darcy-Weisbach friction factor and the diameter.

We start with the first pipe and simply guess a maximum velocity – 100 m/s would for example be a very conservative one – and calculate the friction factor *f* that would lead to. The time step can then be selected to satisfy equation 7.5.1. The procedure is repeated for every pipe, and the strictest one – meaning the smallest time step required by any pipe – is chosen for all pipes. Using that time step, the imaginary steady-state speed of sound for pipe number *k* is calculated according to equations 7.2.1 and 7.2.2, which means:

$$a_{sk\ ss} = \frac{l_k}{2\Delta t} \tag{7.5.2}$$

To make sure we do not violate equation 7.5.1 at any time during the computations, we monitor it in each grid point and time step. If we approach the stability limit, we just increase the speed of sound in all pipes according to equation 7.5.2 and continue. We get even faster convergence if we allow the program to modify $max(f_{i,j}/d \cdot |v_{i,j}|)$, once we have beginning convergence. If it turns out that the expected maximum velocity was

too conservative – maximum velocity is typically lower once the initial transients have died out - we may reduce the speed of sound in all pipes. The computational work involved in increasing or reducing the time step does not much differ from the work involved in making a time step, so it pays to do it quite frequently during the process of finding the steady-state values - for instance for every 5. iteration.

7.5.3 Steady-state convergence criteria

In order to know when steady-state has been reached, we need some criteria to check the results against. We may simply compare the results from the last time step with those of the previous time step. When the relative difference is below a certain threshold, meaning the system has stabilized, we accept the result. We do not need to compare both velocities and pressures, since they do not vary independently. If we use the velocities as reference, the relative velocity difference is computed as the length of the difference vector, divided by the length of the velocity vector. Once that relative difference is smaller than some maximum steady-state relative error, e_{ss}, we accept the results:

$$\frac{\sqrt{\sum_{all\ gridpoints\ ,all\ pipes}\left(v_j - v_{j-1}\right)^2}}{\sqrt{\sum_{all\ gridpoints\ ,all\ pipes} {v_j}^2}} < e_{ss} \tag{7.5.3}$$

There is one problem with this approach, though. We may encounter cases where the velocities are zero, and that will lead to division by zero in equation 7.5.3. To avoid that, we need to define a lower limit, v_{min} , which takes over in case the velocities become too small:

$$\frac{\sqrt{\sum_{all\ gridpoints\ ,all\ pipes}\left(v_{i,j} - v_{i,j-1}\right)^2}}{\sqrt{\sum_{all\ i,j,k} max\left({v_{min}}^2, {v_j}^2\right)}} < e_{ss} \tag{7.5.4}$$

It seems to work well to set $v_{min} = 0.01$ and $e_{ss} \leq 10^{-5}$ in most practical situations.

 For non-commercial use only

7.5.4 Steady-state example

Let us try this on the system shown in figure 7.5.1 to see how it works. The first thing to do when simulating the system is numbering the pipes, as well as deciding which direction to be consider positive, see figure 7.5.2:

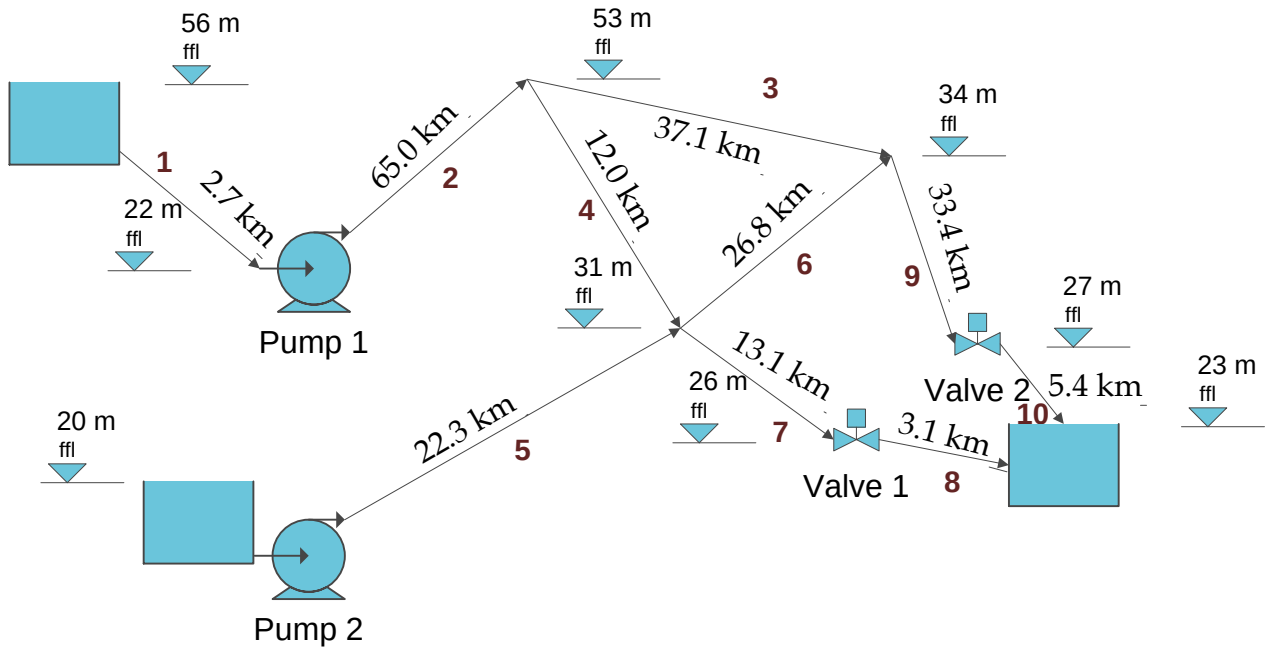


Figure 7.5.2. Network with pipe numbers and positive direction shown.

All pipes are of the same make, having inner diameter $d = 0.296\ m$, and the velocity of sound is $a = 1213\ m/s$. To simplify manual checks of how the simulation program is performing, the Darcy-Weisbach friction factor is held constant at $f = 0.02$ (rather than updated as the Reynolds number changes, which is of course the normal procedure when not checking). The surrounding pressure is $10^5\ Pa$, and all pressures are measured in absolute terms (so that $0\ Pa$ is vacuum).

The valves follow equation 7.3.10, and K_f can go *from* 1.0 (fully open) *to* 10^{10} (fully closed, as explained in chapter 7.3.2.)

Both pumps follow equation 7.3.12 with $k_{p1} = -3000$, $k_{p2} = 200$ and $k_{p3} = 100$, and n/n_0 can be run *from* 0 *to* 1. Both pumps have check valves installed so backflow cannot occur (not shown on the already overloaded figure).

Suppose we run both pumps at $n/n_0 = 1$, and set both valves at $K_f = 1{,}000$. We want to find the steady-state velocities in each pipe.

The purpose here is to illustrate the difference between short and long time steps when calculating the steady-state conditions, and we simply choose two alternative step sizes (rather than doing it intelligently by using equations 7.5.1 and 7.5.2). First, we use the shortest pipe as the one we refer all other velocities to. *Pipe 1* is *2.7 km* and shortest, and we allow it to keep its actual velocity of sound during the first experiment. The longest pipe, *pipe 3*, is *13.7* times as long, and so the speed of sound must be adjusted upwards accordingly, to *16,667 m/s*. Similar modifications of the velocity of sound are done for the other pipes. We set all velocities and pressures to zero before iteration starts, and want to iterate until the relative error is $e_{ss} = 10^{-5}$.

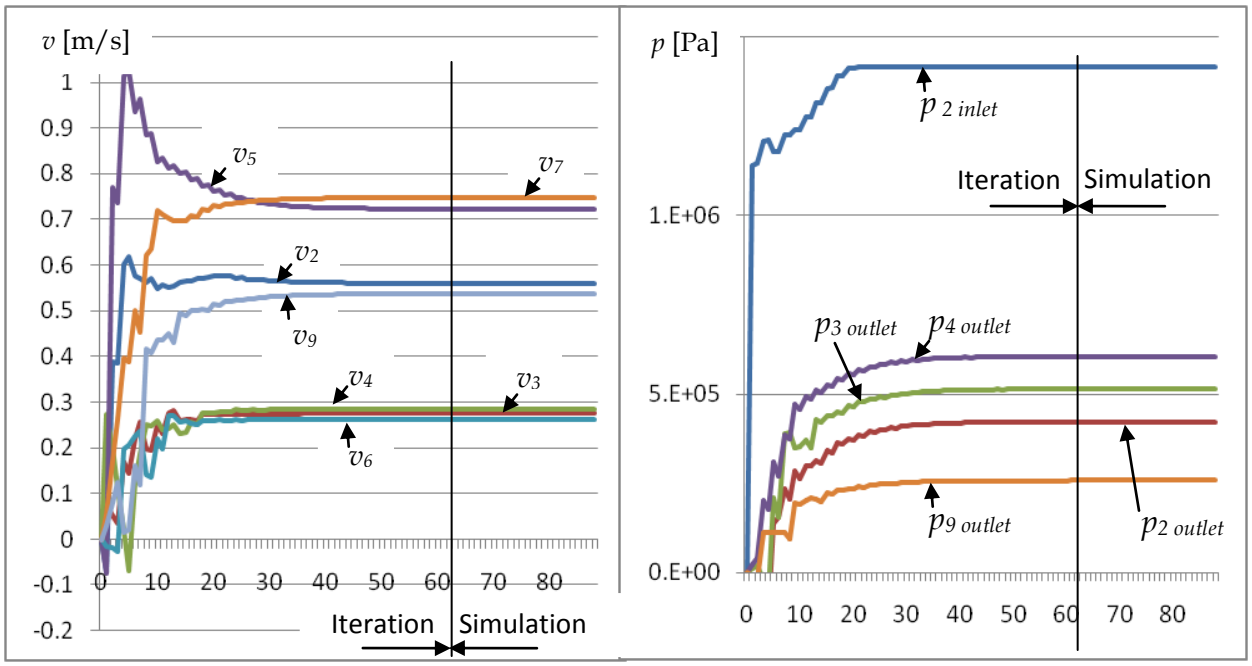


Figure 7.5.3. Velocities and absolute pressures during iteration to steady-state. After 63 iterations, convergence is reached, and the program starts simulating transients. It is the velocities in the middle of the pipes which have been plotted – they do of course become equal in the whole pipe once steady-state convergence is achieved.

It turns out convergence is reached after 521 iterations. That takes only a fraction of a second on a modest laptop computer. If we use the longest pipe as reference so all other speeds of sound are adjusted downwards, we get much faster convergence: It takes only 49 iterations. As expected, (already good enough) convergence is speeded up by a factor almost proportional to the reduction in speed of sound. If we had checked the velocities with equation 7.5.1, we would have seen that the last calculations brought

 For non-commercial use only

us close to the stability limit, so the time step used here is about as good as it gets when using constant time step. We could have improved this significantly by using variable time steps.

Figure 7.5.3 shows how some of the velocities and pressures developed during the iteration process. We see some of the velocities overshoot the final result at first, and it looks like they stabilize after around 30 iterations. As already mentioned, however, accuracy kept improving, and out strict convergence criteria was met only after 49 iterations.

After the steady-state velocities had been established, transient simulations were also carried out, but without introducing any transients. The grid in each pipe was re-adjusted according to the actual speeds of sound. In each grid point, the velocity was set to the same value as found for steady-state. The inlet pressure p_0 was also the same as found in the steady-state computations, and the pressure in each grid point downstream was found as the inlet pressure minus the pressure due to friction and elevation. For point i (i grid-points from the pipe inlet) we then get:

$$p_j = p_0 - \rho \frac{l}{N_x} i \left(\frac{f}{2d} v|v| + g \sin\theta \right) \tag{7.5.5}$$

After having inserted that, and selecting $N_{x1} = 10$ in the shortest pipe (*pipe 1* in our example), we start transient simulation immediately after the steady-state iteration has finished. For illustration purposes, the first part of the transient simulations have been plotted in the same figures as the steady-state iterations (the steady-state iterations are of course not normally plotted at all, since they do not correspond to any physical phenomenon and are only of interest when learning about the method). The switch is completely smooth, and that tells us the transient program has been given correct starting values. Otherwise, transients would have started, as the transient model would try to bring the flow towards what it considered to be steady-state. This is in fact one of the checks we should use both when debugging a program and when using an existing program on new examples – steady-state and transient calculations must agree at the moment we switch from one to the other.

7.6 Simulating transients in pipe networks, an example

Let us now look at some of the results from dynamic simulation of the same system as already described in the previous example. One of the first things we observe from figure 7.5.3, even before starting the dynamic simulations, is that none of the velocities are very high – at least not with the valve positions chosen when testing the steady-state methods in the previous chapter, see figure 7.5.3. The highest velocity appears to be the one in *pipe 7* (and *pipe 8*, since it is in series with *pipe 7*), around *0.75 m/s*. Even immediate stoppage cannot produce higher instant pressure rise or fall than that predicted by equation 7.2.16, which is $\Delta p = 0.91\ MPa$. Chapter 7.4 revealed that friction disappearing as the liquid stops can produce additional pressure rise similar to the initial friction, and in our example, that can be higher than the instantaneous pressure increase. In *pipe 2*, the initial velocity is around *0.56 m/s*. If the pump somehow stopped instantly, that could in principle produce a pressure drop behind the pump of around *0.68 MPa*. Since the initial pressure ($p_{2\ inlet}$) is nearly *2 MPa*, that pressure drop should not be sufficient to create cavitation at the pump outlet. To be on the safe side, we usually want to go through the entire system to identify all likely problem areas.

To verify some of these considerations, figure 7.6.1 shows some results from simulating a stop of *pump 1*. The pump's speed is reduced from full ($n/n_0 = 1$) to stop ($n/n_0 = 0$) in 10 seconds with a linear speed reduction. *Pump 2* is running at full speed throughout the simulation, and the valves are half-open, as explained for the steady-state experiments in figure 7.4.3.

According to the simulations, the pressure at *pipe 2*'s inlet is around *1.4 MPa* until the pump shutdown starts, then falls to around *0.70 MPa*. That is a pressure reduction of about *0.70 MPa*, which is very close to what was expected. The pressure increase at the suction side of the pump is smaller, however, from around *0.4* to *0.75 MPa*, which amounts to around *0.35 MPa*. The reason is that *pipe 1* is only *2.7 km* long, so the pressure wave has time to travel to the tank at *pipe 1*'s inlet and back to the pump in around 4.5 s, or less than half the time it takes to stop the pump.

The fact that the pressure upstream of the pump continues to fall after the pump has come to a complete stop is because the friction in *pipe 2* gradually diminishes as the liquid slows down in a larger and larger part of the pipe.

 For non-commercial use only

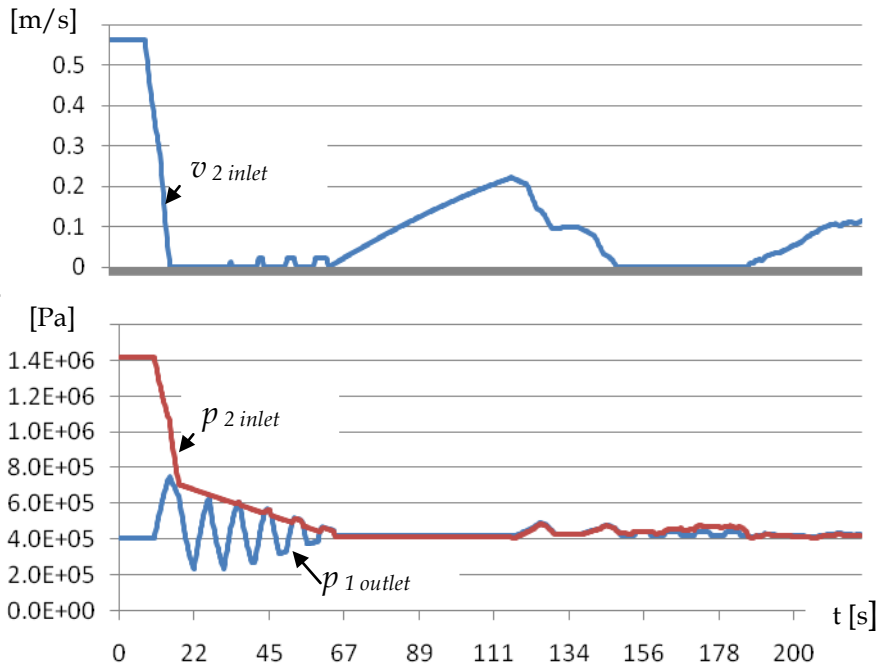


Figure 7.6.1. Velocity through pump 1 into pipe 2 and pressures in front of and after pump 1. Closure starts 10 s after simulation started, and is completed 10 s later.

Notice also that since *pipe 2* is connected to the rest of the pipe network, other reflected waves come back to *pump 1* after awhile. Backflow is prevented by a built-in check valve, so we never see negative velocities through the pump. But positive velocities occurred even after the pump was stopped. The pump is actually very large compared to the pipes, and so at times when the pump inlet experiences even modestly higher pressure than pump discharge (so small that it is not even visible on figure 7.4.4) a considerable flow goes through it. That can alternatively be achieved by having a bypass in parallel with the pump. That bypass must of course have a check valve in it, so liquid does not leak from pump outlet to inlet during normal pumping operation.

Another detail to note is the somewhat awkward time scale. The need for an integer number of grid-points in each pipe (and a correspondingly bound Δt) means simply plotting the results at every time step usually produces results like this. Commercial programs have some interpolation methods built into the plotting routine to produce a nice time scale anyway. But the user needs to be aware of that, in case the interpolation creates unexpected plotting details which have nothing to do with the hydraulics.

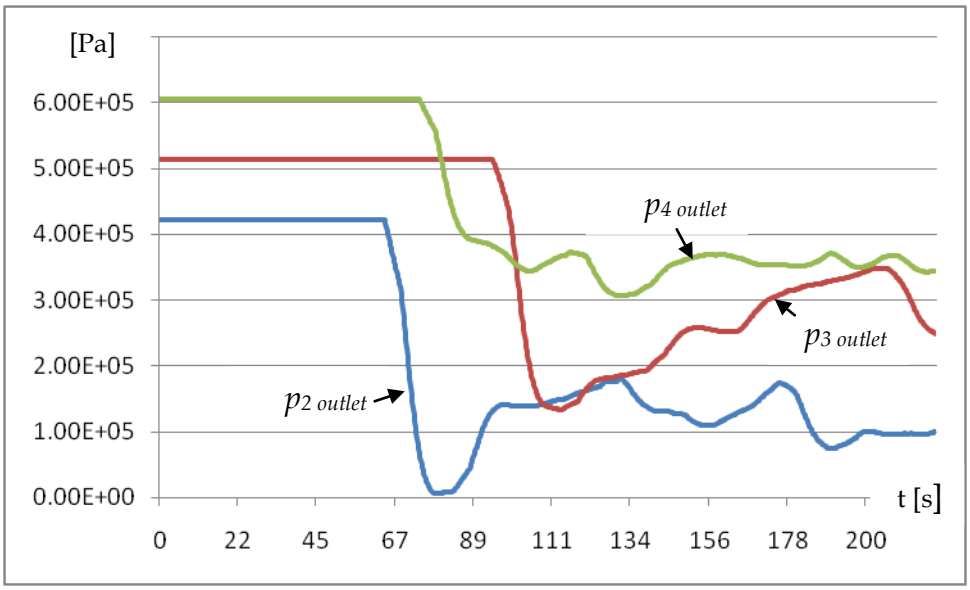


Figure 7.6.2. Pressures in the grid-points.

When we investigate the pressures in each grid point, we immediately see that the one with the highest elevation – the one called $p_{2\ outlet}$ – experiences very low pressure after around *80 s*, and cavitation may occur. It is not hard to imagine other situations where the pressure is likely to fall even lower, for instance if both pumps stop simultaneously (here, only one pump stopped) or the valves being fully open (here, they were only partly open), so this would probably require improved system design or strict operational procedures. Possible action would be to install air inlet valves at those points where cavitation could otherwise occur. In systems where that is unacceptable, damping chambers or accumulators may be installed. On some pipelines, additional valves have been inserted at strategic locations and 'intelligently' controlled during shutdown to avoid undesired pressures – in principle a simple concept, but often complicated and expensive to implement in a sufficiently reliable way. Changing the pipeline route to avoid a high-lying point in the middle – the source of the problems here – is for obvious reasons often not an option.

This simple example showed how we can use simulations to investigate and improve the proposed system design. Let us now have closer look at the method's stability properties.

 For non-commercial use only

7.7 Stability considerations

Numerical integration may create instabilities which make the integration 'explode', typically showing up in the results as numbers becoming infinite. To be useful, or *well-posed*, as it is normally called, a numerical integration method must be stable, consistent and convergent. We are not going to focus much on the latter two criteria. More information about them can be found in books about numerical mathematics, for instance those by Smith (1978) or Polyanin et al. (2004). For our purpose, we are simply going to state that the method of characteristics, as outlined in chapter 7.1, is consistent and convergent, and we will investigate under which conditions it is stable.

Let us start by formulating the equations for the straight pipe in figure 7.6.1. We have chose to set $N_x = 2$, which leads to 3 grid points.

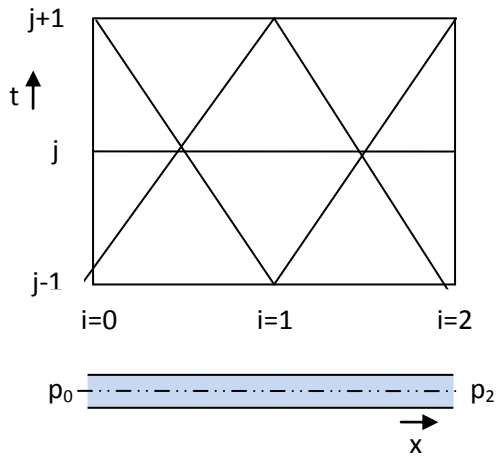


Figure 7.6.1. Grid for pipe with $N_x = 2$.

By considering p_0 and p_2 to be known boundary conditions and using equations 7.2.11, 7.2.13, 7.2.12 and 7.2.14, we get:

$$p_{1,j+1} = \frac{1}{2}\left(K_{A0,j} + K_{B2,j}\right)$$

$$v_{0,j+1} = \frac{p_{0,j+1}}{\rho a_s} - \frac{K_{B1,j}}{\rho a_s} \tag{7.7.1}$$

$$v_{1,j+1} = \frac{1}{2\rho a_s}\left(K_{A0,j} - K_{B2,j}\right)$$

$$v_{2,j+1} = -\frac{p_{2,j+1}}{\rho a_s} + \frac{K_{A1,j}}{\rho a_s}$$

Inserting equations 7.2.9 and 7.2.10, but neglecting the elevation terms (they do not affect stability), this becomes:

$$p_{1,j+1} = \frac{1}{2}\left(p_{0,j} + \rho a_s v_{0,j} - \rho a_s \Delta t \frac{f_0}{2d} v_{0,j}\left|v_{0,j}\right| + p_{2,j} - \rho a_s v_{2,j} + \rho a_s \Delta t \frac{f_2}{2d} v_{2,j}\left|v_{2,j}\right|\right)$$

$$v_{0,j+1} = \frac{p_{0,j+1}}{\rho a_s} - \frac{p_{1,j} - \rho a v_{1,j} + \rho a_s \Delta t \frac{f_1}{2d} v_{1,j}\left|v_{1,j}\right|}{\rho a_s}$$

$$v_{1,j+1} = \frac{1}{2\rho a_s}\left(p_{0,j} + \rho a v_{0,j} - \rho a_s \Delta t \frac{f_A}{2d} v_{0,j}\left|v_{0,j}\right| - p_{2,j} + \rho a_s v_{2,j} - \rho a_s \Delta t \frac{f_B}{2d} v_{2,j}\left|v_{2,j}\right|\right) \quad (7.7.2)$$

$$v_{2,j+1} = -\frac{p_{2,j+1}}{\rho a_s} + \frac{p_{1,j} + \rho a_s v_{1,j} - \rho a_s \Delta t \frac{f_A}{2d} v_{1,j}\left|v_{1,j}\right|}{\rho a_s}$$

We will discuss these equations in some detail and see what they mean for stability.

 For non-commercial use only

7.7.1 Frictionless flow

When studying these equation 7.7.2, let us at fist neglect the friction. On matrix form, frictionless flow can be formulated as:

$$\begin{bmatrix} p_1 \\ v_0 \\ v_1 \\ v_2 \end{bmatrix}_{j+1} = \begin{bmatrix} 0 & \frac{\rho a_s}{2} & 0 & -\frac{\rho a_s}{2} \\ -\frac{1}{\rho a_s} & 0 & 1 & 0 \\ 0 & \frac{1}{2} & 0 & \frac{1}{2} \\ \frac{1}{\rho a_s} & 0 & 1 & 0 \end{bmatrix} \begin{bmatrix} p_1 \\ v_0 \\ v_1 \\ v_2 \end{bmatrix}_j + \begin{bmatrix} \frac{1}{2} & \frac{1}{2} \\ \frac{1}{\rho a_s} & 0 \\ \frac{1}{2\rho a_s} & \frac{1}{2\rho a_s} \\ 0 & -\frac{1}{\rho a_s} \end{bmatrix} \begin{bmatrix} p_0 \\ p_2 \end{bmatrix}_j \tag{7.7.3}$$

If we for a moment neglect the contributions from the boundaries, we see that the state we would have after *j+1* time steps would be:

$$\begin{bmatrix} p_1 \\ v_0 \\ v_1 \\ v_2 \end{bmatrix}_{j+1} = \begin{bmatrix} 0 & \frac{\rho a_s}{2} & 0 & -\frac{\rho a_s}{2} \\ -\frac{1}{\rho a_s} & 0 & 1 & 0 \\ 0 & \frac{1}{2} & 0 & \frac{1}{2} \\ \frac{1}{\rho a_s} & 0 & 1 & 0 \end{bmatrix}^j \begin{bmatrix} p_1 \\ v_0 \\ v_1 \\ v_2 \end{bmatrix}_0 \tag{7.7.4}$$

This is a very interesting result, because it shows us that all state variables after *j+1* integrations depend solely on the initial conditions (*j=0*) and a matrix, let us call it *A*, in power *j*.

To get a feeling for what this means, let us first reflect on a simpler system of only 1 state variable, so that *A* becomes a scalar, and the equation of interest would be on the form $y = A^j x$). We easily realize that if $|A| > 1$, the results would grow and grow as *j* became ever larger with each subsequent step, and it would eventually approach infinity ($\lim_{j\to\infty} A^j = \infty \; if \; |A| > 1$). If, on the other hand, $|A| < 1$, any influence from the initial condition would gradually die out, since $\lim_{j\to\infty} A^j = 0 \; if \; |A| < 1$. Errors entering

the system during the integration would also diminish and eventually disappear. If, on the other hand, $|A| > 1$, any errors would magnify, and eventually, the calculations would 'explode'.

When A is a matrix, as it is in equation 7.7.4, the same applies, but it is A's eigenvalues which must now be considered. All eigenvalues need to be shorter than *1* for all errors to disappear gradually.

But what if one or more of the eigenvalues were of length unity? The influence from the initial condition would live on forever, and so would errors, but they would at least not increase towards infinity. It is therefore generally acknowledged that eigenvalues of length unity will not destroy the stability.

It is well known from mathematics that the eigenvalues λ can be found by:

$$|A - \lambda I| = 0 \tag{7.7.5}$$

where I is the identity matrix. For our A-matrix in equation 7.7.4, that means:

$$\begin{vmatrix} -\lambda & \frac{\rho a_s}{2} & 0 & -\frac{\rho a_s}{2} \\ -\rho a_s & -\lambda & 1 & 0 \\ 0 & \frac{1}{2} & -\lambda & \frac{1}{2} \\ \frac{1}{\rho a_s} & 0 & 1 & -\lambda \end{vmatrix} = 0 \tag{7.7.6}$$

This turns out to lead to a very simple fourth order polynomial:

$$\lambda^4 - 1 = 0 \tag{7.7.7}$$

Or:

 For non-commercial use only

$$(\lambda + 1)(\lambda - 1)(\lambda^2 + 1) = 0 \tag{7.7.8}$$

We obviously get 2 imaginary and 2 real eigenvalues:

$$\lambda_1 = \frac{1}{2} + \sqrt{\frac{3}{4}}i, \;\; \lambda_2 = \frac{1}{2} - \sqrt{\frac{3}{4}}i, \;\; \lambda_3 = 1, \;\; \lambda_4 = -1 \tag{7.7.9}$$

All 4 eigenvalues are of length *1*.That means simulations are going to be stable. Also, we see that the eigenvalues are independent of the time step, something which is unusual for explicit methods.

If we use a finer grid by increasing N_x, finding the eigenvalues is more work, but we end up with the same nice result: For frictionless flow, the method of characteristics is unconditionally stable.

7.7.2 Flow with laminar friction

When setting the Darcy-Weisbach friction factor $f = 64/Re$, the A-matrix changes to:

$$A = \begin{bmatrix} 0 & \frac{\rho a_s}{2}\left(1 - \Delta t \frac{32\nu}{d^2}\right) & 0 & -\frac{\rho a_s}{2}\left(1 - \Delta t \frac{32\nu}{d^2}\right) \\ -\frac{1}{\rho a_s} & 0 & 1 - \Delta t \frac{32\nu}{d^2} & 0 \\ 0 & \frac{1}{2}\left(1 - \Delta t \frac{32\nu}{d^2}\right) & 0 & \frac{1}{2}\left(1 - \Delta t \frac{32\nu}{d^2}\right) \\ \frac{1}{\rho a_s} & 0 & 1 - \Delta t \frac{32\nu}{d^2} & 0 \end{bmatrix} \tag{7.7.7}$$

It is still manageable to find an analytical solution to the eigenvalues by following the same procedure as for the friction-less case:

$$\lambda^4 + \Delta t \frac{32\nu}{d^2}\left(1 - \Delta t \frac{32\nu}{d^2}\right)\lambda^2 - \left(1 - \Delta t \frac{32\nu}{d^2}\right)^3 = 0 \tag{7.7.8}$$

If we define:

$$k = \Delta t \frac{32\nu}{d^2} \tag{7.7.9}$$

We get:

$$\lambda^2 = \frac{1}{2}\left[k(1-k) \pm \sqrt{k^2(1-k)^2 + 4(1-k)^3}\right] \tag{7.7.10}$$

We may plot these results in a diagram:

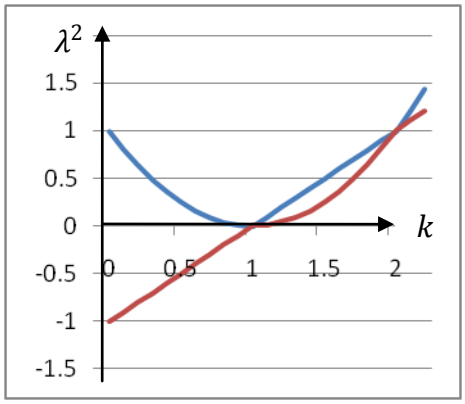


Figure 7.7.1. Plot of equation 7.7.10.

Figure 7.7.10 shows that $\lambda^2 (and\ also\ \lambda) \leq 1$ if:

$$k = \Delta t \frac{32\nu}{d^2} \leq 2 \tag{7.7.11}$$

We also see λ^2 can only take negative values if $k < 0$, meaning complex eigenvalues only occur in the lowest half of the k-values ensuring stability.

The result shows that the method of characteristics will be stable for laminar flow if the time step is not too large, the viscosity is not to large, and/or the diameter is not too small. More generally, the results seem to indicate that high friction (high ν and/or low d) requires smaller times steps than flow with lower friction. Laminar flow tends to occur in pipes with high viscosity and low diameter. Consider, for instance, a *0.02 m* diameter pipe with a fluid of viscosity $10^{-5}\ m^2/s$. According to equation 7.7.11, this

means $\Delta t \leq 0.8$. This does not pose a problem, particularly since pipes with single-phase, laminar liquid flow usually are relatively short, and we can afford a quite dense grid without ending up with an unmanageable amount of equations. But we see that if the diameter is very much smaller, such as in micro-channels or blood vessels, simulating the dynamics with the method of characteristics can result in problematic time step restrictions.

This result were based on $N_x = 2$. But what happens if N_x takes any value, such as $N_x = 10$ or $N_x = 100$?

k=0	k=0.5	k=0.99	k=1	k=2	k=2.1
-0.9511 + 0.3090i	0.807	-0.95	0	1	-1.0023
-0.9511 - 0.3090i	0.6068 + 0.3631i	-0.8047	0	-1	-1.0091
-0.8090 + 0.5878i	0.6068 - 0.3631i	0.95	0	1	-1.0198
-0.8090 - 0.5878i	0.6196	0.8047	0	-1	-1.0335
0.9511 + 0.3090i	0.4408 + 0.5529i	-0.5763	0	1	-1.0488
0.9511 - 0.3090i	0.4408 - 0.5529i	0.5763	0	-1	-1.0644
0.8090 + 0.5878i	0.2318 + 0.6680i	-0.2759	0	-1	-1.0974
0.8090 - 0.5878i	0.2318 - 0.6680i	0.2759	0	1	-1.09
-0.5878 + 0.8090i	0.0000 + 0.7071i	-0 + 0.1i	0	-1	-1.0786
-0.5878 - 0.8090i	0.0000 - 0.7071i	-0 - 0.1i	0	-1	1.0023
0.5878 + 0.8090i	-0.2318 + 0.6680i	-0.0363	0	1	1.0091
0.5878 - 0.8090i	-0.2318 - 0.6680i	0.0363	0.9511	1	1.0198
-0.3090 + 0.9511i	-0.4408 + 0.5529i	-0.0174	0.809	1	1.0335
-0.3090 - 0.9511i	-0.4408 - 0.5529i	-0.0124	0.5878	-1	1.0488
0.3090 + 0.9511i	-0.6068 + 0.3631i	-0.0105	0.309	1	1.0974
0.3090 - 0.9511i	-0.6068 - 0.3631i	0.0174	0	-1	1.09
0 + 1.0000i	-0.807	0.0124	-0.9511	1	1.0786
0 - 1.0000i	-0.6196	0.0105	-0.809	-1	1.0644
1	0.5	0.01	-0.309	1	1.1
-1	-0.5	-0.01	-0.5878	-1	-1.1

Table 7.7.1. Eigenvalues for different k when $N_x = 10$.

For large N_x, finding an analytical expression like the one in equation 7.7.10 is more difficult. But expanding the A-matrix is straight forward, and we may use a commercial software package to compute the eigenvalues. Here, Matlab, a popular scientific program package for technical computing, has been used (The Mathworks, Inc. 2007). The results are shown in table 7.7.1. Interestingly, we get results very similar to those

we saw for $N_x = 2$: For $k = 0$, which corresponds to frictionless flow, all eigenvalues have length one. Complex eigenvalues exist for to $k < 1$, and all eigenvalues are shorter than 1 as long as $k < 2$. The stability criterion in equation 7.7.11 is therefore equally valid for $N_x = 10$ as it was for $N_x = 2$. Trying other N_x, for instance $N_x = 100$ leads to the same result.

7.7.3 Turbulent flow

If we have turbulent friction, the linear theory developed in chapter 7.7.1 and 7.7.2 does not apply. But we can do the next best thing: We linearize by determining the system's Jacobi matrix. Jacobi matrixes are defined in general mathematics books, and they are also partly explained in chapter 10.3. If we set $N_x = 2$, we get results very similar to those in equation 7.7.6:

$$J = \begin{bmatrix} 0 & \frac{\rho a}{2}\left(1 - \Delta t \frac{f_{0,j}}{d}|v_{0,j}|\right) & 0 & -\frac{\rho a}{2}\left(1 - \Delta t \frac{f_{2,j}}{d}|v_{2,j}|\right) \\ -\frac{1}{\rho a} & 0 & 1 - \Delta t \frac{f_{1,j}}{d}|v_{1,j}| & 0 \\ 0 & \frac{1}{2}\left(1 - \Delta t \frac{f_{0,j}}{d}|v_{2,j}|\right) & 0 & \frac{1}{2}\left(1 - \Delta t \frac{f_{2,j}}{d}|v_{2,j}|\right) \\ \frac{1}{\rho a} & 0 & 1 - \Delta t \frac{f_{1,j}}{d}|v_{1,j}| & 0 \end{bmatrix} \tag{7.7.12}$$

It is not strictly correct to simply require all J's eigenvalues to be smaller or equal to 1, as we did for the A-matrix, since the linearization points are going to change for every time step. Doing so anyway may at least give us some useful indications, and we will see that they turn out to be remarkably accurate when compared to simulation results.

If all velocities and friction factors are the same everywhere, we can use direct analogy with equation 7.7.7 to conclude that:

$$\Delta t \frac{f_{i,j}}{d}|v_{i,j}| \leq 2 \tag{7.7.13}$$

 For non-commercial use only

Note, though, that if the v_j at any point in time or space crosses the stability boundary, it has a tendency to produce an instability which never dies out again. Once one of the eigenvalues has become too large it tends to produce an even larger velocity in the next time step, enhancing the instability and leading to the integration 'exploding'. It is therefore probably more accurate and certainly safer to re-formulate equation 7.7.13 and require all velocities to satisfy:

$$\Delta t \frac{1}{d} max\left(f_{i,j}\left|v_{ij}\right|\right) \leq 2 \tag{7.7.15}$$

Since the time step Δt is chosen only indirectly in the simulations, we may introduce equations 7.2.1 and 7.2.2 and re-formulate to:

$$\frac{l}{a_s N_x d} max\left(f_{i,j}\left|v_{ij}\right|\right) \leq 2 \tag{7.7.16}$$

The results tell us that the velocities matter, and that very high velocities may create instabilities, depending on the pipe diameter d and the time step in use, as well as the Darcy-Weisbach friction factor f. Situations leading to very high velocities, for instance because the initial conditions have been incorrectly specified, can therefore create instabilities which make the simulations fail.

For the sake of simplicity, let us assume constant friction factors so that 7.7.16 can be written as:

$$max\left|v_{ij}\right| \leq \frac{2a}{l}\frac{d}{f}N_x \tag{7.7.17}$$

If we experiment with different typical parameters in equation 6.6.16, we quickly realize that we are unlikely to come across numerical instabilities in most situations. Suppose, for instance, we have a pipe where $a_s = 10^3$ *m/s*, $l = 10^3$ *m*, $d = 0.02$ *m* and f is in the order of *0.02*. If we choose $N_x = 10$, the restriction this poses on the velocity is $max\left|v_{ij}\right| \leq 20$

m/s. It is hard to achieve such high speed in such a long, thin pipe, at least over a long time. But transients, such as those we encounter when simulating pipe rupture, can bring us above this limit. For the sake of demonstrating what instability means, let us simply try increasing the velocity gradually until instability occurs.

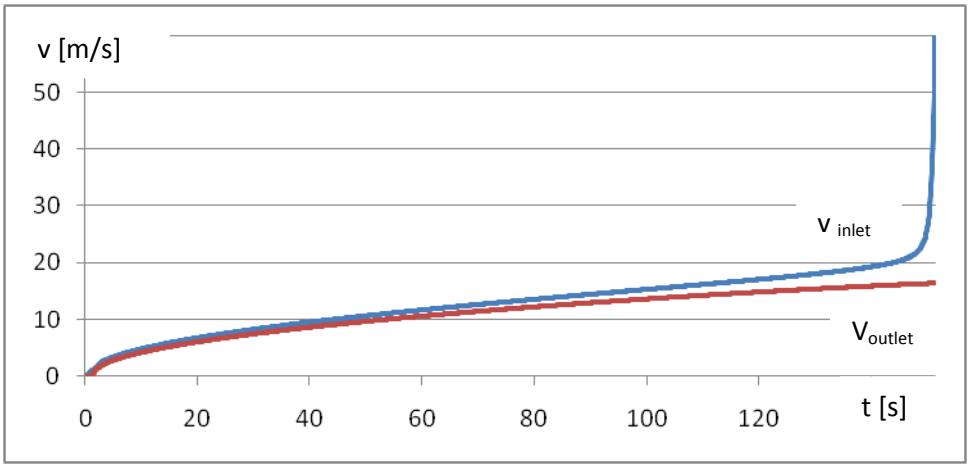


Figure 7.7.2. Velocities in pipe with $a = 10^3$ m/s, $l = 10^3$ m, $d = 0.02$ m, $f = 0.020$.

At the start, everything is at rest, and the pressures and velocities are all zero. The inlet is assumed to be connected to a reservoir where the pressure can be increased linearly with time, while the outlet end is open. The results are plotted in figure 7.7.2. We see that once *20 m/s* is reached – it happens at around $t = 140$ *s* - the velocity goes towards infinity. The inlet pressure has by then had to be increased to around *150 MPa* to trigger this event, so this is indeed a rather imaginary pipeline, but it illustrates very clearly how the numerical instability works: If the velocity becomes large enough to violate the criterion in equation 7.7.16, the method of characteristics is erroneously going to produce velocities and pressures approaching infinity.

7.7.4 Some effects of the characteristic equations being nonlinear

In figure 7.7.3 shows another simulation on the same pipe with identical parameters, but a pressure step of *30 MPa* is imposed on the inlet instead of a gradual pressure buildup.

 For non-commercial use only

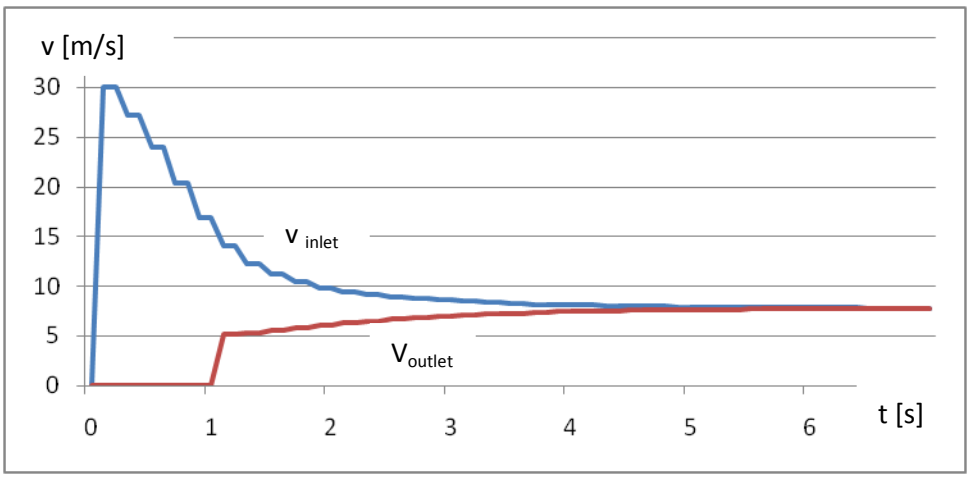


Figure 7.7.3. The same pipe as in figure 7.7.2, but a pressure step is imposed on the inlet.

In this case, the velocity exceeds the *20 m/s* – limit at the inlet end for nearly a second without the system becoming unstable. This shows it is in fact acceptable to violate equation 7.7.16 for a few integrations. Note, though, that we were not much above the limit here, and only in part of the pipe for a very short time. If repeating the simulations with a moderately higher pressure step (*40 MPa*), we do in fact run into trouble. Figure 7.7.4 shows what happens. The result may at first seem completely surprising, because we expected some sort of instability to develop. But instead of any values growing infinitely, we get a constant inlet velocity of *40 m/s*, while all other state variables stay at zero!

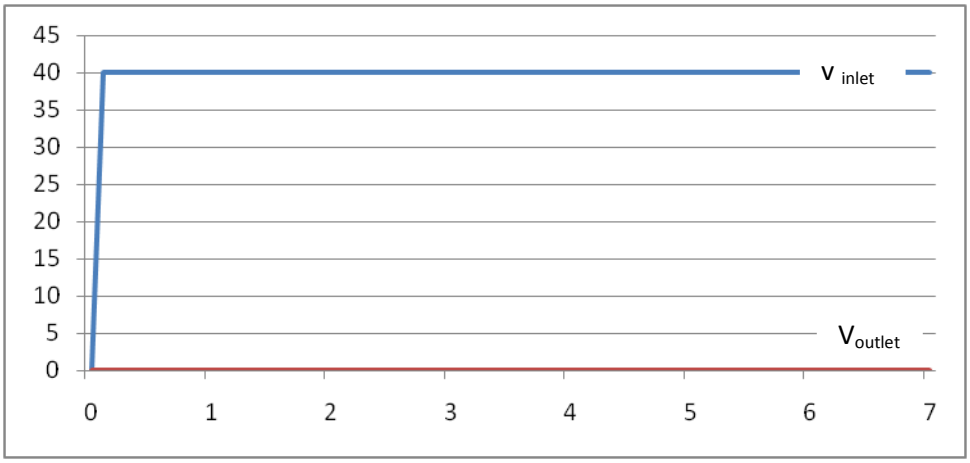


Figure 7.7.4. As figure 7.7.3, but the pressure step has been increased.

It is not so difficult to see directly from equations 7.2.7-7.2.14 that this oddity may happen. At the first time step, anything to the right of the pipe inlet is zero. From

equation 7.2.13 it follows that $v_C$at the inlet has to be $p_{C\ inlet}/\rho a$, since K_B refers to a point some distance into the pipe, where both p and v is still zero. Inserting numbers, we see that this leads to $v_C = 40\ m/s$, just as the simulations show.

When we move to the next grid point, something strange happens. It turns out that according to equation 7.2.9, $K_{A0} = 40\ MPa + 40\ MPa - 80\ MPa = 0$ (given a time step of 0.1 s, which is what we have here). It means that K_{A0}, describing the characteristic from grid-point *0* at time $t = 0$ to grid-point *1* at the next time step becomes *0*. The same is of course true for K_{B2}, given that everything was zero further into the pipe. Therefore, the simulations tell us the velocity wave never propagates anywhere: Everything, except the pressure and inlet velocities, continues to be zero. This is a kind of 'numerical lock', which has no physical counterpart – it is simply mathematics playing us a trick. Fortunately, it is a situation which has little chance of happening by random during simulations – the terms in equation 7.2.9 needed to cancel each other out exactly for it to happen. But it is worth being aware of, since it can be more difficult to detect than the instabilities described in the previous chapter. Here, no parameters approach infinity, and the integration does not 'explode', but the results are incorrect nevertheless.

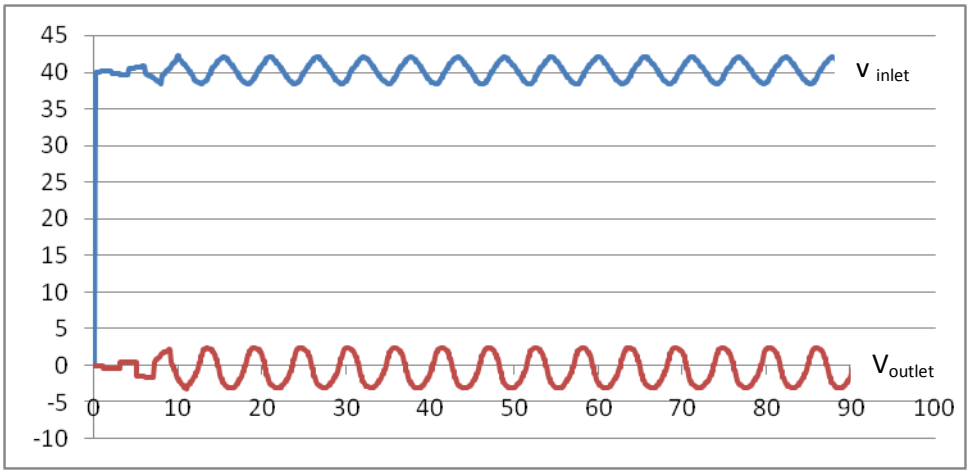


Figure 7.7.4. As figure 7.7.3, but the Darcy-Weisbach friction factor f = 0.0201.

A somewhat likelier, but still rather unlikely numerical oddity arises if we move slightly away from the situation shown in figure 7.7.3. Everything is as for figure 7.7.3, except that *f* has been increased by *0.5 %* to *0.0201*. The result in figure 7.7.4 shows something which has nothing to do with any physical realities in the actual flow: A stable oscillation with an the average velocity at the outlet being zero. This numerical

 For non-commercial use only

phenomenon can easily be overlooked if it happens, in which case erroneous simulations may go undetected.

In figure 7.7.5 we see the results if f is increased further. The velocity does still not propagate as expected, but we run up against the stability problems predicted by equation 7.7.17 in the way we would expect, causing the inlet velocity to 'take off' after around *2.5 s*.

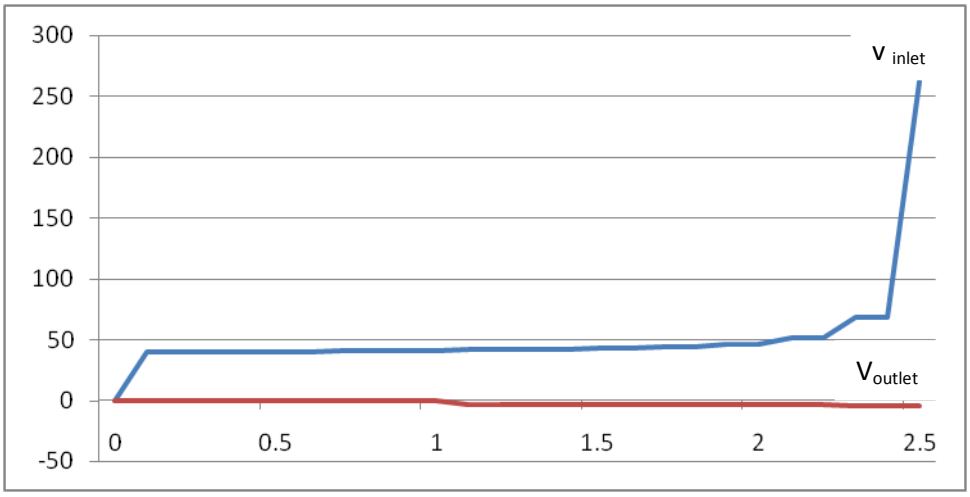


Figure 7.7.5. As figure 7.7.3, but the Darcy-Weisbach friction factor f = 0.021.

The conclusion to all this is that it is best to be conservative when it comes to stability. The stability criterion 7.7.16 should be checked in all grid-points for each time step. If it is violated, the user should be given a warning, and the systems must be given a finer grid if the results are to be reliable.

7.8 Tracking the liquid

Sometimes the liquid entering the pipe does not have constant properties. That means we may have different properties in different parts of the same pipeline, and we need to know where we have which properties in order to determine such important parameters as density, viscosity, and velocity of sound. Contractual and legal requirements may also require tracking since the pipeline operator may send different liquids through the same pipeline in batches. The different batches may even have different owners and customers.

If we integrate the flow Q in each grid-point, it is easy to determine the volume V of liquid which has past those points:

$$\left(\frac{\partial V}{\partial t}\right)_i = Q_i = \frac{\pi d^2}{4} v_i \tag{7.8.1}$$

When we consider possible numerical methods for solving this equation, it is worth noting that $\partial V/\partial t$ does not depend on V itself, and no A-matrix is going to exist. Therefore, there is not going to be any eigenvalues which can become larger than 1, and stability is not going to be a problem.

For best accuracy, one may choose to use a second-order numerical approximation of $\partial V/\partial t$. We will discuss how to do that in later chapters. For now, let us just stick to a first order approximation similar to the ones shown in equations 7.2.3 and 7.2.4 by setting:

$$\left(\frac{\partial V}{\partial t}\right)_i = \frac{V_{i,j+1} - V_{i,j}}{\Delta t} \tag{7.8.2}$$

Inserting that into 7.8.1 leads to:

$$V_{i,j+1} = V_{i,j} + \Delta t \frac{\pi d^2}{4} v_i \tag{7.8.3}$$

By calculating the volume which has passed each grid-point and time step in parallel with the transient calculations this way, it is easy to figure out how far each batch has come at any given time. Note also these extra calculations do not rely on any sort of liquid properties, and they do not slow the computations down significantly.

 For non-commercial use only

7.9 Checking simulation results

When we simulate pipeline or pipe network transients, we generally want to check our results as thoroughly as possible. There are three different types of checks:

i) Checking the theoretical model against measurements to verify the theory.
ii) Checking the computer program for programming 'bugs'.
iii) Checking that the system of interest has been correctly implemented into the computer program.

Fortunately, the method of characteristics has been well documented for liquid flow in lots of publications already and we do not need to put much effort into this part any longer. i) is therefore not of much concern neither to program developers nor program users. That does of course not mean measurements are without value, but the purpose of such measurements are in most cases checks of type ii) and iii).

Whether we have access to measurements or not, there are some simple theoretical methods which will expose many of the errors we may encounter:

1. Check that the transition from steady-state to transient computations runs smoothly, without any transients occurring before we have initiated them. This is the check we discussed in relation to figure 7.5.3.
2. Manually check the continuity equations in the nodes. For large networks, checking at least some of them is useful. Also, check that the pressures are the same at the ends of all pipes connected to the same junction.
3. Plot flows and pressures for pumps, valves, and other components, and check whether they behave as they should according to their characteristics.
4. For pipes with steady-state flow, plot the pressures at both ends and the velocity, and manually check that the pressure loss is as expected.
5. Check whether pressure or velocity waves propagate at the speed of sound. If the friction is so high it smoothens out the wave fronts, study short enough sections to get an acceptable foundation for checking.
6. Check whether the pressure rise or fall during accelerations or retardations agrees with equation 7.2.16 ($\Delta p = \rho a \Delta v$) in the way it was explained in relation to figure 7.4.2. Also, note that as an ever increasing part of the liquid in a pipe is stopped, the friction should also be reduced in the way it was explained for the same example.
7. Try simulations with different grid sizes. Finer mesh (higher N_x, meaning lower Δt) is generally good for accuracy, but bad for computing speed. Compare the

results and settle for as large a time step as acceptable accuracy (and in some cases stability) allows.

8. Experiment with different levels of modeling complexity. Have pumps, valves, bends and other components been modeled with sufficient accuracy? Or are very rough estimates acceptable? Varying input data and comparing results helps clarify this.

7.10 Advantages and limitations when using the method of characteristics

When considering whether or not to use the method of characteristics when simulating single-phase liquid pipe flow, it is useful to keep these advantages and limitations in mind:

Advantages

- The method is very easy to program: The solution is explicit, no iteration or complicated solution methods are needed. The boundary conditions are easy to handle.
- The method has very good and well known stability properties, making it possible to take quite large time steps without the integration 'crashing'. That, together with the explicit (iteration-free) solution algorithm makes the method very fast and well suited for real-time or faster-than-real-time simulations (forecasting).
- The model is very well documented and tested against lots of examples, and its possibilities and limitations are well known.
- Implementing a steady-state network solver in the dynamic simulation program is programmatically very easy by using thee steady-state characteristics method.
- As we will see in the next two chapters, it is easy to implement the energy equation as an additional equation without interfering directly with the method used for calculating p and v. Existing liquid simulation programs with no built-in thermodynamic calculations can therefore be expanded by simply adding the energy equation in addition to the existing, already tested ones.

Disadvantages

- The simplifications done in the continuity equation, as described in equation 7.1.7, means very compressible fluids are poorly modeled. In practice, that means the method is suited only for liquids, not gases.

 For non-commercial use only

- The liquid velocity has to be much smaller than the speed of sound. If not, the propagation velocity would be considerably different for waves travelling upstream and downstream, and that would deform the characteristic grid. This can have an effect when the speed of sound is extremely low, such as in blood vessels, but it is less often of concern in industrial systems.
- The model does of course carry with it all imperfections in the underlying theory, such as inaccuracies in the friction factor, possibly inaccurate liquid compressibility properties and pipe wall elasticity.

References

Allievi, L. (1913): *Teoria del colpo d'ariete*. (Theory of water-hammer.) Atti del Collegio degli Ingegneri ed Architetti Italiani, Milan, Italy (in Italian). (English translation by E.E. Halmos, 1925)

Cross, H. (1946): *Analysis of Flow in Networks of Conduits or Conductors.* University of Illinois, Bull. 286, Nov.

Stepanoff, A.J. (1957): *Centrifugal and Axial Flow Pumps. Theory, Design and Applications.* John Wiley & Sons, Inc.

Smith, G.D. (1978): *Numerical solution of Partial Differential Equations: Finite Difference Methods.* Oxford University Press. Second Edition.

Ham, A. (1982): *On The Dynamics of Hydraulic Lines Supplying Servosystems.* Laboratorium Voor Verktuigkundige Meet – En Regeltechniek, Delft.

Streeter, V.L., Wylie, E.B., (1983): *Fluid Transients.* FEB Press.

Reid, R.C., Prausnitz, J.M., Poling, B.E. (1987): *The Properties of Gases & Liquids.* Fourthe Edition, McGraw-Hill Inc.

Bratland, O., Jensen, P. (1989): *Simulation Models of Pressure Steps in Very Long Hoses or Pipes with Viscoelastic walls.* 6th International Symposium on Pressure Surges, Cambridge, England.

Polyanin, A.D., Zaitsev, V.F. (2004): *Handbook of Nonlinear Partial Differential Equations.* Chapman & Hall/CRC.P

The Mathworks, Inc. (2007): *Matlab Users Guide*. www.mathworks.com

For non-commercial use only

"Thermodynamics is the only physical theory of universal content which I am convinced will never be overthrown, within the framework of applicability of its basic concepts."
Albert Einstein

8 Heat exchange

This chapter covers heat exchange the fluid and the pipe's environment:

- Heat through several radial layers of insulation
- Forced convection between fluid and pipe wall
- Forced convection between the pipe's outer layer and surrounding air or water
- Buried pipe heat loss
- Thermal conductivity tables for common materials

8.1 General about heat through layered insulation

Heat transfer between the fluid and the pipe's surroundings can be important for a number of reasons, and a general simulation program for transient pipe flow must be able to take it into account. Removing or adding heat can alter the viscosity, it can cause cavitation or the fluid freezing solid, it can cause the surroundings to melt or freeze, and for gases, it significantly affects the density. Our conservation equations take heat into account in the form of q in equation 6.3.12, but it does not reveal how to estimate q itself. That is the subject of this chapter.

Heat flow in pipes is a well studied science, and many useful calculation methods have been published. Even though some of the equations are highly empirical and somewhat inaccurate, the main challenge is most often to know the relevant underlying data well enough to use the equations efficiently. For instance, in the model developed here we are going to neglect radiation and instead only take into consideration forced

convection and conduction. Forced convection takes place where the inner pipe surface is in contact with the fluid it transports. It may also occur at the outside of the pipe if wind or currents contribute to cooling or heating.

Conduction is the mechanism at work when heat is transported through the pipe wall, including through layers of coating or insulation. The average rate at which heat passes through a surface can in general be expressed as:

$$Q = UA\Delta T \tag{8.1.1}$$

Where Q *[W]* is the heat transfer rate, U is the heat transfer coefficient *[W/(m²K)]*, A is the surface area *[m²]* and ΔT is the temperature difference between the two sides of the surface *[K]*.

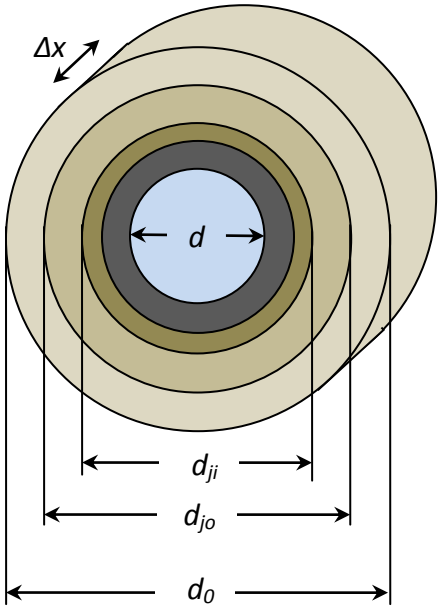
When we have n layers on top of each other, the heat transfer coefficient for all the layers combined can be calculated as:

$$\frac{1}{U_{tot}} = \frac{1}{U_1} + \frac{1}{U_2} + \frac{1}{U_3} + \cdots + \frac{1}{U_n} \tag{8.1.2}$$

In the case of a pipe, layers outside each other have different diameters, and it is convenient to refer each layer's heat coefficient to the specific diameter it is based on. If we prefer to let A in equation 8.1.1 stand for the outer area of the outermost insulation layer, we can do so by calculating:

$$\frac{1}{U_o d_o} = \frac{1}{U_1 d_1} + \frac{1}{U_2 d_2} + \frac{1}{U_3 d_3} + \cdots + \frac{1}{U_n d_n} \tag{8.1.3}$$

 For non-commercial use only



Where U_o is the overall heat transfer coefficient based on the outer diameter of the outermost layer d_o. The diameters d_1, d_2… are the diameter used to calculate each particular layer's heat transfer coefficient. The innermost 'layer' – or the inner boundary - describes the heat transfer coefficient between the flowing liquid and the innermost pipe material, typically the coating or the main pipe material. D_{1i} is therefore most often the pipe's inner diameter. The outermost 'layer' is also special. Its coefficient is between the surroundings and the outer-diameter of the outermost insulation layer.

Figure 8.1.1. Pipe layers.

The diameters in equation 8.1.3 can be regarded as a way of weighing each layer so that it refers to the outermost diameter when used in 8.1.1. The area A can be based on the outer diameter, d_o, for all. U_0 for the n layers is hence computed as:

$$U_o d_o = \frac{1}{\frac{1}{U_1 d_1} + \frac{1}{U_2 d_2} + \frac{1}{U_3 d_3} + \cdots + \frac{1}{U_n d_n}} \tag{8.1.4}$$

For a pipe section of length Δx, the outer area is $\pi d_o \Delta x$, and equation 8.1.1 becomes:

$$Q = U_o \pi d_o \Delta x \left(T_o - T_f\right) \tag{8.1.5}$$

where T_f is the fluid's temperature *[K]* and T_o is the outer (surrounding) temperature *[K]*. Remember that in the total energy equation 6.3.12, the term q representing heat

added to the fluid from the environment should be taken pr. unit volume of fluid. It means that for a section of the pipe of length Δx, we have:

$$q = \frac{Q}{\pi \frac{d^2}{4} \Delta x} \tag{8.1.6}$$

where d as before is the pipe's inner diameter. Inserting equation 8.1.5 into equation 8.1.6 yields:

$$q = \frac{4 U_o d_o}{d^2} (T_o - T_f) \tag{8.1.7}$$

Where $U_o d_o$ has to be calculated by equation 8.1.4.

Let us now examine how to estimate the heat transfer coefficient U_i for each layer, starting with the innermost, the one between fluid and pipe wall.

8.2 Heat transfer coefficient between fluid and pipe wall

The situation when it comes to estimating the heat transfer coefficient for forced convection is a bit like the one for estimating the Darcy-Weisbach friction factor: Many researchers have studied the subject for a long time, and numerous alternative correlations have been proposed. Unlike for the friction factor, however, it is harder to state which approximation is the most accurate one, and several are shown here.

The various correlations are generally based 3 dimensionless numbers: The familiar Reynolds number *Re*, the Prandtl number *Pr*, and the Nusselt number *Nu*:

$$Nu = \frac{Ud}{k_f} \tag{8.2.1}$$

 For non-commercial use only

where U is the heat transfer coefficient we are seeking *[(W/m²K)]*, and k_f is the fluid's thermal conductivity *[W/(m·K)]*. *Pr* is defined:

$$Pr \stackrel{\text{def}}{=} \frac{\nu}{\alpha} = \frac{c_p \mu}{k_f} \tag{8.2.2}$$

Where ν is kinematic viscosity *[m²/s]*, μ is dynamic viscosity *[kg/(m·s)]*, α is thermal diffusivity *[m²/s]*, and c_p is specific heat at constant pressure *[J/(kg·K)]*. The most important thing to know about *Pr* is that it is a pure fluid property, so it can be tabulated as function of temperature and pressure. We do not really need its definition to use *Pr* in the heat calculations.

We see that if we are able to establish a correlation between *Nu*, *Pr* and *Re*, we can determine *U*. As is most often the case, laminar flow is easiest to handle. According to Tosun (2002), Sieder and Tate's correlation (1936) still seems to be the most widely accepted for laminar flow:

$$Nu = 1.86 \left(RePr \frac{d}{l} \right)^{1/3} \left(\frac{\mu}{\mu_w} \right)^{0.14} \tag{8.2.3}$$

The different terms are defined for the average pressure and temperature at each location in the fluid, except μ_w, which is the dynamic viscosity at the pipe's surface.

Note that equation 8.2.3, like so many other correlations for forced convection in pipes, contains the term *d/l*. This term has to do with the entrance effect near the pipe inlet, and may be important when designing heaters or coolers. It is less so in long pipelines. Therefore, we focus exclusively on situations where the pipe is long, meaning *d/l* is close to *0*. In that case, the laminar flow correlation reduces to:

$$Nu = 3.66 \tag{8.2.4}$$

This is an amazingly simple result, since the heat transfer coefficient turns out to be independent of the flow. Both equation 8.2.3 and 8.2.4 are valid only under the following stated limitations:

$$\begin{gathered} 13 \leq Re \leq 2300 \\ 0.48 \leq \mathrm{Pr} \leq 16{,}700 \\ 0.0044 \leq \frac{\mu}{\mu_w} \leq 9.75 \end{gathered} \tag{8.2.5}$$

We see that the equation is not valid all the way down to *Re = 0*. The cooling down in a pipeline in case of shutdown is often of interest, since there can be limits on how far down the temperature is allowed to fall before problems like freezing or wax or hydrate deposition start to occur. In most practical situations, however, the volume changes due to the cooling itself and is typically enough to bring *Re* above *13* even if the pipe has no net flow, making equation 8.2.4 valid.

For turbulent flow, most of the early correlations suffer from the problem that they have relatively limited validity, making them unsuited for high *Re*. One of the most widely used equations is probably that of Petukhov and Kirilov (1970):

$$Nu = \frac{\frac{f}{8} RePr}{1.07 \; + \; 12.7 \left(\frac{f}{8}\right)^{1/2} (Pr^{2/3} - 1)} \tag{8.2.6}$$

We see that equation 8.2.6 contains the Darcy-Weisbach friction factor *f*. Petukhov and Kirilov used something called the Filonenko-correlation to estimate the friction factor – a correlation from 1954 which is inaccurate for high *Re*, and was only intended for

 For non-commercial use only

smooth pipes. It is now common practice to insert more accurate friction factors into equation 8.2.6 and assume the results to be accurate enough for most engineering applications.

The somewhat newer Gnielinski-correlation (1976, 1983) is considered an improvement over the Petukhov-Kirilov correlation. Gnielinski introduced a very modest modification of 8.2.6, and his correlation is probably the best one available at present:

$$Nu = \frac{\frac{f}{8}(Re - 1{,}000)Pr}{1.07 + 12.7\left(\frac{f}{8}\right)^{1/2}(Pr^{2/3} - 1)} \tag{8.2.7}$$

The stated validity of equation 8.2.7 is:

$$2300 \leq Re \leq 5 \cdot 10^6$$
$$0.5 \leq \mathrm{Pr} \leq 2{,}000 \tag{8.2.8}$$

As explained earlier, transition between laminar and turbulent flow is somewhat difficult to predict accurately, so we should expect both equation 8.2.4 and 8.2.7 to be relatively unreliable around Re = 2,300. Another limitation is that equation 8.2.7 is, according to its author, invalid for the very high *Re* we may encounter in high-pressure gas pipelines.

The heat transfer coefficient *U* calculated by equation 8.2.4 or 8.2.7 corresponds to the innermost 'layer' in equation 8.1.4. It means:

$$U_1 d_1 = k_f Nu \tag{8.2.9}$$

The fluid properties involved in the calculations, such as Pr, ν and k, vary with temperature and to some extent also with pressure. Describing such properties accurately in a way the simulation program can access fast in real time is a science in itself, and some companies specialize in developing such program modules.

8.3 Heat transfer coefficients for the pipe wall, coating and insulation layers

If we consider the pipe itself, as well as any coating and insulation, to be separate thermal layers, we may write:

$$U_j\, d_j = \frac{2k_j}{ln\left(\frac{d_{jo}}{d_{ji}}\right)} \tag{8.3.1}$$

Common pipe materials	k_j [W/(m K)]
Steel	45 - 52
Ductile iron	52
Aluminum	200
Copper	380
High Density Polyethylene	0.36
PVC	0.19
Concrete	0 .85 - 1.73
Fiberglass	0.176
Fiberglass (Centron)	0.418
Fiberglass (Smith)	0.36
Rubber (Hard)	0.087
Rubber (Para)	0.109
Rubber (Soft)	0.075 - 0.092

Common coating materials	k_j [W/(m K)]
Asphalt	0.17
Cement	1.05
Concrete (insulating)	0.10-0.60
Concrete (weight)	0.86-1.73
Fusion bonded epoxy	0.251
Glass fiber	0.04
Neoprene	0.25
Polystyrene	0.157
Polystyrene foam	0.029 - 0.035
Polyurethane foam	0.024 - 0.035
PVC	0.19
PVC foam	0.04

Table 8.3.1. Thermal conductivity for common pipe materials, coatings and insulation materials.

For non-commercial use only

Where U_j is the heat transfer coefficient for layer No. j *[W/(m²K)]*, k_j is thermal conductivity for the material layer No. *j* is made up of *[W/(m K)]*, d_{ji} and d_{jo} is the layer's inner and outer diameter [m].

8.4 Heat transfer coefficient for outermost layer

8.4.1 Buried pipe

If the pipeline is buried, the environment around it can consist of such things as peat, sand, gravel, or any combination of them. In addition moisture may have an effect. For such environments, Bau & Sadhal (1982) have developed a correlation for estimating the heat transfer coefficient for fully buried pipes, and Morud & Simonsen (2007) have developed a correlation for partially buried pipes. A simpler and in most cases adequate correlation was presented by King (1984). It states:

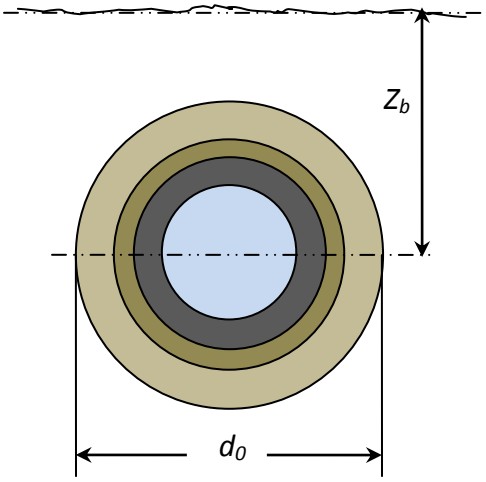


Figure 8.1.1. Pipe layers.

$$U_n d_n = \frac{2k_{soil}}{cosh^{-1}\left(\frac{2Z_b}{d_o}\right)} \quad (8.4.1)$$

Z_b is the pipe centerline's depth below the surface *[m]*, k_{soil} is the soil's thermal conductivity *[W/(m·K)]* and the diameter involved, d_o, is the outer diameter of the outermost insulation layer (= d_n).

k_{soil} does of course vary greatly with the type of soil as well as how much water content it has. Some example values are given in table 8.4.1.

Soil material	k_j [W/(m K)]
Peat (dry)	0.17
Peat (wet)	0.54
Peat (icy)	0.89
Loam	0.175
Sandy soil (dry)	0.4-0.7
Sandy soil (moist)	0.85-1.05
Sandy soil (soaked)	1.90-2.45
Clay soil (dry)	0.35-0.50
Clay soil (moist)	0.7 -0.85
Clay soil (wet)	1.05-1.60
Clay soil (frozen)	2.51
Gravel	0.95
Gravel (sandy)	2.51
Limestone	1.3
Sandstone	1.63-2.08
Ice (0 C)	2.2
Ice (-40 C)	1.63-2.08
Snow (loose)	0.12
Snow (hard packed)	1.2

Table 8.4.1 Typical thermal conductivity for some common soil types.

8.4.2 Above-ground pipe

In case of above-ground pipelines surrounded by air, the pipe is comparable to a cylinder with air flowing perpendicular to its axis. A number of researchers have studied the heat exchange around such cylinders, and the most widely accepted empirical equation coming out of that work is probably the one proposed by Churchill and Bernstein (1977). It covers the entire range of Re for which data is available, as well as for a wide range of *Pr*. It has a form comparable to the one used for forced internal convection, equation 8.2.1:

$$Nu_o = 0.3 + \frac{0.62 {Re_o}^{1/2} {Pr_o}^{1/3}}{\left[1 + \left(\frac{0.4}{Pr_o}\right)^{2/3}\right]^{1/4}} \left[1 + \left(\frac{Re_o}{282{,}000}\right)^{5/8}\right]^{4/5} \qquad (8.4.2)$$

For non-commercial use only

The index 'o' stands for outer, indicating all parameters are based on outer diameter, outer temperature and so on. The Churchill-Bernstein equation is recommended for $Re_o Pr_o > 0.2$, which means it is not strictly valid if the air or water around the pipeline is at rest. In most practical situations that is not really a limitation, since even the most minute wind or current would bring the equation into its valid area. Nature rarely provides environments as static as that, and the pipeline's influence can itself easily create enough disturbances to make the equation valid.

The two most common surrounding fluids are of course air and water. For those air temperatures and pressures we typically encounter (say $223 < T < 333$ *K* and $p = 10^5$ *Pa*), it is sufficiently accurate (to within 3 %) to approximate air's *thermal conductivity*, *kinematic viscosity* and *Prandtl number* by simple linear functions:

$$k_{f\ air} = 6.55 \cdot 10^{-5} T + 0.00594 \tag{8.4.3}$$

$$\nu_{air} = 0.0818 \cdot 10^{-6} T - 8.6471 \cdot 10^{-6} \tag{8.4.4}$$

$$Pr_{air} = -1.587 \cdot 10^{-4} T + 0.759 \tag{8.4.5}$$

Water properties are less linear, and more terms are needed to approximate them for $273 < T < 333$ *K*. Submerged pipelines may have much higher surrounding pressure than one atmosphere, but that only affects the data moderately, so we are well within other errors involved when neglecting it. For the purpose of heat exchange, we may use the following, somewhat simplified but fast curve fit which is based on data taken from Wagner & Kretzschmar (2007), estimated to be within 4% or real values for temperatures below *333 K*:

$$k_{f\ water} = -2.5 \cdot 10^{-5} T^2 + 0.0166 T - 2.1136 \tag{8.4.6}$$

$$\nu_{water} = 10^{25.22[log_{10}(T)]^2 - 131.76 log_{10}(T) + 165.58} \tag{8.4.7}$$

$$Pr_{water} = 10^{28.343[log_{10}(T)]^2 - 148.12 log_{10}(T) + 193.76} \tag{8.4.8}$$

Note that when using these results to estimate a pipeline's outer heat transfer coefficient, Pr_o is of course based on the surrounding fluid's properties. The Reynolds number is also based on the outside conditions:

$$Re_o = \frac{v_{perp\ surr}\, d_o}{\nu_{surr}} \tag{8.4.9}$$

Where $v_{perp\ surr}$ is the surrounding fluid's velocity before being retarded by the pipe, and ν_{surr} is the surrounding fluid's kinematic velocity.

If the fluid does not flow perpendicular to the pipe's center axis, the component being perpendicular is used. This is not a completely accurate approximation as it implies that axial components of the flow do not have any effect, which is of course not so. When estimating the cooling in risers on offshore platforms, better models may be required. Also, equation 8.4.2 is based on a cylinder with flow around it on both sides, which is not the actual situation if the pipe lies on the ground. If so, the real heat exchange due to the outside fluid flow may be somewhat less than what is predicted here. Pipelines in contact with the ground can also exchange heat with the ground directly, and the best estimate may in those cases be achieved by trying to take both effects into account simultaneously. In most cases, though, using the model directly, as it is presented here, is adequate.

There are also other, competing empirical relations for computing Nu, for instance the Whitaker correlation (1972). The two correlations can give quite different results. Tosun reports the Churchill-Bernstein relation giving up to 70% higher heat transfer coefficient than the Whitaker correlation, which indicates significant limitations in the equations themselves. Comparing several equations may be worth the efforts in situations when the outer heat transfer coefficient turns out to be important, such as when the pipe is un-insulated or when cooling-down times after pipeline shut-in are being simulated.

Either way, the heat transfer coefficient, to be used in equation 8.1.3, is computed as:

$$U_n d_n = k_o Nu_o \tag{8.4.4}$$

 For non-commercial use only

8.5 The heat models' limitations

8.5.1 Transient versus steady-state heat flow

Which heat model to use depends on exactly what one wants to investigate. The presented model is steady-state in the sense that it does not account for time delays due to for instance heat being stored in the pipe wall itself. That does not pose a problem if we are investigating flows which last for a long time, and it can be a quite good approximation even when simulating highly transient temperature situations. Consider, for instance, steel pipe carrying water. Water has nearly 9 times as high specific heat capacity as steel, while its density is around 8 times lower, making the heat capacities for both almost proportional to the area they occupy in ach cross section. In most pipelines, the liquid-carrying cross-section is much larger than the pipe wall's cross section, meaning little heat energy is stored in the pipe wall compared to in the liquid.

More generally, if the flow area is $\pi d^2/4$ and has a specific heat capacity c_p and density ρ, while the pipe wall has cross-sectional area $\pi(d_o^2-d^2)/4$, we get:

$$\frac{Pipe\ wall\ heat\ capacity}{Liquid\ heat\ capacity} = \frac{\rho_{wall}\, c_{p\ wall}}{\rho c_p}\frac{\left(d_o{}^2 - d^2\right)}{d^2} \tag{8.5.1}$$

By inserting values for our actual pipeline and considering exactly what sort of heat phenomenon we are interested in, we get a feeling for how large error we introduce by neglecting the pipe wall's heat capacity. If we insert typical values for liquid-carrying pipelines in equation 8.5.1, we often find that the wall has less than 10 % of the liquid's heat capacity. That is of the same order as other errors in the heat calculations, so it rarely makes sense to put too much effort into improving the model in this respect. For gas flow, this can be a bit different. The pipe wall can have larger impact, but rarely enough to necessitate a more accurate model.

For buried pipelines, we can expect a larger part of the surroundings to take part in the heating and cooling, so it generally takes somewhat longer to increase or decrease temperatures than our model suggests.

8.5.2 Other accuracy considerations

The heat model shown here does not include any terms to do with radiation. That is because radiation tends not to be important, though it can have an impact on un-insulated pipes carrying relatively hot fluids. For insulated above-ground pipelines, as well as for both insulated and un-insulated buried pipelines, the main thermal resistance is typically found in the insulation material. Therefore, the outer layer often ends up with nearly the same temperature as the surroundings, rendering radiation irrelevant.

References

Sieder, E.N., G.E. Tate. (1936): Heat *transfer and pressure drop of liquids in tubes*, Ind. Eng. Chem, 28, 1429.

Petukhov,B.S., (1970): *Heat Transfer and Friction in Turbulent Pipe Flow with Variable Physical Properties.* Advances in Heat Transfer, Vol. 6, J. P. Hartnett and T. F. Irvine, eds., Academic, San Diego, CA, pp.504-564.

Whitaker, S., (1972): Forced convection heat transfer correlations for flow in pipes, past flat plates, single cylinders, single spheres, and for flow in packed beds and tube bundles, AIChE Journal 18, 361.

Gnielinski, V. (1976): *New Equations for Heat and Mass Transfer in Turbulent Pipe and Channel Flow*. Int Chem Eng Vol. 16 p. 10.

Churchill, S.W. and M. Bernstein, (1977): A correlating equation for forced convection from gases and liquids to a circular cylinder in cross flow, J. Heat Transfer, 99, 300.

Bau, H.H., Sadhal, S.S. (1982): Heat *Losses from Fluid Flowing in a Buried Pipe.* International Journal of Heat and Mass Transfer 25(11): 1621-1629, 1982.

Gnielinski, V. (1983): *Single-Phase Convective Heat Transfer*, Ch. 2. 5, section 1-1t o 2-9, Hemisphere Publishing Corporation.

King, G.G. (1984): Equation Predicts *Buried Pipeline Temperatures* Oil and Gas Journal, pp. 65-72, March 16.

Tosun, I., (2002): Modelling in transport phenomena. A conceptual approach. First edition, Elsevier Science.

Wagner, W., Kretzschmar, H.J. (2007): *International Steam Tables*. Springer, 2. edition.

 For non-commercial use only

Morud, J.C., Simonsen, A. (2007): *Heat Transfer from Partially Buried Pipes.* 16th Australian Fluid Mechanics Conference.

"Software is like entropy. It is difficult to grasp, weighs nothing, and obeys the second law of thermodynamics; i.e. it always increases."
Norman R. Augustine

9 Adding heat calculations to the characteristics method

This chapter covers:

- Using the energy equation and heat exchange to calculate liquid temperatures
- Traditional solution methods
- Problems caused by numerical dissipation and dispersion
- Modern, efficient spatial discretization models

9.1 The energy equation's characteristic

In chapter 7, we learned how elegantly the continuity and momentum equations could be solved using the method of characteristics. We did not have to use the energy equation at all. In many cases, that is all there is to it and we can do lots of useful

For non-commercial use only

calculations that way. But if we want to have a closer look at how the liquid's temperature develops or how much heat the pipe exchanges with its surroundings, the energy equation becomes essential.

Let us start by re-writing the energy equation on the form shown as equation 6.3.10, but with the terms somewhat re-arranged:

$$\frac{\partial}{\partial t}\left[\rho\left(u+\frac{v^2}{2}+gz\right)\right]+\frac{\partial}{\partial x}\left[\rho v\left(u+\frac{v^2}{2}+gz\right)\right]=-\frac{\partial(vp)}{\partial x}+q+w \tag{9.1.1}$$

If we introduce the specific energy E_s according to equation 6.3.8, we get:

$$\frac{\partial}{\partial t}(\rho E_s)+\frac{\partial}{\partial x}(\rho v E_s)=-\frac{\partial(vp)}{\partial x}+q+w \tag{9.1.2}$$

Recall that in the liquid transient model, the density was kept constant, independent of both ρ and T. Furthermore, we remember that p and v were found independently of anything to do with heat. Therefore, as far as the energy equation 9.1.2 is concerned, p and v are simply (variable) constants – they are not functions of the main variables in equation 9.1.2. Therefore, we may simplify to:

$$\rho\frac{\partial E_s}{\partial t}+\rho v\frac{\partial E_s}{\partial x}=-\frac{\partial(vp)}{\partial x}+q+w \tag{9.1.3}$$

This is in fact a classical first order quasi-linear hyperbolic equation. We can see that by inserting:

$$dE_s=\frac{\partial E_s}{\partial t}dt+\frac{\partial E_s}{\partial x}dx \tag{9.1.4}$$

If we eliminate $\partial E/\partial t$ between equations 9.1.3 and 9.1.4, we get:

$$\frac{\partial E_s}{\partial x}(\rho dx - \rho v dt) + \left[\left(-\frac{\partial (vp)}{\partial x} + q + w\right)dt - \rho dE_s\right] = 0 \tag{9.1.5}$$

This equation is independent of $\partial E/\partial t$, and it can also be made independent of $\partial E/\partial x$ by choosing dy/dx so that:

$$\rho dx - \rho v dt = 0 \tag{9.1.6}$$

From equations 9.1.5 and 9.1.6 it follows that:

$$\left(-\frac{\partial (vp)}{\partial x} + q + w\right)dt - \rho dE_s = 0 \tag{9.1.7}$$

In other words if we choose $dx/dt = v$, which in our case describes the characteristic, we may set:

$$\frac{dE_s}{dt} = \frac{1}{\rho}\left(-\frac{\partial (vp)}{\partial x} + q + w\right) \tag{9.1.8}$$

This is similar to when we turn on the shower in the morning: It is only the upstream conditions (the hot water tank, say) which affect the temperature. The time it takes for the first hot water to reach the shower cap depends upon the water's velocity. When later studying gas and multi-phase flow, the same applies, and the shower-example serves well as a mental reference.

 For non-commercial use only

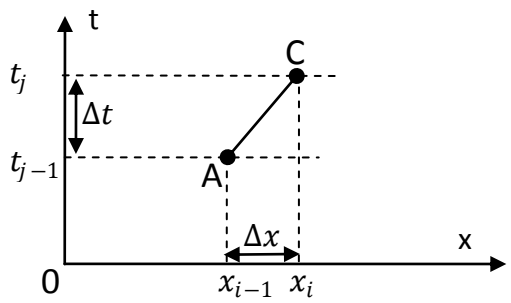


Figure 9.1.1. Characteristic line for E in the xt-plane.

This is very similar to how we found a solution for the continuity and momentum equations in chapter 7. One important difference here is that there is only one characteristic, not two. If we construct a grid using similar ideas as the ones figure 7.1.1 is based on, we get figure 9.1.1. The conditions in point C some time into the future is only affected by what went on upstream some time before – anything happening downstream is irrelevant.

In the special case where $v = 0$, the characteristic becomes flat, we see that $dx/dt = 0$. That means we need infinite grid density along the x-axis, something which is of course impossible. Therefore, we cannot expect the characteristic to provide a good basis for describing the heat if $v = 0$.

At first glance it may seem that we now have a complete model for simulating liquid flow with heat at this point, at least if $v \neq 0$. It looks like dE/dt could be approximated the same way we did in equations 7.2.3 and 7.2.4 by setting:

$$\frac{dE_s}{dt} = \frac{E_{s\,C} - E_{s\,A}}{\Delta t} \; for \; \frac{dx}{dt} = v \; if \; v > 0$$

$$\frac{dE_s}{dt} = \frac{E_{s\,C} - E_{s\,B}}{\Delta t} \; for \; \frac{dx}{dt} = v \; if \; v < 0 \qquad (9.1.9)$$

$$\frac{dE_s}{dt} is \; not \; defined \; if \; v = 0$$

The upstream point seems to be the appropriate one to use when calculating the derivative, we but simply check which way the flow goes and pick the appropriate one from those in equation 9.1.9.

But there is a problem with this approach. The grid used to calculate the specific energy E_s would have to be different to the one used for pressure- and velocity transient calculations: We would need one *thermo-grid* satisfying $dx/dt = v$, and a *pressure-velocity-grid* satisfying $dx/dt = a_s$. Since a_s typically is two orders of magnitude larger than v, it is difficult to bring information from one grid to the other. The grid-points are not going to overlap, at least not most of the time. If both grids had been fixed, we could probably have lived with that by using interpolation. But since transients make the velocity vary over time, and the thermo-grid's mesh size depends on precisely the velocity, this approach is impractical.

From the above, we conclude as follows:

- For liquid flow, the pressures and velocities are not much affected by temperatures, and the energy equation may be omitted in many calculations just as we did in chapter 7. The temperature is most relevant for calculating viscosity and detecting such things as ice formation or cavitation, while its effect on density is so small that it is in fact neglected in the model. Even when the energy equation is included, it can be treated as an add-on to the continuity and momentum equations, with a very weak coupling back to affect p and v (it only affects the viscosity ν and thereby to some extent the friction). The coupling the other way is much more significant, p and v strongly affects E_s (and thereby the temperature).
- When adding the energy equation, it turns out that it follows a characteristic described by $dx/dt = v$, meaning it is only affected by liquid coming from upstream, and that the specific energy in the liquid propagates at a velocity similar to the liquid's velocity.
- No meaningful characteristic for the specific energy can be defined if the velocity is *0*.
- Since the pressure and liquid transients travel at the speed of sound, while the energy turns out to travel at the fluid's speed, we are faced with a system where more than one characteristic speed is present at the same time. This leads to different grid density preferences in time and space for different parts of the conservation equations.

Although the energy equation's characteristic was useful in understanding the nature of how the energy propagates, it did not lead to a practical computation algorithm. Therefore, we need to look for alternative ways to add the energy equation in simulations where p and v is calculated by the method of characteristics.

 For non-commercial use only

9.2 Solving the energy equations using the explicit Lax-Wendroff's method

Since it turned out to be difficult to solve the energy equation by introducing yet another characteristics method, we return to equation 9.1.3 and try to approximate $\partial E/\partial t$ and $\partial E/\partial x$ directly. Nothing better than a first order approximation may seem appropriate, given that the continuity and momentum equations rely on the first-order approximations in equations 7.2.3 and 7.2.4. A first order approximation leads to an unstable numerical method if applied to equation 9.1.3, though. Instead, we use a second-order method – not because we need the better accuracy such a method brings, but because it is stable.

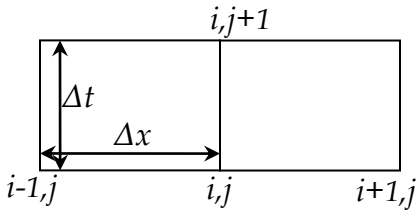


Figure 9.2.1 Rectangular discretization grid.

Consider the grid in figure 9.2.1. Let us use the point *i,j* and find expressions for the derivatives around it using Taylor expansion.

Taylor expansion in the time-direction, from point *i,j* to *i,j+1* follows directly from Taylor's theory:

$$E_{s\,i,j+1} = E_{i,j} + \Delta t \left(\frac{\partial E_s}{\partial t}\right)_{i,j} + \frac{1}{2}\Delta t^2 \left(\frac{\partial^2 E_s}{\partial t^2}\right)_{i,j} + \cdots, \tag{9.2.1}$$

Finding direct estimates of the second order time derivative is not possible without introducing more than one time level, something we would rather avoid since it is less convenient to program and takes up more memory (more time levels must be remembered). Instead, we take advantage of the fact that equation 9.1.3 is linear by re-writing it to:

$$\frac{\partial E_s}{\partial t} = -v\frac{\partial E_s}{\partial x} - \frac{1}{\rho}\left[\frac{\partial (vp)}{\partial x} - q - w\right] \tag{9.2.2}$$

We also need an expression for the second derivative:

$$\frac{\partial^2 E_s}{\partial t^2} = \frac{\partial}{\partial t}\left(-v\frac{\partial E_s}{\partial x}\right) - \frac{\partial}{\partial t}\left\{\frac{1}{\rho}\left[\frac{\partial (vp)}{\partial x} - q - w\right]\right\} \tag{9.2.3}$$

The shape of the ∂E_s-curve in the E_s-t plane must be similar to the shape of the ∂E_s-curve in the E_s-x plane, with the difference of the factor $-v$ and a constant set-off, corresponding to the 'constant' term in the square parenthesis. For the purpose of finding the second-derivative, we can therefore ignore the constant term (since it does not affect the shape of the first-derivative curve and therefore does not influence the second-derivative), and pretend:

$$\frac{\partial E_s}{\partial t} = -v\frac{\partial E_s}{\partial x} \tag{9.2.4}$$

Time derivation of the left-hand side of equation 9.2.2 must therefore correspond to spatial derivation of the right-hand side, and we may apply equation 9.2.3 to find the second derivative of 9.2.2, so we get:

$$\frac{\partial^2 E_s}{\partial t^2} = v^2\frac{\partial^2 E_s}{\partial x^2} \tag{9.2.5}$$

Inserting equations 9.2.2 and 9.2.5 into the Taylor-expansion 9.2.1, and ignoring derivatives of higher order than second, gives:

$$E_{s\,i,j+1} = E_{s\,i,j} + \Delta t\left(-v\frac{\partial E_s}{\partial x} - \frac{1}{\rho}\left[\frac{\partial (vp)}{\partial x} - q - w\right]\right)_{i,j} + \frac{1}{2}\Delta t^2\left(v^2\frac{\partial^2 E_s}{\partial x^2}\right)_{i,j} \tag{9.2.6}$$

 For non-commercial use only

The only job remaining here is to insert approximations for the first and second order spatial derivative of E_s.

It follows directly from the definition of a derivative that $\partial E/\partial x \approx \Delta E/\Delta x$ if Δx is small. For instance, we may use a central difference and set:

$$\frac{\partial E_{s\,i,j}}{\partial x} = \frac{E_{s\,i+1,j} - E_{s\,i-1,j}}{2\Delta x} \tag{9.2.7}$$

To estimate the second derivative, we may start by estimating the derivative in a point half way between *i,j* and *i+1,j*:

$$\frac{\partial E_{s\,i+1/2,j}}{\partial x} = \frac{E_{s\,i+1,j} - E_{s\,i,j}}{\Delta x} \tag{9.2.8}$$

A similar approximation at the other side would be:

$$\frac{\partial E_{s\,i-1/2,j}}{\partial x} = \frac{E_{s\,i,j} - E_{s\,i-1,j}}{\Delta x} \tag{9.2.9}$$

Combining equations 9.2.8 and 9.2.9 gives:

$$\frac{\partial^2 E_{s\,i,j}}{\partial x^2} = \frac{\frac{\partial E_{s\,i+1/2,j}}{\partial x} - \frac{\partial E_{s\,i-1/2,j}}{\partial x}}{\Delta x} = \frac{E_{s\,i+1,j} - 2E_{s\,i,j} + E_{s\,i-1,j}}{\Delta x^2} \tag{9.2.10}$$

Inserting equations 9.2.6 and 9.2.9 into 9.2.5 now gives us:

$$E_{s\,i,j+1} = E_{s\,i,j} - \frac{v}{2}\frac{\Delta t}{\Delta x}\left(E_{s\,i+1,j} - E_{s\,i-1,j}\right) + \frac{1}{2}v^2\left(\frac{\Delta t}{\Delta x}\right)^2\left(E_{s\,i+1,j} - 2E_{s\,i,j} + E_{s\,i-1,j}\right) - \frac{\Delta t}{\rho}\left[\frac{\partial(vp)}{\partial x} - q - w\right]_{i,j} \tag{9.2.11}$$

By re-arranging, the final result becomes:

$$E_{s\,i,j+1} = \frac{v}{2}\frac{\Delta t}{\Delta x}\left(1 + v\frac{\Delta t}{\Delta x}\right)E_{s\,i-1,j} + \left[1 - \left(v\frac{\Delta t}{\Delta x}\right)^2\right]E_{s\,i,j} - \frac{v}{2}\frac{\Delta t}{\Delta x}\left(1 - v\frac{\Delta t}{\Delta x}\right)E_{s\,i+1,j} - \frac{\Delta t}{\rho}\left[\frac{\partial(vp)}{\partial x} - q - w\right]_{i,j} \tag{9.2.12}$$

This tells us that if we know the conditions at one time step *j*, we can use equation 9.2.12 to find them at the next time step, *j+1*. The last term contains various 'constants' from the solution of the continuity and momentum equations as well as the heat flow q between the pipe liquid and the environment. There is also a term which has to do with any added or removed work w (relevant of pumps, compressors or turbines are present).

For $\partial(vp)/\partial x$, we may use a first-order central approximation similar to the one in equation 9.2.7:

$$\left[\frac{\partial(vp)}{\partial x}\right]_{ij} = \frac{v_{i+1,j}p_{i+1,j} - v_{i-1,j}p_{i-1,j}}{2\Delta x} \tag{9.2.13}$$

 For non-commercial use only

9.3 Boundary conditions for the thermo equation

9.3.1 The problem with lack of neighboring grid-points at the boundary

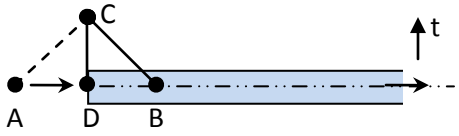


Figure 9.3.1. Inlet boundary

When we use equation 9.2.12 to calculate $E_{s\,i,j+1}$, called point C in figure 9.3.1, we generally need information from the previous time step in point A, B and D. This can pose a problem at the pipe boundaries, since the inlet and outlet do not have points at both sides.

At the inlet boundary, the specific energy E_s is obviously not a function of what goes on inside the pipe, it is determined by the fluid coming into the pipe. Equation 6.3.8 tells us that E_s is a function of the incoming fluid's internal energy u, velocity v and pipe inlet elevation Z. They are calculated elsewhere.

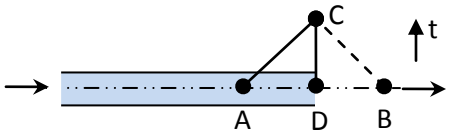


Figure 9.3.2. Outlet boundary

At the outlet boundary, things are more complicated. E_s is of course going to be a function of what the fluid has experienced on its journey through the pipe, and so equation 9.2.13 is valid, but impossible to use, given the lack of a point B.

The problem may be solved by extrapolating data from neighboring grid-points. The simplest solution would be to simply set $E_{s\,C} = E_{s\,A}$. Doing so would mean ignoring any energy transformations going on in the last part of the pipe. For a very long pipeline with lots of grid-points, that might not be so bad, at least if the purpose of the calculations is to estimate heat loss. If, for instance, $N_x = 10^3$, the error in doing so should be in the order of 10^{-3}. That is far less than the uncertainty involved in calculating the heat loss according to the procedure outlined in chapter 8.

A better approximation would be to assume the temperature to be the same in C as in A, but update E_s according to changes in the other (known) data E_s consists of.

The best type of extrapolation can be achieved by using several neighboring points in the estimate, for instance by drawing a straight line through the two closest points to the left of the outlet (point A and a point to the left of it in figure 9.3.2).

The most accurate and general solution can be created by going back to equation 9.2.5, and reducing the order by neglecting the last term:

$$E_{s\,i,j+1} = E_{s\,i,j} + \Delta t\left(-v\frac{\partial E_s}{\partial x} - \frac{1}{\rho}\left[\frac{\partial (vp)}{\partial x} - q - w\right]\right)_{i,j} \tag{9.3.1}$$

We modify the central approximation in equation 9.2.6 to a left approximation:

$$\frac{\partial E_{s\,i,j}}{\partial x} = \frac{E_{s\,i,j} - E_{s\,i-1,j}}{\Delta x} \tag{9.3.2}$$

And get:

$$E_{s\,i,j+1} = E_{s\,i,j} - v\frac{\Delta t}{\Delta x}\left(E_{s\,i,j} - E_{s\,i-1,j}\right) - \frac{\Delta t}{\rho}\left[\frac{\partial (vp)}{\partial x} - q - w\right]_{i,j} \tag{9.3.3}$$

Re-arranging:

$$E_{s\,i,j+1} = v\frac{\Delta t}{\Delta x}E_{s\,i-1,j} + \left(1 - v\frac{\Delta t}{\Delta x}\right)E_{s\,i,j} - \frac{\Delta t}{\rho}\left[\frac{\partial (vp)}{\partial x} - q - w\right]_{i,j} \tag{9.3.4}$$

Equation 9.3.4 only relies on information from A and D in order to get to C, so it can be used as it is directly (apart from $\partial(vp)/\partial x$, equation 9.2.12 also having to be replaced by a left approximation). Note that equation 9.3.2 should only be allowed to replace equation 9.2.11 at the outlet, not in the whole pipe, otherwise the integration becomes unstable.

Note also our boundary conditions are no longer symmetrical, as they were for the continuity and momentum equations. Inlet and outlet must be treated differently. It means we must check the direction of v both at the inlet and outlet at each time step and use the appropriate condition. The transients may of course result in the inlet and outlet

 For non-commercial use only

flow reversing at different times, there may be instances where inflow or outflow happens in both ends of a pipe simultaneously. That does not create problems for the simulations, but it increases the amount of code somewhat, and both pipe ends must be able to handle both situations.

If outflow happens at what has been defined at pipe inlet, we may develop an equation similar to 9.3.4 by using right side derivatives:

$$E_{s\,i,j+1} = \left(1 + v\frac{\Delta t}{\Delta x}\right)E_{s\,i,j} - v\frac{\Delta t}{\Delta x}E_{s\,i+1,j} - \frac{\Delta t}{\rho}\left[\frac{\partial(vp)}{\partial x} - q - w\right]_{i,j} \tag{9.3.5}$$

Note that boundary conditions are much more thoroughly treated in chapters 11 and 12.

9.3.2 Junctions, pumps, valves and other components

There are fewer sorts of components to be handled by the energy equation than by the continuity and pressure equations. Valves, for instance, neither add nor remove energy, and as far at the energy equation is concerned, they don't do anything special. Their effect is accounted for indirectly by the data from the other equations (p and v). Pumps and turbines are simple, too: They create a value for w.

Junctions, on the other hand, are slightly more complicated: If there is more than one inlet, the fluids mix and create an average temperature. It is also possible for the inflowing liquids to have different properties. At an oil field, for instance, it is common for oil from different wells to be piped to a manifold and into the same pipeline. The different wells may deliver oils of different chemical properties as well as different temperatures to the pipeline. The resulting temperature (and E_s) is some average of the different inlets. The sum of all energy flowing in has to be the same as the sum of everything flowing out:

$$\sum_{All\ inflowing\ \ k} E_{s\,k}\rho_k A_k v_k = E_{s\,mix}\rho_{mix} \sum_{All\ outflowing\ \ k} A_k v_k \tag{9.3.6}$$

In case all liquids have the same chemical properties and the density is constant, the resulting Es_{mix} is going to be close to a weighted average of everything incoming:

$$E_{s\,mix} = \frac{\sum_{All\ inflowing\ \ k} E_{s\,k} A_k v_k}{\sum_{All\ outflowing\ \ k} A_k v_k} \tag{9.3.6}$$

9.4 Determining secondary variables

When we simulate our equation system, meaning equations 7.2.9-7.2.12, as well as 9.2.12, we get values for p, v and E_s. But we also need to know the temperatures as they are often of direct interests and besides required in the heat loss calculations.

A liquid's specific internal energy is a fluid property and can be tabulated or fitted based on measurements. Alternatively, we may use values for the specific enthalpy h as input. From equation 6.3.8 and 6.3.11 it follows that:

$$h = E_s + \frac{p}{\rho} - \frac{v^2}{2} - gz \tag{9.4.1}$$

To utilize this equation, we need a correlation between h, T and p for the liquid in question. Such properties depend on which liquid we are dealing with and which temperature and pressure ranges we are in.

When inserting starting values, we may start out with a set of temperatures, and equation 9.4.1 is simply reversed to calculate the initial specific energies:

$$E_s = h - \frac{p}{\rho} + \frac{v^2}{2} + gz \tag{9.4.2}$$

We also want to be able to calculate the temperature at all grid-points as the simulation progresses, so we need a method to determine $T = T(p, h)$, as well. When high accuracy is required, values must of course be found from tables, from curve-fitted formulas, or

 For non-commercial use only

from special computer programs designed for that purpose. This is discussed in greater detail for gases in chapter 10.6, where we point out more general ways of doing this, such as the Peng-Robinson curve fit method. General methods are relatively computer-intensive and easily end up taking more than half the computing capacity.

Liquids, which are what we are dealing with when we use the method of characteristics, are somewhat easier to handle than gases, and tabulated values can normally be curve-fitted quite easily for convenient representation in a computer program. h tends to be only weekly dependent on p, and it is often accurate enough to model h as a function of T only. As an example, figure 9.4.1 shows how close the 3 curves are for water for as different pressures as *0.1*, *50* and *100 MPa*. For moderate pressures, using the specific heat for constant pressure, c_p, and setting $h = c_p(T - T_{ref})$, may be adequate even when the pressure is not constant.

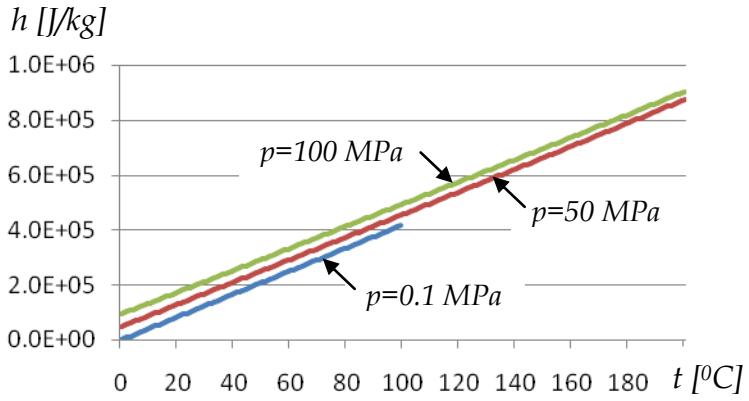


Figure 9.4.1. Specific enthalpy for water

Pr, ν and k_f also tend to depend far less on pressure than on temperature for those pressures and temperatures most often dealt with, and simple approximations of the sort shown in equations 8.4.6 - 8.4.8 are adequate.

9.5 Computing starting values

In chapter 7.5.1, we observed how easy it is to determine steady-state pressures and velocities to be used as initial conditions for the transients we want to investigate. When the energy equation is included, we need starting values for E_s as well.

At steady-state flow, nothing changes over time, and $\partial E_s/\partial t = 0$. That can be inserted into 9.1.3:

$$\frac{\partial E_s}{\partial x} = \frac{1}{\rho v}\left[-\frac{\partial (vp)}{\partial x} + q + w\right] \tag{9.5.1}$$

Suppose we have already found v to be positive, so the liquid flows into what was initially assumed to be the pipe's inlet end. We may then simply start at that end and continue computing towards the outlet. To achieve that, we use a right approximation for the derivative:

$$\left(\frac{\partial E_s}{\partial x}\right)_i = \frac{E_{s\,i+1} - E_{s\,i}}{\Delta x} \tag{9.5.2}$$

Inserted into equation 9.5.3, this leads to:

$$\frac{E_{s\,i+1} - E_{s\,i}}{\Delta x} = \frac{1}{\rho v}\left[-\frac{\partial (vp)}{\partial x} + q + w\right]_i \tag{9.5.3}$$

By re-arranging:

$$E_{s\,i+1} = E_{s\,i} + \frac{\Delta x}{\rho v}\left[-\frac{\partial (vp)}{\partial x} + q + w\right]_i \tag{9.5.4}$$

This turns out to be a very simple recursive formula. At the inlet, $E_{s\,1}$ is known as a boundary condition – it is the inflowing fluid's specific energy. Therefore, $E_{s\,2}$ can easily be computed using equation 9.5.4. When determining q, we found in chapter 8 that we need to know the liquid's temperature. For the first section, we use the inlet

 For non-commercial use only

temperature based on $E_{s\,1}$, as determined by equation 9.4.2. Similarly, $E_{s\,3}$ is computed as a function of $E_{s\,2}$ and so on, until we have found starting values for all the temperatures.

We get better accuracy – and also better agreement with the dynamic model – if we replace the first-order approximation 9.5.2 with a second-order approximation:

$$\left(\frac{\partial E_s}{\partial x}\right)_i = \frac{E_{s\,i+1} - E_{s\,i-1}}{2\Delta x} \tag{9.5.5}$$

Inserting this into equation 9.5.1 leads to:

$$E_{s\,i+1} = E_{s\,i-1} + \frac{2\Delta x}{\rho v}\left[-\frac{\partial(vp)}{\partial x} + q + w\right]_i \tag{9.5.6}$$

This equation can obviously not be used at the boundary ($i = 0$), since that point does not have a grid point to the left of it ($i - 1$ does not exist). Therefore, we need to use equation 9.5.4 at the boundary, and then go on with equation 9.5.6 for the rest of the grid.

If v is negative, the liquid flows in at what was assumed to be the outlet end, and we must of course start the recursive calculations there. By replacing equation 9.5.2 with a left approximation, 9.5.4 can be modified to:

$$E_{s\,i-1} = E_{s\,i} - \frac{\Delta x}{\rho v}\left[-\frac{\partial(vp)}{\partial x} + q + w\right]_i \tag{9.5.7}$$

Similarly, equation 9.5.6 is replaced by:

$$E_{s-1} = E_{s\,i+1} - \frac{2\Delta x}{\rho v}\left[-\frac{\partial(vp)}{\partial x} + q + w\right]_i \tag{9.5.8}$$

This method is so fast and easy one may use a finer grid for these computations than for the later transient simulations, especially if better starting-value accuracy is desirable. In most cases, though, that is not necessary, since slightly incorrect starting values for T or E_s do not tend to create transients travelling back and forth in the way incorrect starting pressures or velocities do.

This method can easily be applied to a general network in this way:

i) Compute steady-state p and v as it is was explained in chapter 7.
ii) Start with the pipes where a known liquid comes into the system, typically from a reservoir with known temperature. Use equation 9.4.2 to compute E_s, and use equation 9.5.4 or 9.5.5 to compute E_s in the other grid-points.
iii) When ii) has been completed and the outlet temperatures from some of the pipes are known, there will be at least one or more junctions where all inflowing temperatures are known (otherwise, the found starting values for v are wrong). Use the junction methods from chapter 9.3.1 to find E_s in those junctions, and calculate starting values in all pipes flowing out from those junctions.
iv) Repeat iii) until all pipes have been given starting values.
v) If the calculations reveal temperatures resulting in very different viscosities compared to the ones assumed when computing p and v, the calculations could be repeated with new, updated viscosities to improve the result's accuracy.

9.6 Stability considerations for the energy solution

The A-matrix for equation 9.2.12, which is of interest to stability, is a diagonal matrix on the form

$$A = \begin{bmatrix} a & b & & & & & & & \\ c & a & b & & & & & & \\ & c & a & b & & & & 0 & \\ & & c & a & b & & & & \\ & & & c & a & b & & & \\ & & & & c & a & b & & \\ & 0 & & & & c & a & b & \\ & & & & & & c & a & b \\ & & & & & & & c & a \end{bmatrix} \tag{9.6.1}$$

Where the factors a (not to be confused with speed of sound), b and c can be read from equation9.2.12 as:

$$a = 1 - \left(v\frac{\Delta t}{\Delta x}\right)^2, b = -\frac{v}{2}\frac{\Delta t}{\Delta x}\left(1 - v\frac{\Delta t}{\Delta x}\right), c = \frac{v}{2}\frac{\Delta t}{\Delta x}\left(1 + v\frac{\Delta t}{\Delta x}\right) \tag{9.6.2}$$

It can be shown (Smith, 1978) that the eigenvalues for a *N x N*-matrix on this form are:

$$\lambda_s = a + 2(bc)^{1/2}\cos\frac{s\pi}{Nx+1}, s = 1,2,\dots,N \tag{9.6.3}$$

Applied to 9.6.2 (where $N = Nx + 1$):

$$\lambda_s = 1 - \left(v\frac{\Delta t}{\Delta x}\right)^2 + v\frac{\Delta t}{\Delta x}\left[\left(v\frac{\Delta t}{\Delta x}\right)^2 - 1\right]^{1/2}\cos\frac{s\pi}{Nx+1}, s = 1,2,\dots,Nx+1 \tag{9.6.4}$$

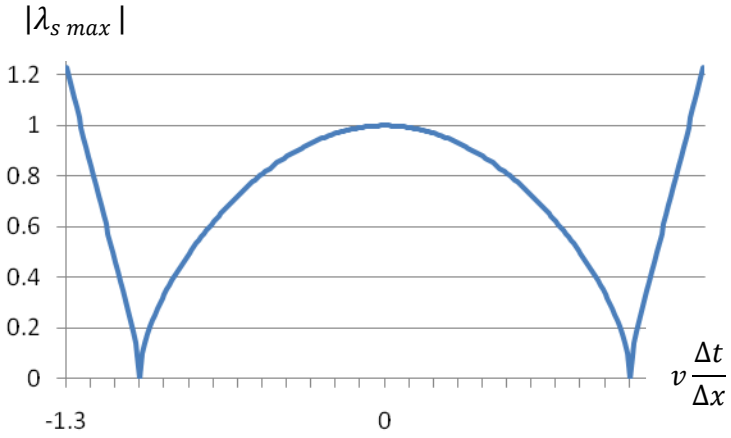


Figure 9.6.1. Longest eigenvalue plotted as function of $(v\,\Delta t/\Delta x)$.

We may simply select a high value for N_x, say $N_x = 1000$, and allow s to run through all N_x for each choice of $(v \cdot \Delta t/\Delta x)$. When selecting the largest $|\lambda_s|$ for each $(v \cdot \Delta t/\Delta x)$, we get the results plotted in figure 9.6.1.

We see that $|\lambda_{s\,max}| \leq 1$ as long as $|v\,\Delta t/\Delta x|$ is below a certain value, and that value turns out to be slightly higher than 1. Conservatively, we may require that:

$$v\frac{\Delta t}{\Delta x} \leq 1 \tag{9.6.5}$$

If we use the same grid as for the pressure and velocity simulations, where we recall that $\Delta x/\Delta t = a$, we can write the stability criterion 9.6.5 as:

$$\frac{|v|}{a} \leq 1 \tag{9.6.6}$$

This is a very simple result, and it reveals stability is never going to be a problem. After all, we are not dealing with liquid velocities higher than the speed of sound. If we were, other assumptions in the model, such as the grid structure for the methods of characteristics and the Allievi simplifications, would break down anyway. So the added energy equation, equation 9.2.12, is going to be stable and will work well as long as the other equations do. Our complete model is therefore very robust and can accept even very long time steps, the only stability limitation being the one developed previously as equation 7.7.15.

Note that a special situation arises if $v = 0$. The largest eigenvalue's length reaches 1, which happens to be the longest length acceptable before stability brakes down, though equation 9.2.12 becomes:

$$E_{s\,i,j+1} = E_{s\,i,j} - \frac{\Delta t}{\rho}\left[\frac{\partial(vp)}{\partial x} - q - w\right]_{i,j} \tag{9.6.7}$$

 For non-commercial use only

Unlike the results we ended up with when investigating the thermodynamic characteristic in chapter 9.1, equation 9.6.7 provides us with a useful correlation even for $v = 0$. The transport-parts of the equation (the terms containing v) have disappeared, and the internal energy is simply going to increase for as long as heat or work is added. As explained earlier, the empirical equation used to calculate q, equation 8.2.4, does not handle $v = 0$ well, so care should be taken if the velocity stays at zero for a long time.

9.7 Numerical dissipation and dispersion

9.7.1 How numerical dissipation and dispersion can affect the simulations

We have seen that the thermodynamic model is stable and easy to program with Lax-Wendroff's method. Lest us try to do so and simulate a simple example to see what happens.

A buried pipeline transports hot water from a spring to a far-away city. The pipe's length $l = 100\ km$, inner diameter $d = 0.50\ m$, outer diameter $d_0 = 0.52\ m$ while the inner surface is smooth. It is un-insulated and buried at $Z_b = 1.5\ m$ depth, and the soil is wet sand with thermal conductivity $k_f = 2.0\ W/(m{\cdot}K)$ and temperature $t_0 = 4\ ^0C$ above it. The inlet temperature is $T_{in} = 90\ ^0C$, and the pipe elevation can be considered constant ($Z_{in} = Z_{out} = 0\ m$). The inlet and outlet pressures are $p_{in} = 1.25\ MPa$ and $p_{out} = 0.10\ MPa$.

When we run the steady-state part of the simulations with $N_x = 10$, it shows that the velocity becomes $v = 1.0\ m/s$, and the outlet temperature $t_{out} = 50\ ^0C$.

To see how temperatures propagate with the flow, it was decided to let the inlet temperature t_{in} make a sudden step down to $10\ ^0C$ after $25{,}000\ s$. We would expect that step to propagate with the flow and start to become visible at the outlet end after another $100{\cdot}10^3\ m\ /\ 1\ m/s = 100{,}000\ s$.

Unfortunately, the results in figure 9.7.1 show the outlet starts responding to the step already 70,000 s after closure, and that is obviously before any fluid has even reached the outlet! As if that was not surprising enough, it also takes nearly double that time before the new outlet temperature has reached its new equilibrium. It is clearly physically impossible for the outlet to be affected by the temperature step before the colder liquid has had time to arrive. One might at first presume the velocity profile could make particles in the center of the pipe travel faster than the average, so that some effect became evident earlier. That cannot be the explanation here, since the velocity profile is not modeled at all, meaning even if this effect could have an impact in

the real world, our model is incapable of taking it into account. Besides, turbulence would prevent any particle from staying consistently in the center of the pipe anyway.

The 'smearing out'-effect of the temperature step was also unexpected. The gradual heating of the pipe wall cannot be the explanation, given that the heat model is in fact steady-state in the sense that it does not include any delays due to heat gradually building up in the pipe wall or surrounding soil. So even if that is what would happen in practice, it should not be reflected in these results.

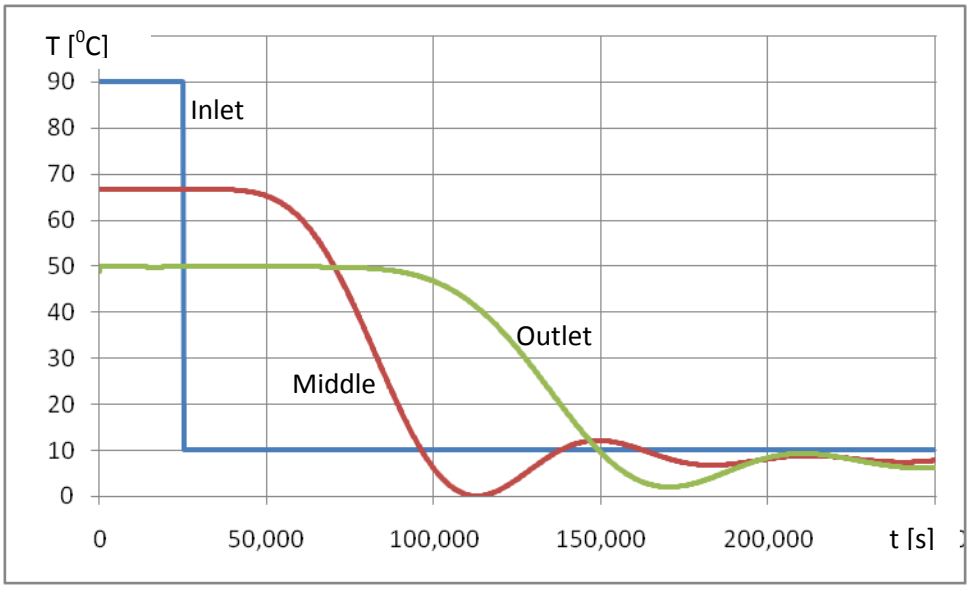


Figure 9.7.1. Temperature as function of time. Simulation results for N_x = 10.

The reason for the unexpected results can be found in the numerical method itself. It is discussed in greater detail later, but for now, let us just say that many researchers have tried to find ways to counter this problem, and we will present one of them.

The smearing effect is sometimes called *numerical dissipation*, even though energy does not necessarily get lost in this undesirable numerical phenomenon. We see another unexpected result, too: The temperature drop at the outlet does in fact overshoot the steady-state value it finally settles at. That is physically impossible, and is also a result of the numerical method not behaving quite the way we would want it to. It is called *numerical dispersion*, and it, too, requires some more attention.

 For non-commercial use only

9.7.2 Easy ways to reduce numerical dissipation and dispersion

One obvious improvement would of course be to increase N_x. Using only $N_x = 10$ in a pipeline as long as this is after all not very conservative. If we increase N_x *to 100*, we get the results in figure 9.7.2. This has improved things: The temperature step at the outlet has become sharper, but we still have an overshoot and oscillations.

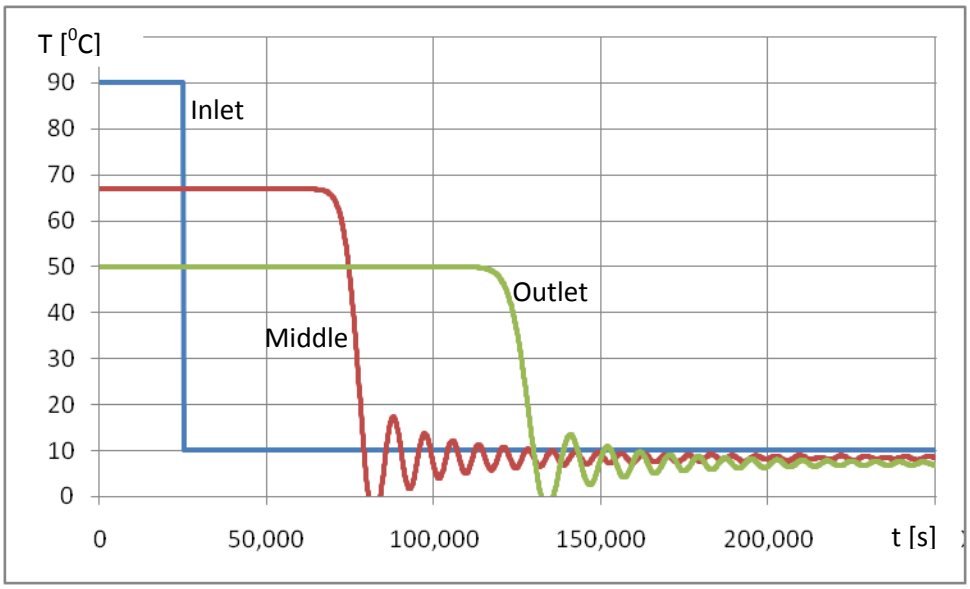


Figure 9.7.2. Temperature as function for time. Simulation results for $N_x = 100$.

We can increase the grid density even more, of course, but at the cost of increased computing work. Since it is only the thermodynamic part we have problems with, it is most efficient to make a separate, denser grid for the thermodynamic calculations, while leaving the characteristics grid for the p and v calculations as it is. Interpolating the necessary v *and* $\partial(vp)/\partial x$*-variables* from the roughest grid is easy, since the grid spacing can be kept constant. That way, one does not have to decrease the time step when creating a finer mesh for the temperature calculations, and the increase in computational work is far less than it otherwise would have been. Note, though, that the stability criterion 9.6.6 would change accordingly when using this method. If the temperature grid is made 20 times denser in the spatial dimension, stability requires $20 \cdot |v|/a \leq 1$, and that should not be a problem for most practical situations.

It is, however, possible to modify the Lax-Wendroff method to make it unconditionally stable by sacrificing its second-order properties. To see how that is done, let us go back to equation 9.2.12. The last term in that equation, as estimated by equations 9.2.5 and 9.2.10, is what gives the method its second order. Suppose we only partly included that

second-order term. We could do so by multiplying it with a factor k_{o2} between *1* and *0*. That would modify equation 9.2.10 also, and by going through the development again , we see that equation 9.2.12 would become:

$$E_{s\,i,j+1} = \frac{v}{2}\frac{\Delta t}{\Delta x}\left(1 + k_{o2} v \frac{\Delta t}{\Delta x}\right) E_{s\,i-1,j} + \left[1 - k_{o2}\left(v\frac{\Delta t}{\Delta x}\right)^2\right] E_{s\,i,j} - \frac{v}{2}\frac{\Delta t}{\Delta x}\left(1 - k_{o2} v \frac{\Delta t}{\Delta x}\right) E_{s\,i+1,j} - \frac{\Delta t}{\rho}\left[\frac{\partial (vp)}{\partial x} - q - w\right]_{i,j} \tag{9.7.1}$$

If we use equation 9.6.3 to investigate the stability for this method for different choices of k_{o2}, we can make the same sort of plot as in figure 9.6.1.

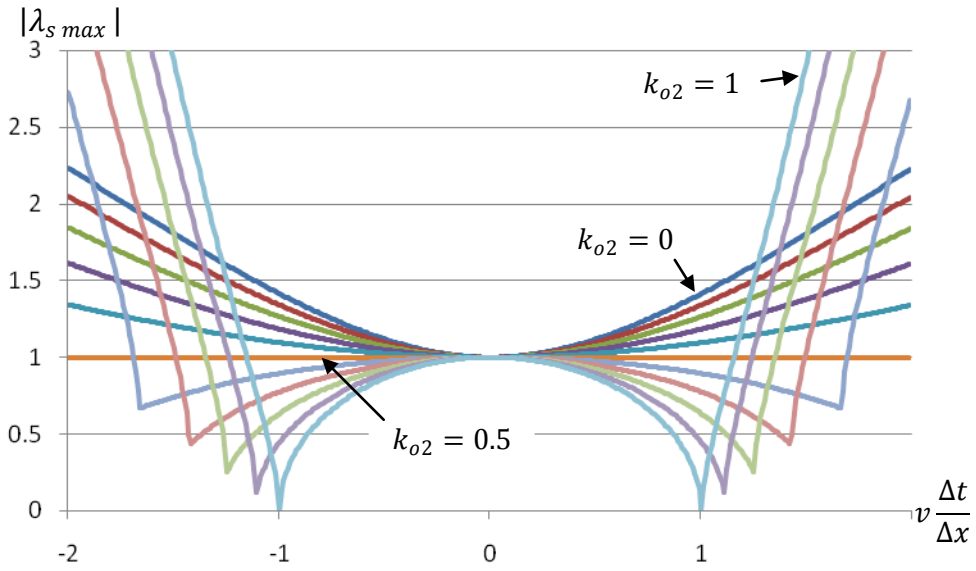


Figure 9.7.3. Longest eigenvalues.

We see that if $k_{o2} = 0$, the longest eigenvalue is going to be longer than 1 no matter how fine grid we use, meaning setting $k_{o2} = 0$ results in an unconditionally unstable method – clearly not a good choice. The same can be said for $k_{o2} = 0.1, 0.2, 0.3\ and\ 0.4$. $k_{o2} = 1$ bringing us back to the traditional Lax-Wendroff equation, and we do of course get the same result as in figure 9.6.1. Reducing k_{o2} from *1* increases the stability area somewhat, until we get to $k_{o2} = 0.5$, when something interesting happens: The method becomes *stable at any* $v \cdot \Delta t/\Delta x$. Inserting that into equation 9.7.1 leads to:

 For non-commercial use only

$$E_{s\,i,j+1} = \frac{v}{2}\frac{\Delta t}{\Delta x}\left(1+\frac{1}{2}v\frac{\Delta t}{\Delta x}\right)E_{s\,i-1,j} + \left[1-\frac{1}{2}\left(v\frac{\Delta t}{\Delta x}\right)^2\right]E_{s\,i,j} - \frac{v}{2}\frac{\Delta t}{\Delta x}\left(1-\frac{1}{2}v\frac{\Delta t}{\Delta x}\right)E_{s\,i+1,j} - \frac{\Delta t}{\rho}\left[\frac{\partial(vp)}{\partial x} - q - w\right]_{i,j} \quad (9.7.2)$$

Equation 9.7.2 thus enables us to make the grid much denser for the thermodynamic part of the calculations than for the pressure and velocity transient calculations without risking stability problems. Using a dense grid, however, does not completely solve the problems with dissipation and dispersion. Doing so requires more advanced numerical methods, and the Kurganov-Tadmor scheme shown in the next chapter offers one of the best solutions.

9.7.3 Modern, effective ways to counter dissipation and dispersion

Numerical mathematics is a relatively young discipline, in the sense that its use has been driven by the fact that computers have become more and more commonplace. One of the most important advances concerning hyperbolic equations is the 2. order method developed by Nessyahu and Tadmor (1990) and later improved to 3. order by Kurganov and Tadmor (1999), we will refer to it as the KT3 method. The theory is well documented in their original papers, and the full details will not be shown here. Instead, we will describe the main ideas behind it, focus on how to implement the algorithm, and explain how it affects the simulation results.

It has long been recognized that each section of the liquid can be considered a cell with distinct borders, and numerical methods can be developed by expressing what crosses those borders. If we consider grid point *i* to be located in the middle of such a cell, the borders are located half-way to its two neighboring grid points. We index the half-way points *i-1/2* and *i+1/2*. KT3 is based on estimating E_s in those midpoints, which again are based on the values in the neighboring cell midpoints, see figure 9.7.4.

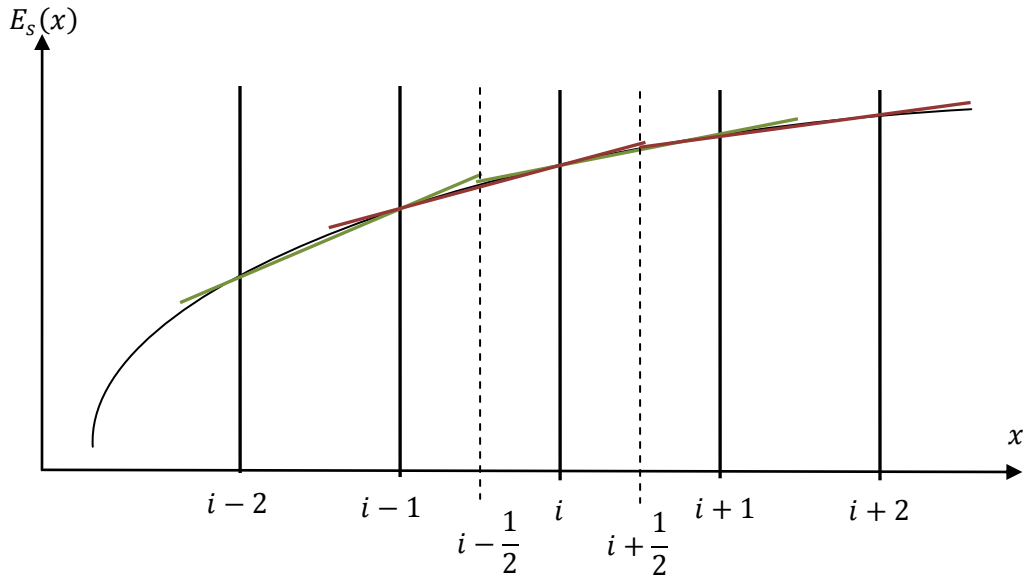


Figure 9.7.4. Lines through neighboring grid-points to cell boundaries.

We see that each midpoint can be extrapolated from both its sides. For instance, $E_{s\ i\text{-}1/2}$ can be estimated from the left as:

$$E^L{}_{s\,i-1/2} = E_{s\,i-1} + 0.5(E_{s\,i} - E_{s\,i-1}) \tag{9.7.3}$$

Rather than using that estimate directly, the last term is multiplied by a factor $\Phi(r_i)$. When that factor is *1*, we are back to equation 9.7.3, and if it is *0*, we have $E^L{}_{s\,i-1/2} = E_{s\,i-1}$. $\Phi(r_i)$ can take values between *0* and *2*. How it varies can be determined by first defining:

$$r_i = \frac{E_{s\,i} - E_{s\,i-1}}{E_{s\,i+1} - E_{s\,i}} \tag{9.7.4}$$

Then, upper and lower limits are defined to avoid r_1 from becoming too large or too small. It has been shown by several authors, including Kurganov and Tadmor (1999), limiting r_i according to the so-called *Minmod*-function can strongly reduce or even eliminate dissipation and dispersion:

 For non-commercial use only

$$\Phi(r_i) = \max[0, \min(1, r_i)] \tag{9.7.5}$$

Or, alternatively, by the so-called *Superbee*-function:

$$\Phi(r_i) = max\{0, \max[min(2r_i, 1), min(2, r_i)]\} \tag{9.7.6}$$

The *Superbee*-function tends to perform best at reducing dissipation, but the Minmod-function has an edge when it comes to reducing dispersion. The so-called *Van Ler* limiter represents a compromise between the two:

$$\Phi(r_i) = \frac{r_i + |r_i|}{1 + |r_i|} \tag{9.7.7}$$

All 3 limiters perform well in most practical situations, but Superbee is probably the best on average. Very sharp temperature steps do not occur in most pipelines, and even the Superbee-limiter does not allow any notable dispersion is such cases.

Equation 9.7.3 can now be written as:

$$E^L{}_{s\,i-1/2} = E_{s\,i-1} + 0.5\Phi(r_{i-1})(E_{s\,i} - E_{s\,i-1}) \tag{9.7.3}$$

Similarly, we may estimate $E_{s\,i\text{-}1/2}$ from the right side as:

$$E^R{}_{s\,i-1/2} = E_{s\,i} - 0.5\Phi(r_i)(E_{s\,i+1} - E_{s\,i}) \tag{9.7.4}$$

Doing the same for $E_{s\,i\text{-}1/2}$:

$$E^{L}{}_{s\,i+1/2} = E_{s\,i} + 0.5\Phi(r_i)(E_{s\,i+1} - E_{s\,i}) \tag{9.7.5}$$

And:

$$E^{R}{}_{s\,i+1/2} = E_{s\,i+1} - 0.5\Phi(r_{i+1})(E_{s\,i+2} - E_{s\,i} + 1) \tag{9.7.6}$$

The average of these values, together with the local propagation speed v, is used to compute function values for the spatial derivatives on each side of point i. From equation 9.2.2, we recall that the spatial derivative-term was $v\frac{\partial E_s}{\partial x}$. The KT3 scheme instructs us to set:

$$\begin{aligned} f_{i-1/2} = \frac{1}{2}\{&[v_{i-1/2}E^{L}{}_{s\,i-1/2} + v_{i-1/2}E^{R}{}_{s\,i-1/2}] \\ &+ |k_{i-1/2}|[E^{L}{}_{s\,i-1/2} - E^{R}{}_{s\,i-1/2}]\} \end{aligned} \tag{9.7.7}$$

And:

$$\begin{aligned} f_{i+1/2} = \frac{1}{2}\{&[v_{i+1/2}E^{L}{}_{s\,i+1/2} + v_{i-1/2}E^{R}{}_{s\,i+1/2}] \\ &+ |k_{i+1/2}|[E^{L}{}_{s\,i+1/2} - E^{R}{}_{s\,i+1/2}]\} \end{aligned} \tag{9.7.8}$$

Where k in our simple, linear case can be read directly from equation 9.2.2 as the factor in front of $\frac{\partial E_s}{\partial x}$, which happens to be v. We need to use the max of $|v_{i-1/2}|$ and $|v_{i+1/2}|$. Inserting that into equations 9.7.7 and 9.7.8 we get:

$$\begin{aligned} f_{i-1/2} = \frac{1}{2}\{&[v_{i-1/2}E^{L}{}_{s\,i-1/2} + v_{i-1/2}E^{R}{}_{s\,i-1/2}] \\ &+ max(|v_{i-1/2}|, |v_{i+1/2}|)[E^{L}{}_{s\,i-1/2} - E^{R}{}_{s\,i-1/2}]\} \end{aligned} \tag{9.7.9}$$

And:

$$f_{i+1/2} = \frac{1}{2}\{[v_{i+1/2}E^L{}_{s\,i+1/2} + v_{i-1/2}E^R{}_{s\,i+1/2}] + max(|v_{i-1/2}|, |v_{i+1/2}|)[E^L{}_{s\,i+1/2} - E^R{}_{s\,i+1/2}]\} \quad (9.7.10)$$

The boundary velocities can be estimated from velocities in the grid-points as follows:

$$v_{i-1/2} = (v_{i-1} + v_i)/2 \quad (9.7.11)$$

$$v_{i+1/2} = (v_i + v_{i+1})/2 \quad (9.7.12)$$

Finally, we calculate the time derivative according to equation 9.2.2 and KT3 using a central difference bases on $f_{i-1/2}$ and $f_{i+1/2}$:

$$\frac{\partial E_s}{\partial t} = -\frac{1}{\Delta x}(f_{i+1/2} - f_{i-1/2}) - \frac{1}{\rho}\left[\frac{\partial (vp)}{\partial x} - q - w\right]_i \quad (9.7.13)$$

The time derivative can be estimated is several different ways. Here, we will use the simplest possible first order approximation:

$$\left(\frac{\partial E_s}{\partial t}\right)_{i,j} = \frac{E_{s\,i,j+1} - E_{s\,i,j}}{\Delta t} \quad (9.7.14)$$

The regime becomes:

$$E_{s\,i,j+1} = E_{s\,i,j} - \frac{\Delta t}{\Delta x}\left(f_{i+1/2,j} - f_{i-1/2,j}\right) - \frac{\Delta t}{\rho}\left[\frac{\partial(vp)}{\partial x} - q - w\right]_{i,j} \qquad (9.7.15)$$

We see that this method cannot be used at the boundaries, since grid-points there do not have neighbors at both sides of them. The lowest grid point index (at the pipe inlet end) is 0, and the highest is N_x-1. We therefore use the KT3 scheme only for $1 \le i \le N_x$, and even there we need to modify it a bit. Near the outlet, we see that 9.7.2 stretches into $N_x + 2$, where no grid point exists. We can therefore not use the limiter function there, and we use instead:

$$E^R{}_{s\,i+1/2} = 0.5(E_{s\,i} + E_{s\,i+1}) \; when \; i = N_x \qquad (9.7.16)$$

A similar problem arises near the inlet, where r_i is not defined for equation 9.7.3, and we replace it with:

$$E^R{}_{s\,i-1/2} = 0.5(E_{s\,i-1} + E_{s\,i}) \; when \; i = 1 \qquad (9.7.17)$$

At the inlet boundary the model breaks down altogether, and we need to go back to the same first-order approximations we used in chapter 9.3. For the inlet, E_s is calculated from the inlet enthalpy according to equation 9.4.2. If the liquid flows out of the 'inlet end', meaning $v_0 < 0$, we use first order approximations for both derivatives:

$$E_{s\,0,j+1} = E_{s\,0,j} - v\frac{\Delta t}{\Delta x}\left(E_{s\,0,j} - E_{s\,1,j}\right) - \frac{\Delta t}{\rho}\left[\frac{\partial(vp)}{\partial x} - q - w\right]_{i,j} \qquad (9.7.18)$$

For the outlet boundary, we calculate:

 For non-commercial use only

$$E_{s\,Nx+1,j+1} = E_{s\,Nx+1,j} - v\frac{\Delta t}{\Delta x}\left(E_{s\,Nx+1,j} - E_{s\,Nx,j}\right) - \frac{\Delta t}{\rho}\left[\frac{\partial(vp)}{\partial x} - q - w\right]_{Nx+1,j} \qquad (9.7.19)$$

When $v_{Nx+1} > 0$, we use equation 9.7.19, otherwise we use equation 9.4.2.

When using this method on the same pipeline as in figure 9.7.2, setting $N_x = 100$ and using the Superbee-limiter, we get the results in figure 9.7.5. The temperature fronts have become very sharp, and there is no need to use a denser grid to get accurate results for this purpose.

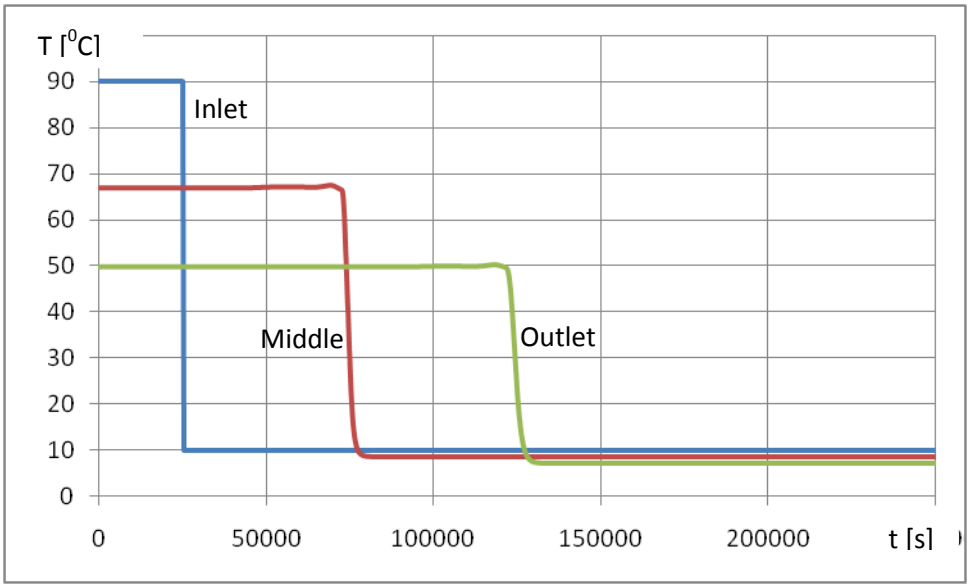


Figure 9.7.5. Temperature as function for time. Simulation results for $N_x = 100$.

It is interesting that these amazing results can be achieved by very fast calculations. All 250,000 seconds – nearly 7 hours of operation time on a 100 km long pipeline – was simulated in only a few minutes on a standard laptop computer from 2007.

Although the theory behind the KT3 method is relatively complicated, we saw that the algorithm it produces is explicit and very easy to program.

For every time step in every grid point, all liquid properties were updated, and so was the Darcy-Weisbach friction factor. Even so, the simulations ran 3 orders of magnitude

faster than real time, making this method well suited for forecasting or real-time simulations.

References

Smith, G.D. (1978): *Numerical solution of Partial Differential Equations: Finite Difference Methods*. Oxford University Press. Second Edition.

Van Leer, B. (1979): *Towards the Ultimate Conservative Difference Scheme. V.A. Second Order Sequel to Godonov's Method*, Journal of Comput. Phys. 32 pp. 101-136

H.Nessyahu and E.Tadmor. (1990): Non-*oscillatory Central Differencing for Hyperbolic Conservation Laws*, Journal of Comput. Phys. 87, 408.

Quarteroni, A. (1997): *Advanced Numerical Approximation of Nonlinear Hyperbolic Equations*. Springer.

Kurganov, A., Tadmor, E. (1999): *New High-Resolution Central Schemes for Nonlinear Conservation Laws and Convection-Diffusion Equations*, Journal of Comp. Phys., 160, 214–282.

 For non-commercial use only

"Perfect gases are like perfect people: They do not exist."
Unknown origin

10 Solving the conservation equations

Solving the conservation equations without major simplifications:

- The conservation equations on matrix form
- Perfect and real gas conservation equation fundamentals
- Using the Kurganov-Tadmor-scheme for the matrix formulation
- Why Runge-Kutta 4 and Kurganov-Tadmor 3 fit well together
- Calculating p, T and h from ρ, ρv and E

10.1 Problem formulation

In chapter 7 – 9, we saw how easy it was to solve the conservation equations for liquid flow. The thermodynamic calculations, as described by the energy equation, could be regarded as almost a separate 'add-on' program part which could be omitted if we were not interested in temperatures or heat. For gas flow, we cannot do all the simplifications liquid flow allows, and consequently end up with a slightly more complicated solution. Density can no longer be regarded as independent of temperature, and unless we assume isothermal or isentropic flow, we need to take heat exchange with the

environment into account. That is best done by solving the continuity, momentum and energy equations together. This is of course also a valid way to solve the equations for liquid flow, but may in some cases be unnecessarily complicated, at least when developing simulation programs exclusively for liquid calculations.

Equations 6.1.5, 6.2.12 and 6.3.12 written on matrix form:

$$\frac{\partial}{\partial t}\begin{bmatrix}\rho\\ \rho v\\ \rho\left(u+\frac{v^2}{2}+gz\right)\end{bmatrix}=-\frac{\partial}{\partial x}\begin{bmatrix}\rho v\\ p+\rho v^2\\ \rho v\left(h+\frac{v^2}{2}+gz\right)\end{bmatrix}+\begin{bmatrix}0\\ -\frac{f\rho}{2d}v|v|-\rho g sin\theta\\ q+w\end{bmatrix} \tag{10.1.1}$$

Since we have more unknowns than equations, we need more correlations to close the system and make it possible to find a solution.

Let us first repeat equation 6.3.11, since it correlates two variables in equation 10.1.1:

$$h=u+\frac{p}{\rho} \tag{10.1.2}$$

We know that density is a function of pressure and temperature. For perfect gases, that correlation is simple, but for real gases, it is less so. In general, we need to know the two fluid properties:

$$p=p(T,\rho) \tag{10.1.3}$$

And:

$$T=T(p,h) \tag{10.14}$$

Various different ways of modeling these properties exist, some of the most common being the Peng-Robinson and Redlich-Kwong equations of state (Moran & Shapiro, 2006). The methods are well described in various literature, but they do of course rely

 For non-commercial use only

on empirical, tabulated data for the different components the fluid consists of, and we cannot easily reverse them to express for instance $p(T,h)$. Besides, it is common for third-party software to handle the fluid's properties, and we do not always know all the details in the model used. Therefore, we will keep equations 10.1.13 and 10.1.14 in the general form shown here, and assume both $p(T,h)$ and $T(p, \rho)$ to be available from that software, too. If unavailable, they can be calculated as outlined in chapter 10.7.

The heat and friction calculations also require three additional fluid properties - the kinematic viscosity, ν, the thermal conductivity, k_f, and the Prandtl number Pr - to be available. Both ν, k_f, and Pr are functions of both pressure and temperature. For gases, the dynamic viscosity μ $(= \nu\rho)$ tends to be less pressure-dependent than ν, and so using μ allows less frequent updates and is therefore somewhat more convenient. In general terms, we get:

$$k_f = k_f(p,T) \tag{10.1.5}$$

$$\mu = \mu(p,T) \tag{10.1.6}$$

$$Pr = Pr(p,T) \tag{10.1.7}$$

By introducing the fluid's internal energy pr unit volume, E, as:

$$E = \rho\left(u + \frac{v^2}{2} + gz\right) \tag{10.1.8}$$

as well as equation 6.3.11, this can be re-formulated as:

$$\frac{\partial}{\partial t}\begin{bmatrix}\rho\\ \rho v\\ E\end{bmatrix} = -\frac{\partial}{\partial x}\begin{bmatrix}\rho v\\ p+\rho v^2\\ v(E+p)\end{bmatrix} + \begin{bmatrix}0\\ -\frac{f\rho}{2d}v|v| - \rho g sin\theta\\ q+w\end{bmatrix} \tag{10.1.9}$$

Equations 10.1.2 – 10.1.9 together provide complete closure, so the equations can be solved. Exactly how to do it we will look at in the next chapter, but let us for convenience first define an even shorter way of expressing equation 10.1.9:

$$\frac{\partial Y}{\partial t} = -\frac{\partial F}{\partial x} + \mathrm{D}, \quad \text{where}$$

$$\mathrm{Y} = \begin{bmatrix} y_1 \\ y_2 \\ y_3 \end{bmatrix} = \begin{bmatrix} \rho \\ \rho v \\ E \end{bmatrix}, \mathrm{F} = \begin{bmatrix} f_1 \\ f_2 \\ f_3 \end{bmatrix} = \begin{bmatrix} \rho v \\ p + \rho v^2 \\ v(E+p) \end{bmatrix}, \mathrm{D} = \begin{bmatrix} d_1 \\ d_2 \\ d_3 \end{bmatrix} = \begin{bmatrix} 0 \\ -\frac{f\rho}{2d} v|v| - \rho g sin\theta \\ q + w \end{bmatrix} \tag{10.1.10}$$

10.2 Some initial, simplified considerations

No gas is perfect, and in high pressure gas pipelines, assuming the gas to be perfect leads to significant errors. We therefore need to deal with real gases (or liquids) when solving equation 10.1.9, and we will later show how that can be accounted for in the model. It can still be advantageous to start by discussing a perfect gas to reduce chances of getting lost in fluid property correlations before we have had time to formulate the overall model. Besides, nearly all publications discussing the latest advances in numerical methods for solving equation 10.1.9 use perfect gas simplifications in their test cases, and a perfect gas can be a good tool for debugging a simulation program during the development process. We will also simplify a bit further by presuming the pipe to be horizontal. That rids us of all terms to do with elevation (z and $sin\theta$), and it does not have any consequences for the main properties we are out to investigate in this chapter. Elevation terms are easy to include again later.

The pρT-correlation for a perfect gas is really simple:

$$p = \rho R_g T \tag{10.2.1}$$

where $R_g = R/M_g$ is a characteristic constant for the particular gas.

 For non-commercial use only

For a perfect gas, the internal energy u also depends on T only. That gives us a second equation of state:

$$u = u(T) \tag{10.2.2}$$

We recall from equation 10.1.2 that $h = u + p/\rho$, so it follows from 10.2.1 that:

$$h = u(T) + R_g T = \mathrm{h}(T) \tag{10.2.3}$$

meaning the enthalpy is also only a function of temperature. That simplifies the definitions of specific heat at constant volume, c_v, and at constant pressure, c_p, to:

$$c_v = \frac{du}{dT}, \quad c_p = \frac{dh}{dT} \tag{10.2.4}$$

Derivation of equation 10.2.3 and inserting 10.2.4 leads to:

$$R_g = c_p - c_v \tag{10.2.5}$$

Suppose that gas is *calorically perfect*, meaning c_v and c_p are constant, then we may integrate equation 10.2.4 to get:

$$h = c_p(T - T_0) \tag{10.2.6}$$

For simplicity, we define h to be zero at absolute zero temperature, meaning $T_0 = 0$.

The correlation between E and u, equation 10.1.8 reads $E = \rho\left(u + \frac{v^2}{2} + gz\right)$. Since we presume the pipe to be horizontal, $z = 0$. We use equation 10.1.2 to eliminate u, set $\kappa = \frac{c_p}{c_v}$ and eliminate h and T by combining equations 10.2.1, 10.2.3, 10.2.5 and 10.2.6:

$$p = (\kappa - 1)\left(E - \frac{\rho v^2}{2}\right) \tag{10.2.7}$$

The velocity v can easily be expressed in terms of the two state variables ρ and ρv, as:

$$v = \frac{(\rho v)}{\rho} \tag{10.2.8}$$

and we finally get:

$$p = (\kappa - 1)\left(E - \frac{(\rho v)^2}{2\rho}\right) \tag{10.2.9}$$

This shows that for a perfect gas, we do have a very simple correlation between p and primary variables ρ, ρv, and E.

Inserting equations 10.2.8 and 10.2.9 into equation 10.1.9 yields:

$$\frac{\partial}{\partial t}\begin{bmatrix}\rho\\ \rho v\\ E\end{bmatrix} = -\frac{\partial}{\partial x}\begin{bmatrix}\rho v\\ (\kappa-1)E + (3-\kappa)\frac{(\rho v)^2}{2\rho}\\ \frac{(\rho v)}{\rho}\left\{\kappa E - (\kappa-1)\frac{(\rho v)^2}{2\rho}\right\}\end{bmatrix} + \begin{bmatrix}0\\ -\frac{f\rho}{2d}v|v|\\ q+w\end{bmatrix} \tag{10.2.10}$$

10.2.10 is now in itself a closed set of equations and can be simulated directly, but some additional correlations may be useful when defining starting- and boundary conditions.

 For non-commercial use only

The internal energy pr. unit volume, E, for instance, follows from equation 10.1.8, as well as the simplifications due to the pipe being horizontal and the gas perfect:

$$E = \rho\left(c_p T + \frac{(\rho v)^2}{2\rho}\right) - p \tag{10.2.11}$$

The speed of sound, a, is another useful parameter. In chapter 7.9, we saw it can be used to check the simulation program by comparing it to the propagation speed appearing in simulation results. We will later see a is in fact also used in some of the most useful numerical schemes for solving the conservation equations.

From perfect gas dynamics it is known that the speed of sound can be found as:

$$a = \sqrt{\kappa R_g T} \tag{10.2.12}$$

In chapter 7.2.1, we saw that for liquid flow, the pressure increase after instantaneous closure of a valve in a pipe with initial velocity v_0 is $\Delta p = \rho a v_0$. The argument can also be reversed: If the liquid at rest is exposed to a pressure step Δp, a velocity step v_0 is instantaneously going to result. The correlation gives us many ways to manually check parts of simulation results for liquid flow. For both perfect and non-perfect gas flow, it can also be used for calculations if the pressure step is small enough so that the density and speed of sound does not to change significantly during the step.

10.3 The conservation equations' main properties

We are going to use the KT3 spatial discretization method outlined in chapter 9.7.3 to solve the conservation equations. We saw that in order to do so, we needed to know a characteristic velocity for the equations to be solved. It that example, where the energy equation was the only one to be solved by KT3, the characteristic velocity turned out to be the liquid's velocity. We need to solve all of the equations in 10.1.9 simultaneously (or 10.2.12 in the case of a perfect gas), and we need to know the characteristic velocities for that equation set. Since the equations are non-linear, we cannot study their

eigenvalues directly. Instead, we linearize by finding the Jacobi-matrix and use its eigenvalues.

The Jacobi matrix is defined as:

$$J \stackrel{\text{def}}{=} \begin{bmatrix} \frac{\partial f_1}{\partial y_1} & \frac{\partial f_1}{\partial y_2} & \frac{\partial f_1}{\partial y_3} \\ \frac{\partial f_2}{\partial y_1} & \frac{\partial f_2}{\partial y_2} & \frac{\partial f_2}{\partial y_3} \\ \frac{\partial f_3}{\partial y_1} & \frac{\partial f_3}{\partial y_2} & \frac{\partial f_3}{\partial y_3} \end{bmatrix} = \begin{bmatrix} \frac{\rho v}{\partial \rho} & \frac{\rho v}{\partial \rho v} & \frac{\rho v}{\partial E} \\ \frac{\partial (p+\rho v^2)}{\partial \rho} & \frac{\partial (p+\rho v^2)}{\partial \rho v} & \frac{\partial (p+\rho v^2)}{\partial E} \\ \frac{\partial v(E+p)}{\partial \rho} & \frac{\partial v(E+p)}{\partial \rho v} & \frac{\partial v(E+p)}{\partial E} \end{bmatrix} \tag{10.3.2}$$

It is not possible to come up with an analytical solution to J based on the general, undefined correlations 10.1.3 and 10.1.4. Instead, let us again use the perfect gas assumption and equation 10.2.11 as base and simplify the Jacobi matrix accordingly, so we get:

(10.3.11)

$$J = \begin{bmatrix} \frac{\partial y_2}{\partial y_1} & \frac{\partial y_2}{\partial y_2} & \frac{\partial y_2}{\partial y_3} \\ \frac{\partial \left[(\kappa-1)\left(y_3 - \frac{{y_2}^2}{2y_1}\right) + \frac{{y_2}^2}{y_1}\right]}{\partial y_1} & \frac{\partial \left[(\kappa-1)\left(y_3 - \frac{{y_2}^2}{2y_1}\right) + \frac{{y_2}^2}{y_1}\right]}{\partial y_2} & \frac{\partial \left[(\kappa-1)\left(y_3 - \frac{{y_2}^2}{2y_1}\right) + \frac{{y_2}^2}{y_1}\right]}{\partial y_3} \\ \frac{\partial \left[\frac{y_2 y_3}{y_1} + (\kappa-1)\left(\frac{y_2 y_3}{y_1} - \frac{{y_2}^3}{2{y_1}^2}\right)\right]}{\partial y_1} & \frac{\partial \left[\frac{y_2 y_3}{y_1} + (\kappa-1)\left(\frac{y_2 y_3}{y_1} - \frac{{y_2}^3}{2{y_1}^2}\right)\right]}{\partial y_2} & \frac{\partial \left[\frac{y_2 y_3}{e_1} + (\kappa-1)\left(\frac{y_2 y_3}{y_1} - \frac{{y_2}^3}{2{y_1}^2}\right)\right]}{\partial y_3} \end{bmatrix}$$

and hence:

$$J = \begin{bmatrix} 0 & 1 & 0 \\ \frac{\kappa-3}{2}v^2 & (3-\kappa)v & \kappa-1 \\ (\kappa-1)v^3 - \frac{\kappa v E}{\rho} & \frac{\kappa E}{\rho} - \frac{3}{2}(\kappa-1)v^2 & \kappa v \end{bmatrix} \tag{10.3.3}$$

The eigenvalue-vector λ is defined from the identity-matrix I as:

 For non-commercial use only

$$|J - \lambda I| = 0 \tag{10.3.4}$$

By solving equation 10.3.4, the 3 eigenvalues become:

$$\lambda_1 = v - \left[\frac{\kappa(\kappa - 1)\left(E - \rho\frac{v^2}{2}\right)}{\rho}\right]^{1/2}$$

$$\lambda_2 = v \tag{10.3.5}$$

$$\lambda_3 = v + \left[\frac{\kappa(\kappa - 1)\left(E - \rho\frac{v^2}{2}\right)}{\rho}\right]^{1/2}$$

We see that $E - \rho\frac{v^2}{2} = \rho u = \rho c_v T$, and the expression inside brackets are in fact $\kappa(c_p - c_v)\mathrm{T}$ or $\kappa R_g \mathrm{T}$, which according to equation 10.2.12 is the square of the speed of sound for a perfect gas. That simplifies our result to:

$$\lambda_1 = v - a_s, \lambda_2 = v + a_s, \lambda_3 = v \tag{10.3.6}$$

Equation 10.3.6 makes a lot of sense: Sound waves can be expected to travel at the speed of sound, a_s, compared to the fluid. Since the fluid itself flows at velocity v, sound waves travel at $v \pm a_s$. The energy, on the other hand, simply travels with the flow and leads to $\lambda_3 = v$.

The eigenvalue with the largest absolute value, which is the parameter needed in the KT3 metod, is obviously:

$$max|\lambda_s| = |v| + |a_s| \tag{10.3.7}$$

When the gas is not perfect, determining the Jacobi matrix is not as straight forward, but it seems reasonable that the same thing happens and that the flow is characterized by the speed of sound, together with the fluid's velocity itself.

Determining the speed of sound for non-perfect gases is more difficult than for perfect ones, and numerous estimates have been proposed over the years. Having an accurate estimate is important when using ultrasound devices for fiscal measurements, and much of the available theory is based on work which has been carried out in order to improve such measurements. One of the most trusted sources nowadays is AGA 10, see American Gas Association (2003), which gives detailed guidelines. It turns out that the speed of sound can be estimated as:

$$a_s = \left\{ \frac{c_p}{c_v} \frac{RT}{M_g} \left[Z + \rho \left(\frac{\partial Z}{\partial p} \right)_T \right] \right\}^{1/2} \tag{10.3.8}$$

A perfect gas can be seen as a special case where $Z = 1$, $(\partial Z/\partial p)_T = 0$, $R_g = R/M_g$, and of course $\kappa = c_p/c_v$. As we would expect, inserting those values leads us back to equation 10.2.12.

For real gases, we need to get the parameters in equation 10.3.16 from tables or databases. If $(\partial Z/\partial p)_T$ is not tabulated directly, it can be estimated by varying p while keeping T constant, and then comparing that to how much Z changes. One important thing to note here, though, is that neglecting $(\partial Z/\partial p)_T$ leads to incorrect velocity of sound, and Z needs to be modeled both as a function of p and T in order to get accurate results.

Example: A pipeline contains gas at $p = 12\ MPa$ and $278\ K$. The gas composition is *87.5% Methane, 7.0% Ethane, 2.1% Propane, 0.25% n-Butane, 0.03%, iso-butane 0.3%, n-Pentane, 0.06% iso-Pentane, 1.4% Nitrogen* and *1.4% Carbon Dioxide*. What is the speed of sound?

From AGA 10 (or tabulated data, not shown in details here) we come up with $c_p = 3{,}756\ J/(kg \cdot K)$, $c_v = 1.758\ J/(kg \cdot K)$, $M_g = 0.01845\ kg/mol$, $Z = 0.6985$, $\rho =$

 For non-commercial use only

137.1 kg/m^3, $(\partial Z/\partial p)_T = -8.83 \cdot 10^{-4}\ m^3/kg$, and the universal gas constant R is as always $R = 8.32\ J/(kg \cdot mol)$. Inserting these values into equation 10.3.8 gives $a_s = 393\ m/s$. Note that if we had neglected Z being a function of p (by setting $(\partial Z/\partial p)_T = 0$, the result would have become $a_s = 433\ m/s$, which is too high.

10.4 Selecting time integration and spatial discretization methods

In chapter 9.7, we saw that the convective transport is characterized by the fluid's velocity. For liquid flow, that may typically be two orders of magnitude slower than the pressure and velocity transients, which are characterized by the speed of sound. In gas flow, the fluid's velocity can at times approach the speed of sound, but we must still expect to have to deal with fast and slow phenomena at the same time. Fast phenomena show up as large eigenvalues in the system matrix. All known explicit numerical integration methods for ordinary differential equations have stability limits determined by the fastest phenomena it simulates, which in our pipe flow is determined by the speed of sound. That leads to relatively small maximum time steps. If we want to study how the temperature develops in a gas particle as it travels through a long pipeline, say from Norway to Germany, the simulations must cover the time that particle takes to complete its journey. Small time steps, combined with long travel time, can easily lead to time consuming simulations.

The traditional way to address that problem has been to use implicit difference schemes. Such schemes can be constructed to make the integration stable at any step length, but at the cost of having to iterate a set of equations for every time step. That is sometimes done with fixed-point iteration. Getting good convergence properties for the iteration normally involves computing or at least approximating a Jacobi-matrix and inverting it for each time step, and that is in itself time consuming. Another problem is that an implicit method is quite a blunt tool in that it integrates nearly everything, producing seemingly stable results even if the physical system is unstable, and even if the program contains serious programming or data input errors. Explicit methods, on the other hand, are far more sensitive, and most unintended errors result in the integration becoming unstable, giving the user a useful warning that something is wrong. The implicit methods' unconditional stability is also what has made them so popular, however, since no instability occurs even when using long time steps.

Recent advancements in non-oscillatory spatial discretization methods make implicit methods less attractive for single-phase flow, and high speed computations can instead be achieved by focusing on high order methods. This does not mean implicit methods never have their advantages. But implicit methods are easier to program, and as explained above, they are also somewhat safer to work with.

Godunov (1959) has shown that higher order schemes for solving partial differential equations (PDSs) become oscillatory if they have order higher than 1. His theorem states that *linear numerical schemes for solving PDE's, having the property of not generating new extrema (monotone scheme), can be at most first-order accurate*. In general, to get around the Godunov's theorem, one must use non-linear high order schemes. This was long thought to be the final word on higher order methods, they were expected to be if little use due to dissipation and dispersion, as it was illustrated in figures 9.7.1 and 9.7.2. We now know that is not quite so, however. In general, two alternative strategies are possible. The first consists in *preventing* the generation of numerical oscillations by acting on the production mechanism, while the second consists in *damping* the generated oscillations by using artificial dissipation terms. The KT3 scheme adopts the first approach. We can say that the limiters it uses act on the computed numerical advective fluxes, and they deal with Gudonov's theorem by reducing the order locally for short time periods when it is necessary to prevent oscillations from being generated. This temporary reduction of order does not seem to affect the overall accuracy unfavorably, and for practical purposes, it is meaningful to call it an order 3-method.

When solving the general conservation equations 10.1.9, the KT3 scheme transforms the equations into ordinary differential equations. To take full advantage of its high order, we must use an integration method of no lesser order when simulating. It is also necessary to use a high order approximation at the boundaries. In chapter 11, we will see how such boundary approximations can be developed.

But first let us consider doing time integration using one of the very popular third or fourth order explicit Runge-Kutta integration methods, we will call them RK3 and RK4. Explicit methods, sometimes called forward methods, are very easy to program, but as stated before, they are not unconditionally stable. If we use a third order spatial discretization, and third or higher order time discretization, the overall order should be 3, so we can expect to achieve the same accuracy as can only be obtained with much finer grids when using lower order methods.

 For non-commercial use only

Besides, should one later wish to switch to an implicit method, for instance an implicit multistep method, it can at least in principle be done by simply changing the time integration method without altering the spatial discretization scheme.

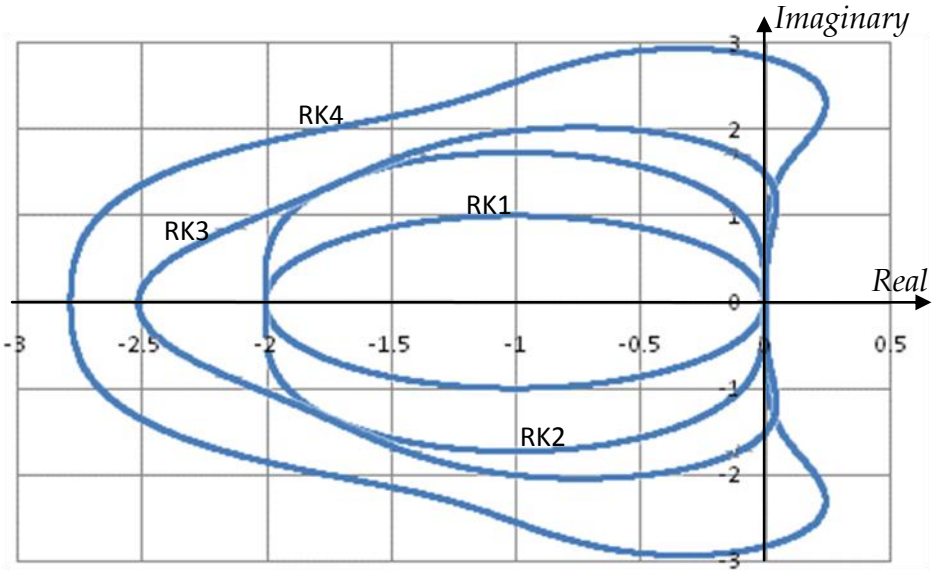


Figure 10.3.1. Runge-Kutta integration methods' stability area.

The RK-method's stability areas are shown in figure 10.3.1. All the simulated system's eigenvalues, λ_s, multiplied with the time step, Δt, have to fall within the curve relevant to the method used. To understand what this means, let us look at a linear system on the form:

$$\frac{dy}{dt} = At \tag{10.4.1}$$

where y and t are vectors, and A is a square matrix. Such a system is physically stable if all A's eigenvalues have zero or negative real-parts.

If we use RK-integration to simulate a physically stable system on this form, the calculations are also always going to be stable as long as we use small enough time steps. Interestingly, RK4's stability area actually stretches into a tiny part of the physically unstable area, so it is possible for the simulation results to tell us everything is stable even when it is not. That is in practice not much of a problem for explicit RK4, though, since the discrepancies are so small. Most of the known implicit methods, on the other hand, have stability areas stretching far into the physically unstable area, meaning they are generally poor at recognizing physical instabilities. They may

conclude a valve regulator is going to perform well in situations when it actually is going to be physically unstable!

Once we have decided to use an RK-method, we need to decide which to use. Two considerations matter. First, we want at least as high order as in the spatial discretization method we use, otherwise we are wasting accuracy and therefore have to take smaller time steps to reach a target overall accuracy. That would make the simulations slower.

Second, we want to be able to take as large a time step as possible compared to the number of function calls the integration method makes for each time step. For the RK-methods of order 4 or less, we generally have to make as many function calls as the order of the method. RK4, for instance, uses 4 function calls to get one time step into the future. Lower order means fewer function calls pr. time step, but also smaller stability area. The RK3-method stretches only down to -2.5 along the real axis, compared to -2.8 for RK3. It means the step length must be reduced to around 90% to maintain stability if we switch from RK4 to RK3, while the computational work is reduced by around 25%. If the system contains only real eigenvalues, it is therefore around 16% more efficient to use RK3 than RK4. That conclusion changes if we consider systems with eigenvalues on the imaginary axis. Our complete system may include components like pumps, regulators, and other devices. Depending on how they have been modeled, they may lead to the presence of complex eigenvalues. RK4 allows 60% longer time steps than RK3 for systems where pure complex eigenvalues are time step limiting, making RK4 the fastest of the two. RK2 and RK1 perform poorly for systems having eigenvalues close to the imaginary axis, so they are less attractive as a general tool when simulating pipe system flow.

The conclusion is that of the explicit RK methods, RK3 and RK4 are best for our purpose, and RK4 is probably the best overall method when other components than pipes are included in the simulations.

The RK methods can easily be designed to vary their time steps as they integrate. They do so by comparing a higher order method with one of lower order. A RK4-5 method uses one additional function call per time step to get both 4^{th} and 5^{th} order results. By comparing those results, it works out whether to accept the last integration step, and what step length to use for the next integration. Interestingly, the RK5-method is unstable, so it can only be used for error estimation, and the overall order is determined by RK4. The extra work per time step is usually more than compensated for by the constantly optimized step length, so variable step methods tend to be faster than fixed

 For non-commercial use only

step methods. Variable step methods also has the added advantage of producing an estimate of the global error, and that results in better control of which accuracy we reach (for the time integration, anyway, but it does not tell us anything about the spatial discretization errors).

Medovikov (1999) has developed a class of ordinary differential equation solvers called DUMKA, an alternative worth mentioning. They seem to compare well with RK4. Both his third order method, DUMKA3, and the fourth order method, DUMKA4, have a stability area which stretches further to the left than RK4, meaning it allows longer time steps for systems with real eigenvalues. That makes them well suited for hyperbolic equations. There are also other alternatives, and an internet search for Ordinary Differential Equation (ODE)-solvers may reveal alternatives like Runge–Kutta–Chebyshev (RKC)-methods, various implicit Runge-Kutta methods, and Patankar. Since we are developing a general model for pipe systems, where regulators and other components may be part of the system we simulate, we stick to the well-known and somewhat simpler RK4-methods, which have proven to be quite robust for all stable systems.

Many spatial discretization methods have been developed over the years, and Liska and Wendroff (2003) have tested some of the most interesting ones. As with most available comparisons, they focus mainly on how well the different explicit methods perform when simulating shocks (fluid speed approaching speed of sound) and discontinuities (temperature, pressure or velocity experiencing an instantaneous step), but that is not the most interesting situations to most pipeline simulations. Liska and Wendroff show that several other methods are able to reproduce discontinuities even more accurately than Nessyahu and Tadmor's (1990) original central scheme and the KT3 scheme, but also point out that KT3 has advantages due to its simplicity. That simplicity leads to relatively fast simulations and easy programming.

10.5 How to account for friction and heat in the KT3 scheme

Kurganov and Tadmor (1999) dealt with equations of a similar form as equation 10.1.10 in their paper, but with $D = 0$. That corresponds to flow without friction, elevation, heat or work. They did not show how D should be included without destroying the method's high order. In chapter 9.7.3, we included heat, but without discussing how in greater detail. In this chapter, we will look at how to extend the KG3 method to include

D, as well as how to efficiently calculate the local eigenvalues the KG3-method requires to work properly.

For the state variables at the cell boundaries we have:

$$Y^L{}_{i-1/2} = Y_{i-1} + 0.5\Phi(r_{i-1})(Y_i - Y_{i-1}) \tag{10.5.1}$$

$$Y^R{}_{i-1/2} = Y_i - 0.5\Phi(r_i)(Y_{i+1} - Y_i) \tag{10.5.2}$$

$$Y^L{}_{i+1/2} = Y_i + 0.5\Phi(r_i)(Y_{i+1} - Y_i) \tag{10.5.3}$$

$$Y^R{}_{i+1/2} = Y_{i+1} - 0.5\Phi(r_{i+1})(Y_{i+2} - Y_{i+1}) \tag{10.5.4}$$

where:

$$r_i = \frac{Y_i - Y_{i-1}}{Y_{i+1} - Y_i} \tag{10.5.5}$$

And the limiter $\Phi(r_i)$ can for instance be the Superbee function in equation 9.7.6.

Once $Y^L{}_{i-1/2}$, $Y^R{}_{i-1/2}$, $Y^L{}_{i+1/2}$ and $Y^R{}_{i+1/2}$ have been computed, we use the procedures explained in chapter 10.8 to find the secondary variables p, v and T at the cell boundaries. We then have all the variables we need to calculate the flux F at the boundaries, too. The *KT3 scheme* instructs us to set:

$$F_{i-1/2} = \frac{1}{2}\left\{\left[F\left(Y^L{}_{i-1/2}\right) + F\left(Y^R{}_{i-1/2}\right)\right] + \bar{a}_{i-1/2}\left[Y^L{}_{i-1/2} - Y^R{}_{i-1/2}\right]\right\} \tag{10.5.6}$$

$$F_{i+1/2} = \frac{1}{2}\left\{\left[F\left(Y^L{}_{i+1/2}\right) + F\left(Y^R{}_{i+1/2}\right)\right] + \bar{a}_{i+1/2}\left[Y^L{}_{i+1/2} - Y^R{}_{i+1/2}\right]\right\} \tag{10.5.7}$$

 For non-commercial use only

Where

$$\bar{a}_{i-1/2} = \bar{a}_{i+1/2} = max\left[rad\left(\frac{\partial F}{\partial Y}\right)_{i-1/2}, rad\left(\frac{\partial F}{\partial Y}\right)_{i}, rad\left(\frac{\partial F}{\partial Y}\right)_{i-1/2}\right] \quad (10.5.8)$$

Where *rad* means spectral radius for the Jacobian matrix for the flux, which is the largest eigenvalue in the respective locations $i-1/2$, i and $i+1/2$. We remember from chapter 10.2 that for a perfect gas, we found the largest eigenvalue to be simply the speed of sound plus the fluid velocity. For a real fluid, it is harder to prove this in a strictly mathematical way, but we can get the results we are after by using equation 10.3.8 to calculate the velocity of sound a_s, adding the liquid velocity, and taking the largest of the ones at the boundaries and the center of cell *i*:

$$\bar{a}_{i-1/2} = \bar{a}_{i+1/2} = max\left[(a+|v|)_{i-1/2}, (a+|v|)_{i}, (a+|v|)_{i-1/2}\right] \quad (10.5.9)$$

Calculating an incorrect velocity of sound according to equation 10.2.6 makes the overall results inaccurate, but it does not alter the propagation velocity significantly. It is therefore possible to check if all parameters have been connected correctly in the finished simulation program by looking at how fast a step in pressure or flow propagates along the pipe. That propagation speed can be compared to the values found when using equation 10.2.6.

The time derivative is the only remaining derivative after the spatial dimension has been dicretisized. Kurganov and Tadmor showed that if *D* in equation 10.1.10 had been zero, the final derivative could then be computed as:

$$\frac{dY_i}{dt} = \frac{\partial Y_i}{\partial t} = -\frac{F_{i+1/2} - F_{i-1/2}}{\Delta x} \quad (10.5.10)$$

Obviously, unless the flow is frictionless, the pipe horizontal and no heat flow exists, *D* is not zero, and Kurganov and Tadmor did not show how to include that. By going through their paper, though, it is possible to see that including the source term, which mathematicians often call *D* (not to be confused with pressure and mass flow sources

discussed regarding boundary conditions in chapter 11), would have modified equation 10.5.10 to:

$$\frac{dY_i}{dt} = \frac{\partial Y_i}{\partial t} = -\frac{F_{i+1/2} - F_{i-1/2}}{\Delta x} + \frac{1}{\Delta x}\int_{x_{i-1/2}}^{x_{i+1/2}} D\, dx \qquad (10.5.11)$$

The integral indicates that D should be taken as the average value for the whole cell. Due to the nonlinearities in D, that is not quite the same as calculating D using the state variables for the cell averages (the ones indexed i). When we look at equation 10.1.9, we can see how the different terms vary:

- The friction term is proportional to $\rho v|v|$. The other parameters in the friction term, such as the friction factor f, vary so little within a cell that it is quite accurate to consider it constant for this purpose.
- The elevation term is proportional to $\rho \cdot sin\theta$.
- The heat q varies in a somewhat more complicated way, as outlined in chapter 8. We recall that both the Re number and the Pr took part in the calculation of the overall heat transfer coefficient U. That coefficient, together with the temperature difference between the liquid and the pipe's environment, determines the heat. How U varies with the other parameters depend on pipe insulation thickness, outside weather and temperature, as well as many other parameters, but it is relatively easy to establish simple approximations for any particular pipe. In this general approach, we presume all parameters used as input according to chapter 8 to vary linearly in each cell.

The calculation procedure outlined in equations 10.5.1 - 10.5.10 requires us to calculate both primary and secondary variables at 3 locations in each cell: At its boundaries and for the cell average. The cell average is not necessarily the value we have at the cell center, but it is most often going to be very close. We therefore combine the 3 known values by using Simpson's rule to integrate. From that, we calculate an average value:

$$\left(\overline{\rho v|v|}\right)_i = \frac{(\rho v|v|)_{i-1/2} + 4(\rho v|v|)_i + (\rho v|v|)_{i+1/2}}{6} \qquad (10.5.12)$$

 For non-commercial use only

For the elevation term, we similarly get:

$$\overline{(\rho \cdot sin\theta)}_i = \frac{(\rho \cdot sin\theta)_{i-1/2} + 4(\rho \cdot sin\theta)_i + (\rho \cdot sin\theta)_{i+1/2}}{6} \tag{10.5.13}$$

For the heat terms, the more complicated correlations make it easiest, if also slowest, to make 3 complete heat calculations for each cell, and then average them afterwards:

$$\bar{q}_i = \frac{q(\rho, T, v, \dots)_{i-1/2} + 4q(\rho, T, v, \dots)_i + q(\rho, T, v, \dots)_{i+1/2}}{6} \tag{10.5.14}$$

These values are used to calculate the source matrix:

$$\frac{1}{\Delta x}\int_{x_{i-1/2}}^{x_{i+1/2}} D\,dx = \begin{bmatrix} 0 \\ -\frac{f}{2d}\overline{(\rho v|v|)}_i - g\overline{(\rho \cdot sin\theta)}_i \\ \bar{q}_i + w \end{bmatrix} \tag{10.5.15}$$

We see that equations 10.5.11, 10.5.14, 10.5.12 and 10.5.13 make it possible to calculate $\frac{dY_i}{dt}$.

How to handle the boundary conditions is explained in great detail in chapter 11.

10.6 Calculating secondary from primary variables

We see from equation 10.1.9 that as we integrate equation 10.1.9, we use ρ, ρv and E as primary variables. But we also need to know the secondary variables v, h, T and p for each time step. In addition, we need to update k_f, μ and Pr, but they are less interwoven into the main calculations and may not necessarily be worth updating at every grid-point for each time step.

The velocity follows directly from the first two primary variables:

$$v = \frac{\rho v}{\rho} \tag{10.6.1}$$

For non-perfect gases, the other 3 secondary variables depend on each other as well as the primary variables. Equation 10.1.8 together with the general equations 10.1.3 and 10.1.4 tell us that:

$$h = \frac{E + p}{\rho} - \frac{v^2}{2} - gz$$

$$T = T(p, h) \tag{10.6.2}$$

$$p = p(T, \rho)$$

Where h, T and p are the unknowns to be solved. If we have a good enough guess for the initial pressure p, typically the pressure from the previous time step, we may simply use that to compute h, T and p. We can continue going through the equations again and again several times, getting a better estimate each time. Convergence can be expected within anything between 1 and 50 iterations, depending on how good initial guess we made. The method has the advantage of being both very simple and also valid for both gases and liquids, but it can be relatively slow. It does not always guarantee convergence, either, and such fixed-point iteration is not recommended for solving the equations.

Fortunately, there are better ways to iterate a solution to equations 10.6.2. The most efficient method can be achieved if we have access to h expressed explicitly as a function of p and ρ so that we do not have to involve T in the iteration:

$$h = h(p, \rho) \tag{10.6.3}$$

Using this, together with the first equation in 10.6.2, we may set:

 For non-commercial use only

$$h(p,\rho) - \frac{E+p}{\rho} + \frac{v^2}{2} + gz = 0 \tag{10.6.4}$$

The only un-known here is p. It can be solved using Newton-iteration:

$$p_{n+1} = p_n - \left[\left(\frac{\partial h}{\partial p}\right)_\rho - \frac{1}{\rho}\right]_n^{-1} \left[h(p,\rho) - \frac{E+p}{\rho} + \frac{v^2}{2} + gz\right]_n \tag{10.6.5}$$

If we compare this equation with the one for perfect gas, equation 10.2.9, we notice they are quite similar, the difference being that 10.9.6 requires a few rounds of iteration to be solved. This is of great help when we later develop boundary conditions, and it is also used to calculate p, and T from ρ, ρv and E in each cell.

Equation 10.6.4 gives us a simple way to estimate the absolute error, and therefore also a criteria for when to stop the iteration. We stop when:

$$\left|h(p,\rho) - \frac{E+p}{\rho} + \frac{(\rho v)^2}{2\rho^2} + gz\right| < \varepsilon_p \tag{10.6.7}$$

How small to choose ε_p is a tradeoff between speed and accuracy, but setting $\varepsilon_p = 10^{-3}$ seems to work well in most cases. It typically leads to only one or two iterations in most parts of the pipe if the pressure from the previous time step is used as start value.

Sometimes it can be convenient to use perfect gas properties when testing out the program. It follows from equation 10.2.1 and 10.2.6 that for perfect gases, we can easily express $h(p,\rho)$ directly:

$$h(p,\rho) = \frac{c_p}{R_g}\frac{p}{\rho} \tag{10.6.8}$$

By simple derivation, we can also express:

$$\left(\frac{\partial h}{\partial p}\right)_{\rho} = \frac{c_p}{R_g}\frac{1}{\rho} \tag{10.6.9}$$

When inserting these values, the results should agree with equation 10.2.9 if we have implemented everything correctly.

10.7 Determining indirect fluid properties

We recall that the most important fluid properties typically occur on the form shown in equations 10.1.3 and 10.1.4, where we had $p = p(T, \rho)$ and $h = h(T, \rho)$.

Suppose that we are seeking a way to solve $T(p, \rho)$ or $\rho(p, T)$. That can be formulated as a solution to the function f_p defined as:

$$f_p = p_{exact} - p(T, \rho) = 0 \tag{10.7.1}$$

This equation can be solved by Newton-iteration as:

$$T_{n+1} = T_n + \frac{p_{exact} - p(T_n, \rho)}{\left(\frac{\partial p}{\partial T}\right)_{\rho}} \tag{10.7.2}$$

or

$$\rho_{n+1} = \rho_n + \frac{p_{exact} - p(T, \rho_n)}{\left(\frac{\partial p}{\partial \rho}\right)_{T}} \tag{10.7.3}$$

 For non-commercial use only

The partial derivatives can be found by two function calls:

$$\left(\frac{\partial p}{\partial T}\right)_{\rho} = \frac{p(T,\rho) - p(T-\Delta T,\rho)}{2\Delta T} \tag{10.7.4}$$

And:

$$\left(\frac{\partial p}{\partial \rho}\right)_{T} = \frac{p(T,\rho) - p(T,\rho-\Delta \rho)}{2\Delta \rho} \tag{10.7.5}$$

Where ΔT and $\Delta\rho$ are chosen as small quantities, for instance $\Delta T = 0.1K$ and $\Delta\rho = 0.1\,kg/m^3$. Notice that the function call $p(T_n,\rho)$ is part of both equation 10.7.2 and 10.7.4, so we do not need to calculate it more than once. Each iteration requires two function calls, and we typically end up doing 2-5 iterations, so it takes considerably longer to calculate indirectly modeled properties.

We can use the value from the previous time step as a starting value, and iterate until:

$$|f_p| = |p_{exact} - p(T,\rho)| \leq \varepsilon_p \tag{10.7.6}$$

The convergence criteria ε_p may be in the order of $10^{-3}\,Pa$. Solving indirect variables from enthalpy is similarly simple:

$$T_{n+1} = T_n + \frac{h_{exact} - h(T_n,\rho)}{\left(\frac{\partial h}{\partial T}\right)_{\rho}} \tag{10.7.7}$$

and

$$|f_h| = |h_{exact} - h(T,\rho)| \leq \varepsilon_h \tag{10.7.8}$$

Typical numerical values for h may be an order of magnitude or two lower than those for p, depending on the system we are studying. It is best to adjust the convergence criteria accordingly, for instance so that $\varepsilon_h = 10^{-5}\, J/(kg \cdot K)$.

Notice that since the indirect calculations may be an order of magnitude slower than the direct calculations, it can be tempting to create a separate, direct curve fit for each. For instance, we could attempt to describe $T(h,\rho)$ directly. If so, one has to take care to make $T(h,\rho)$ agree accurately with $h(T,\rho)$, otherwise the energy balance will be violated. When we simulate the pipe flow, we are jumping back and forth between the primary variables $\rho, \rho v, E$ and the secondary variables p, v, T, h for every function call. Lack of symmetry can result in pumping energy into or out of the pipe for each jump, something which produces incorrect results. When having only one curve fit for each physical property correlation, as described here, that problem is avoided.

References

Godunov, S, K. (1959): *A Difference Scheme for Numerical Solution of Discontinuous Solution of Hydrodynamic Equations*, Math. Sbornik, 47, 271-306, translated US Joint Publ. Res. Service, JPRS 7226, 1969.

H.Nessyahu and E.Tadmor: (1990). Non-*oscillatory Central Differencing for Hyperbolic Conservation Laws*, Journal of Comput. Phys. 87, 408.

Medovikov, A.A. (1998): *High Order Explicit Methods for Parabolic Equations.* BIT, 38. 2, pp. 372–390.

Kurganov, A., Tadmor, E. (1999): *New High-Resolution Central Schemes for Nonlinear Conservation Laws and Convection-Diffusion Equations*, Journal of Comp. Phys., 160, 214–282.

American Gas Association (2003): Speed of sound in Natural Gas and Other Related Hydrocarbon Gases. Report No. 10.

Liska, R., Wendroff, B. (2003): *Comparison of Several Difference Schemes on 1D and 2D Test Problems for the Euler Equations*. SIAM J. Sci. Comput., Vol. 25, No. 3, pp 995-1017.

Kermani, M. J., Gerber, A. G., Stockie, J. M. (2003): *Thermodynamically Based Moisture Prediction Using Roe's Scheme*. The 4th Conference of Iranian AeroSpace Society, Amir Kabir University of Technology, Tehran, Iran, January 27–29.

 For non-commercial use only

Moran, M.J., Shapiro, H.N. (2006): *Fundamentals of Engineering Thermodynamics*, John Wiley & Sons Ltd.

"An idea, like a ghost, must be spoken to a little before it will explain itself."
Charles Dickens

11 Ghost cells

Inserting ghost cells at each end of the pipe, a first approach:

- What ghost cells are
- Various ways to insert values into the ghost cells
- Calculating ρ and E from ρv, $p + (\rho v)^2/\rho$ and $v(E + p)$

11.1 Some general considerations

At the pipe boundaries, meaning at the inlet and outlet ends, certain properties have to be known from the way the pipe is connected to the outside world. At each end, either the pressure or the mass flow, or a correlation between the two, has to be known. In addition, the temperature must be known for the inflowing fluid. These are the boundary conditions we face, and they are explained in greater detail in chapter 12.

One problem with our KT3 model is that each cell uses information from two neighbors at each side of itself when calculating the time derivatives. At the boundaries, some of the neighboring cells fall outside the pipe and therefore do not exist. This is not a unique problem to the KT3 scheme; it is common for many spatial discretization methods. One possible solution, and the one adopted here, is to create 'ghost cells', or imaginary cells outside the physical pipe. For that to be useful, we also need ways to insert imaginary values for $\rho, \rho v$ and E in those ghost cells. How to do so does not follow from the KT3 scheme, so we need to develop methods for it separately.

How to treat boundary conditions properly is still subject to much research. One of the most relevant sources at this stage seems to be the one by Leveque (2002), and some of the methods shown here have been inspired by his approach.

 For non-commercial use only

The methods shown in this chapter follow relatively conventional thinking, but some new elements have been added. Later, after the boundary conditions have been more thoroughly discussed in chapter 12, we are going to show a less traditional way of filling the ghost cells in chapter 13. To this author's knowledge, some of the methods in chapter 11.3-11.5 and those in chapter 13 have never been published before, but they have been tested on numerous examples and found to work well.

11.2 Inserting ghost values: A simple method

Figure 10.2.1 shows how the inlet boundary, with ghost cells and all, is arranged. The first real cell starts where the pipe starts, so the cell's center is located some distance inside the pipe. The pipe's boundary conditions are therefore enforced at the cell's boundary, not at the cell's center.

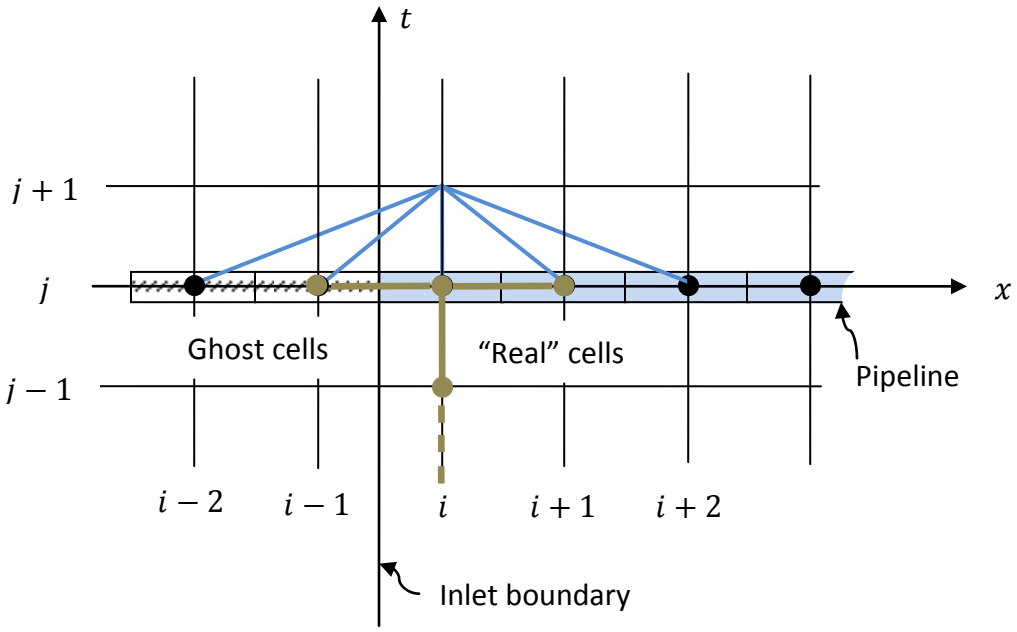


Figure 11.2.1.Pipe inlet end with 2 ghost cells. Getting from cell i,j to i, j+1 requires information from the two ghost cells at i-1,j and i-2,j, as well as from i,j itself, and from i+1,j and i+2,j. For that to be possible, we need to estimate values for the ghost cells first. The figure hints how a ghost cell's state can be estimated based on information from past and present states in the nearest cell inside the pipe. As we will see below, information from i,j-1 and i,j and i,j-1 makes it possible to estimate for the values we need for cell i-1,j.

Before we start discussing how to fill the ghost cells, let us look at how to index them. The most common convention is probably to give the first real cell index 1, meaning the two adjacent ghost cells get indexes $i = 0$ and $i = -1$. The problem with this naming convention is that many programming languages cannot use negative vector indexes, so we may end up having to re-index everything when going from theory to computer code. To avoid that, we set $i = 0$ at the first ghost cell, so that the first real cell gets index $i = 2$. If we have a total of N_x cells inside the pipe, the index for the last real cell becomes $N_x + 1$, while the last ghost cell corresponds to $i = N_x + 3$. Regardless of how we choose to index the first real cell, figure 11.2.1 is valid, since it refers all indexes to the first real cell's index without inserting numerical values.

The simplest possible way to create values for the ghost cells is to copy the values from the nearest neighbors. Using the notation in equation 10.1.10 for the ghost cells at the inlet boundary, that would mean:

$$Y_{i-2,j} = Y_{i-1,j} = Y_{i,j} \tag{11.2.1}$$

where i is the index for the first real cell, typically chosen to be 2. At the outlet, we would fill the two ghost cells to the right of the last 'real cell by setting:

$$Y_{i+2,j} = Y_{i+1,j} = Y_{i,j} \tag{11.2.2}$$

Where index i may be $N_x + 1$ if we use the naming convention explained above.

This is not a very accurate way of filling in the ghost cells, but still more accurate than some authors have claimed. At first glance, it may look like an approximation of order zero, and so it would have been if we had used it along the whole pipe. Order zero (O0) means that decreasing the distance between nodes by making the mesh finer does not result in improved overall accuracy, and such a method is not going to be convergent, meaning it is not going to work.

The most common approach to determining a method's order goes like this: When we try to increase a method's accuracy by increasing the number of grid points, we also increase the number of computations producing roundoff-errors. For this to give a

 For non-commercial use only

favorable net contribution, the accuracy gain pr. roundoff-error must be higher than the loss due to increased number of terms producing roundoff-errors. Put another way, the global roundoff error is one order lower than the local roundoff error, since one of the orders is spent compensating for the increased number of terms producing such errors. The local roundoff-error has to be order *2* for the global one to be of order *1*, which is the lowest order it is possible to have for a convergent method.

The situation at the boundary is somewhat different, though. Making the mesh finer does not increase the number of ghost cells, so the global error is not one order lower than the approximation used at the boundary. It is easy to show with Taylor-expansion that the ghost cell approximation shown in equation 12.2.1 has a local roundoff error of *1*, and the global consequence of that error is going to be *1* as well. The boundary approximations become a smaller and smaller part of the total number of grid-points the finer the grid is chosen. That means increasing the grid density actually does increase accuracy, and that also shows the global order is *1*.

The fact that it is relatively acceptable to use a method with local order lower at the boundaries compared to what we do in the rest of the pipe is significant, and we will return to it several times later. It shows the very simple approximation in equation 11.2.1 is in fact at least better than order *0*, but still far from order *3*, which the KG3-scheme is capable of. The overall global order is determined by the weakest link in the computation chain, so it falls down to a mere *1*, wasting part of what was so attractive with the KT3 scheme. If we still use it and plot the resulting (ρv) along the pipe, the curve typically shows a sharp bend near the boundaries even after the simulation has had time to reach steady-state. Since continuity requires (ρv) to be the same in the whole pipe at steady-state, such results are not accurate. The problem can be countered by using very high grid density, but that is of course precisely what we want to avoid by using a high-order method for the main computations. Besides, when Δx is reduced, Δt must also be reduced to maintain stability. All in all, that makes this method much slower than what can be achieved with more sophisticated boundary conditions.

On the positive side, handling the boundary conditions according to equation 11.2.1 and 12.2.2 is very easy and results in a robust solution as long as N_x is chosen high enough, and it is a quite common strategy. It can also represent a simple reference to compare against when testing more advanced ghost cell filling methods.

11.3 An improved ghost cell approximation

The ghost cell values should preferably comply with equation 10.1.10, just like the rest of the pipe flow model. The general Taylor-expansion equation, 11.3.1, can help us achieve that:

$$F(x_i + \Delta x) = F(x_i) + \Delta x \left(\frac{\partial F}{\partial x}\right)_i + \frac{1}{2}(\Delta x)^2 \left(\frac{\partial^2 F}{\partial x^2}\right)_i + \frac{1}{6}(\Delta x)^3 \left(\frac{\partial^3 F}{\partial x^3}\right)_i + \ldots \qquad (11.3.1)$$

With an eye to equation 10.1.10, we observe that Taylor-expansion from a point x_i to a point Δx to the right of it can be used to create an estimate for the derivative by re-arranging this somewhat:

$$\left(\frac{\partial F}{\partial x}\right)_i = \frac{F(x_i + \Delta x) - F(x_i)}{\Delta x} - \frac{1}{2}\Delta x \left(\frac{\partial^2 F}{\partial x^2}\right)_i - \frac{1}{6}(\Delta x)^2 \left(\frac{\partial^3 F}{\partial x^3}\right)_i + \ldots \qquad (11.3.2)$$

The further out in the (infinite) Taylor-expansion we go, the smaller the terms become. Since we cannot use an infinite amount of terms, we must break off the expansion at some point, and this is the main source of error. The smallest of the terms shown in equation 11.3.2 is going to be the one to the right. That term is proportional to $(\Delta x)^2$. If we ignore that term, the resulting error will be proportional to $(\Delta x)^2$. If we use a small Δx, the error is going to be small. More importantly, we see that reducing Δx leads to the error shrinking proportional to the square of the reduction. That is what we mean when we say the method's order is 2, it is simply the order Δx occurs in for the first ignored term in the Taylor expansion. For reasons already explained, the global consequence of errors at the boundary is one order higher than would have been the result of errors being repeated in all cells throughout the pipe.

In our case, the 2. order approximation of $\partial F/\partial x$ looks like this:

 For non-commercial use only

$$\left(\frac{\partial F}{\partial x}\right)_{i,j} = \frac{F_{i+1,j} - F_{i,j}}{\Delta x} - \frac{1}{2}\Delta x\left(\frac{\partial^2 F}{\partial x^2}\right)_{i,j} \tag{11.3.3}$$

If we do the Taylor-expansion towards the left side by studying $F(x_i - \Delta x)$, we can easily show that the following approximation also holds true:

$$\left(\frac{\partial F}{\partial x}\right)_{i,j} = \frac{F_i - F_{i-1}}{\Delta x} + \frac{1}{2}\Delta x\left(\frac{\partial^2 F}{\partial x^2}\right)_{i,j} \tag{11.3.4}$$

Similarly, we may estimate the time derivative as:

$$\left(\frac{\partial Y}{\partial t}\right)_{i,j} = \frac{Y_{i,j} - Y_{i,j-1}}{\Delta t} + \frac{1}{2}\Delta t\left(\frac{\partial^2 Y}{\partial t^2}\right)_{i,j} \tag{11.3.5}$$

At the inlet, we can insert equations 11.3.4 and 11.3.5 into 10.1.10 and get an estimate for $F_{i-1,j}$, and thereby calculate the state variables for the nearest ghost cell. By repeating that process after reducing the spatial index i by one, we also get values for the outermost ghost cell at the inlet. The same can be done for the ghost cells at the outlet, but equation 11.3.3 has to replace 11.3.4, and the values to compute are of course those in $F_{i+1,j}$.

But what should we do with the second derivatives in equations 11.3.3, 11.3.4 and 11.3.5?

Simply dropping them is one option. That would make the local order for the boundary approximations 1, and as explained earlier, the global consequence of that error is going to be of order close to 2. A possible additional simplification would be to neglect the time derivative altogether, but that would obviously reduce the accuracy even further. But it would at least approach the correct solution when the flow approaches steady-state, since that means the time derivate becoming zero anyway. For relatively slow pressure and mass flow changes at the boundaries, the most common situation in long pipelines, we get surprisingly accurate results by simply setting $\partial Y/\partial t = 0$ at the

boundary. If we insert that, together with the first order terms of equation 11.3.4 into equation 10.1.10, we get:

$$0 = -\frac{F_i - F_{i-1}}{\Delta x} + \mathrm{D} \tag{11.3.6}$$

If we set $i = 2$, corresponding to the first real cell at the inlet end, we can estimate the closest ghost cell by setting:

$$F_{i-1} = F_i - \Delta x \cdot \mathrm{D} \tag{11.3.7}$$

Once that is done, we simply set $i = 1$ and re-calculate to fill the outermost cells. At the outlet, we first set $i = N_x + 1$, and thereafter $i = N_x + 2$ to fill the ghost cells with:

$$F_{i+1} = F_i + \Delta x \cdot \mathrm{D} \tag{11.3.8}$$

We will discuss how to do so in greater detail in the next chapter, but at this point, let us just make two important observations regarding this way of extrapolating the values:

1. It is the ghost values we extrapolate, not values being part of the final result of our computations. Even though the time derivative is neglected in computing ghost values, it does not mean boundary values cannot change over time. The outermost real cells are 'fed' the actual, time-varying values corresponding to the last known pressure (for pressure sources) or mass flow (for mass flow sources). The overall consequences of neglecting the time derivative when calculating the ghost values is therefore going to be less severe than one might at first expect.
2. When determining for instance $F_{i+1,j}$ from $F_{i,j}$ according to equation 10.10.7, we get the flux terms f_1, f_2 and f_3, which according to equation 10.1.10 corresponds to ρv, $p + \rho v^2$ and $v(E + p)$. What we are seeking is of course ρ, ρv and E, so we need to solve a set of nonlinear equations after we have determined $F_{i+1,j}$.

 For non-commercial use only

11.4 Further ghost cell improvements

The first thing to do to improve the ghost cell approximations even further is to include the time derivative. That modifies equation 11.3.7 to:

$$F_{i-1} = F_i - \Delta x \cdot \mathrm{D} + \Delta x \left(\frac{\partial Y}{\partial t}\right)_{i,j} \tag{11.4.1}$$

At the outlet, we modify equation 11.3.8 to:

$$F_{i+1} = F_i + \Delta x \cdot \mathrm{D} - \Delta x \left(\frac{\partial Y}{\partial t}\right)_{i,j} \tag{11.4.2}$$

We may at first think that $\partial Y/\partial t$ can be estimated from the first term in equation 11.3.5 directly. The problem is that the higher order Runge-Kutta integration methods, which we propose to use when simulating, make intermediate function calls. Therefore, ghost cell values are required not only at the time steps *j-1, j, j+1* and so on, but also in-between. The most used RK4-method, for instance, starts the process of integrating from time-level *j* to *j+1* by requesting all $\partial y/\partial t$-values at time j. That is not problematic. We have already shown how to create values for the ghost cells there. But the second call requests values for time *j+1/2*, and other integration methods may require function values at other intermediate times. Equation 11.3.5 does not tell us how to predict such values. We can modify it, however, so it becomes possible to extrapolate to a point lying $\delta \cdot \Delta t$ past time-layer *j*. We simply develop the Taylor-expansion around $Y_{j+\delta}$ rather than around Y_j:

$$\left(\frac{\partial Y}{\partial t}\right)_{i,j+\delta} = \frac{Y_{i,j+\delta} - Y_{i,j}}{\delta \cdot \Delta t} + \frac{1}{2}\delta \cdot \Delta t \left(\frac{\partial^2 Y}{\partial t^2}\right)_{i,j+\delta}, 0 < \delta \leq 1 \tag{11.4.3}$$

At $\delta = 0$, we can obviously not use the first term on the right-hand side of equation 11.4.3, so for the first call, we use equation 11.3.5 in its original form. For intermediate calls, however, we use equation 11.4.3.

This looks like a simple and straight forward way of estimating the ghost cell values. Unfortunately, there is a snag. If we include the time derivative of both $\rho, \rho v$ and E, the integration becomes unstable. This appears to be because doing so results in the boundary conditions becoming over-specified, since time history and neighboring cell values are not independent of each other. Coelcho et al. (2006) showed that for a perfect gas, it was possible to include both $\partial \rho v / \partial t$ and $\partial E / \partial t$ at outlet boundary where the pressure was kept constant. Perfect gases are fundamentally different from real gases in that the enthalpy h depends only on T, while in real gases it also depends on the pressure, and thus the simulation becomes unstable. At both inflowing and outflowing boundaries, it is necessary to set $\partial \rho / \partial t = 0$ and $\partial E / \partial t = 0$, while $\partial (\rho v) / \partial t$ can be estimated with equation 11.3.5 or 11.4.3.

This leads to the following robust if not perfect method for calculating ghost values:

1. For the first function call in a time step, calculate $\partial (\rho v) / \partial t$ according to equation 11.3.5, neglecting the higher order term. For intermediate time steps, use equation 11.4.3. Set $\partial \rho / \partial t = 0$ and $\partial E / \partial t = 0$.
2. Insert this into equation 11.4.1 or 11.4.2 and calculate ghost values for the ghost cells nearest the pipe ends first, thereafter for the outermost cells in a way similar to the one explained in chapter 11.3.

11.5 Computing state variables from flux variables

One important task still remains. The equations developed so far enable us to compute F, which corresponds to $(\rho v), p + (\rho v)^2 / \rho$ and $v(E + p)$ in the ghost cells. That is a step in the right direction, but our goal is to estimate $\rho, (\rho v)\ and\ E$. When developing a way to do so, we do not want to limit ourselves to perfect gases, so we have to rely on general correlations for the fluid properties.

We start by calculating f_1, f_2 and f_3 according to equations 11.4.1 or 11.4.2 as described above. From equation 10.1.10 we recall that those factors are defined as:

$$(\rho v) = f_1 \tag{11.5.1}$$

 For non-commercial use only

$$p + \frac{(\rho v)^2}{\rho} = p + \frac{{f_1}^2}{\rho} = f_2 \tag{11.5.2}$$

$$\frac{(\rho v)}{\rho}(E + p) = \frac{f_1}{\rho}(E + p) = f_3 \tag{11.5.3}$$

From equations 10.1.2 and 10.1.8 it follows that:

$$E = \rho\left(h + \frac{{f_1}^2}{2\rho^2} + gz\right) - p \tag{11.5.4}$$

We also need to involve the fluid's main properties, as described in equations 10.1.3 and 10.1.4:

$$p = p(T, \rho) \tag{11.5.5}$$

$$T = T(p, h) \tag{11.5.6}$$

It is obviously possible, though, to combine equations 11.5.5 and 11.5.6 and express h directly as a function of p and ρ:

$$h = h(p, \rho) \tag{11.5.7}$$

That enables us to reduce the number of unknown's to be solved simultaneously to 3, since 11.5.7 can be inserted into 11.5.4, and the result, together with equations 11.5.2 and 11.5.3 can be formulated as:

$$\begin{bmatrix} p \\ \rho \\ E \end{bmatrix} = \begin{bmatrix} f_2 - \frac{{f_1}^2}{\rho} \\ \frac{f_1}{f_3}(E+p) \\ \rho\left\{h(p,\rho) + \frac{{f_1}^2}{2\rho^2} + gz\right\} - p \end{bmatrix} \tag{11.5.8}$$

We can use Newton-iteration to find the solution to:

$$\begin{bmatrix} 0 \\ 0 \\ 0 \end{bmatrix} = \begin{bmatrix} p - f_2 + \frac{{f_1}^2}{\rho} \\ \rho - \frac{f_1}{f_3}(E+p) \\ E - \rho\left\{h(p,\rho) + \frac{{f_1}^2}{2\rho^2} + gz\right\} + p \end{bmatrix} \tag{11.5.9}$$

The Jacobi-matrix follows from derivation of the vector on the right-hand side of equation 11.5.9:

$$J_g = \begin{bmatrix} 1 & -\frac{{f_1}^2}{\rho^2} & \\ -\frac{f_1}{f_3} & 1 & -\frac{f_1}{f_3} \\ 1 - \rho\left(\frac{\partial h}{\partial p}\right)_\rho & -h(p,\rho) - \frac{{f_1}^2}{\rho^2} - gz - \rho\left[\left(\frac{\partial h}{\partial \rho}\right)_p - \frac{{f_1}^2}{\rho^3}\right] & 1 \end{bmatrix} \tag{11.5.10}$$

Newton-iteration can then be done by simply

 For non-commercial use only

$$\begin{bmatrix} p \\ \rho \\ E \end{bmatrix}_{n+1} = \begin{bmatrix} p \\ \rho \\ E \end{bmatrix}_{n} - {J_g}_n^{-1} \begin{bmatrix} p - f_2 + \frac{{f_1}^2}{\rho} \\ \rho - \frac{f_1}{f_3}(E+p) \\ E - \rho\left\{h(p,\rho) + \frac{{f_1}^2}{2\rho^2} + gz\right\} + p \end{bmatrix}_n \tag{11.5.11}$$

If we do not have access to $(\partial h/\partial p)_\rho$ and $(\partial h/\partial \rho)_p$-data for the fluid, it looks like the iteration converges even if they are neglected (set to zero), but it typically takes 5-10 times as many iterations. It therefore pays to estimate them indirectly. $(\partial h/\partial p)_\rho$ can be estimated by making to calls to $h(p,\rho)$ for slightly different p, and then set:

$$\left(\frac{\partial h}{\partial p}\right)_\rho = \frac{h(p,\rho) - h(p-\Delta p,\rho)}{\Delta p} \tag{11.5.12}$$

Similarly, we may estimate:

$$\left(\frac{\partial h}{\partial \rho}\right)_p = \frac{h(p,\rho) - h(p,\rho-\Delta \rho)}{\Delta p} \tag{11.5.13}$$

With careful programming, this enables us to get significantly faster convergence with only two more calls to $h(p,\rho)$ compared to what we would have had to make if $(\partial h/\partial p)_\rho$ and $(\partial h/\partial \rho)_p$ had been neglected. Using the same $(\partial h/\partial p)_\rho$ and $(\partial h/\partial \rho)_p$ over several time steps may also be acceptable at periods when h does not change much.

Iteration is stopped when we are satisfied the result is close enough to the actual solution. We can use equation 11.5.9 for that purpose: We take the norm of the vector at the right-hand side, and see if it is close enough to zero. For each iteration, we estimate the absolute error directly by defining:

$$\begin{bmatrix}\varepsilon_1\\ \varepsilon_2\\ \varepsilon_3\end{bmatrix} = \begin{bmatrix} p - f_2 + \frac{{f_1}^2}{\rho} \\ \rho - \frac{f_1}{f_3}(E+p) \\ E - \rho\left\{h(p,\rho) + \frac{{f_1}^2}{2\rho^2} + gz\right\} + p \end{bmatrix} \tag{11.5.14}$$

We break off the iteration when the error norm:

$$\sqrt{{\varepsilon_1}^2 + {\varepsilon_2}^2 + {\varepsilon_3}^2} < \varepsilon_{p\rho E} \tag{11.5.15}$$

Setting $\varepsilon_{p\rho E} = 10^{-3}$ is more than adequate for most simulations, and it may – with care - be set much higher if speed is important. Relaxing the convergence criteria does normally not make very much of a difference for speed, though, since Newton-iteration converges rapidly anyway.

To get the iteration started, we need initial values for p, ρ and E. Values from the previous time step or from the nearest cell can be used for that purpose. Using values from the past time step has the advantage of approaching the correct value as the flow approaches steady-state, and this is therefore normally the preferred approach.

We may encounter two special cases when solving these equations: We may get $f_3 = 0$, which would obviously lead to division by zero in equation 11.5.11. Also, we may get $f_1 (= \rho v) = 0$, something which would mean equation 11.5.2 no longer contains information about ρ. The last problem can be dealt with in a not too scientific way, but one that seems to work well, by simply checking if f_1 is zero, and then giving it some small value in case it is.

How to deal with $f_3 = 0$ can be seen by going back to the original equations 11.5.1-11.5.3. From 11.5.3 it follows $E = -p$. By inserting this into equation 11.5.4 we get a new density equation, while the pressure equation is kept unchanged. That leads to:

 For non-commercial use only

$$\begin{bmatrix} p \\ \rho \end{bmatrix}_{n+1} = \begin{bmatrix} p \\ \rho \end{bmatrix}_{n} - J_{g\,n}{}^{-1} \begin{bmatrix} p - f_2 + \dfrac{f_1{}^2}{\rho} \\ h(p,\rho) + \dfrac{f_1{}^2}{2\rho^2} + gz \end{bmatrix}_n \tag{11.5.16}$$

The Jacobi matrix has here changed to:

$$J_g = \begin{bmatrix} 1 & -\dfrac{f_1{}^2}{\rho^2} \\ \left(\dfrac{\partial h}{\partial p}\right)_\rho & \left(\dfrac{\partial h}{\partial \rho}\right)_p - \dfrac{f_1{}^2}{\rho^3} \end{bmatrix} \tag{11.5.16}$$

We now have a general recipe for finding ρv for the ghost cells:

1. Compute f_1, f_2 and f_3 using equations 11.4.1 or 11.4.2.
2. Use equations 11.5.10 and 11.5.11 and Newton-iteration to determine ρ and E, while (ρv) follows directly from equation 11.5.1.

We have seen in previous chapters that in case the fluid is a perfect gas, h simplifies to $h = c_p T$. By derivation it follows that that for perfect gases, we have:

$$\left(\frac{\partial h}{\partial p}\right)_\rho = 0$$

$$\left(\frac{\partial h}{\partial \rho}\right)_p = -\frac{c_p}{R_g}\frac{p}{\rho^2} \tag{11.5.17}$$

Using these simple perfect-gas correlations may be of help when testing out the simulation program.

References

Godunov, S, K. (1959): *A Difference Scheme for Numerical Solution of Discontinuous Solution of Hydrodynamic Equations*, Math. Sbornik, 47, 271-306, translated US Joint Publ. Res. Service, JPRS 7226, 1969.

Leveque, R.J. (2002): *Finite Volume Methods for Hyperbolic Problems.* Cambridge University Press.

Coelho, R.M.L., Lage, P. L. C., Silva Telles, A. (2006): *A Comparison of Hyperbolic Solvers for Ideal and Real Gas Flows.* Brazilian Journal of Chemical Engineering, April 19.

 For non-commercial use only

"Knowledge once gained casts a light beyond its own immediate boundaries."
John Tyndall

12 Boundary conditions

This chapter explains how to deal with:

- Known pressure at the end, fluid flowing into the pipe
- Known pressure at the end, fluid flowing out of the pipe
- Known mass flow into the pipe
- Known mass flow out of the pipe
- Causality in junctions
- Boundary conditions for valves and other components

12.1 General

When simulating pipe networks, we want to be able to connect pipes to other pipes, reservoirs, nodes, valves compressors, and many other common pipe network components. In the computer code, a pipe is typically programmed as an object, and that object needs to be very general – it must be able to handle both flow directions at both pipe ends. It must also be able to handle any causality in each end, both pressure and mass flow sources. As described more thoroughly in chapter 12.1.1, a pressure source is defined as a situation where the pipe's environment defines the pressure, for instance in the form of a pressure vessel or a pressure regulator, while the pipe responds by determining the mass flow. If so, pressure is *cause*, while mass flow is *effect*.

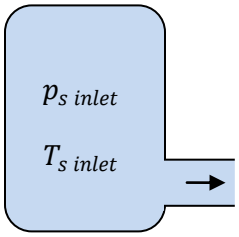
A mass flow source is defined as the environment controlling the mass flow, while the pipe responds by determining the pressure at that end.

There is no direct connection between boundary conditions at the two ends of a pipe. It is, for example, completely possible to temporarily have inflowing fluid at both ends at the same time. It is in fact possible to have any combination of boundary conditions at the two pipe ends at a given time. Therefore, the boundary conditions in our transient model are determined individually, so that the boundary conditions in one end are determined without regard for how it is in the same pipe's other end.

Also, keep in mind that boundaries with known pressure is not quite analogous to boundaries with known mass flow, since those two variables take part in the conservation equations in quite different ways - (ρv) is a primary variable, while p is a secondary variable. We should therefore not be surprised when we subsequently see they are not symmetrical in the way they occur in the different possible boundary conditions.

The four different types of boundary conditions each end can experience are explained in chapters 12.1.1-12.1.4.

12.1.1 Boundary condition 1: Pressure source, inflowing fluid



Both the pressure and the temperature are known at the boundary because the pipe's environment 'decides' it, for instance because the pipe is connected to a tank with a specific (known) pressure and temperature. As seen from the pipe, both $p_{s\ inlet}$ and $T_{s\ inlet}$ are sources, while (ρv) is effect.

When implementing this, we may start by having another look at figure 11.2.1. We recall that the first real cell, meaning the first cell inside the pipe, has its left boundary at the pipe inlet. This means the boundary conditions are enforced at the cell boundary, not at the cell center.

Since both the pressure and the temperature are decided from the outside sources $p_{s\ inlet}$ and $T_{s\ inlet}$, this also determines the density according to the fluid's properties, as for instance described by equation 10.1.3 or further elaborated in equation 10.7.3. Therefore, the density at the boundary is forcibly set to:

 For non-commercial use only

$$\rho = \rho^{L}{}_{i-1/2} = \rho^{R}{}_{i-1/2} = \rho(p_{s\ inlet}, T_{s\ inlet})\ at\ the\ inlet$$
$$\rho = \rho^{L}{}_{i+1/2} = \rho^{R}{}_{i+1/2} = \rho(p_{s\ outlet}, T_{s\ outlet})\ at\ the\ outlet \quad (12.1.1)$$

For the KT3 scheme, this means equations 10.5.1 and 10.5.2 are simply replaced by the first of the 12.1.1-equations for $\rho_{i-1/2}$ at the inlet, while equations 10.5.3 and 10.5.4 are replaced by the $\rho_{i+1/2}$ –equation, 12.1.1, at the outlet. The mass flow is not determined by the environment here, so $(\rho v)_{i-1/2}$ is simply computed as the selected computation scheme dictates, equations 10.5.1-10.5.3, without any modifications enforced at the boundary. That way, $(\rho v)_{i-1/2}$ becomes effect, as it is supposed to.

E, on the other hand, is also determined by the pressure and temperature sources, and it follows from equations 10.1.8 and 10.1.2 that at the inlet, we get:

$$E^{L}{}_{i-1/2} = \rho\left[h(p_{s\ inlet}, T_{s\ inlet}) + \frac{(\rho v)^{L}{}_{i-1/2}{}^{2}}{2\rho_{i-1/2}{}^{2}} + g z_{i-1/2}\right] - p_{s\ inlet} \quad (12.1.2)$$

$$E^{R}{}_{i-1/2} = \rho\left[h(p_{s\ inlet}, T_{s\ inlet}) + \frac{(\rho v)^{R}{}_{i-1/2}{}^{2}}{2\rho_{i-1/2}{}^{2}} + g z_{i-1/2}\right] - p_{s\ inlet} \quad (12.1.3)$$

At the outlet end, a pressure source with inflowing fluid would of course lead to similar equations, but with the cell boundary index being $i + 1/2$ rather than $i - 1/2$.

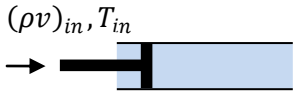
Also, remember that pressures and temperatures at $i - 1/2$ at the inlet is always set to $p_{s\ inlet}, T_{s\ inlet}$ (or at $i + 1/2$ in case of outlet, set to $p_{s\ outlet}, T_{s\ outlet}$) for all calculations where they are used.

12.1.2 Boundary condition 2: Pressure source, out-flowing fluid

In this case the pressure is decided by the pipe's environment, and the mass flow and temperature is the pipe's response. Note that boundary condition *1* switches to condition *2* and vice versa when the flow direction reverses.

These are the easiest boundary conditions to enforce. All computations are run using equations 10.5.1-10.5.4, almost as if there were no boundary, the only difference being that pressure is determined by pressure source rather than according to equation 10.6.5. If fluid flows out at the inlet, ${p^L}_{i-1/2}$ and ${p^R}_{i-1/2}$ for the first real cell is set to $p_{s\ inlet}$. At the outlet, this situation means ${p^L}_{i+1/2}$ and ${p^R}_{i+1/2}$ for the last cell is set to $p_{s\ outlet}$.

12.1.3 Boundary condition 3: Mass flow source, in-flowing fluid



The mass flow and the temperature are determined by the environment, while the pressure is determined by the pipe.

This means ρ is calculated from equations 10.5.1-10.5.4, as in the main calculations, while ${(\rho v)^L}_{i-1/2} = {(\rho v)^R}_{i-1/2} = (\rho v)_{s\ inlet}$ in case this occurs at the inlet. For the outlet, we get ${(\rho v)^L}_{i+1/2} = {(\rho v)^R}_{i+1/2} = (\rho v)_{s\ outlet}$.

The energy equation at the inlet is very similar to equation 12.1.2, the main difference being that the pressure has to be found from the fluid property, equation 10.1.3:

$$E^L_{\ i-\frac{1}{2}} = \rho^L_{\ i-1/2}\left[h\left(p^L_{\ i-1/2}, T_{s\ inlet}\right) + \frac{(\rho v)_{s\ inlet}^{\ 2}}{2\rho^L_{\ i-1/2}^{\ 2}} + g z_{i-1/2}\right] - p^L_{\ i-1/2}$$

$$p^L_{\ i-1/2} = p(T_{s\ inlet}, \rho^L_{\ i-1/2}) \tag{12.1.4}$$

And:

$$E^R_{\ i-\frac{1}{2}} = \rho^R_{\ i-1/2}\left[h\left(p^R_{\ i-1/2}, T_{s\ inlet}\right) + \frac{(\rho v)_{s\ inlet}^{\ 2}}{2\rho^R_{\ i-1/2}^{\ 2}} + g z_{i-1/2}\right] - p^R_{\ i-1/2}$$

$$p^R_{\ i-1/2} = p(T_{s\ inlet}, \rho^R_{\ i-1/2}) \tag{12.1.5}$$

In case this occurs at the outlet end, we similarly set:

$$E^L{}_{i+\frac{1}{2}} = \rho^L{}_{i+1/2}\left[h\left(p^L{}_{i+1/2}, T_{s\ outlet}\right) + \frac{(\rho v)_{s\ inlet}{}^2}{2\rho^L{}_{i+1/2}{}^2} + gz_{i+1/2}\right] - p^L{}_{i+1/2}$$

$$p^L{}_{i+1/2} = p(T_{s\ outlet}, \rho^L{}_{i+1/2}) \tag{12.1.6}$$

And:

$$E^R{}_{i+\frac{1}{2}} = \rho^R{}_{i+1/2}\left[h\left(p^R{}_{i+1/2}, T_{s\ outlet}\right) + \frac{(\rho v)_{s\ inlet}{}^2}{2\rho^R{}_{i+1/2}{}^2} + gz_{i+1/2}\right] - p^R{}_{i+1/2}$$

$$p^R{}_{i+1/2} = p(T_{s\ outlet}, \rho^R{}_{i+1/2}) \tag{12.1.7}$$

The temperature at $i-1/2$ at the inlet is always set to $T_{s\ inlet}$ (or at $i+1/2$ in case of outlet, set to $T_{s\ outlet}$) for all calculations where they are used.

12.1.4 Boundary condition 4: Mass flow source, out-flowing fluid

The mass flow is 'decided' by the pipe's environment, while the pressure and temperature is the pipe's response. Boundary condition *3* switches to condition *4* and vice versa when the flow direction reverses.

Only the mass flow state variable is modified compared to equations 10.5.1-10.5.4 by setting $(\rho v)_{i-1/2}{}^L = (\rho v)_{i-1/2}{}^R = (\rho v)_{s\ inlet}$ (or setting $(\rho v)_{i+1/2}{}^L = (\rho v)_{i+1/2}{}^R = (\rho v)_{s\ outlet}$ for the outlet end).

12.2 Selecting boundary conditions in junctions

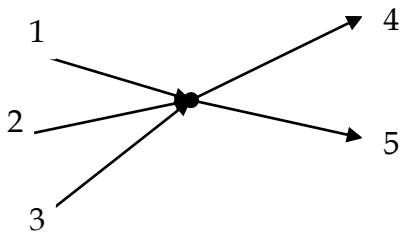


Figure 12.2.1. Junction of 5 pipes.

In chapter 7.3.7, the method of characteristics for liquid flow allowed us to develop boundary conditions for junctions by using simple algebra. The general conservation model we now develop is more complex, and that makes it hard to develop similarly simple correlations. Instead, we are going to borrow some results from power

bond graph theory.

Karnopp and Rosenberg (1974) and subsequent authors have outlined an elaborate theory on how to formulate state equations for various dynamic systems. One of the cornerstones in the theory is the concept of *causality*, the theory clarifies how to keep account of what is *cause* and what is *effect* for all state variables throughout various dynamic systems. When we apply the causality concept to a junction, where all pressures must be equal, the bond graph theory tells us only one pipe can decide what the pressure will be, while the others have to comply with that pressure as 'slaves'. One pipe provides the pressure source, while the others provide mass flow sources. This is not a way to grant one pipe more authority than the others, but simply a method of formulating the system equations without accidentally over- or under-specifying parts of it. It does not matter which pipe is selected to be 'master' of pressure (and therefore 'slave' when it comes to flow) in each junction, the result is going to be the same, only the way of formulating the equations are different.

When we are developing a general pipe network simulation program, focusing on causalities allows us to structure the program very efficiently. We simply create a general pipe-class which can accept either a known pressure or a known flow at each end in the way it was outlined in chapters 12.1.1 - 12.1.3. Every pipe in the system is represented as an object which is an instance of the same pipe class. In each junction, we allow one pipe to play the role of the pressure source, while the others are mass flow sources.

Suppose, for instance, that *pipe 4* is chosen as pressure source for the junction in figure 12.2.1. Since *pipe 4* decides the pressure, it cannot also decide its own mass flow at the same end, and is instead forced to accept the mass flow from the other pipes. As the situation appears when seen from *pipe 4*, it is therefore connected to a 'known flow' at its inlet. That flow is taken directly from the other pipes in a way which satisfies continuity:

$$(\rho v)^4{}_{in} = \frac{A^1}{A^4}(\rho v)^1{}_{out} + \frac{A^2}{A^4}(\rho v)^2{}_{out} + \frac{A^3}{A^4}(\rho v)^3{}_{out} - \frac{A^5}{A^4}(\rho v)^5{}_{in} \qquad (12.2.1)$$

where A is the cross-sectional area. For the pressures, all other pipes have to accept the pressure decided by *pipe 4* so that:

 For non-commercial use only

$$p^1{}_{out} = p^2{}_{out} = p^3{}_{out} = p^5{}_{in} = p^4{}_{i=0} \tag{12.2.2}$$

The temperature in the node is a consequence of the mixing which takes place there, as was explained for liquids in chapter 9.3.2. In the general case, we have:

$$E_{mix} = \frac{\sum_{All\ inflowing\ \ k} E^k (\rho v)^k A^k}{\sum_{All\ outflowing\ \ k} (\rho v)^k A^k} \tag{12.2.3}$$

The fluid's energy is E_{mix} in the node. When that fluid flows into branches, the inlet enthalpy must comply with equations 10.1.8, 10.1.2, and the temperature can thereafter be calculated from equation 10.1.4 (or its 10.7.2-variant). Suppose, for instance, a situation where all flow directions are positive, so the fluid flows as assumed in figure 12.2.1 for all branches. For *pipe 4*, that would mean:

$$h_{mix} = \frac{E_{mix} - p}{\rho_{mix}} - \frac{1}{2}\left[\frac{(\rho v)^{k=4}}{\rho_{mix}}\right]^2 - g z_{node} \tag{12.2.4}$$

The temperature then follows from the fluid's properties according equation 10.1.4 (or the variant of it shown in equation 10.7.2).

This would mean that *pipe 4* experiences *boundary condition 3*, as explained in chapter 12.1.3. If the flow direction changes for pipe 4, it will experience *boundary condition 4*. Pipe 5, on the other hand, experiences *boundary condition 1*, but that would of course change to *boundary condition 2* if the flow reverses. For *pipes 1, 2* and *3*, we have to use *boundary condition 2*, but must change it to *boundary condition 1* in case the flow changes direction.

12.3 Other boundary conditions

The same causality considerations can be used to handle any other boundary conditions. All component inserted into the system, be it valves, compressors, pumps, pigs, accumulators or anything else, must generally always act as either the pressure or

the mass flow sources. They can always be modeled in a way that fits our standard pipe object.

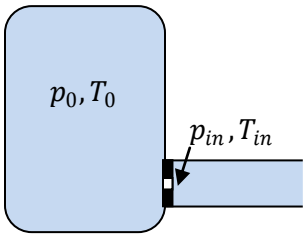


Figure 10.6.4. Choke at pipe inlet.

As an example, let us consider a simple nozzle at the inlet of a pipe. For simplicity, we assume perfect gas, that the friction can be neglected in the nozzle, and that the flow is subsonic. In that case, ρv is known from gas dynamics to be:

$$(\rho v) = \frac{1}{A_{nozzle}} \frac{2\kappa}{\kappa - 1} p_0 \left[1 - \left(\frac{p_{in}}{p_0} \right)^{\frac{\kappa-1}{\kappa}} \right] \qquad (12.3.1)$$

We are free to choose the nozzle's causality as we wish, but the form it is written on makes it most convenient to have it decide the mass flow into the pipe. That makes the pipe experience *boundary condition 3* at the inlet. It means the pipe object will return p_{in}, while the equation 12.3.1 can be used to calculate the mass flow directly.

The temperature, which is also required at the pipe inlet, drops as the gas accelerates towards the nozzle, but increases again when the gas (nearly) stagnates at the other side. Since this is a perfect gas, those two effects cancels each other out, and some distance behind the nozzle, $T_{in} = T_0$.

Making similar models for other components is straight forward.

References

Karnopp, D. C., Rosenberg, R. C. (1974): *System Dynamics, a Unified Approach.* John Wiley & Sons, Inc.

 For non-commercial use only

"Simplicity is the ultimate sophistication."
Leonardo da Vinci

13 Filling the ghost cells by using the boundary conditions directly

This chapter shows an alternative, novel way to fill in ghost cell values:

- General principle
- How it works for flow sources
- How it works for pressure sources

13.1 General philosophy

In chapter 11, we presented several methods for inserting values into the ghost cells. Those methods work relatively well, but we saw that they had some considerable disadvantages: Stability considerations prevented us from taking $\partial\rho/\partial t$ and $\partial E/\partial t$ into account when filling them. We must expect that to have a negative impact on accuracy at times when those two terms become relatively large at the boundaries.

An alternative approach is to start out by asking this question: Which values do the primary variables in the ghost cells need to have in order to impose the correct boundary values on the outermost cell boundaries? Answering this means going into how the method in question (we focus on KT3) uses the boundary values. Since we already have discussed the various boundary conditions in chapter 12, as well as the KT3 method in chapter 10, it is possible to pursue this approach.

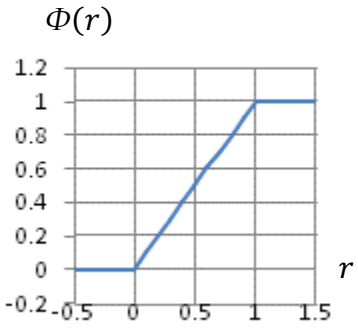


Figure 13.1.1. The Minmod limiter

Consider the already mentioned Minmod limiter described by:

$$\Phi(r) = Max[0, Min(1, r)] \tag{13.1.1}$$

If we focus on the part where $0 \leq r \leq 1$, we see that $\Phi(r) = r$. For such values of r, we can ignore the limiter function. We recall that r was defined as:

$$r_i = \frac{Y_i - Y_{i-1}}{Y_{i+1} - Y_i} \tag{13.1.2}$$

If we insert 13.1.2 into equations 10.5.1 and 10.5.2, we get:

$$Y^L{}_{i-1/2} = 0.5Y_{i-1} + 0.5Y_{i-2} \tag{13.1.3}$$

$$Y^R{}_{i-1/2} = 0.5Y_i + 0.5Y_{i+1} \tag{13.1.4}$$

This tells us there are three cells contributing to the conditions at the left boundary of cell *i*: Cell *i-2*, cell *i-1,* and cell *i* itself. If cell *i* happens to be the first real cell at the pipe inlet (corresponding to *i=2* when we start indexing *i=0* for first ghost cell), it means that equations 13.1.3 and 13.1.4 must satisfy the boundary conditions. For some situations,

 For non-commercial use only

this can actually be solved if we also require the left and the right computations to give the same result:

$$Y^L{}_{i-1/2} = Y^R{}_{i-1/2} \tag{13.1.5}$$

Even though equations 13.1.3 and 13.1.4 are not strictly valid outside $0 \leq r \leq 1$, limiting does not happen most of the time, and the method works well in practice.

In the following, we will see what that means for the two main types of boundary conditions: Flow and pressure sources.

13.2 Mass flow source

If the pipe inlet has a source mass flow $(\rho v)^L{}_{s\ inlet} = (\rho v)^R{}_{s\ inlet} = (\rho v)_{s\ inlet}$, equations 13.1.3 and 13.1.4 become:

$$(\rho v)_{s\ inlet} = 0.5(\rho v)_{i-1} + 0.5(\rho v)_{i-2} \tag{13.2.1}$$

$$(\rho v)_{s\ inlet} = 0.5(\rho v)_{i} + 0.5(\rho v)_{i-1} \tag{13.2.2}$$

This can be solved so that the mass flows for the two ghost cells become known:

$$(\rho v)_{i-1} = 2(\rho v)_{s\ inlet} - (\rho v)_{i} \tag{13.2.3}$$

$$(\rho v)_{i-2} = 2(\rho v)_{s\ inlet} - (\rho v)_{i-1} \tag{13.2.4}$$

13.2.1 Inflowing fluid

If the fluid flows in a positive direction, meaning into the end defined as the inlet end, the inlet temperature is also a source. Even though the temperature is not a primary variable, it is logical to extrapolate it in the same way as the mass flow so that:

$$T_{i-1} = 2T_{s\ inlet} - T_i \tag{13.2.5}$$

$$T_{i-2} = 2T_{s\ inlet} - T_{i-1} \tag{13.2.6}$$

We are not claiming that the temperature of the fluid about to flow into the pipe depends on the temperature inside the pipe; that would be physically impossible. What we are saying is simply that the selected ghost cell temperature is 'designed' to produce as accurate results as possible when it later takes part in calculating the (known) boundary temperature.

We need to know one more variable in the ghost cells before all primary and secondary variables can be determined. Since no more variables are given directly by the boundary conditions, we need to adapt a different strategy for the last variable. One strategy which seems to work well is to extrapolate the pressure from known values in the nearest real cells. We may use the Taylor expansion explained in equation 11.3.1. We can see directly from that equation that if we include all terms up to and including the second order derivative, we get a third order approximation (since Δx occurs in the third power for in the first ignored Taylor-term). The two lowest order derivatives can be estimated directly as:

$$\frac{\partial p_i}{\partial x} = \frac{p_{i+1} - p_i}{\Delta x} \tag{13.2.7}$$

$$\frac{\partial^2 p_i}{\partial x^2} = \frac{\frac{p_{i+1} - p_i}{\Delta x} - \frac{p_i - p_{i-1}}{\Delta x}}{\Delta x} = \frac{p_{i+1} - 2p_i + p_{i-1}}{(\Delta x)^2} \tag{13.2.8}$$

 For non-commercial use only

It is actually very easy to estimate at third order derivative, too, and it seems to have some stability benefits. The third order derivative cannot be estimated directly around cell i, but it can easily be calculated at location $i+\frac{1}{2}$, which is near enough to be taken as an estimate for location i:

$$\frac{\partial^3 p_i}{\partial x^3} = \frac{\frac{\partial^2 p_{i+1}}{\partial x^2} - \frac{\partial^2 p_i}{\partial x^2}}{\Delta x} = \frac{p_{i+2} - 3p_{i+1} + 3p_i - p_{i-1}}{\Delta x} \tag{13.2.9}$$

This leads to:

$$p_{i-1} = \frac{9}{4}p_i - \frac{3}{2}p_{i+1} + \frac{1}{4}p_{i+2} \tag{13.2.10}$$

$$p_{i-2} = \frac{9}{4}p_{i-1} - \frac{3}{2}p_i + \frac{1}{4}p_{i+1} \tag{13.2.11}$$

Once both p and T are known in each ghost cell, ρ is of course determined by the fluid's properties, for instance the one by equation 10.7.3. The last primary variable, E, then follows from equations 10.1.8 and 10.1.2:

$$E = \rho\left[u + \frac{(\rho v)^2}{2\rho^2} + gz\right] - \mathrm{p} \tag{13.2.12}$$

13.2.2 Outflowing fluid

In case the fluid flows out of the inlet end, the temperature is of course not given by the boundary conditions as described by equations 13.1.9 and 13.1.10. In that case, we may extrapolate the temperature in the same way as the pressure, or we may alternatively extrapolate both ρ and E directly. Choosing the first alternative, we simply replace 13.2.5 and 13.2.6 with equations 13.2.13 and 13.2.14 when the flow reverses:

$$T_{i-1} = \frac{9}{4}T_i - \frac{3}{2}T_{i+1} + \frac{1}{4}T_{i+2} \tag{13.2.13}$$

$$T_{i-2} = \frac{9}{4}T_{i-1} - \frac{3}{2}T_i + \frac{1}{4}T_{i+1} \tag{13.2.14}$$

At the outlet end, we get a similar set of equations, with some minor differences due to the ghost cells lying to the right of the last real cell. Equations 13.2.1 and 13.2.2, for instance, change to:

$$(\rho v)_{i+1} = 2(\rho v)_{s\ outlet} - (\rho v)_i \tag{13.2.15}$$

$$(\rho v)_{i+2} = 2(\rho v)_{s\ outlet} - (\rho v)_{i+1} \tag{13.2.16}$$

Where $i = Nx + 1$. Similarly, the pressure extrapolation changes to:

$$p_{i+1} = \frac{9}{4}p_i - \frac{3}{2}p_{i-1} + \frac{1}{4}p_{i-2} \tag{13.2.17}$$

$$p_{i+2} = \frac{9}{4}p_{i+1} - \frac{3}{2}p_i + \frac{1}{4}p_{i-1} \tag{13.2.18}$$

13.3 Pressure source

This is very similar to what has been explained for pressure mass flow source in chapter 13.2. The pressure source is set as:

 For non-commercial use only

$$p_{i-1} = 2p_{s\ inlet} - p_i \tag{13.3.1}$$

$$p_{i-2} = 2p_{s\ inlet} - p_{i-1} \tag{13.3.2}$$

The temperature is given by equation 13.2.5 and 13.2.6 for inflowing fluid, and by 13.2.13 and 13.2.14 for discharging fluid. The third variable can be the velocity, extrapolated as:

$$v_{i-1} = \frac{9}{4}v_i - \frac{3}{2}v_{i+1} + \frac{1}{4}v_{i+2} \tag{13.3.3}$$

$$v_{i-2} = \frac{9}{4}v_{i-1} - \frac{3}{2}v_i + \frac{1}{4}v_{i+1} \tag{13.3.4}$$

We then have all the secondary variables in the ghost cells, and the primary variables can be found directly from the property equations 10.1.3, 10.1.4, as well as 10.2.8, 10.1.8 and 10.1.2.

References

Godunov, S, K. (1959): *A Difference Scheme for Numerical Solution of Discontinuous Solution of Hydrodynamic Equations*, Math. Sbornik, 47, 271-306, translated US Joint Publ. Res. Service, JPRS 7226, 1969.

Leveque, R.J. (2002): *Finite Volume Methods for Hyperbolic Problems.* Cambridge University Press.

Coelho, R.M.L., Lage, P. L. C., Silva Telles, A. (2006): *A Comparson of Hyperbolic Solvers for Ideal an Real Gas Flows.* Brazilian Journal of Chemical Engineering, April 19.

"As far as we know, our pipe flow simulation software has never made an undetected error."
Tim Weisert, modified

14 Simulation results and program testing

Ways to test simulation results against known physical laws:

- Simulation examples with plot of revealing parameters
- The Joule-Thomson effect
- Rupture simulations
- Cooling after a gas pipeline is shut down
- Test against commercial software packages
- Result testing checklist for the fully transient simulations

14.1 Simulating one of the world's longest gas pipelines

Transient pipe flow simulations, especially gas simulations, are relatively complicated, and there is always some scope for errors. Whether we are developing the simulation program ourselves or using off-the-shelf simulation software, we generally want to have ways of testing results. If measurements are available, we should of course use

For non-commercial use only

them as a reference. Else, we need other ways of testing. In chapter 7.4.2, we looked at various simple tests we can perform to check the results when simulating liquid transients. Similar tests can be used for gas transients, too. When used systematically, such tests enable us to detect most of the errors we are likely to encounter.

Let us start by simulating the same pipeline as was considered manually in chapter 6.4.2. We recall that for the *813 km* long pipeline with a diameter of *966.4 mm*, an inlet pressure of *15 MPa* and outlet pressure of *9.6 MPa*, When we used equation 6.4.17, we found that we would get a steady-state mass flow of around *318 kg/s* if the pipeline is horizontal and if the flow is isothermal.

Gas	Molar %
N_2	1.37
CO_2	1.38
Methane	87.42
Ethane	6.97
Propane	2.13
Isobutane	0.30
Butane	0.25
Ipentane	0.06
Pentane	0.03
Hexane	0.09
Sum	**100**

Table 14.1.1. Gas composition.

The gas composition is a shown in the table to the left. This determines $p(T,\rho)$ and $h(T,\rho)$, even though the details of how to establish those properties are outside the scope of this book. As mentioned earlier, there are books, standards, tables and dedicated software available to assist with that. Some of the property data are shown graphically in figures 14.1.1-14.1.3.

The average dynamic viscosity *is* $\mu = 16.9 \cdot 10^{-6}$ kg/(m·s²), as before, the gas' average Prandtl number *Pr = 1.2,* and the average thermal conductivity k_f*=0.03* W/(m·K).

The pipeline is coated with a *70 mm* layer of weight concrete having a thermal conductivity around *1.2 W/(m·K)*, and we assume the current perpendicular to it to be 0.5 m/s. For simplicity, we neglect the elevation; it has only minor influence on the capacity in this case anyway.

We set the number of cells, *Nx*, to 100. That is a very low number for such a long pipeline, but as we will see later, our method's high order makes it sufficient for many sorts of simulations.

The inlet temperature is chosen identical to the seawater temperature at 273 K.

The simulations are carried out using the *Minmod* limiter and a fourth-order variable step-size Runge-Kutta integration method (RK4-5). The ghost cell filling method is the one described in chapter 13. Since the pipe is hydraulically smooth for the Reynolds numbers we encounter, it does not matter which uniformity factor we use for the pipe surface in equation 2.9.4. Starting conditions are set to *9.6 MPa* pressure in the entire

pipeline, and the gas is initially at rest. At time $t = 0$, the pressure at the inlet is increased linearly to *15 MPa* during $2 \cdot 10^5$ *s* (*2.3 days*) as the gas slowly accelerates towards normal production flow, followed by $8 \cdot 10^5$ *s* (*9.3 days*) of steady-state operation.

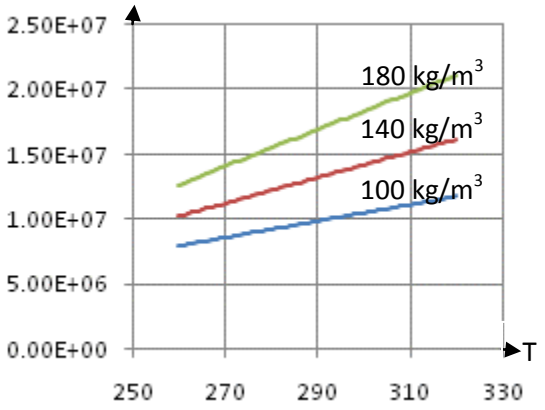


Figure 14.1.1. Pressure as function of temperature for 3 different densities.

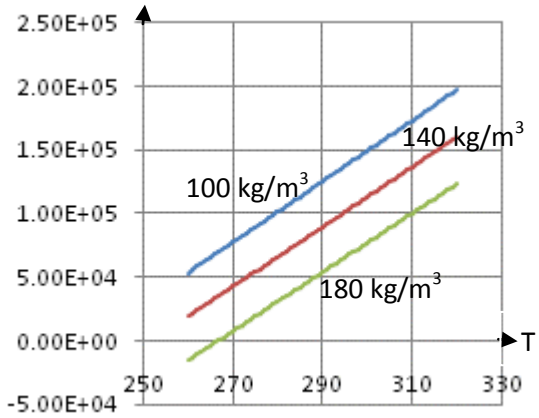


Figure 14.1.2. Enthalpy as function of temperature for 3 different densities.

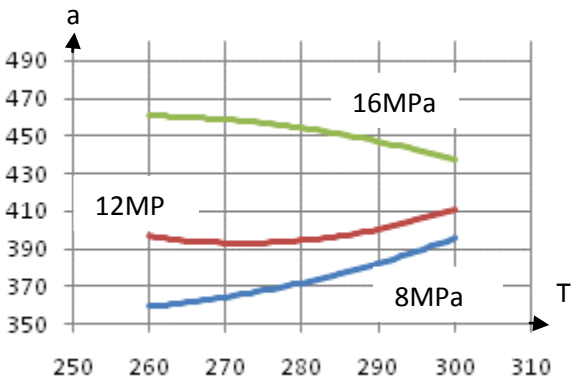


Figure 14.1.3. Speed of sound as function of temperature for 3 different pressures.

For non-commercial use only

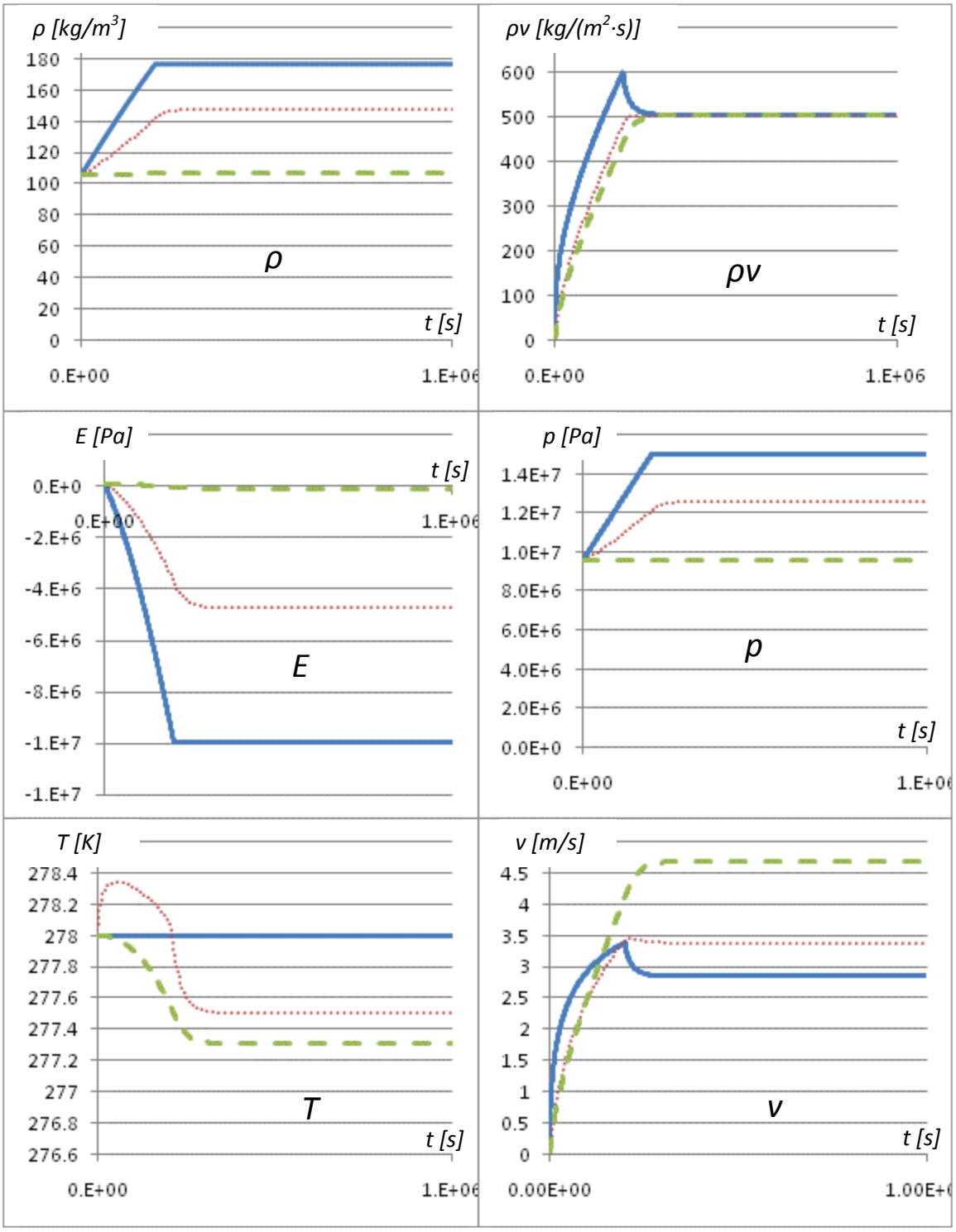


Figure 14.1.4. Simulation results. The 3 primary and 3 secondary variables plotted as function of time from t = 0 to t = 10^6 s (nearly 12 days). Solid line is inlet, dashed line outlet, and dotted line is at the middle of the pipe.

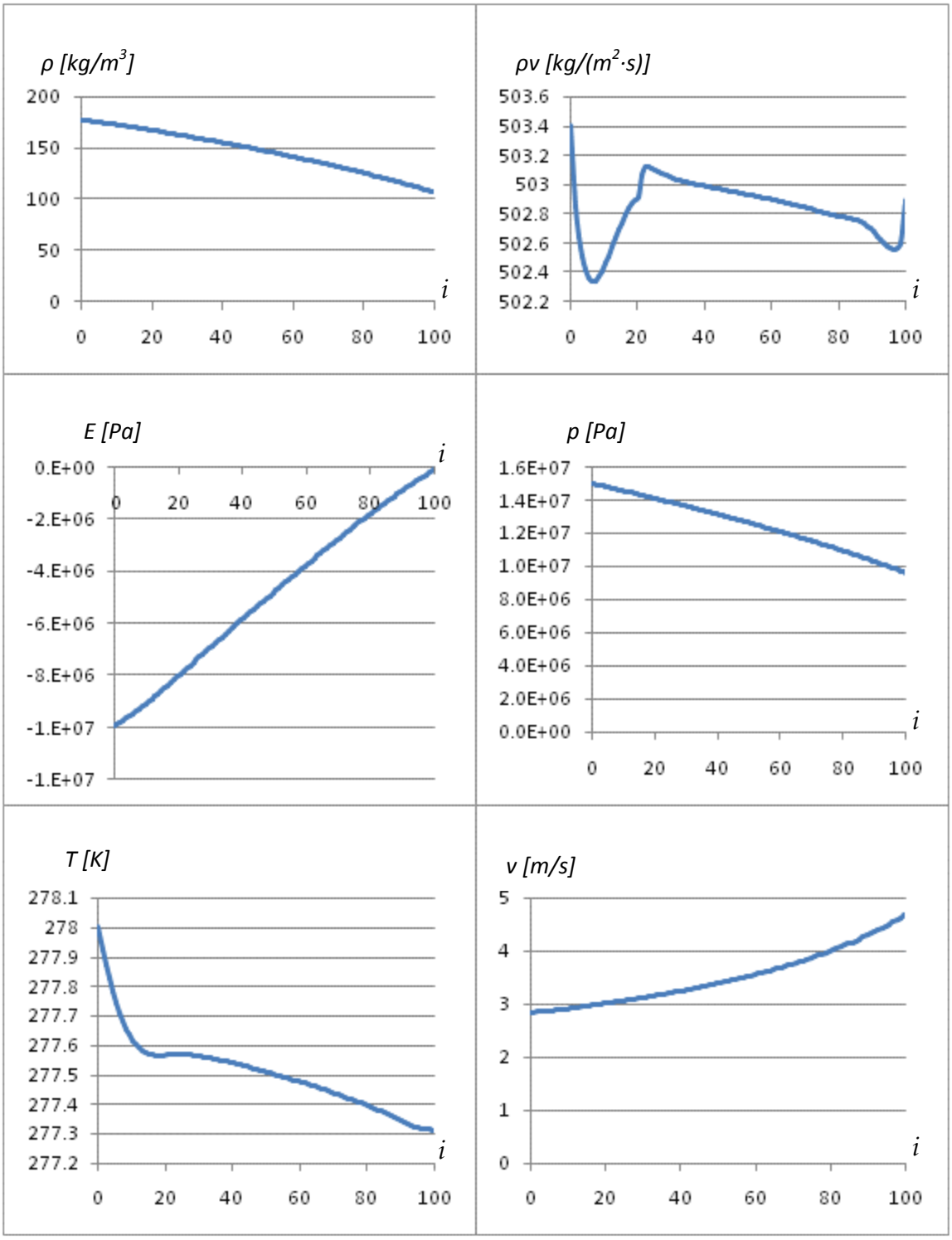


Figure 14.1.5. Simulation results. The various parameters' distribution along the pipeline from inlet (left-hand side) to outlet (right-hand side).

For non-commercial use only

The simulations were done with all fluid properties as well as the Darcy-Weisbach friction factor updated for every function call. The full simulation, covering 11.6 days of pipeline operation, was done in less than an hour on a relatively cheap laptop computer bought in 2007.

We are using a very slow pressurization in this example, and we can see from the results in figure 14.1.4 that the gas mass flow increases steadily as the inlet pressure rises. At the beginning, the inlet mass flow is larger than the outlet flow, since some additional gas is stored in the pipeline as the average pressure increases. Within hours after the increase has stopped, the mass flow stabilizes and becomes close to constant in the whole pipeline. This is in fact one of the reliable checks we are able to perform for the simulations. The mass flow has to become constant in the whole line as we approach steady-state. Whether that actually happens in our simulations can be seen more clearly from figure 14.1.5, where the mass flow has been plotted along the pipeline at the end of the simulations. Even though the variations have been scaled up to make them more visible, we see that they are very small: $\rho v = 502.8 \pm 0.6$ kg/(s·m²) – a variation of only 0.12%.

The temperature turns out to be fairly constant, showing that a thin layer of weight concrete does – as expected - not offer much thermal insulation for such a long pipeline. In this particular case, it would therefore have been a good approximation to assume isothermal flow and do away with the energy equation from the start.

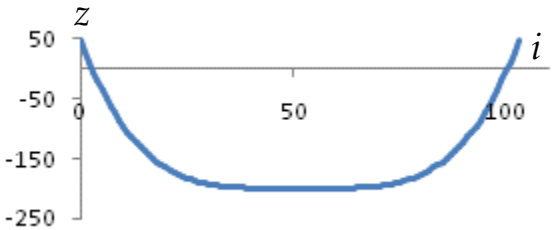


Figure 14.1.7. Pipe elevation profile, including elevation for ghost cells.

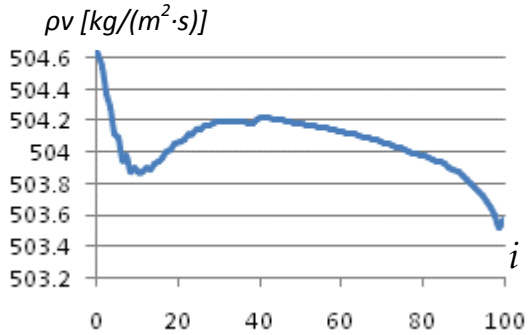


Figure 14.1.8. Pipe elevation profile taken into account.

If we multiply the steady-state ρv with the pipe's cross-sectional area, we get *369 kg/s*. That is very close to the *362 kg/s* we came up with when using equation 6.4.17 in chapter

6.4. Comparing steady-state simulation results with equation 6.4.17 is one of the useful checks we can make for most types of gas flow. That equation is only valid for horizontal, isothermal flow, which happens to be what we have here, but the results are not very different even if these conditions are not fully met, so equation 6.4.17 is useful in any event. The example below throws some light on how large role the elevation profile plays.

If we assume the pipe elevation profile to be as shown in figure 14.1.7, we see that the mass flow increases only around *1 %* compared to the simulations where elevations were neglected. For such moderate elevations as these, the influence is minimal, but that can of course be different for mountain crossings or considerably deeper sea beds. Note that in order to be able to do the simulations with such a small number of cells, we have had to make sure the ghost cells have elevations which are natural extensions of the actual profile, so that the ghost-part of the pipe continue the same way the pipe ends are pointing. If care is not taken to assure this, a significant increase in error can be expected.

14.2 Gas temperature in insulated pipelines

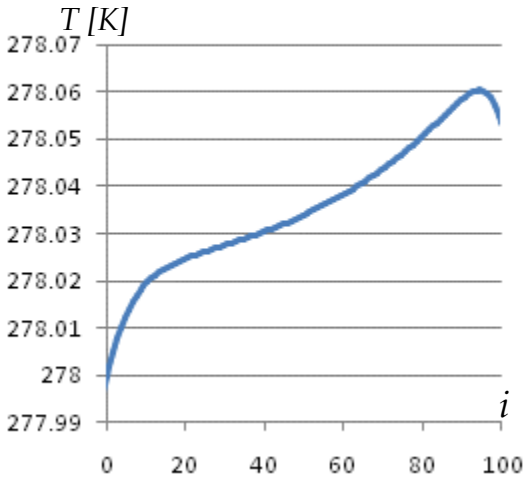


Figure 14.2.1. Simulated temperature profile for a perfect gas, steady-state flow and infinite thermo-insulation around the pipe.

We know from thermodynamics that a fluid flowing from one reservoir through a nozzle or a pipe maintains its enthalpy if no external work or heat is added to or taken out of the flow. For a perfect gas, that means the temperature remains constant. Our pipeline is poorly insulated and heat is obviously exchanged with the surrounding sea. But for the sake of verifying that the simulations agree with physics in this respect, we can remove the heat loss by simply setting the insulation's thermal conductivity to zero or near zero, or we can remove the heat loss terms if our program allows us to.

 For non-commercial use only

In figure 14.2.1, everything is as for the example in figure 14.1.4, except the heat exchange with the environment is set to zero, and the gas is modeled as perfect. When taking the amplified vertical scale into account, we see the temperature actually stays very close to constant as expected.

For a real gas, this does not have to be so. We remember that the enthalpy h can be expressed as a function of T and ρ, and that also p is a function of T and ρ. It is therefore obviously true that T is correlated to p and h in such a way that $T = T(p,h)$.

How much the temperature changes when the pressure changes while the enthalpy stays constant is therefore a fluid property we can determine by looking at a factor μ_J defined as:

$$\mu_J \stackrel{\text{def}}{=} \left(\frac{\partial T}{\partial p}\right)_h \tag{14.2.1}$$

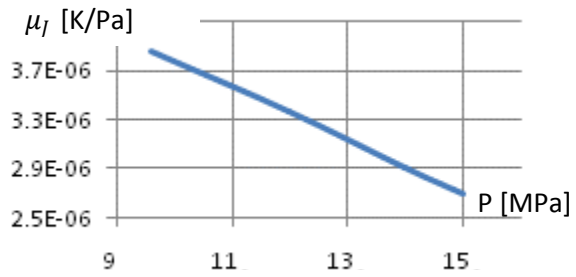


Figure 14.2.2. Joule-Thomson coefficient μ_J as a function of pressure in MPa.

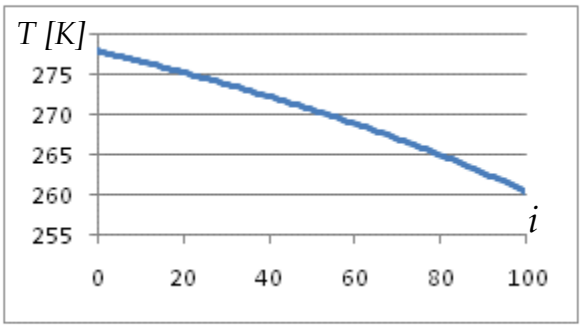


Figure 14.2.3. Simulated temperature profile for a real gas, steady-state flow and infinite thermo-insulation around the pipe.

The factor is called the *Joule-Thomson coefficient*, and we can easily determine it for our particular gas by combining the data in figures 14.1.1 and 14.1.2. By doing so, we get the curve in figure 14.2.2.

In our pipeline, where the pressure drops from *15* to *9.6 MPa*, the average μ_J is going to be around $3.27 \cdot 10^{-6}$ K/Pa. Setting $\Delta p = -5.4 \cdot 10^6 Pa$, equation 14.2.1 leads us to expect a temperature drop of around $\Delta T = -5.4 \cdot 3.27\ K = -17.6\ K$ if the pipeline is perfectly insulated. This gives us yet another opportunity to verify the simulations.

The simulation results in figure 14.2.3 shows the temperature drops from the

inlet temperature, *278 K*, to an outlet temperature of *260.4 K* as it travels through the pipeline. That happens to be a temperature drop of *17.6 K*, exactly as expected from the manual calculation.

14.3 Simulating pipe rupture

Simulating pipe rupture has several challenges compared to most other simulations: The velocity can reach the speed of sound so choking occurs, and the temperature may drop so much that the gas starts to form droplets, making the flow multi-phase rather than single-phase. The last situation can obviously not be handled properly with a single-phase simulation program, but it can at least tell us whether we approach the conditions where multi-phase flow would occur. What happens in detail after that can only be calculated with a multi-phase simulation program, but our single-phase program can give us important clues.

Simulating the situation occurring when we approach speed of sound, we encounter two challenges.

First, we know gas flowing through a pipe cannot exceed the speed of sound, choking prevents that from happening. But is this effect built into our model, or must we manually check the gas's velocity at each time step and limit it artificially if it approaches the speed of sound? It is well known that the traditional liquid flow model described in chapter 7 does not limit the speed automatically. The reason is that the Allievi-simplifications have removed the physical foundation for choking. But the model we use here relies on fewer simplifications, and it automatically replicates choking conditions. All we have to do is simply to simulate normally, and speeds higher than the speed of sound is not going to occur simply because the model we use has the relevant part of the physics built into it. We could easily test that by removing the friction and increasing the inlet pressure to see how high velocities the model allows us to create.

Second, each cell is very long in our *813 km* pipeline, no less than *8.13 km* if we choose to use only *100 cells*, as we did in the simulations shown in figures 14.1.4 and 14.1.2. In case of a rupture, it is the gas nearest the rupture which will experience the most dramatic temperature fall and the highest speed. The model can obviously not reproduce that if the steepest velocity gradient occurs in a small part of one single cell. We would therefore need to have much shorter cells near the rupture to get realistic results.

 For non-commercial use only

To illustrate this problem, let us first do a simulation with $N_x = 400$, meaning each cell is around 2 km long. Suppose the pipe is cut near one of the ends, but at *190 m* depth under the sea's surface where the outside pressure is around $2 \cdot 10^6$ *Pa*. The pipeline is pressurized to *9.6 MPa* before the rupture, and the gas is assumed to be at rest. We are interested in what happens without any operator or control system intervention, meaning no valves are being closed down to limit the damage.

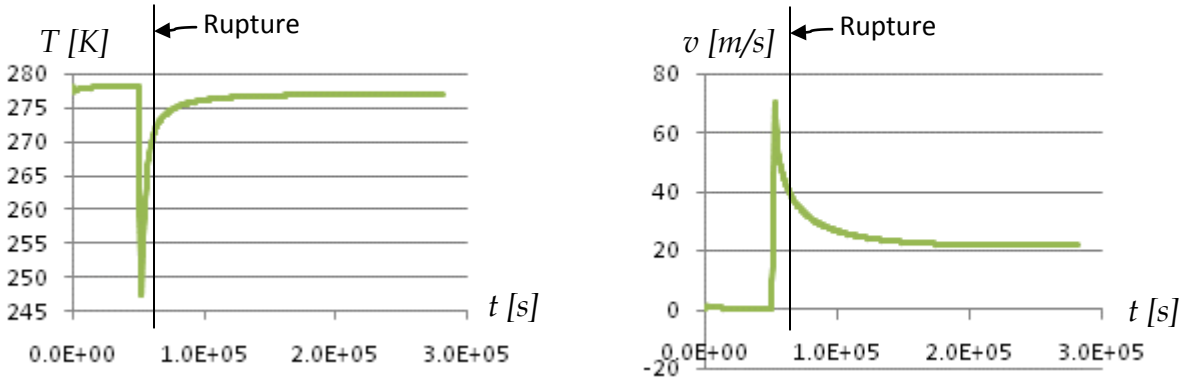


Figure 14.3.1. Simulated temperature and velocity by the rupture as a function of time. The rupture is assumed to be near the pipe outlet at 200 m depth, and the plots are relevant to the upstream part of the ruptured pipeline.

Figure 14.3.1 shows the results. The steady-state velocity seen after $2 \cdot 10^5$ *s* is the result of the inlet pressure being kept constant at *9.6 MPa* even after the rupture occurred – not exactly what most responsible operators would allow, but simply what we decided to investigate here.

The most important result is that peak flow starts to recede almost immediately after it was reached, and the most extreme flow lasts for around 10^4 s, which is only 2-3 hours. Given that such a catastrophic event would take days or weeks to deal with in a pipeline as long as this one, the error due to limited resolution near the rupture is not really significant when it comes to forecasting the damage. But for the sake of understanding the physics at work here, it is worth pointing out that the model cannot possibly be accurate during those first hours: In a real situation, the velocity would have reached the speed of sound when the outside pressure is this much lower than the inside pressure. The model fails to show that simply because of the limited resolution we have used. A finer grid would have lead to more accurate results, but it would also capture an even larger temperature reduction closest to the rupture (it can be seen to fall to around *242 K* at figure 14.3.1). When trying that out (not included here), we see that

even a modest increase in N_x leads to the temperature falling so much that it results in condensation. That means a rupture would lead to multi-phase flow locally, and our single-phase model would run into problems if trying to simulate that in detail. Simulating with a very fine grid is therefore not really useful in this case.

14.4 How cooling affects the flow after shutdown

Let us consider the long pipeline from chapter 14.1 once again. We use slightly different boundary conditions this time: The outlet is connected to a mass flow source, meaning a particular mass flow is taken out of the outlet end. It is at first set to *503 kg/s*. At the inlet, we have a constant pressure of *15 MPa*. If we compare these data with what we had in chapter 14.1, we see that they are virtually identical, the only difference being that we have changed the causality at the outlet. But we have done it so that the mass flow we impose is the same as we got as response when we used a pressure source of *9.6 MPa* at the outlet. Therefore, we expect the same pressure to arise this time, too. This is actually one of the tests we are able to do to check the simulations: Comparing simulations with causalities chosen differently and see that they agree. Poorly specified boundary conditions tend not to.

The system is allowed to operate for a long time so the flow becomes steady-state. 10^4 *s* after the plotting was started, we close the outlet.

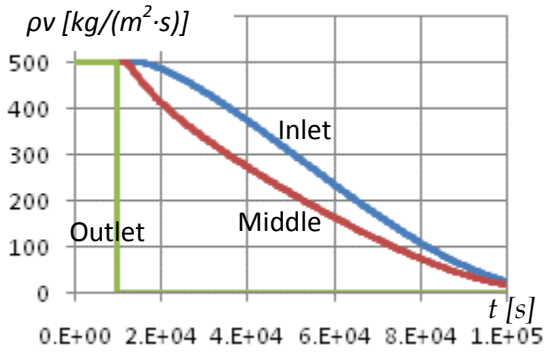


Figure 14.4.1. Specific mass flow as function of time.

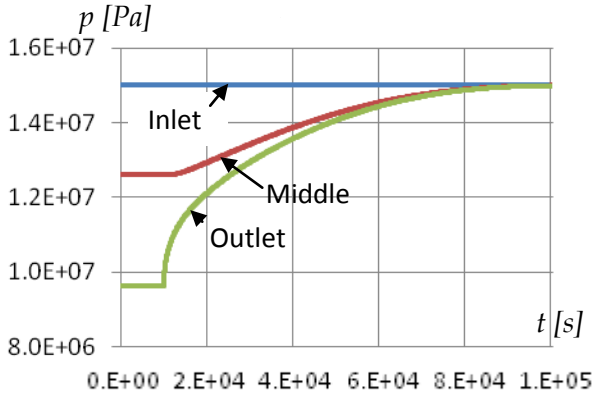


Figure 14.4.2. Pressure as a function of time.

 For non-commercial use only

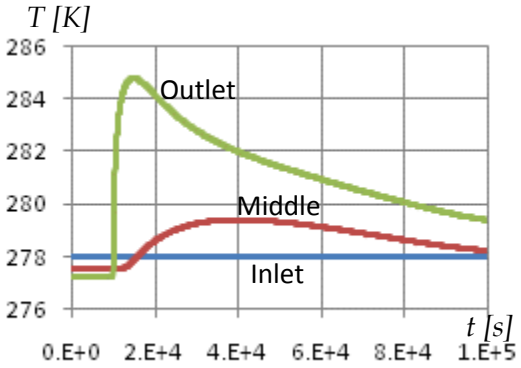


Figure 14.4.3. Temperature as function of time.

The results show the steady-state outlet pressure before closure is around *9.6 MPa*, as expected. After the outlet has been closed, the inlet flow gradually decreases as the pressure approaches *15 MPa* in the whole pipeline. The temperature plot in figure 14.4.3 shows that the outlet closure at first leads to a temperature increase of *6 K* or so, but the temperature falls back to the same temperature as the environment as cooling takes effect.

Let us now compare these results to what would have happened if the pipeline was perfectly insulated. We simply set the thermal conductivity K_f= *0.0 W/(m·K)* and repeat the simulations.

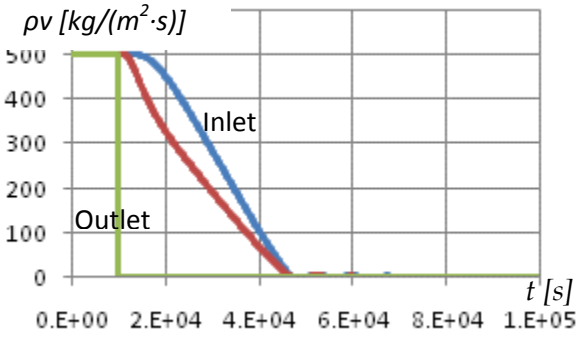


Figure 14.4.4. Specific mass flow as function of time.

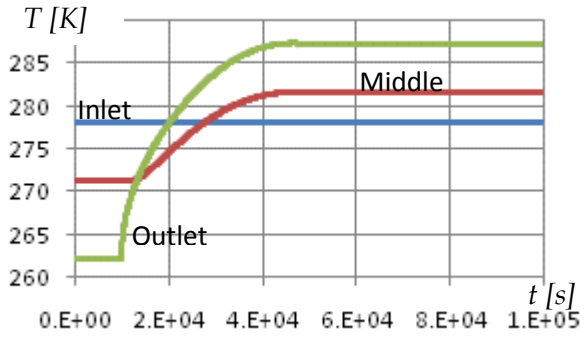


Figure 14.4.5. Temperature as function of time.

As explained in chapter 14.2, the Joule-Thomson effect leads to a significant temperature difference for the steady-state flow when the pipe is so well insulated. Also as expected, time is not going to even out the temperature differences when no heat can go through the pipe wall. But there is another striking difference compared to the results in figures 14.4.1-14.4.3: In the perfectly insulated pipe, the gas comes to rest much faster after pipe closure. This shows that it is the gradual cooling which keeps the fluid moving long after it would otherwise have fallen to rest. It gives us a feeling for how much even minute temperature changes affect the flow in a very long, shut-down

pipeline. We recall the heat equations, as described in chapter 8, relies on the fluid not being completely at rest, or else they are going to be invalid. Since even tiny temperature changes turn out to create considerable flow in a gas pipeline, our model is going to be valid for most practical situations.

14.5 Comparing with other simulation programs

When more than one simulation program is available, it can help to use several and see how well the results compare. Be aware, however, that some of the commercially available programs have been developed by the same developers even when they a marketed under different brand names, so it is important to know whether one actually compares with a different one as intended.

We have chosen two of the most well-known commercial steady-state multi-phase simulation programs to compare our results from chapter 14.1 with. Our gas flow example is of course single phase flow, but multi-phase simulation programs can also handle single-phase flow.

Interestingly, one of the tested programs requires input data in a way which may at first glance appear to violate the causality theory outlined in chapter 12: It requires both pressure and mass flow to be given at the same pipe end. That sounds as if the program imposes a pressure and mass flow source at the same end simultaneously, which is physically impossible. At the other end, it does not impose any sources at all, which seems equally impossible. But since steady-state means the mass flow is constant in the whole pipeline, the mass flow given at the inlet is going to be the same as at the outlet, so it does not matter which end the flow refers to. Therefore, this is equivalent to having a pressure source at the inlet and a flow source at the outlet, something which is perfectly possible.

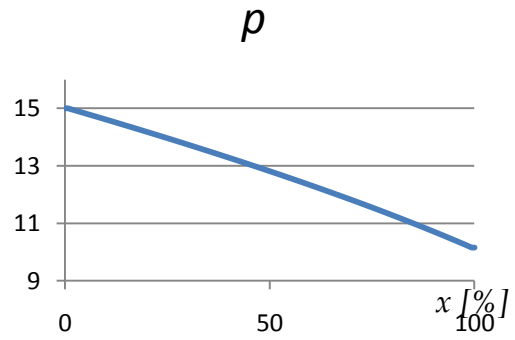


Figure 14.5.1. Simulations, commercial software A.

Results from using the methods described here have been compared to results from *commercial software A*. We saw in chapter 14.1 that the elevation profile was relatively unimportant in this case, and for simplicity, both pipelines have been assumed horizontal.

 For non-commercial use only

The results, figure 14.5.1, are relatively similar to those we got in chapter 14.1, but *software A* results in a somewhat higher downstream pressure: *10.1 MPa*, as opposed to *9.6 MPa* in chapter 14.1. The pressure loss from inlet to outlet differs by as much as *9 %* for the given flow.

We recall this pipeline is hydraulically smooth for the Reynolds numbers we encounter, and also that relatively recently published friction measurements have made it possible to create better Darcy-Weisbach predictions than previously. The inlet Reynolds number is according to *software A* $Re = 2.352 \cdot 10^7$, something which according to AGA report No. 10 (Uhl et al, 1965) leads to $f = 0.007301$, while Colebrook & White (and the Moody diagram) gives $f = 0.007182$, and if using the surface uniformity formulae for $u_s = 1$ gives $f = 0.007485$. We see that the difference between the two last ones is around 4 %, so it could have explained some of the simulation differences, though not all. The remaining 5 % difference must have to do with differences in solution method or gas properties.

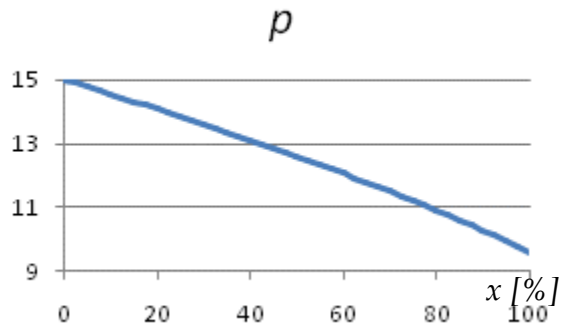


Figure 14.5.2. Simulations, commercial software B

When repeating the simulations with *commercial software B*, which requires us to give the inlet pressures at both ends, we get a mass flow of *376.0 kg/s*, which is only 2 % more than we got in chapter 14.1. *Software B*'s manual states that it uses the Moody diagram to calculate the friction factor, which is not what we used in chapter 14.1, and this can fully explain the difference.

It is of course possible to compare any of the other parameters the simulations produce, too, as well as to simulate modifications of the system. When using *software B* to calculate the temperature reduction for infinite insulation to investigate the Joule-Thomson effect illustrated in figure 14.2.3, it gives a temperature loss of 16.4 K. That is 93 % of what we came up with as plotted in figure 14.2.3.

Interestingly, when using AGA pressure drop calculations, a selectable option in *software B*, the iteration no longer converged, and no results were obtained. This is an example of the fact that even well-renowned and expensive pipe flow simulation programs contain a considerable amount of 'bugs', and evaluating the results is indeed

a very important part of the engineer's job. We will therefore have a closer look at some of the test we can do to check the results.

14.6 How to verify gas flow simulations, an overview

14.6.1 See if the integrations runs at all

As mentioned before, most severe programming and data input errors tend to lead to the simulation program not working at all, at least if an explicit integration method like explicit RK4 is used. This is in itself a good check, if the program runs, chances are the most severe errors have been eliminated.

The type of integration routine used is important to how much we can read out of whether the simulation runs at all. Even implicit methods are not always stable if severe bugs are present, they have their own (admittedly large) stability areas, and the iteration methods they use rely on accurate enough starting values to converge.

If we have problems making the simulation program run properly, simplifying the system is a god strategy. Remove all non-essential components, use a very course grid (low N_x in all pipes), and consider switching off all regulators so valves and pumps are fixed. This is how we should start the modeling process in the first place anyway: Begin with a simplified system and then add complexity after some initial simulations. Also, remember that the physical system itself can be unstable, in which case the simulation 'crash' can be mirroring how the physical system would 'crash', too. Detecting such potential problems is of course one of the reasons why we are simulating.

14.6.2 Do the same checks as for liquid flow.

Most checks for liquid flow simulations, as listed in chapter 7.9, are valid for gas flow, too, but with some modifications. Check No. 2 about verifying the nodes manually, for instance, should also include verifying mixing and resulting temperature, as explained in chapter 12.2.

Check No. 4 regarding the steady-state pressure loss is also somewhat different, since equation 6.4.17 is valid only for horizontal pipes. It is possible to modify it to include elevation terms. That is relatively cumbersome for manual calculations, however, and it is often better to use it as is, and to estimate the elevation's contribution to the pressure as $\bar{\rho} g \Delta z$, where $\bar{\rho}$ is an average density for the pipe in question. Alterntively, the pipe

 For non-commercial use only

may at first be modeled as horizontal in the simulation program simply to make comparison with equation 6.4.17 easy (but of course modeled correctly in the main simulations).

Check 5, investigating whether waves propagate at the speed of sound as calculated by 10.3.16, can be more important here, depending on which spatial discretization one uses. We remember that KT3 uses the speed of sound to calculate $max|\lambda_s|$ according to equation 10.3.7, and this parameter takes part in the numerical method directly the way it was outlined in chapter 10.5. If the program somehow ends up calculating an incorrect speed of sound, that is going to lead to incorrect damping, but it will not affect the propagation speed significantly. Such an error can therefore be detected by comparing the propagation speed coming out of the simulations with the one predicted by equation 10.3.16.

Check 6, the pressure rise after instantaneous valve closure, does not follow equation 7.2.16 when the fluid is a gas. For small pressure steps which do not alter the speed of sound much, however, it is a god approximation, and for perfect gases, simple, accurate correlations between Δp and Δv exist.

14.6.3 Checking the boundary and ghost cell approximations for steady-state flow

As mentioned before, one of the difficulties in using the high order KT3 method is the need for imaginary ghost cells outside the actual pipe. Generating inaccurate or even outright wrong values in these ghost cells is one of the potential error scenarios we want to check against. For steady-state flow, such errors tend to show up as discontinuities near the ends of the pipe for all the variables we compute in each time step. We can easily check that by making plots similar to the ones in figure 14.1.5. The mass flow plot tends to be the most revealing one of those plots.

As an example, let us study the ρv-plot at the top right corner of figure 14.1.5. The vertical scale is amplified, so the tiny variations of ± *0.15 %* around the medium value are not very significant to the results' accuracy. But they do show that something is slightly different near the ends than in the main section of the pipe, particularly at the inlet end. If we use less accurate ways of filling the ghost cells, for instance the ones in equation 11.2.1, we get far worse results, and the continuity equation will appear as violated unless the grid density is increased by several orders of magnitude.

We can do this test for all four types of boundary conditions: Pressure source with both inflowing and outflowing fluid, and flow source with inflowing and outflowing fluid.

14.6.4 Checking the boundary and ghost cell approximations for transient flow

The steady-state test described in chapter 14.6.3 cannot necessarily reveal errors or inaccuracies during the transient simulations. But there are some ways of checking such simulations, too. For instance, we may impose a known flow source at one end, and see if it leads to the mass buildup it is supposed to.

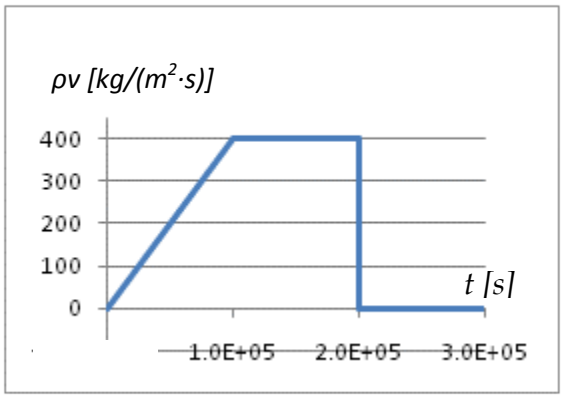


Figure 14.6.1. Specific mass flow source at inlet, example.

To illustrate this, consider a pipe modeled with a mass flow source at the inlet and a pressure source at the outlet. Initially, the pipe is pressurized to *10 MPa*, and the outlet pressure source is also *10 MPa*, the inlet flow source is *0*, and the fluid is at rest. We then start to increase the mass flow source ρv linearly, over 10^5 *s* until it becomes $500\ kg/(s \cdot m^2)$, keep it there for 10^5 *s*, and then abruptly set the flow source back to 0 again, as illustrated on figure 14.6.1.

The outlet pressure is kept at *10 MPa* throughout the process, and we simulate until a new steady-state situation has stabilized. The outlet end is open all the time, so mass flow in upstream and out downstream is eventually going to stabilize at the same value.

What is important here is that we are able to calculate the total mass manually, and that can be compared to the simulation results. Total area-specific mass is obviously $m_A = \left(400\frac{kg}{m2 \cdot s} \cdot 10^5\ s\ \cdot \frac{1}{2}\right) + \left(400\frac{kg}{m2 \cdot s} \cdot 10^5\ s\ \right) = 6 \cdot 10^7 kg/m^2$.

In the simulation model, we simply add an equation for the cell at the outlet boundary, to be integrated in parallel with the other equations:

$$\frac{dm_A}{dt} = (\rho v)_{i+1/2} \tag{14.6.1}$$

 For non-commercial use only

When simulating this system over a very long time, until it has stabilized, the m_A coming out of the simulations shall agree with the one calculated manually.

This test can be done with lots of different specific mass flow source profiles, for instance by also using negative flows. We can also keep the flow source at zero all the time, and vary the pressure source. If we start and end up at the same pressure, we know the net mass flow in and out of the pipe once steady-state has been reached has to become zero.

It is also possible to change the causalities. We may for instance first make a run with the mass flow source shown in figure 14.6.1, and save the resulting inlet pressure. Afterwards, the model's causality is changed so that the pipe inlet has a pressure source. We then make a new simulation run with the pressure source being identical to the pressures we got from the mass flow source simulations. If the simulations are correct, the mass flow profile at the inlet coming out of these simulations should be identical to the one in figure 14.6.1.

14.6.5 Check that the program uses correct fluid properties

Fluid properties can at times be buried quite deep in the simulation program, and it is wise to check the properties manually using tables or other sources. If we compare p, ρ and T, it is obviously possible to check $p(T, \rho)$, and we may also want to have a look at h and check $h(T, \rho)$ in a couple of points.

If we make a simulation run with an infinitely insulated pipe, we are also able to check the Joule-Thompson effect the way it was explained in chapter 14.2. In that example, the pipe was horizontal. Otherwise, elevation would have had to be taken into account, too.

This check of course only helps us find out whether the program uses the same underlying fluid data as is should. It does not tell us anything about whether the fluid's composition is correctly estimated in the first place. Not knowing exactly what the gas consists of is a relatively common problem, and so varying it slightly in order to find out how sensitive the results are to composition uncertainties can be a good idea, too.

14.6.6 Check the heat flow calculations manually

In is in some cases possible to use the heat flow equations from chapter 8 to manually check the heat flow results coming out of the simulation program. It is easiest to do so under steady-state conditions. If the program itself is not steady-state, just run the simulations until pressures, mass flows and heat flows stabilizes. It is best to concentrate on a relatively short section of the pipe so that the temperature is nearly constant for the whole section. With inside and outside temperatures and all other relevant data known from the simulations, it is straight forward to insert it all into the heat flow equations from chapter 8 and see if it adds up.

Transient temperatures can also to some extent be checked by using the approximations shown in chapter 6.4.3.

14.6.7 Increase the velocity until choking occurs

If we are unfamiliar with the design of the simulation program we are using – not an uncommon situation in engineering practice – it can be useful to make choking tests. We simply reduce the friction factor down to zero if it is possible, or we may increase the inlet pressure or mass flow enough to see whether it is possible to increase the fluid's speed beyond the speed of sound. That is not physically possible in a pipe, so if the simulation program allows it, we know that it is based on simplifications in this respect. The model outlined in chapter 10 will automatically limit the maximum speed, while the more simplified models, such as the one in chapter 7 and some of those in chapter 15, do not. The simplifications do not necessarily give us unacceptable results if we only use it to simulate much lower velocities, but this test can be of help when investigating the simulation program's possibilities and limitations.

If the program is based on simplifications, it is quite common to limit the maximum velocity by using a simple test-criteria in the program. Therefore, we can generally not use the test the other way and conclude the underlying model is very advanced even if the program prevents supersonic flow from occurring.

14.6.8 Things which may confuse result interpretation

It is amazing how many things can go wrong when simulating pipe flow - one encounters some new challenges in nearly all new system simulation. Here, we will discuss some of the more common ones.

 For non-commercial use only

Variable-step methods – those which determine the time steps by comparing results from two different integration methods (such as RK4-5) may respond to stability problems by reducing the time step to a very small value. If well programmed, this should lead to user warnings. But the integration method may be third-party software, and it may not know what counts as 'very small' as seen from the physical system it is dealing with. In some cases, it can instead lead to the integration getting virtually nowhere in time even after very long simulation runs, and it does not necessarily tell the user that there is a problem. The underlying problem can of course be erroneous input data or errors in the program itself, or even actual physical instabilities in the system we are simulating.

The calculation of chemical properties can also play tricks in some simulation programs. If the gas reaches a temperature and pressure where condensation starts to appear, the program should recognize that and give a user warning. Chemical properties are often calculated by third-party software, and it may simply try to feed two-phase properties back to the single-phase transient calculations. This may or may not be handled properly; depending on how well the program system has been designed and tested. In poorly designed programs the integration may simply 'crash'.

Plotting programs can also introduce unexpected results. They are most often created by another organization than the one who developed the simulation program, and it may contain functions the pipe flow program would be better off without. For instance, many advanced plotting programs can do various types of filtering or smoothing of the curves. If this is happening without the user's knowledge, sharp edges may appear as nice and smooth, and that can be very misleading. Also, if the simulation produces results at varying time intervals, it is important the results are not plotted with constant spacing for each point so the time scale gets distorted.

Friction factor calculations are another common source of errors. As explained in chapter 2, there are many different friction calculation methods in use, and some simulation programs allow the user to choose which method to use. Whether the method is selectable or not, it is important to avoid the sources of confusion explained in chapter 2.13.

References

Uhl, A.E. (1965): *Steady Flow in Gas Pipelines.* Institute of Gas Technology, Technical Report No. 10, American Gas Association.

 For non-commercial use only

"Everything should be as simple as possible, but no simpler."
Albert Einstein

15 Simplified models

Simplified models of the conservation equations include:

- Steady-state equation formulation
- Simplifications for isothermal flow
- Neglecting inertia terms to create a simplified transient model
- The importance of including real gas properties

15.1 General

The fully transient model described in chapters 10-14 works well, but it is also quite expensive in terms of required computer resources. When dealing with complex networks, the fully transient model can lead to relatively slow computations. That problem obviously diminishes as the technology progresses, but it is still true that simplified models are much used. This chapter argues that some of the simplifications seem to survive mostly for historical reasons. Improved numerical methods and cheap computers make the fully transient models more practical now than they were before. We will examine some of the most common simplifications, though, starting out with a steady-state model.

For non-commercial use only

15.2 Steady-state calculations

If we go back and take a look at equation 10.1.9, we recall the left-hand side of it is the time derivative. In a steady-state situation, everything has stabilized, so by definition, the time derivative is zero. That means:

$$\frac{\partial}{\partial x}\begin{bmatrix}\rho v\\ p+\rho v^2\\ v(E+p)\end{bmatrix}=\begin{bmatrix}0\\ -\frac{f\rho}{2d}v|v|-\rho g sin\theta\\ q+w\end{bmatrix} \tag{15.2.1}$$

The first equation simply states that $\partial(\rho v)/\partial x = 0$, meaning the mass flow has to be kept the same though the whole pipe. That is obviously something we manage to do without dedicating an equation for it in each grid point, so we can ignore it in the calculations.

Equations 15.2.1 can be simplified even further if we neglect the inertia term of the momentum equation. The $\partial/\partial x(\rho v)^2$-term arises because the gas accelerates as it expands from the inlet to the outlet. For the long pipeline investigated in chapter 14.1, the velocity plot in figure 14.1.5 shows v =2.9 *m/s* at the inlet, and each fluid particle accelerates to around *4.5 m/s* by the time it reaches the outlet after a time period of several days. That is a very slow acceleration indeed, and the pressure reduction it causes is obviously totally insignificant compared to the more than *5 MPa* pressure loss caused by friction. For that pipeline, as for most long pipelines, we can safely neglect that inertia for steady-state calculations and set:

$$\frac{\partial}{\partial x}\begin{bmatrix}\mathrm{p}\\ v(E+p)\end{bmatrix}=\begin{bmatrix}-\frac{f\rho}{2d}v|v|-\rho g sin\theta\\ q+w\end{bmatrix} \tag{15.2.2}$$

If we use the previously described methods to correlate the primary variables ρ, ρv, and E with the secondary variables p, v, T, and h, we can find the steady-state solution by solving equation 15.1.2. It is not difficult to do so, the left-hand side has very weak feedback to the right-hand side of the equation, so nearly any convergent

 For non-commercial use only

approximation of $\partial/\partial x$ is going to be stable and non-oscillatory. For instance, we may use a simple first-order approximation such as:

$$\frac{\partial y}{\partial x} = \frac{Y_{i+1} - Y_i}{\Delta x} \tag{15.2.3}$$

Where the definition of Y is:

$$Y = \begin{bmatrix} y_1 \\ y_2 \end{bmatrix} = \begin{bmatrix} p \\ v(E+p) \end{bmatrix} \tag{15.2.4}$$

If, for instance, we want a pipeline to carry *369 kg/s* with an upstream pressure of *15 MPa* (as in the example in chapter 14.1) and wonder what the downstream pressure needs to be to achieve that, we can insert equation 15.2.3 into 15.2.2 and set:

$$\begin{bmatrix} \mathrm{p} \\ v(E+p) \end{bmatrix}_{\mathrm{i+1}} = \begin{bmatrix} \mathrm{p} \\ v(E+p) \end{bmatrix}_{\mathrm{i}} + \begin{bmatrix} -\frac{f\rho}{2d} v|v| - \rho g sin\theta \\ q + w \end{bmatrix}_{\mathrm{i}} \tag{15.2.5}$$

We simply start by inserting p and $v(E+p)$ at the inlet. Note that E can be calculated from equation 10.1.8, 10.1.2 and 10.1.4 at the inlet. Elsewhere, we set $\rho = \rho(p,T)$, $v = (\rho v)/v$ and $E = \frac{{y_2}^2}{v} - p$. Equation 15.2.5 is used repeatedly for ever increasing i until we get to the outlet end of the pipe.

In case the flow is isothermal, as it actually turned out to be in our poorly insulated and very long pipeline in chapter 14.1, we do not need the last equation to keep track of the temperature. We therefore end up with only one equation:

$$\mathrm{p_{i+1}} = \mathrm{p_i} - \frac{f_i \rho_i}{2d} v_i |v_i| - \rho_i g sin\theta_i \tag{15.2.6}$$

That makes the calculations even simpler and faster. It is also possible to increase the method's order to 2 by modifying equation 15.2.3 to:

$$\frac{\partial y}{\partial x} = \frac{\mathrm{Y_{i+1}} - \mathrm{Y_{i-1}}}{2\Delta \mathrm{x}} \tag{15.2.7}$$

But we need to put in some extra effort to get started, since the first calculation from the inlet is going to produce values only for Y_{i+1}, thereby ignoring Y_i. To get started, we need to use a first order approximation like 15.2.3 for the first step. We can choose to use one order of magnitude smaller Δx combined with an order of magnitude more steps when calculating that Y_i in order to maintain a fully second order accuracy. Doing so means that we simply use a denser grid near the boundary where we are forced to use a lower order approximation.

15.3 Fully transient isothermal model

Although the steady-state model in chapter 15.2 is useful in some cases, such as when finding starting values for the transient models, is suffers from one very obvious drawback: It cannot tell us how things like pressure or mass flow develop over time. That also makes the model unable to give us detailed information about how different parts of the pipeline can be used to store gas, of instance to meet peak demands in areas where large consumers are located.

Let us go back to the full model as described by equations 10.1.9. When the flow is isothermal, we do not need the third equation to determine the temperature, and we simplify to:

$$\frac{\partial}{\partial t}\begin{bmatrix}\rho \\ \rho v\end{bmatrix} = -\frac{\partial}{\partial x}\begin{bmatrix}\rho v \\ p + \rho v^2\end{bmatrix} + \begin{bmatrix}0 \\ -\frac{f\rho}{2d} v|v| - \rho g sin\theta\end{bmatrix} \tag{15.3.1}$$

 For non-commercial use only

The pressure can now be found directly from the property equation $p = p(T, \rho)$, excluding the need for any iteration even for real gases.

Apart from that, we can solve the equations in the same way as before using the KT3 scheme. The reduced number of equations, together with the simpler and therefore faster switch between primary and secondary variables, can speed up the computations by a factor of 1.5-5. That is of course nice, but not necessarily enough to be significant with today's low computer costs.

15.4 Neglecting part of inertia for isothermal flow

We have already argued that the sort of inertia associated with the $\partial/\partial x(\rho v)^2$-term in the state equations is of little or no relevance to most long pipeline flow. We may therefore in most cases neglect it in the transient equations, too. If, in addition, our flow is isothermal, we end up with the following equations:

$$\frac{\partial}{\partial t}\begin{bmatrix}\rho \\ \rho v\end{bmatrix} = -\frac{\partial}{\partial x}\begin{bmatrix}\rho v \\ \mathrm{p}\end{bmatrix} + \begin{bmatrix}0 \\ -\frac{f\rho}{2d}v|v| - \rho g sin\theta\end{bmatrix} \tag{15.4.1}$$

The gas property equation to sue is of course the familiar real-gas equation $p = p(T, \rho)$.

For the sake of investigating what sort of equation 15.4.1 is, let us look at the special case in which the gas is a perfect gas. We can then insert equation 10.2.1 and eliminate p:

$$\frac{\partial}{\partial t}\begin{bmatrix}\rho \\ \rho v\end{bmatrix} = -\frac{\partial}{\partial x}\begin{bmatrix}0 & 1 \\ R_g T & 0\end{bmatrix}\begin{bmatrix}\rho \\ \rho v\end{bmatrix} + \begin{bmatrix}0 \\ -\frac{f\rho}{2d}v|v| - \rho g sin\theta\end{bmatrix} \tag{15.4.2}$$

The eigenvalues are defined by:

$$\begin{vmatrix}-\lambda & 1 \\ R_g T & -\lambda\end{vmatrix} = 0 \tag{15.4.3}$$

This leads to:

$$\lambda = \pm\sqrt{R_g T} \tag{15.4.4}$$

This shows that our equations are hyperbolic, just like the ones we have encountered before. That would also have been the case even if our gas was not perfect, it would just mean the constant factor $R_g T$ would have to be replaced by some other function of T (as well as of p). So even though we are aware hyperbolic equations like 15.4.2 can be described by characteristics, we also realize that expressing those characteristics may be complicated for real gases. But we can at least in principle use some sort of quasi-perfect gas, and we can solve the equations in much the same way as the method of characteristics shown in chapter 6.

A more general way of solving equation 15.4.2 is to use the KT3 method shown earlier. If we do that, we gain little in terms of simulation speed by introducing these simplifications, so we may as well return to the full model from chapter 10.

15.5 Neglecting all terms to do with gas inertia

15.5.1 Model formulation

The other term to do with inertia in equation 15.3.1 is $\partial(\rho v)/\partial t$. For relatively slow mass flow changes and/or relatively long pipes (such as pipelines), it often contributes less than *1%* of the friction term. If we neglect it, we end up with these two equations:

$$\frac{\partial \rho}{\partial t} = -\frac{\partial(\rho v)}{\partial x} \tag{15.5.1}$$

$$\frac{\partial p}{\partial x} = -\frac{f\rho}{2d} v|v| - \rho g sin\theta \tag{15.5.2}$$

As before, the fluid property $p = p(T, \rho)$ is used to close the equations.

 For non-commercial use only

It is hard to see any obvious ways to solve the equations as they stand, but we can transform them in a way which makes it easier to solve them numerically. We start by changing equation 15.5.1 into the form shown in equation 6.1.10:

$$\frac{\partial \rho}{\partial t} = -\mathrm{v}\frac{\partial \rho}{\partial x} - \rho\frac{\partial v}{\partial x} \tag{15.5.3}$$

Now let us try to find expressions for $\partial\rho/\partial x$ and $\partial v/\partial x$. Since $p = p(\rho, T)$, it follows:

$$\frac{\partial p}{\partial x} = \left(\frac{\partial p}{\partial \rho}\right)_{\mathrm{T}} \cdot \frac{\partial \rho}{\partial x} + \left(\frac{\partial p}{\partial T}\right)_{\rho} \cdot \frac{\partial T}{\partial x} \tag{15.5.4}$$

For isothermal flow, $\partial T/\partial x = 0$, and we end up with:

$$\frac{\partial p}{\partial x} = \left(\frac{\partial p}{\partial \rho}\right)_{\mathrm{T}} \cdot \frac{\partial \rho}{\partial x} \tag{15.5.5}$$

Note that $(\partial p/\partial \rho)_{\mathrm{T}}$ is simply a fluid property and may typically be pulled out of some third-party fluid property program. It does not take part in the numerical integration of the equations, so the mathematics is not quite as complex as it may at first appear from the number of partial derivatives.

Inserting equation 15.5.5 into equation 15.5.2, we get:

$$\frac{\partial \rho}{\partial x} = \left(\frac{\partial p}{\partial \rho}\right)_{\mathrm{T}}^{-1} \left(-\frac{f\rho}{2d} v|v| - \rho g sin\theta\right) \tag{15.5.6}$$

That gives us an expression for $\partial\rho/\partial x$ to insert into equation 15.3.3, but we still lack an expression for $\partial v/\partial x$. We can find one by further derivation of 15.5.6:

$$\frac{\partial^2\rho}{\partial x^2} = \left(\frac{\partial p}{\partial \rho}\right)_T^{-1}\left[-\frac{f}{2d}\left(v|v|\frac{\partial \rho}{\partial x} + 2\rho v\frac{\partial v}{\partial x}\right) - \frac{\partial \rho}{\partial x}gsin\theta\right] - \left(\frac{f\rho}{2d}v|v| + \rho gsin\theta\right)\frac{\partial\left(\frac{\partial p}{\partial \rho}\right)_T^{-1}}{\partial x} \quad (15.5.7)$$

Solving this for $\partial v/\partial x$:

$$\frac{\partial v}{\partial x} = -\frac{d}{f\rho v}\left[\left(\frac{\partial p}{\partial \rho}\right)_T\frac{\partial^2\rho}{\partial x^2} + \left(\frac{fv|v|}{2d} + gsin\theta\right)\frac{\partial \rho}{\partial x}\right] - \left(\frac{v}{2} + \frac{gdsin\theta}{fv}\right)\frac{\partial\left(\frac{\partial p}{\partial \rho}\right)_T^{-1}}{\partial x} \quad (15.5.8)$$

Eliminating $\partial\rho/\partial x$ by inserting equation 15.5.6, we get:

$$\frac{\partial v}{\partial x} = -\frac{d}{f\rho v}\left[\left(\frac{\partial p}{\partial \rho}\right)_T\frac{\partial^2\rho}{\partial x^2} + \left(\frac{fv|v|}{2d} + gsin\theta\right)\left(\frac{\partial p}{\partial \rho}\right)_T^{-1}\left(-\frac{f\rho}{2d}v|v| - \rho gsin\theta\right)\right] - \left(\frac{v}{2} + \frac{gdsin\theta}{fv}\right)\frac{\partial\left(\frac{\partial p}{\partial \rho}\right)_T^{-1}}{\partial x} \quad (15.5.9)$$

We are now able to insert equation 15.5.6 and 15.5.9 into 15.5.3. We get:

 For non-commercial use only

$$\frac{\partial \rho}{\partial t} = \left(\frac{\partial p}{\partial \rho}\right)_T^{-1} \left(\frac{f\rho v^3}{2d} v|v| + \rho g v sin\theta\right) + \frac{d}{fv}\left[\left(\frac{\partial p}{\partial \rho}\right)_T \frac{\partial^2 \rho}{\partial x^2} - \left(\frac{fv|v|}{2d} + gsin\theta\right)\left(\frac{\partial p}{\partial \rho}\right)_T^{-1} \left(-\frac{f\rho}{2d} v|v| - \rho g sin\theta\right)\right] + \rho\left(\frac{v}{2} + \frac{gdsin\theta}{fv}\right)\frac{\partial \left(\frac{\partial p}{\partial \rho}\right)_T^{-1}}{\partial x} \quad (15.5.10)$$

Basic algebra simplifies equation 15.5.10 into:

$$\frac{\partial \rho}{\partial t} = \left(\frac{\partial p}{\partial \rho}\right)_T^{-1} \left(\frac{f\rho v^3}{2d} v|v| + \rho g v sin\theta\right) + \frac{d}{fv}\left(\frac{\partial p}{\partial \rho}\right)_T \frac{\partial^2 \rho}{\partial x^2} - \frac{d\rho}{fv}\left(\frac{fv|v|}{2d} + gsin\theta\right)^2 \left(\frac{\partial p}{\partial \rho}\right)_T^{-1} + \left(\frac{\rho v}{2} + \frac{\rho g d sin\theta}{fv}\right)\frac{\partial \left(\frac{\partial p}{\partial \rho}\right)_T^{-1}}{\partial x} \quad (15.5.11)$$

We immediately realize this equation cannot be solved alone, since both ρ and v occur as unknowns in it. We therefore need one more equation, and we simply use the last equation in 15.3.1. If we also insert equation 15.5.5 to eliminate p, we get:

$$\frac{\partial(\rho v)}{\partial t} = -\left(\frac{\partial p}{\partial \rho}\right)_T \cdot \frac{\partial \rho}{\partial x} - \frac{\partial \rho v^2}{\partial x} - \frac{f\rho}{2d} v|v| - \rho g sin\theta \quad (15.5.12)$$

This may look like something of a paradox, because we are in fact re-introducing the inertia-terms we neglect in equation 15.3.17. What was then the point of neglecting them in the first place? And besides, if we have to solve equations 15.3.17 and 15.3.18 in parallel, why not rather solve the more accurate equation set 15.3.1 instead?

To answer these questions, let us first observe that the coupling between the two equations 15.5.11 and 15.5.12 is very weak. ρv, computed by equation 15.5.12, is only affecting 15.5.11 indirectly via the friction term. Also, we saw that equation 15.5.11 describes $\partial\rho/\partial t$ as it would have been if $\partial(\rho v)/\partial t = 0$, based on the assumption that $\partial\rho/\partial t$ is not going to be much affected by whether $\partial(\rho v)/\partial t$ is zero or not. This assumption is not the same as forcing $\partial(\rho v)/\partial t$ to become zero, so we do not expect equation 15.5.12 to necessarily end up telling us $\partial(\rho v)/\partial t = 0$, and hence it does not have to result in (ρv) being constant over time. What we have done is create a set of equations with numerical properties mostly determined by one of them, namely equation 15.5.11. That equation happens to be on the same format as the familiar heat equation, which is well described in literature, and it is known to be parabolic (Cannon, 1984).

This model has benefits simply because it is easy to solve. We just have to remember that no part of the inertia terms (neither $\partial(\rho v)/\partial t$ nor $\partial\rho v^2/\partial x$) are accounted for correctly, so we can only expect accurate results when friction and/or elevation forces dominate over inertia. That is a common situation in pipelines and many pipe networks, but may be inadequate when we want to investigate fast transients, for instance rapid valve operations, compressor failure or pipe rupture.

The model presumes isothermal flow, but it allows both pressure and mass flow to develop over time, so it can give much more information about the pipe flow than a purely steady-state model can. But it is not a fully transient model, even though some commercial programs relying on it are being marketed as transient without explaining the limitations.

15.5.2 Numerical approximations

We can use second order approximations for all spatial derivatives:

$$\frac{\partial^2\rho}{\partial x^2} = \frac{\rho_{i+1} - 2\rho_i + \rho_{i-1}}{(\Delta x)^2} \tag{15.3.19}$$

 For non-commercial use only

And:

$$\frac{\partial \rho}{\partial x} = \frac{\rho_{i+1} - \rho_{i-1}}{2\Delta x} \tag{15.5.20}$$

The spatial derivative of the fluid property $\left(\frac{\partial p}{\partial \rho}\right)_T^{-1}$ is equally easy to estimate as:

$$\frac{\partial \left(\frac{\partial p}{\partial \rho}\right)_T^{-1}}{\partial x} = \frac{\left(\frac{\partial p}{\partial \rho}\right)_{T\ i+1}^{-1} - \left(\frac{\partial p}{\partial \rho}\right)_{T\ i-1}^{-1}}{2\Delta x} \tag{15.5.21}$$

At the boundaries, we need to modify, and there are a number of ways to do so. Here, we will simply use one ghost cell at each end of the pipe and insert values in those ghost cells in exactly the way it was described for the KG3-scheme in chapter 11.

15.5.3 Important observations regarding neglecting the gas inertia

Neglecting inertia is quite a popular approach when simulating gas pipe flow, and many of the commercially available simulation programs are based on this assumption. One reason for that is simply the fact that the model was described in Streeter & Wylie's much used book (1983, though earlier editions exist). Before the KG3-scheme was invented, the numerical benefits were very important, too. Note, though, that most of the models found in literature only describe how to neglect the inertia when simulating perfect gases, and perfect gas models have limited validity.

We remember from equation 10.2.1 that for a perfect gas, $p = \rho R_g T$. In that case:

$$\left(\frac{\partial p}{\partial \rho}\right)_T = R_g T \text{ and } \left(\frac{\partial p}{\partial \rho}\right)_T^{-1} = \frac{1}{R_g T} \tag{15.5.22}$$

In our isothermal model, T is by definition constant, and:

$$\frac{\partial \left(\frac{\partial p}{\partial \rho}\right)_T^{-1}}{\partial x} = 0 \tag{15.5.23}$$

This means the last term in equation 15.5.11 vanishes for perfect gases, and the term is most often neglected in inertia-free models in literature. Equation 15.5.11 gets the form:

$$\frac{\partial \rho}{\partial t} = \frac{1}{R_g T}\left(\frac{f\rho v^3}{2d} v|v| + \rho g v sin\theta\right) + \frac{d}{fv} R_g T \frac{\partial^2 \rho}{\partial x^2} - \frac{d\rho}{fv}\left(\frac{fv|v|}{2d} + g sin\theta\right)^2 \frac{1}{R_g T} \tag{15.5.24}$$

For real gases, though, a very significant error can result from neglecting how $(\partial p/\partial \rho)_T$ varies along the pipe. If we use equations 15.5.11 and 15.5.12 to simulate the same pipeline as in chapter 14.1, the steady-state results converges towards the same values as before. If the last term in equation 15.5.11 is neglected, the results turn out to not even converge towards a steady-state where the mass flow is constant in the whole pipeline.

The other important comment about assuming isothermal flow and neglecting the inertia terms is that recent improvements have removed most of the motives to do so. The full model, as shown in equation 10.1.9, is so efficiently solved with the KG3-scheme on a modern computer that it rarely is necessary to introduce these simplifications any longer. The only simplifications offering very significant speed gains over the fully transient model are the steady-state simplifications outlined in chapter 15.2. As already explained, those simplifications limit the model's value significantly and are best used to calculate starting values for the transient calculations.

References

Streeter, V.L., Wylie, E.B., (1983): *Fluid Transients.* FEB Press.

 For non-commercial use only

Cannon, J., (1984): *The One-Dimensional Heat Equation, Encyclopedia of mathematics and its applications*. Addison-Wesley.

Osiadacz, A. J., (1996): *Different Transient Models – Limitations, Advantages and Disadvantages.* Pipeline Simulation Interest Group.

Nomenclature

Latin letters

a_s	Speed of sound	[m/s]
A	Cross-sectional area	[m^2]
A	General square matrix	
c_v	Spesific heat at constant volume	[J/kg·K]
c_p	Spesific heat at constant pressure	[J/kg·K]
C	Chezy's coefficient for friction calculations,	SI-irrelevant
C_d	Factor in the Kolmogorov spectrum	Dimensionless
C_e	Factor in the Kolmogorov spectrum	Dimensionless
C_h	Hazen-Williams-factor, rarely used in the SI-system	SI-irrelevant
C_v	Valve flow coefficient used in the imperial unit system	[$in^{7/2}lb^{-1/2}$],
d	Inner pipe diameter	[m]
d_h	Hydraulic pipe diameter, as defined by equation 3.1.1	[m]
d_i	Inner annular diameter, as defined in figure 3.4.1	[m]
d_o	Outer annular diameter, as defined in figure 3.4.1	[m]
D	Vector defined by equation 10.1.10	
e_{ss}	Steady-state relative iteration error, equations 7.5.3 and 7.5.4	Dimensionless
E	Volume-specific power	[Pa]
E_s	Energy pr. unit mass	[J/kg]
$E(\sigma)$	Kolmogorov spectrum	
f	Darcy-Weisbach friction factor	Dimensionless
f_m	Darcy-Weisbach friction factor for power-law fluids	Dimensionless
f_r	Rough pipe friction factor used by the AGA calculation method	Dimensionless
f_s	Smooth pipe friction factor used by the AGA calculation method	Dimensionless
F	Flux vector, as defined by equation 10.1.10	
g	Gravitational acceleration	[m/s^2]
h	Specific enthalpy	[J/kg]
h	Height	[m]
H	Hurst exponent, in this book's context used to characterize surfaces	Dimensionless
H'	Surface texture parameter used by Sletfjerding	Dimensionless
J	Jacobi-matrix	
J_g	Jacobi-matrix for ghost cell calculations as defined in equation 11.5.10	

For non-commercial use only

k	Constant defined by equation 7.7.9	Dimensionless
k_c	Compressibility	[kg/s^2·m]
k_d	Delay-factor defined by equation 2.10.1	Dimensionless
k_g	Geometric correction factor for friction as defined by equation 3.3.1	Dimensionless
k_j	Thermal conductivity for layer No. j	[M/(mK)]
k_k	Constant in the Kolmogorov-spectrum	Dimensionless
k_k	Constant defined by equation 2.8.12	Dimensionless
k_s	Sand grain roughness, equivalent sand grain roughness	[m]
k_ε	Constant defined by equation 2.8.11	Dimensionless
k_τ	Constant defined by equation 2.8.5.	Dimensionless
k_1, k_2	Constants used to defined friction in piping components in chapter 4	Dimensionless
K_A,K_B	Factors defined by equations 7.2.9 and 7.2.10	[Pa]
K_f	Friction factor defined by equation 4.1.1	Dimensionless
K_v	Valve flow factor used for easy comparison with imperial units	[m $^{7/2}$kg$^{-1/2}$]
K_0	Factor for pseudoplastic and dilatants fluids as def. by equation 5.2.1	Varies
l	Length, total pipe length unless specified otherwise	[m]
l_e	Equivalent length	[m]
l_w	Distance between welds, as defined in figure 4.4.1,	[m]
m	Mass	[kg]
$\dot{m}$	Mass flow	[kg/s]
n	Non-newtonian fluid power law exponent	Dimensionless
n	Pump speed	[rev./min]
n_d	Factor for defining local friction factor minimum, equation 2.10.2	Dimensionless
n_s	Vector normal to surface, as defined by equation 6.1.1	[m]
n_0	Reference pump speed	[rev./min]
Nu	Nusselt number	Dimensionless
N_x	Number of grid points or cells (ghost-cells not included)	Dimensionless
m_n	Friction factor used in Manning's formula	[m$^{1/3}$·s]
p	Pressure	[Pa]
$p_{A,B,C}$	Pressure, indexed according to figure 7.1.1.	[Pa]
Pr	Prandtl number	Dimensionless
q	Volume-specific heat	[J/m^3]
Q	Flow	[m^3/s]
Q	Heat transfer rate	[W]
r	Inner pipe radius	[m]
r_i	Argument in the flux limiter, see equations 9.7.4 and 10.5.5	Dimensionless

R	Universal gas constant	[J/(K·mol)]
R_a	Arithmetic mean surface roughness	[m]
R_g	Mean peak-to-valley surface height	[m]
R_g	Characteristic gas constant for a particular ideal gas	[J/kg·K]
R_0	Bend radius	[m]
R_a	Arithmetic mean surface roughness	[m]
R_q	Root mean square surface roughness	[m]
R_z	Peak-to-valley surface height difference	[m]
Re	Reynolds number (=v·d/ν)	Dimensionless
Re_d	Reynolds number for local friction factor minimum, equation 2.10.2	Dimensionless
Re_m	Power-law Reynolds number defined by equation 5.2.10	Dimensionless
s	Turbulence eddy size	[m]
s_m	Slope as defined for Manning's formula	Dimesnionless
S	Surface, as defined by equation 6.1.1	[m^2]
t	Time	[s]
T	Absolute temperature	[K]
u	Specific internal energy	[J/kg]
u_s	Surface structure uniformity factor	Dimensionless
U	Heat transfer coefficient	[W/(m2K)]
v	Fluid velocity, average over the cross-section	[m/s]
$v_{A,B,C}$	Fluid velocity, indexed according to figure 7.1.1	[m/s]
v_{sl}	Large scale eddy velocity	[m/s]
v_{es}	Turbulence eddies' velocity based on kinetic energy	[m/s]
V	Volume	[m^3]
w	Volume-spcific work	[J/m^3]
w	Width	[m]
x	Axial direction; integration variable defined by equation 2.8.18	
y	Distance from pipe wall (= d/2 – r)	[m]
Y	Primary variables vector, as defined by equation 10.1.1	
z	Elevation from reference level	[m]
Z	Compressibility factor for real gas	Dimensionless
$\bar{Z}$	Averaged compressibility factor for real gas	Dimensionless

Greek letters

α	Angle defining partly filled pipe as defined in figure 3.2.1	Radians
α	Thermal diffusivity	[m2/s]
α_c	Junction angles defined in chapter 4	Radians
β	Constant defined by equation 2.8.10	Dimensionless
β_c	Cone and junction angles defined in chapter 4	Radians

For non-commercial use only

$\boldsymbol{\delta}$	Relative iteration error	Dimensionless
$\boldsymbol{\delta_l}$	Laminar sub-layer thickness	[m]
$\boldsymbol{\delta_w}$	Weld thickness, as defined in figure 4.4.1	[m]
ε	Rate of dissipation in the Kolmogorov-spectrum	[m2/s3]
$\boldsymbol{\varepsilon_{p\rho E}}$	Error norm, as defined by equations 11.5.14 and 11.5.15	
$\boldsymbol{\Phi(r_i)}$	Flux limiter function	Dimensionless
$\boldsymbol{\eta}$	Kolmogorov viscous micro length scale	[m]
$\boldsymbol{\varphi_G}$	Gaussian probability function	Dimensionless
$\boldsymbol{\kappa}$	Ideal gas isentropic exponent	Dimensionless
$\boldsymbol{\lambda}$	Eigenvalue	Dimensionless
$\boldsymbol{\mu}$	Dynamic viscosity ($= \nu\rho$)	[kg/(m·s)]
$\boldsymbol{\mu_J}$	Joule-Thomson coefficient, as defined by equation 14.2.1	[K/Pa]
$\boldsymbol{\mu_a}$	Apparent viscosity for power-law fluids, def. by equation 5.2.2	[kg/(m·s)]
$\boldsymbol{\mu_p}$	Apparent viscosity for Birmingham plastic fluids, eq. 5.3.1	[kg/(m·s)]
$\boldsymbol{\mu_s}$	Surface roughness mean	[m]
$\boldsymbol{\nu}$	Kinematic viscosity ($= \mu/\rho$)	[m^2/s]
$\boldsymbol{\rho}$	Density	[kg/m^3]
$\boldsymbol{\rho v}$	Area-specific mass flow	[kg/s·m]
σ	Inverse wave number in the Kolmogorov spectrum	[m^{-1}]
σ^2	Surface roughness variance	[m^2]
$\boldsymbol{\tau}$	Shear stress	[N/m^2]
$\boldsymbol{\tau_w}$	Shear stress between fluid and pipe wall	[N/m^2]
$\boldsymbol{\tau_0}$	Minimum shear stress to initiate non-Newtonian fluid flow	[N/m^2]
θ	Pipe elevation angle, positive is upwards	Radians
θ_b	Bend angle	Radians

Subscripts

i	Cell and grid point No.
j	Time step No. (for integration), layer No. (for insulation, see figure 8.1.1)
k	Pipe No.
ss	Steady-state
o, i	Outer , inner (relevant to insulation layers, see figure 8.1.1)

Superscripts

L	Left (calculated from left-side values, equations 9.7.3, 9.7.5, 10.5.1, 10.5.3)
R	Right (calculated from right-side values, equations 9.7.4, 9.7.6, 10.5.2, 10.5.4)

Index

- A -

Accuracy, 1, 4, 14, 75, 77, 82, 88, 182, 187, 204, 205, 206, 222, 229, 236, 239, 240, 266, 268, 269, 275, 282, 283, 285, 303, 325, 334
Acquisition, 6
AFT pipeline, 15
AGA, 4, 1, 12, 29, 41, 46, 47, 63, 65, 74, 76, 79, 82, 264, 323, 344
AGA Program, 12
American Gas Association, 90, 130, 264, 278, 329
Annular cross-section, 2, 99, 100
API, 11, 19
Application programming interface, 11
Aspen Yysys®, 13
Aspen Traflow, 19
Atmos Pipeline Software, 15

- B -

Bends, 2, 89, 102, 106
Bentonitic clay, 123
Birmingham plastic, 2, 122, 127, 128, 346
Blausius, 82
Blood, 22, 87, 121, 122, 197, 207
Boundary conditions, 3, 4, 5, 165, 233, 295
Boundary layer, 48, 50, 53, 57, 58, 61, 89
Buried, 3, 4, 217, 221, 222, 243, 327

- C -

Capacity, 4, 3, 4, 10, 13, 16, 22, 28, 88, 97, 129, 147, 161, 180, 181, 221, 237, 311
CAPE-OPEN, 12
Cavitation, 12, 106, 110, 165, 188, 190, 209, 228
Centrifugal pump, 3, 169, 170, 173
Characteristic, 3, 4, 33, 56, 156, 158, 159, 165, 172, 200, 202, 207, 224, 226, 227, 228, 243, 258, 261
Characteristics, 5, 3, 4, 34, 44, 90, 123, 145, 152, 155, 159, 161, 165, 169, 170, 172, 181, 182, 183, 191, 195, 196, 200, 205, 206, 224, 228, 229, 237, 242, 245, 299, 336
Check, 3, 7, 152, 172, 179, 184, 185, 189, 205, 227, 234, 261, 271, 311, 318, 320, 324, 325, 327, 328
Chezy's coefficient, 81, 344
Clay-water suspensions, 123
Codes, 4
Colebrook & White, 37, 38, 39, 40, 46, 47, 63, 64, 65, 74, 75, 82, 323
Commercial software, 3, 197, 310, 322, 323
Commissioning, 7
Complexity, 9, 14, 147, 181, 206, 324
Components, 2, 4, 13, 26, 46, 102, 103, 139, 205, 206, 220, 235, 257, 268, 269, 295, 302, 324, 345
Compressibility, 3, 29, 146, 153, 154, 207, 346
Condensate, 10, 13
Conical contraction, 113
Conical diffuser, 112
Conservation, 5, 2, 4, 132, 134, 135, 138, 141, 142, 144, 152, 209, 228, 255, 261, 266, 296, 299, 331
Conservation form, 135
Continuity equation, 134, 135, 137, 139, 182, 206, 325

For non-commercial use only

Convergence, 3, 38, 181, 182, 183, 184, 186, 187, 265, 274, 277, 278, 291, 292
Cooling, 2, 5, 138, 148, 210, 214, 220, 221, 320, 321
Corrosion, 14, 80, 88
Corrugated, 60, 61
Crane, 79, 80, 90, 101, 104, 110, 112, 119

- D -

Data collection, 6
Delay-factor', 72
Diameter changes, 2, 102, 111
Dilatant, 123, 125
Discretization, 4, 224, 229, 261, 265, 266, 267, 268, 269, 280, 325
Dispersion, 4, 224, 243, 244, 245, 247, 248, 249, 266
Displacement pump, 3, 173
Dissipation, 4, 49, 52, 62, 224, 243, 244, 245, 247, 248, 249, 266, 346
DPDL, 17
DRA, 129
Drag-reducing agents, 129
Drillmuds, 123

- E -

Eddies, 26, 48, 49, 50, 52, 54, 55, 56, 57, 58, 61, 62, 87, 129, 346
Eigenvalues, 156, 194, 195, 196, 197, 198, 199, 204, 241, 246, 262, 263, 265, 267, 268, 269, 270, 335
Elevation profile, 315, 316, 322
Elliptic cross-section, 2, 100
Empirical factors, 48, 73
Energy cascade, 48
Energy conservation, 2, 132, 138
Energy equation, 141
Energy spectrum, 49
Erosion, 3, 14, 35, 106

- F -

Fanning's factor, 80, 81
Flow assurance, 8
Flow source, 5, 305
FlowDesk, 15
Flowmaster, 7, 15
Fluid properties, 3, 4, 6, 3, 63, 135, 138, 153, 216, 256, 257, 276, 288, 315, 327
FluidFlow3, 15
Flux variables, 5, 288
Frequency-dependent friction, 86
Friction, 4, 7, 1, 2, 3, 4, 10, 21, 22, 23, 24, 26, 28, 29, 30, 31, 32, 33, 35, 36, 37, 38, 40, 41, 42, 43, 44, 45, 46, 47, 48, 50, 51, 56, 60, 61, 62, 63, 65, 66, 67, 68, 72, 73, 75, 76, 77, 78, 79, 80, 81, 82, 83, 84, 85, 86, 87, 88, 89, 90, 94, 95, 96, 97, 100,뭙102, 103, 106, 107, 108, 110, 111, 112, 113, 114, 121, 123, 124, 125, 126, 127, 128, 129, 135, 145, 147, 153, 154, 161, 163, 177, 178, 179, 182, 183, 185, 187, 188, 193, 195, 196, 198, 199, 202, 203, 205, 207, 212, 214, 228, 253, 257, 269, 272, 302, 315, 318, 323, 328, 329, 332, 336, 340, 344, 345
Friction factor errors, 77
Frictionless flow, 3, 193
Friction-reducing fluids, 2, 129

- G -

GAP, 17
Gas inertia, 6, 336, 341
GasPack™, 13
GasVLE, 13
GASWorks, 15
Gaussian distribution, 41, 42, 45, 72
Ghost cells, 5, 280
Gioia, 7, 48, 92
Glycol, 14
Gnielinski-correlation, 215

Graphical user interface, 11, 19
Grytaaga, 74
GUI, 11

- H -

H2OCALC, 15
Haaland, 39, 64, 68, 82, 90
Hardy Cross, 181
Hazen-Williams, 80, 81, 344
Heat, 3, 4, 138, 209, 212, 216, 217, 222, 223, 343, 345, 346
Heat model, 221, 222, 244
Heat transfer, 210, 211, 212, 213, 214, 215, 217, 220, 222, 272
Hydrates, 13
Hydraulic diameter, 93, 94, 96, 97, 99, 100
HYSYS Pipe Segment, 17
HYSYS Pipesys, 17

- I -

Idelchik, 91, 97, 99, 100, 101, 104, 106, 107, 108, 109, 111, 112, 117, 120
Inertia, 6, 86, 136, 331, 332, 335, 336, 340, 341, 342
Inlet loss, 2, 110
Instantaneous valve closure, 3, 163, 176
Insulation, 3, 4, 3, 138, 142, 148, 209, 210, 211, 216, 217, 222, 272, 315, 316, 317, 323, 347
Integration, 4, 12, 54, 56, 60, 143, 183, 191, 194, 199, 202, 206, 234, 265, 266, 267, 268, 287, 288, 311, 324, 329, 337, 346, 347
Isothermal flow, 6, 17, 29, 138, 148, 154, 315, 316, 331, 335, 337, 340, 342
Iteration, 38, 67, 68, 161, 184, 186, 187, 206, 265, 274, 275, 277, 291, 292, 323, 324, 335, 344, 346

-J -

Jacobi-matrix, 262, 265, 290, 344
Joule-Thomson coefficient, 317, 346
Junctions, 2, 4, 102, 114, 235

- K -

Kolmogorov, 1, 31, 48, 49, 50, 52, 53, 56, 82, 89, 91, 344, 346, 347
KT3, 5, 4, 247, 250, 251, 252, 253, 261, 263, 266, 269, 270, 280, 283, 297, 304, 325, 335, 336
Kurganov, 5, 247, 248, 254, 255, 269, 271, 278

- L -

Laminar, 3, 22, 24, 25, 26, 27, 31, 44, 48, 50, 53, 55, 57, 61, 66, 75, 76, 82, 83, 84, 85, 86, 98, 99, 100, 101, 121, 122, 123, 124, 125, 128, 129, 195, 196, 213, 215
Lax-Wendroff's method, 4, 229, 243
Leak detection, 14
Liquefied Natural Gas, 2
Lucendro, 74

- M -

Manning's formula, 81, 345
Mass conservation, 2, 132, 142
Matlab, 15, 197, 207
Measurements, 35, 61, 74, 92, 112, 131
MEG, 18
Methanol, 14
Method of characteristics, 5, 165, 197, 336
Momentum conservation, 2, 132, 135
Momentum equation, 137, 138, 142, 143, 144, 145, 332

 For non-commercial use only

Moody, 4, 1, 21, 31, 32, 36, 39, 40, 41, 43, 44, 46, 47, 54, 56, 57, 58, 60, 62, 63, 65, 66, 73, 74, 75, 76, 77, 79, 80, 81, 82, 83, 88, 89, 148, 323
Multiflash, 13
Multi-phase, 3, 1, 4, 9, 10, 12, 14, 16, 17, 18, 19, 20, 101, 151, 226, 318, 320, 322

- N -

Nessyahu, 247, 254, 269, 278
Network analysis, 3, 180
Newton's law, 23, 24, 84
Newtonian, 1, 2, 15, 23, 63, 88, 121, 122, 123, 124, 125, 128, 130, 131
Newton-iteration, 67, 68, 168, 275, 276, 290, 292, 293
Nikuradse, 1, 21, 30, 31, 32, 33, 34, 35, 36, 37, 40, 41, 42, 43, 44, 46, 47, 48, 54, 55, 57, 58, 60, 66, 72, 78, 82, 89
Noise, 86, 87, 89
Non-circular pipes, 1, 93
Non-Newtonian, 122, 123
Numerical instability, 200
Numerical lock, 202
Nusselt, 212, 345

- O -

OLGA, 12, 16, 18, 19
Ormen Lange, 5, 16, 18, 20
Overshoot, 68, 187, 244, 245

- P -

Partially-filled pipe, 1, 94
Peng-Robinson, 237, 256
Pigging, 14
Pipe flow, 3, 5, 1, 4, 7, 8, 9, 13, 14, 15, 16, 17, 19, 22, 24, 29, 37, 40, 48, 63, 66, 75, 80, 89, 91, 135, 138, 161, 181, 206, 209, 265, 278, 284, 310, 323, 328, 329, 340, 341
Pipe rupture, 5, 200, 318, 340
PIPEFLO, 17
Pipeline, 22
Pipelines, 3, 4, 5, 2, 3, 5, 6, 7, 10, 16, 17, 18, 22, 28, 46, 77, 79, 86, 88, 91, 92, 102, 104, 108, 110, 129, 138, 144, 147, 148, 167, 190, 213, 215, 218, 219, 221, 222, 249, 258, 285, 310, 316, 322, 332, 336, 340
Pipeline design, 6
Pipeline politics, 2
Pipeline projects, 1, 3, 4, 72, 77, 88
PipelineStudio, 15
Pipephase, 12, 17, 19
PipeSim, 17
Prandtl, 36, 46, 82, 92, 127, 131, 212, 219, 257, 311, 345
Pressure step, 84, 164, 200, 201, 261
PRO/II, 13
PROFES, 17
ProFES transient, 19
Profilometer, 34
Program testing, 5, 310
Pseudoplastic, 123, 345
Pulsations, 83, 87, 89, 174
PVT-data, 11, 12, 13, 15
PVTp, 13
PVTsim, 13

- R -

Real gase, 5, 146, 256, 258, 264, 288, 335, 336, 342
Rectangular pipe, 2, 97
Regulator
Regulators, 86, 87, 89, 268, 269, 324
Reynolds number, 4, 22, 27, 29, 30, 32, 40, 43, 44, 48, 51, 53, 62, 72, 76, 86, 88, 91, 93, 96, 97, 121, 125, 126, 154, 179, 181, 185, 212, 220, 323, 345

Richardson, 48, 89, 131
Right-of-way, 6
Rk4, 266, 267, 268, 269, 287, 311, 324, 329
Roughness, 4, 21, 22, 30, 31, 32, 33, 34, 35, 36, 39, 40, 41, 43, 44, 45, 46, 51, 53, 58, 61, 62, 65, 66, 74, 75, 76, 78, 79, 80, 81, 88, 89, 129, 176, 179, 345, 346, 347
Route selection, 2, 5, 6
Runge-Kutta, 5, 255, 266, 267, 269, 287, 311

- S -

Sand grain roughness, 33, 34, 63, 345
Secondary variables, 4, 236, 270, 272, 273, 274, 278, 306, 309, 313, 332, 335
Sigmoid, 72
SIMONE, 15
Simplified models, 6, 331
SimSuite Pipeline, 19
Simulations, 3, 4, 3, 4, 5, 1, 5, 7, 9, 10, 11, 12, 13, 14, 15, 16, 68, 85, 138, 148, 171, 176, 179, 180, 181, 182, 187, 188, 190, 195, 199, 201, 202, 203, 205, 206, 228, 235, 240, 242, 243, 253, 265, 268, 269, 292, 310, 311, 315, 316, 317, 318, 320, 321, 323, 324, 325, 326, 327, 328
Single-phase, 1, 9, 14, 15, 91
Sletfjerding, 7, 33, 34, 35, 58, 77, 78, 79, 80, 82, 91, 92, 344
Slugging, 10
Specific enthalpy, 237, 344
Specifications, 3, 4, 22
Speed of sound, 28, 153, 158, 159, 163, 164, 175, 176, 179, 182, 183, 186, 205, 207, 228, 241, 242, 261, 263, 264, 265, 269, 271, 318, 319, 325, 328
Stability, 3, 4, 152, 191, 240, 303
Steady-state calculations, 6, 332
Steel pipes, 6, 78
Stoke's law, 23
Stoner pipeline simulator, 15
Submerged, 3
Subsea, 3, 4, 5, 6, 7, 18, 20, 147, 148
Surface profile, 33, 34, 35
Surface roughness, 1, 3, 10, 24, 30, 32, 40, 43, 44, 60, 61, 62, 63, 65, 75, 77, 78, 79, 81, 87, 88, 129, 345
Surface structure uniformity factor, 45, 64, 88, 176
Surfaces, 1, 21, 30, 32, 33, 34, 35, 36, 40, 41, 43, 47, 54, 61, 62, 63, 65, 73, 78, 79, 80, 129, 344

- T -

TACITE, 12, 17, 19
Tadmor, 5, 247, 248, 254, 255, 269, 271, 278
Temperature, 5, 3, 10, 12, 13, 29, 138, 141, 146, 147, 148, 152, 154, 210, 211, 213, 214, 216, 219, 221, 222, 225, 226, 228, 233, 235, 236, 237, 238, 240, 243, 244, 245, 249, 253, 255, 256, 257, 259, 265, 269, 272, 280, 296, 297, 298, 299, 301, 302, 306, 307, 309, 311, 312, 315, 316, 317, 318, 319, 321, 323, 324, 328, 329, 333, 334, 346
Thermal conductivity, 213, 217, 218, 219, 243, 257, 311, 316, 321
Third-party software, 257, 329
Thixotropic, 123
Tolerances, 75
Tracking, 3, 203
Traditional moody, 40, 66, 76
Transient, 4, 5, 6, 9, 10, 12, 13, 15, 16, 17, 19, 22, 29, 68, 83, 85, 86, 87, 89, 135, 144, 145, 147, 170, 180, 181, 187, 204, 205, 209, 221, 225, 228, 240, 247, 296, 310, 326, 329, 331, 334, 335, 340, 342
Transition, 31, 36, 44, 57, 64, 66, 76, 82, 88, 205, 215
TUFFP pro, 17

For non-commercial use only

Turbulent, 7, 1, 21, 26, 31, 48, 49, 52, 61, 63, 82, 89, 129, 130, 244

- U -

Uhl, 46, 82, 90, 323, 329
Unconditionally stable, 195, 245, 266
Uniformity-based, 65, 73, 82, 148, 179

- V -

Valves, 2, 102, 104, 235
Verify, 5, 7, 188, 205, 317, 324
Visco-elastic, 87, 89
Viscosity, 3, 12, 23, 24, 27, 52, 63, 121, 122, 123, 124, 129, 152, 154, 176, 196, 203, 209, 213, 219, 228, 257, 311, 346
Von karman, 24, 25, 26, 30, 36, 51, 56, 82, 127

- W -

Wax, 4, 13, 214
Welds, 2, 108

- Y -

Yield stress, 122, 123

- Z -

Zagarola, 63, 64, 65, 76, 77, 78, 91



The author, Dr. Ove Bratland, was awarded his PhD from the Norwegian Institute of Technology in 1985. He has 28 years of experience in the petroleum industry as lecturer, consultant, and manager, and has worked in various countries in Europe and Asia. His technical qualifications cover an unusually broad range of skills, including hydraulics and pneumatics, pipe flow with special emphasis on flow assurance, flow measurement, dynamic simulations, software development, dynamic system analysis, and automation. He has worked hands-on with most systems common to the upstream petroleum industry, particularly those found on oil rigs and subsea in the Norwegian sector of the North Sea.

This book is the first in a series of two, and it focuses mostly on single-phase flow. The second book deals with flow assurance for multi-phase flow.

- Explores topics essential to studying single-phase liquid and gas pipe flow.
- Includes a marked survey of commercially available multi- and single-phase simulation programs.
- New, improved diagrams and formulas for more accurate friction calculations.
- How to include junctions, bends, valves, pumps and other common components.
- Both steady-state and transient simulations.
- The methods are built on the very latest from numerical mathematics, fluid mechanics, software development and market studies.
- Resources for the book can be found at www.drbratland.com

Pipe Flow 1

Single-phase Flow Assurence

An up-to-date reference for engineers and developers involved with liquid or gas pipelines and networks.